

2014

Design, synthesis, and exploration of a chimeric antioxidant and new crosslinkers for molecular imprinting

Danielle Songe Meador

Louisiana State University and Agricultural and Mechanical College

Follow this and additional works at: https://digitalcommons.lsu.edu/gradschool_dissertations



Part of the [Chemistry Commons](#)

Recommended Citation

Meador, Danielle Songe, "Design, synthesis, and exploration of a chimeric antioxidant and new crosslinkers for molecular imprinting" (2014). *LSU Doctoral Dissertations*. 1260.

https://digitalcommons.lsu.edu/gradschool_dissertations/1260

This Dissertation is brought to you for free and open access by the Graduate School at LSU Digital Commons. It has been accepted for inclusion in LSU Doctoral Dissertations by an authorized graduate school editor of LSU Digital Commons. For more information, please contact gradetd@lsu.edu.

DESIGN, SYNTHESIS, AND EXPLORATION OF A CHIMERIC ANTIOXIDANT AND
NEW CROSSLINKERS FOR MOLECULAR IMPRINTING

A Dissertation

Submitted to the Graduate Faculty of the
Louisiana State University and
Agricultural and Mechanical College
in partial fulfillment of the
requirements for the degree of
Doctor of Philosophy

in

The Department of Chemistry

by
Danielle Songe Meador
B.S., Louisiana State University, 2009
May 2014

To my family

I dedicate my dissertation to my amazing and supportive husband Weslee who has remained at my side throughout all of my graduate work, and my beautiful and sweet daughter Annabelle as well as future children who have given me light and hope in my pursuit of a doctoral degree in chemistry. I also dedicate my work to my parents Karen and David Songe III who have instilled in me the values required to pursue a higher education and the drive to succeed, as well as my sister Dana who has also been a great cheerleader throughout my graduate studies. And last, but not least I dedicate my dissertation to my beloved grandparents Ann and Phil Gioia Sr. and Marion and David Songe Jr. who have inspired me to have a strong work ethic and most importantly to always be humble.

ACKNOWLEDGEMENTS

I would like to express my deepest and heartfelt gratitude to my graduate advisor and mentor Dr. David Spivak who has helped me develop into an independent thinker and successful chemist. I would also like to sincerely thank Dr. Cristina Sabliov, Dr. Doug Gilman, Dr. Carol Taylor, Dr. Justin Ragains, and Dr. Brenda Tubana for all of their guidance in my pursuit of a doctoral degree. I appreciate all of my colleagues and friends who have also been supportive throughout my graduate career.

TABLE OF CONTENTS

ACKNOWLEDGEMENTS	iii
LIST OF TABLES	vi
LIST OF FIGURES	vii
LIST OF SCHEMES.....	x
LIST OF ABBREVIATIONS.....	xi
ABSTRACT.....	xiii
CHAPTER 1: MOLECULAR IMPRINTING INTRODUCTION	1
1.1 Introduction to Molecular Imprinting	1
1.2 The Traditional Imprinting Approach.....	3
1.3 The OMNiMIP Imprinting Approach	7
1.4 The Improvement of Crosslinkers for Molecular Imprinting.....	8
1.5 References	9
CHAPTER 2: NEW CROSSLINKERS FOR MOLECULAR IMPRINTING	13
2.1 Introduction, Design and Synthesis of New Crosslinkers.....	13
2.2 Experimentals.....	26
2.3 Results and Discussion of New Crosslinkers for Molecular Imprinting.....	38
2.4 New Crosslinking Monomers Overall Conclusions.....	49
2.5 Future Work	51
2.6 References	53
CHAPTER 3: RACEMIC AND SCALEMIC IMPRINTING.....	55
3.1 Introduction to Racemic and Scalemic Imprinting	55
3.2 Experimentals: Syntheses of Crosslinking Monomers and OMNiMIP Polymerizations ...	60
3.3 Racemic and Scalemic Template Imprinting Results and Discussion	64
3.4 Racemic and Scalemic Imprinting Conclusions.....	73
3.5 Racemic and Scalemic Imprinting Future Work.....	74
3.6 References	74

CHAPTER 4: EXPLORATION OF ABSOLUTE CONFIGURATION USING AN ENANTIOMERIC PAIR OF MOLECULARLY IMPRINTED POLYMERS	77
4.1 Introduction to the Determination of Absolute Configuration.....	77
4.2 DuoMIP Design and Synthesis*	81
4.3 Results and Discussion of NOBE DuoMIPs*	86
4.4 Exploration of a Chiral OMNiMIP for AC Analysis	101
4.5 Absolute Configuration Determination Conclusions	104
4.6 Absolute Configuration Future Work	105
4.7 References	106
CHAPTER 5: SYNTHESIS OF A NEW CHIMERIC ANTIOXIDANT	109
5.1 Introduction to Diseases Associated with Oxidative Stress	109
5.2 VECAR Design	113
5.3 VECAR Synthesis and Experimentals	115
5.4 VECAR Conclusion	127
5.5 VECAR Future Work.....	128
5.6 References	128
APPENDIX A: SPECTRA FOR CHAPTER TWO	132
APPENDIX B: SPECTRA FOR CHAPTER THREE.....	152
APPENDIX C: CHROMATOGRAMS FOR CHAPTER FOUR	168
APPENDIX D: SPECTRA FOR CHAPTER FIVE	181
APPENDIX E: LETTERS OF PERMISSION	195
THE VITA	197

LIST OF TABLES

Table 2.1: HPLC results for OMNiMIPs synthesized from the crosslinkers with alteration of polymerizable groups *	40
Table 2.2: HPLC results of the OMNiMIPs synthesized from the three-armed crosslinkers *	43
Table 2.3: HPLC results for OMNiMIPs from the addition of EWG *	46
Table 2.4: HPLC results for the OMNiMIPs synthesized from NAG (100 x 2.1 mm column *)	47
Table 2.5: HPLC results for the OMNiMIPs synthesized from NAG (50 x 2.1 mm column *)	48
Table 3.1: Racemic Imprinting HPLC Results *	64
Table 3.2: Scalemic Imprinting HPLC Results *	70
Table 4.1: NOBE DuoMIPs imprinted with 5% <i>S</i> -BOC-Tyr or <i>R</i> -BOC-Tyr *	87
Table 4.2: NOBE DuoMIP imprinted with 20% <i>S</i> -BOC-Tyr or <i>R</i> -BOC-Tyr *	91
Table 4.3: NOBE DuoMIPs imprinted with BOC-Phe or BOC-Phe-OMe templates *	98
Table 4.4: L-NALA DuoMIP system imprinted with <i>R</i> or <i>S</i> -BOC-Tyr *	102

LIST OF FIGURES

Figure 1.1: Examples of common crosslinkers.....	4
Figure 1.2: BOC-Tyrosine (7) and methacrylic acid (8).....	4
Figure 1.3: Diagram of traditional imprinting*.....	6
Figure 1.4: Imprinting illustration in the laboratory.....	6
Figure 1.5: Illustration of OMNiMIP technique.....	7
Figure 1.6: Non-polar and polar spacer modification designs.....	8
Figure 1.7: Non-polar spacer modifications to NOBE.....	9
Figure 2.1: NAG.....	13
Figure 2.2: 2-acrylamidoethyl acrylate (13) and 2-acrylamidoethyl methacrylate, (14).....	15
Figure 2.3: Structures of three and two armed crosslinkers.....	18
Figure 2.4: Three-armed crosslinkers for OMNiMIP imprinting.....	20
Figure 2.5: A general design placing electron-withdrawing groups on the ends of the structure of NOBE (a) and 2-(2-bromoacrylamido) ethyl 2-bromoacrylate, BrOBE (19, b).....	21
Figure 2.6: Hydrogen bonding interactions between the crosslinker BrOBE (19) and the template BOC-Tyr (7).....	23
Figure 2.7: (2 <i>R</i> ,3 <i>S</i>)-3-methacrylamidobutan-2-yl methacrylate (20).....	24
Figure 2.8: Predicted binding behavior of NOBE (1) with itself and BOC-Tyr (a). Predicted binding behavior of a trifunctional crosslinker (17) with itself and BOC-Tyr (b).....	44
Figure 3.1: (+)- <i>S</i> -2-(6-methoxynaphthalen-2-yl) propanoic acid (a) and (-)- <i>R</i> -2-(6-methoxynaphthalen-2-yl) propanoic acid (b).....	55
Figure 3.2: Structures of alkyl substituted melamines: triethylmelamine (48), triisopropylmelamine (49), tributylmelamine (50), atrazine (R= iPr) (51), simazine (R= Et) (51), cyanazine (R= C(CH ₃) ₂ CN) (51), terbutylazine (R= tBu) (51), propazine (52), and ametryn (R ₁ = Et R ₂ = iPr) (53), prometryn (R ₁ = iPr R ₂ = iPr) (53), terbutryn (R ₁ = Et R ₂ = tBu) (53).....	57
Figure 3.3: (<i>S</i>)-(-)- <i>N</i> -methacryloyl-1-naphthylethylamine (54),	

N-(3,5-Dinitrobenzoyl)- α -methylbenzylamine (55), and ethylene dimethacrylate (3).....	58
Figure 3.4: (<i>S</i>)-2-(2-methyl-acryloylamino)-3-phenyl propionic acid (56), <i>S</i> -bis[1-phenylethyl]amine (57), and <i>R</i> -bis[1-phenylethyl]amine (58).....	59
Figure 3.5: L-NALA imprinted with racemic BOC-Tyr (7) Mobile Phase Polarity Studies.....	66
Figure 3.6: Chromatogram of racemic (7) imprinted polymer using L-NALA*.....	67
Figure 3.7: Scalemic analytes on L-NALA racemic imprinted polymer*.....	68
Figure 3.8: Scalemic Imprinted Chromatograms*.....	71
Figure 3.9: Temperature Experiments on 75% L and 25% D-BOC-Tyr Imprinted Columns.....	72
Figure 4.1: <i>S</i> (66) and <i>R</i> (67) α -methoxy- α -trifluoromethylphenylacetic acid (MTPA) (Mosher's acid).....	78
Figure 4.2: The catalyst homobenzotetramisole (HBTM) is used for CEC analysis. The molecule with the <i>R</i> group (alkyl group) forward reacts faster with the <i>S</i> catalyst compared to the <i>R</i> catalyst. The molecule with the <i>R</i> group (alkyl group) pointing backwards reacts faster with the <i>R</i> catalyst than the <i>S</i> catalyst. The difference in reaction rates of each enantiomer with the enantiomerically pure catalyst enables stereochemical determination.....	79
Figure 4.3: Structures of print molecules used for the DuoMIP syntheses: <i>S</i> -BOC-Tyr (7a), <i>R</i> -BOC-Tyr (7b), <i>S</i> -BOC-Phe (72a), <i>R</i> -BOC-Phe (72b), <i>S</i> -BOC-Phe-OMe (73a), <i>R</i> -BOC-Phe-OMe (73b), <i>S</i> -4-benzyl-2-oxazolidinone (74a) and <i>R</i> -4-benzyl-2-oxazolidinone (74b).....	82
Figure 4.4: DuoMIP system. <i>S</i> -BOC-Tyr fits into the <i>S</i> -BOC-Tyr imprinted site (a), <i>R</i> -BOC-Tyr fits into the <i>R</i> -BOC-Tyr imprinted site (b), and <i>S</i> -BOC-Tyr does not fit into the <i>R</i> -BOC-Tyr imprinted site (c).....	83
Figure 4.5: Absolute configuration analysis of (<i>S</i>)- <i>N</i> -acetyl-tyrosine absolute using the DuoMIP system imprinted with <i>S</i> (a) and <i>R</i> (b)-BOC-Tyr.....	94
Figure 4.6: <i>S</i> -Acetyl-Tyr analyte (85) on NOBE imprinted with 20% <i>S</i> -BOC-Tyr (<i>S</i> -MIP) ^a and <i>S</i> -Acetyl-Tyr analyte on NOBE imprinted with 20% <i>R</i> -BOC-Tyr (<i>R</i> -MIP) ^b	95
Figure 4.7: (<i>S</i>)-phenyllactic acid in the binding cavity of the NOBE OMNiMIP imprinted with 20% <i>S</i> -BOC-Tyr (a), (<i>S</i>)-phenyllactic acid in the binding cavity of the NOBE imprinted with 20% <i>R</i> -BOC-Tyr (b), (<i>S</i>)-phenyl glycinol in the binding cavity of the NOBE OMNiMIP imprinted with 20% <i>S</i> -BOC-Tyr (c), and (<i>S</i>)-phenyl glycinol in the binding cavity of the NOBE OMNiMIP imprinted with 20% <i>R</i> -BOC-Tyr (d).....	96

Figure 4.8: The “strong” and “moderate” hydrogen bonding groups and the “small” and “big” groups are illustrated for BOC-Tyr (7) and the “strong/moderate” group and the “small” and “big” groups are shown for 4-benzyl-2-oxazolidinone (74) print molecules.....	97
Figure 4.9: The “strong” and “moderate” hydrogen bonding groups and the “small” and “big” groups are illustrated for BOC-Phe (72) and BOC-Phe-OMe (73).....	98
Figure 4.10: The structure of L-NALA (9) differs from NOBE (1) by one methyl group in the alpha amido position.....	101
Figure 5.1: Diagram of Atherosclerosis development.....	109
Figure 5.2: Structures of vitamin E molecules: α -tocopherol (93), β -tocopherol (94), γ -tocopherol (95), δ -tocopherol (96), α -tocotrienol (97), β - tocotrienols (98), γ - tocotrienols (99), and δ - tocotrienols (100).....	110
Figure 5.3: Structures of hydrophilic antioxidant molecules: vitamin C (101), carnosine (102), and folic acid (103).....	111
Figure 5.4 Water-soluble vitamin E derivatives.....	112
Figure 5.5 VECAR (106) design.....	113
Figure 5.6 The structure of DPPH (120).....	125
Figure 5.7 DPPH Assay used to determine the inhibition values.....	126

LIST OF SCHEMES

Scheme 2.1: Synthesis of NOBE (1).....	26
Scheme 2.2: Synthesis of 2-acrylamidoethyl acrylate (13).....	27
Scheme 2.3: Synthesis of 2-acrylamidoethyl methacrylate (14).....	28
Scheme 2.4: Synthesis of 1,3-dimethacrylamidopropan-2-yl methacrylate (17).....	28
Scheme 2.5: Synthesis of (<i>S</i>)-2,3-dimethacrylamidopropyl methacrylate (18).....	29
Scheme 2.6: Synthesis of BrOBE (19).....	32
Scheme 2.7: Synthesis of NAG (12).....	33
Scheme 2.8: Synthesis of ((<i>2R,3S</i>)-3-methacrylamidobutan-2-yl methacrylate (20).....	35
Scheme 2.9: Synthesis of the crosslinker 2-(2-(trifluoromethyl)acrylamido)ethyl 2-(trifluoromethyl)acrylate (43).....	52
Scheme 2.10: Synthesis of the crosslinker N-(3-methyl-2-oxobut-3-en-1-yl) methacrylamide (47).....	53
Scheme 3.1: Synthesis of NOS (61).....	60
Scheme 3.2: Synthesis of L-NALA (9).....	62
Scheme 4.1: Synthesis of the <i>S</i> -MIP of DuoMIP System.....	82
Scheme 4.2: Synthesis of D-BOC-Phe-OMe.....	84
Scheme 5.1 VECAR (106) Synthesis.....	116

LIST OF ABBREVIATIONS

α	Separation factor, two analytes from one sample
α'	Separation factor, two analytes from different samples
AC	Absolute configuration
AcOH	Acetic Acid
aq	Aqueous
AIBN	2,2'-Azobis(2-methylpropionitrile)
BOC	<i>Tert</i> -Butyl carbamate
BOC-Phe-OMe	Methyl-2-((<i>tert</i> -butoxycarbonyl)amino)-3-phenylpropanoate
BnOX	4-Benzyl-2-oxazolidinone
br	Broad
BrOBE	2-(2-Bromoacrylamido)ethyl 2-bromoacrylate
CEC	Competing enantioselective conversions
CBZ	Carboxybenzyl
CHCl₃	Chloroform
CDCl₃	Deuterated Chloroform
d	Doublet
dd	Doublet of doublets
DCC	1,3-Dicyclohexylcarbodiimide
DCM	Dichloromethane
DCU	1,3-Dicyclohexylurea
DMAP	4-Dimethylaminopyridine
DMF	Dimethylformamide
DNB	<i>N</i> -(3,5-Dinitrobenzoyl)- α -methylbenzylamine
DuoMIPs	Utilization of two MIP columns for AC determination
EGDMA	Ethylene glycol dimethylacrylate
Et₂O	Diethyl ether
Et₃N	Triethylamine
EtOAc	Ethyl acetate
EWG	Electron withdrawing group
γ	Gamma
HOBt	1-Hydroxybenzotriazole
HBTM	Homobenzotetramisole
HPLC	High Performance Liquid Chromatography
hrs	Hours
<i>i</i>-BuCO₂Cl	<i>Isobutyl</i> -chloroformate
IR	Infrared
k'	Capacity factor
LAH	Lithium aluminum hydride
LDLs	Low density lipoproteins
L-NALA	(<i>S</i>)-2-methacrylamidopropyl methacrylate
m	Multiplet
MAA	Methacrylic Acid
MAPP	(<i>S</i>)-2-(2-Methyl-acryloylamino)-3-phenyl propionic acid

MeCN	Acetonitrile
MeOH	Methanol
MgSO₄	Magnesium sulfate
min	Minutes
MIPs	Molecularly imprinted polymers
MTPA	α -Methoxy- α -trifluoromethylphenylacetic acid
NAG	2-Methyl-N-(3-methyl-2-oxobut-3-enyl)acrylamide
NMM	N-methyl morpholine
NMR	Nuclear magnetic resonance
NOBE	2-(Methacryloylamino)ethyl-2-methylacrylate
NOS	<i>N,O</i> -Bis-methacryloyl L-serine
OMNiMIPs	One monomer molecularly imprinted polymers
ox-LDLs	Oxidized LDLs
PEA	Bis[1-phenylethyl]amine
q	Quartet
rt	Room temperature
sat.	Saturated
s	Singlet
THF	Tetrahydrofuran
t	Triplet
TBM	Tributylmelamine
TEM	Triethylmelamine
TPM	Triisopropylmelamine
<i>t</i>R	Retention time
TRIM	Trimethylolpropane trimethacrylate
<i>t</i>_v	Void volume
Tyr	Tyrosine
UV	Ultraviolet
VCD	Vibrational circular dichroism

ABSTRACT

The improvement and utility of crosslinkers are important topics of molecular imprinting. Crosslinker significance is evident when molecularly imprinted polymer (MIP) composition related to performance as separation media is examined. Crosslinkers account for the bulk of MIP formulations made through traditional imprinting (80-90%) and is even greater when the One Monomer Molecularly Imprinted Polymer (OMNiMIP) approach is utilized (100%). It is not surprising that alteration of the bulk component will result in different separation performances. Crosslinkers studied in this work were designed, synthesized, and evaluated toward improvement in OMNiMIP selectivity. In particular, functionality and number of polymerizable groups, addition of electron withdrawing groups or stereocenters, and maximization of amide content of OMNiMIP crosslinkers were explored using L-BOC-Tyrosine as a standard template. The separation factors (α') obtained from chromatographic studies of these OMNiMIPs were compared to results from 2-(methacryloylamino)ethyl-2-methylacrylate (NOBE), the most successful OMNiMIP crosslinking monomer thus far. Although several of these new OMNiMIPs displayed enantiomeric selectivity toward BOC-Tyr, an increased α' was not observed.

Racemic and Scalemic imprinting as well as absolute configuration (AC) determination were also studied throughout this work to improve MIP utility in academia and industry. Chiral OMNiMIP crosslinkers (*S*)-2-methacrylamidopropyl methacrylate (L-NALA) and *N,O*-bis-methacryloyl L-serine (NOS) were imprinted with racemic BOC-Tyr and both exhibited partial enantiomeric separation by chromatography. L-NALA was further explored through imprinting scalemic templates, and studies also showed enantiomeric separation. Additionally, L-NALA and NOBE were studied in AC determination. Here, a mnemonic was developed to illustrate

template recognition. Limitations on binding factors were also set to determine data reliability in regards to determination of absolute configuration.

A chimeric antioxidant composed of vitamin E and carnosine (VECAR) was designed and synthesized to improve drug delivery. VECAR was fabricated based on the lipophilicity and hydrophilicity of its individual components and is expected to have increased permeability in hydrophilic media while maintaining recognition by key proteins in biological pathways. This new compound displayed similar antioxidant activity as vitamin E *in vitro* and is anticipated to reach more versatile regions of cells, leading to the elimination or reduction of diseases caused by oxidative damage.

CHAPTER 1: MOLECULAR IMPRINTING INTRODUCTION

1.1 Introduction to Molecular Imprinting

Molecular imprinting is a field that started in the 1930's and is increasingly gaining more popularity in the literature.¹ This field is becoming distinctly more important as molecularly imprinted polymers, tailored to encompass selective recognition cavities based on size, shape, and functionality, are being developed and utilized in new and exciting ways.² Ramström and Mosbach described various methods where MIPs have been used in an attempt to increase reaction rates by imprinting a template that was either a substrate, transition state, or product analogue to promote catalysis.³ Haupt's review shows the involvement of MIPs in immunoassays and sensors.⁴ Also, a large number of papers have been published that use the recognition properties of these unique "smart" polymers as chromatographic stationary phases for enantiomeric separations.^{5,6}

MIPs are not just popular for their vast application potential, they are also important because of the unique characteristics that separate them from biological molecules and other solid phase materials. Unlike other systems, these smart polymers can withstand extremely high temperatures and large pH ranges.^{7,8,9} The reusability, long storage times, inexpensive fabrication, and straightforward and simple syntheses are also characteristics of MIPs that account for their attraction.^{1,10,11,12}

There are two bonding techniques used to synthesize MIPs: covalent and non-covalent.² The covalent bonding approach involves a chemical reaction to bind the monomer(s) and template, and another bond breaking reaction to release the template. Although this approach does generate selective MIPs, it still requires a chemical reaction to selectively bind to it again.

For example, Wulff and co-workers used phenyl- α -D-mannopyranoside as the template and covalently bound 4-vinylphenylboronic acid by an esterification reaction to form the imprinted cavity.¹³

A second bonding approach for the formation of MIPs is non-covalent imprinting. Here, one advantage is that there is no need to perform a chemical reaction to add or remove the imprinted template from the binding site; instead non-covalent imprinting utilizes principles of Van der Waals forces, hydrogen bonding, and dipole-dipole interactions. These interactions between the monomer(s) and template(s) in solution cause the binding site cavities to form with specific shape and functionality once polymerized, leading to the recognition abilities of the MIPs.¹⁴

Whether the covalent or non-covalent imprinting approach is used for imprinting, the selectivity of the MIP needs to be tested in order to determine if it is efficient at imprinting a selected target. One method to evaluate MIPs is through studying the polymer's ability to selectively bind a target. High Performance Liquid Chromatography (HPLC) is one analytical instrument that can be used to examine the selectivity of imprinted polymers. Analytes (as a mixture or an isolated molecule) can be injected onto an HPLC column packed with MIP as the stationary phase. The time that it takes the analyte(s) to travel through the column depends on the affinity of the analyte(s) to the imprinted column; stronger binding affinities lead to longer retention times. Once a retention time is observed, a normalization factor called the capacity factor (k'), which is independent of column size or amount of stationary phase can be calculated. The capacity factor is determined by subtracting the void volume (t_V), which accounts for the volume of solvent needed to pass through the column, from the retention time (t_R) of the analyte divided by the void volume (Eq. 1.1).

$$k' = \frac{(t_R - t_V)}{t_V} \quad \text{Eq. 1.1}$$

The capacity factor can be determined for the imprinted analyte as well as non-imprinted analyte(s). Once the k' factors for each analyte are calculated, the selectivity of the MIP can be analyzed by determining the separation factor (α or α'), which is calculated by dividing the k_1' of the most retained by the k_2' of the least retained analyte (α denotes the separation factor for analytes injected on the HPLC at the same time and α' refers to the separation factor calculated for analytes injected individually on the HPLC column, Eq. 1.2). Larger separation factors signify greater performance of analyte separation achieved by the MIP.²

$$\alpha \text{ or } \alpha' = \frac{k_1'}{k_2'} \quad \text{Eq. 1.2}$$

1.2 The Traditional Imprinting Approach

The crosslinker, template, functional monomer, initiator, temperature, and solvent (also referred to as porogen) are all important components used in traditional non-covalent imprinting. It is imperative to take into consideration the design of all components involved in synthesizing the imprinted polymer to ensure high selectivity. Modifying all components to increase non-covalent interactions and form a rigid imprinted cavity to obtain a large α' is the goal of researchers pursuing MIP design.

Comprising 80-90% of the imprinted polymer formed by traditional non-covalent imprinting, the chemical crosslinker is one of the most vital pieces of the MIP formulation.⁵ There are several common crosslinkers shown throughout the literature and a few examples are represented in Figure 1.1.^{5,15,16,17,18,19} Each crosslinker shown has been designed to form a highly crosslinked network polymer whose rigid morphology allows for cavities with strong binding

and re-binding capabilities of the desired analyte. The chemical crosslinker may also possess features that increase non-covalent interactions. For example, the crosslinker 2-(methacryloylamino) ethyl-2-methylacrylate (NOBE, **1**) is able to form hydrogen bonding interactions with templates that contain complementary donor/acceptor abilities.

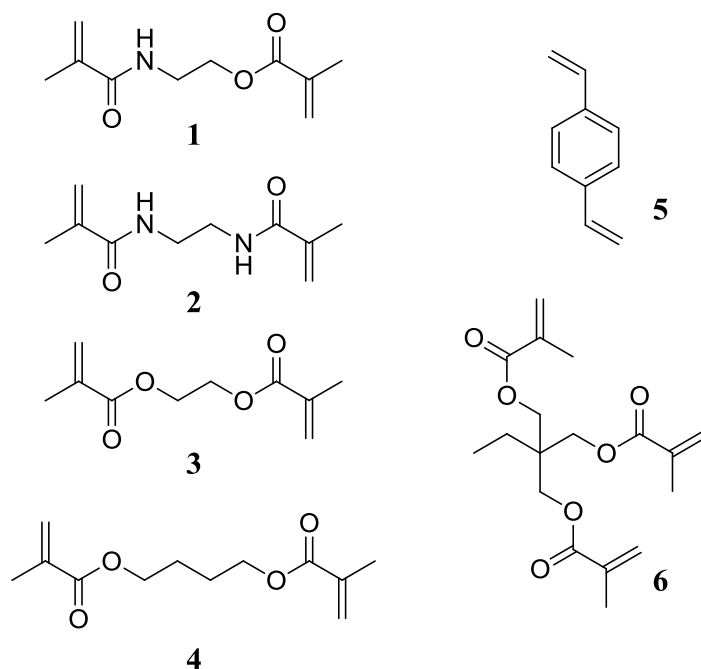


Figure 1.1: Examples of common crosslinkers.

The ability to successfully participate in non-covalent interactions; such as, hydrogen bonding and electrostatic interactions, is an important feature that the template should also encompass. Template size is another key feature that should be taken into account. The molecular weight of the template can range in size from amino acids and drugs, to larger molecules such as proteins; however, as size increases, imprinting becomes more challenging.^{20,21}

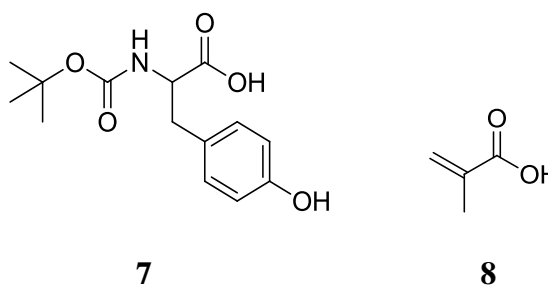


Figure 1.2: BOC-Tyrosine (**7**) and methacrylic acid (**8**).

BOC-Tyrosine (Figure 1.2, **7**) is one

template that has been successfully used when studying imprinted polymers due to its modest size and hydrogen bonding capabilities with the functional monomer. A template size that is too large could cause the template to become permanently encapsulated in the imprinted cavity. Another problem associated with large templates is that their size also inhibits their ability to diffuse into the imprinted cavity upon rebinding.²² The functional monomer chosen should complement the template's non-covalent interactions and provide a strong basis for binding. Methacrylic acid (Figure 1.2, **8**) is a common functional monomer in the literature because of its hydrogen bond donor/acceptor relationship with templates.^{23,24} Once a functional monomer is selected, it is crucial to optimize its concentration in the MIP formulation. The ratio of functional monomer to template, as well as to the crosslinker, needs to be optimized to generate the best selectivity.

The initiator and its concentration in the polymer formulation are also important in imprinting. Piletsky et al. demonstrated that lower concentrations of initiator, approximately 1-2% formed better imprinted polymers than imprinted polymers made with up to 5% initiator.²⁵ They also demonstrated that with less than 1% initiator, a rigid polymer, which is needed to form structurally sound cavities, was not formed. The porogen used for MIP syntheses should dissolve all contents of the formulation without interfering with the non-covalent interactions that occur in the pre-polymer complex. The temperature during polymerization is another factor to take into consideration for MIP syntheses. Results in the literature show that lower temperatures allow for imprinted polymers to form with better selectivity due to better pre-polymer complex formation of the functional monomer and template in solution.^{26,27,28,29}

Once a formulation is derived, molecularly imprinted polymers are traditionally synthesized by first dissolving a functional monomer in solution with a template to allow a pre-

polymer complex to form (Figure 1.3 and Figure 1.4.)³⁰ Next, a crosslinker is added to the

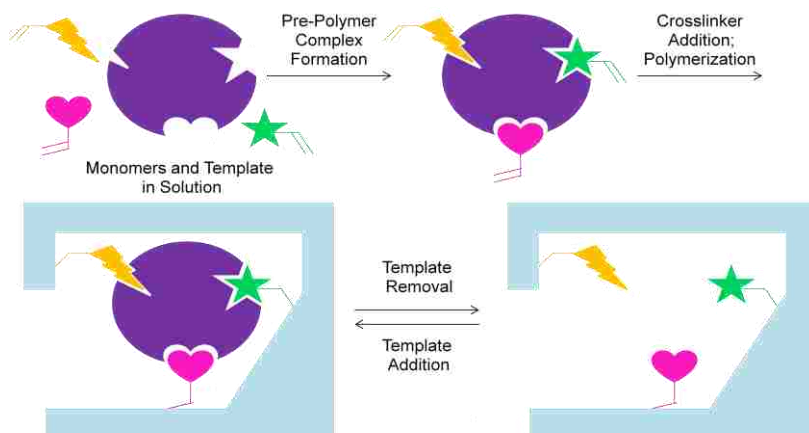


Figure 1.3: Diagram of traditional imprinting.

monomer and template solution. After the crosslinker addition, an initiator such as AIBN is added and the photo polymerization is carried out in a cooled reactor. Once the MIP is made, the template is removed by refluxing solvent through the polymer over several hours using a Soxhlet

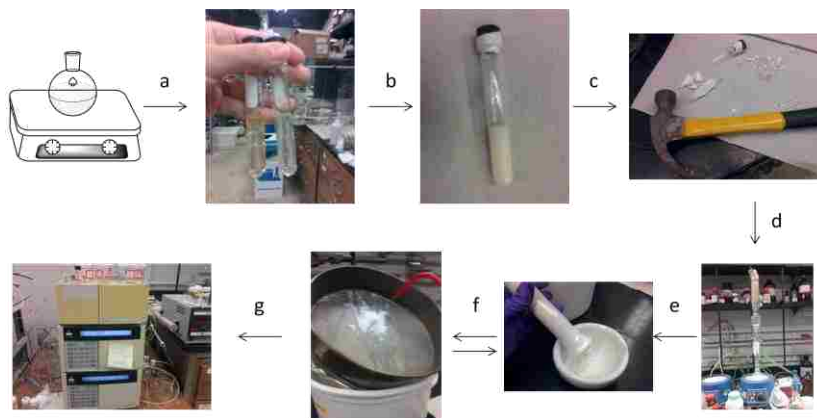


Figure 1.4: Imprinting illustration in the laboratory*.

*Synthesized crosslinker combined with template and initiator dissolved in porogen (a.) Polymerize to solid MIP (b.) Remove MIP (c.) Put MIP in Soxhlet to remove template (d.) After template removal, grind MIP to the desired particle size (e.) Wash and grind until enough material is acquired to pack the HPLC column (f.) Perform HPLC analysis (g.) Reprinted with permission from *Organic Letters* **2014** 16 (5), 1402-1405. Copyright 2014 American Chemical Society.

extractor. The MIP can then be ground and sieved to obtain an optimized particle size for use in chromatographic evaluation to determine its template selectivity and separation ability.²

1.3 The OMNiMIP Imprinting Approach

A new and exciting discovery by the Spivak research group came from studies developing two non-covalent traditional imprinting systems to select for either L-BOC-Tyr or a single enantiomer of bi-naphthol. Here, 2-(methacryloylamino) ethyl-2-methylacrylate (NOBE, **1**) was the crosslinker and methacrylic acid was the functional monomer used in the imprinting process. Throughout the study, the ratio of functional monomer to crosslinker was examined. During these experiments, it was discovered that when NOBE was used 100% in solution without any functional monomer, there was a significantly better imprinting performance for both template systems. These surprising results led to the newly developed non-covalent imprinting approach called the One Monomer Molecularly Imprinted Polymer (OMNiMIP) method invented by the Spivak research group.^{2,31}

The OMNiMIP technique uses a single functional crosslinking monomer in solution with the template to form the imprinted polymer (Figure 1.5.) This new and exciting approach

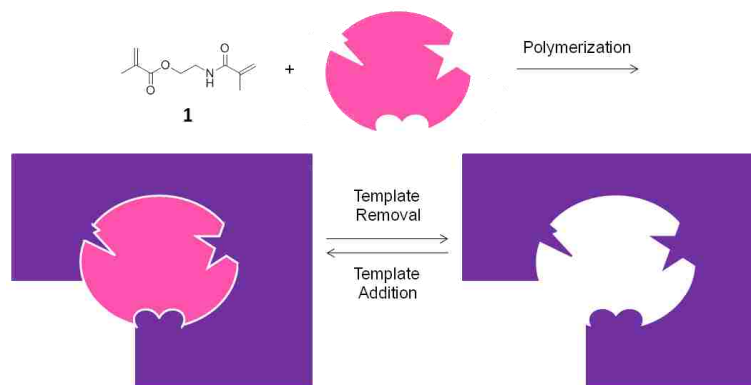


Figure 1.5: Illustration of OMNiMIP technique.

simplifies the conditions to form MIPs making these systems even more efficient. No longer is the type and amount of functional monomer, the ratios of functional monomer to crosslinker, or the ratio of template to functional monomer, considerations that need to be studied for making imprinted polymers.³¹

1.4 The Improvement of Crosslinkers for Molecular Imprinting

Improving the ability of a MIP to separate analytes is an ongoing task of imprinters. The optimization of the crosslinker design in traditional and OMNiMIP imprinting is often studied.^{32,33,34} In particular, the structure of NOBE has been altered, and selectivity based on these alterations has been explored. More specifically, Figure 1.6 depicts spacer modifications possible for NOBE. The spacer was modified by adding non-polar and polar groups between the amide and ester to explore the selectivity resulting from these changes to the crosslinking monomer for OMNiMIP imprinting.³⁵

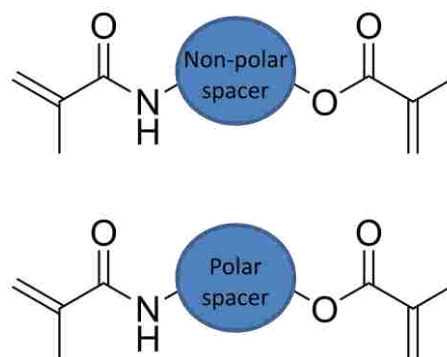


Figure 1.6: Non-polar and polar spacer modification designs.

Non-polar groups such as methyl, isopropyl, and isobutyl have been added to the amido alpha position (Figure 1.6); however, these additions did not improve imprinting. In fact, the larger groups created steric interactions that disrupted the ability of the template to hydrogen bond to the crosslinking monomer. Also, the polymers were “soft”, indicating a low degree of polymerization. A trend showed that with fewer non-covalent interactions between the monomer and template, the imprinted polymers displayed less selectivity when analyzed as a chromatographic stationary phase to separate enantiomers.³³

In a subsequent study, polar groups containing acid, alcohol, amine, and amide functionality were attached to the alpha amido position of NOBE. In this study, only the compound containing the acid addition, *N,O*-bis-methacryloyl L-serine (NOS), was soluble in the polymerization progen and polymerized into an OMNiMIP. While NOS was capable of separating enantiomers of BOC-Tyr, it did not perform better than

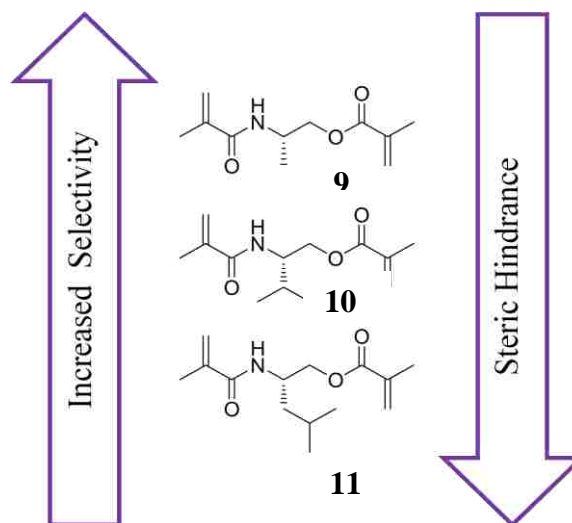


Figure 1.7: Non-polar spacer modifications to NOBE.

NOBE.³⁵ The continued alteration of the chemical structure of NOBE in an attempt to make a better crosslinker for imprinting is a primary focus of this work.

1.5 References

- Alexander, C.; Andersson, H. S.; Andersson, L. I.; Ansell, R. J.; Kirsch, N.; Nicholls, I. A.; O'Mahony, J.; Whitcombe, M. J., Molecular imprinting science and technology: a survey of the literature for the years up to and including 2003. *Journal of Molecular Recognition* **2006**, *19* (2), 106-180.
- Molecularly Imprinted Materials* Marcel Dekker: New York, 2005.
- Ramstrom, O.; Mosbach, K., Synthesis and catalysis by molecularly imprinted materials. *Curr. Opin. Chem. Biol.* **1999**, *3*, 759-764.
- Haupt, K., Imprinted polymers-Tailor-made mimics of antibodies and receptors. *Chemical Communications* **2003**, (2), 171-178.
- Sibrian-Vazquez, M.; Spivak, D. A., Enhanced Enantioselectivity of Molecularly Imprinted Polymers Formulated with Novel Cross-Linking Monomers. *Macromolecules* **2003**, *36* (14), 5105-5113.

6. Haginaka, J., Monodispersed, molecularly imprinted polymers as affinity-based chromatography media. *Journal of Chromatography B* **2008**, *866* (1–2), 3-13.
7. Yoshizako, K.; Hosoya, K.; Iwakoshi, Y.; Kimata, K.; Tanaka, N., Porogen Imprinting Effects. *Anal. Chem.* **1998**, *70*, 386-389.
8. Nam, G. H.; Kim, D., Separation characteristics of molecular imprinted poly(methacrylic acid) for retinoid derivatives. *J. Appl. Polym. Sci.* **2003**, *90*, 1081-1087.
9. Svenson, J.; Nicholls, I. A., On the thermal and chemical stability of molecularly imprinted polymers. *Anal. Chim. Acta* **2001**, *435*, 19-24.
10. Ju, J. Y.; Shin, C. S.; Whitcombe, M. J.; Vulfson, E. N., Imprinted polymers as tools for the recovery of secondary metabolites produced by fermentation. *Biotechnol. Bioeng.* **1999**, *64*, 232-239.
11. Kriz, D.; Mosbach, K., Competitive amperometric morphine sensor based on an agarose-immobilized molecularly imprinted polymer. *Anal. Chim. Acta* **1995**, *300*, 71-5.
12. Mullett, W. M.; Lai, E. P. C., Determination of Theophylline in Serum by Molecularly Imprinted Solid-Phase Extraction with Pulsed Elution. *Anal. Chem.* **1998**, *70*, 3636-3641.
13. Wulff, G.; Vesper, W.; Grobe-Einsler, R.; Sarhan, A., Enzyme-analogue built polymers, 4. On the synthesis of polymers containing chiral cavities and their use for the resolution of racemates. *Die Makromolekulare Chemie* **1977**, *178* (10), 2799-2816.
14. Mayes, A. G.; Whitcombe, M. J., Synthetic strategies for the generation of molecularly imprinted organic polymers. *Advanced Drug Delivery Reviews* **2005**, *57* (12), 1742-1778.
15. Wulff, G.; Sarhan, A., Use of polymers with enzyme-analogous structures for the resolution of racemates. *Angew. Chem., Int. Ed. Engl.* **1972**, *11*, 341.
16. Wulff, G.; Vietmeier, J.; Poll, H. G., Enzyme-analog built polymers. 22. Influence of the nature of the crosslinking agent on the performance of imprinted polymers in racemic resolution. *Makromol. Chem.* **1987**, *188*, 731-40.
17. Kempe, M.; Mosbach, K., Receptor binding mimetics: A novel molecularly imprinted polymer. *Tetrahedron Letters* **1995**, *36* (20), 3563-3566.
18. Schweitz, L.; Andersson, L. I.; Nilsson, S., Capillary Electrochromatography with Predetermined Selectivity Obtained through Molecular Imprinting. *Analytical Chemistry* **1997**, *69* (6), 1179-1183.
19. Shea, K. J.; Spivak, D. A.; Sellergren, B., Polymer complements to nucleotide bases. Selective binding of adenine derivatives to imprinted polymers. *Journal of the American Chemical Society* **1993**, *115* (8), 3368-3369.

20. Sellergren, B., Imprinted polymers with memory for small molecules, proteins, or crystals. *Angew. Chem., Int. Ed.* **2000**, *39*, 1031-1037.
21. Takeuchi, T.; Hishiya, T., Molecular imprinting of proteins emerging as a tool for protein recognition. *Organic & Biomolecular Chemistry* **2008**, *6* (14), 2459-2467.
22. Yan, M.; Ramstrom, O., *Molecularly imprinted materials: science and technology*. Marcel Dekker: New York, 2005; p 1-734.
23. Shi, X.; Wu, A.; Qu, G.; Li, R.; Zhang, D., Development and characterisation of molecularly imprinted polymers based on methacrylic acid for selective recognition of drugs. *Biomaterials* **2007**, *28* (25), 3741-3749.
24. Yongfeng, K.; Wuping, D.; Yan, L.; Junxia, K.; Jing, X., Molecularly imprinted polymers of allyl- β -cyclodextrin and methacrylic acid for the solid-phase extraction of phthalate. *Carbohydrate Polymers* **2012**, *88* (2), 459-464.
25. Mijangos, I.; Navarro-Villoslada, F.; Guerreiro, A.; Piletska, E.; Chianella, I.; Karim, K.; Turner, A.; Piletsky, S., Influence of initiator and different polymerisation conditions on performance of molecularly imprinted polymers. *Biosensors and Bioelectronics* **2006**, *22* (3), 381-387.
26. O'Shannessy, D. J.; Ekberg, B.; Mosbach, K., Molecular imprinting of amino acid derivatives at low temperature (0°C) using photolytic homolysis of azobisnitriles. *Analytical Biochemistry* **1989**, *177* (1), 144-149.
27. Spivak, D.; Gilmore, M. A.; Shea, K. J., Evaluation of Binding and Origins of Specificity of 9-Ethyladenine Imprinted Polymers. *J. Am. Chem. Soc.* **1997**, *119*, 4388-4393.
28. Sellergren, B.; Shea, K. J., Influence of polymer morphology on the ability of imprinted network polymers to resolve enantiomers. *Journal of Chromatography A* **1993**, *635* (1), 31-49.
29. Reinholdsson, P.; Hargitai, T.; Isaksson, R.; Tornell, B., Preparation and properties of porous particles from trimethylolpropane trimethacrylate. *Angew. Makromol. Chem.* **1991**, *192*, 113-32.
30. Meador, D. S.; Spivak, D. A., Absolute Configuration Determination Using Enantiomeric Pairs of Molecularly Imprinted Polymers. *Organic Letters* **2014**, *16* (5), 1402-1405.
31. Sibrian-Vazquez, M.; Spivak, D. A., Molecular Imprinting Made Easy. *Journal of the American Chemical Society* **2004**, *126* (25), 7827-7833.
32. Sibrian-Vazquez, M.; Spivak, D. A., Characterization of molecularly imprinted polymers employing crosslinkers with nonsymmetric polymerizable groups. *Journal of Polymer Science Part A: Polymer Chemistry* **2004**, *42* (15), 3668-3675.

33. LeJeune, J.; Spivak, D., Chiral effects of alkyl-substituted derivatives of N,O-bismethacryloyl ethanolamine on the performance of one monomer molecularly imprinted polymers (OMNiMIPs). *Analytical and Bioanalytical Chemistry* **2007**, *389* (2), 433-440.
34. Whitcombe, M. J.; Chianella, I.; Larcombe, L.; Piletsky, S. A.; Noble, J.; Porter, R.; Horgan, A., The rational development of molecularly imprinted polymer-based sensors for protein detection. *Chemical Society Reviews* **2011**, *40* (3), 1547-1571.
35. LeJeune, J. Design and Development of Chiral and Achiral Molecularly Imprinted Stationary Phases. Louisiana State University, Baton Rouge, 2010.

CHAPTER 2: NEW CROSSLINKERS FOR MOLECULAR IMPRINTING

2.1 Introduction, Design and Synthesis of New Crosslinkers

A. Crosslinkers with Alteration of Polymerizable Groups

The polymerization rate of a monomer is largely dependent on the type of polymerizable group it has; for example vinyl groups polymerize slower than methacrylates. There are two main contributing factors that determine the radical polymerization rates of monomers: the ability of a monomer to form a radical and the stability of the radical formed.¹ An article by Chan et al. examines these factors and discusses the radical polymerization rates of several types of polymerizable groups, such as methacrylates, acrylates, methacrylamides, and acrylamides.² The experiments carried out demonstrate that methacrylates polymerize faster than acrylates. This phenomenon could be attributed to the stable free radical that is formed from the tertiary methacrylate group as opposed to a secondary radical, which is less stable. The article also addressed the fact that methacrylates are more reactive to radical polymerizations than methacrylamide groups. This observation is explained by the amide group's greater participation in resonance versus the ester group, which makes the amide substituent not free to stabilize the radical as much, thus lowering the rate of radical polymerization.

A publication by Sibrian-Vasquez et al. explored nonsymmetrical polymerizable groups, which included examining crosslinkers with a methacrylate and methacrylamide combination (e.g. NOBE, **1**).^{3,4,5,6} Here, the authors showed that the nonsymmetrical crosslinker NOBE performed well in molecularly imprinted polymer systems. In another paper, 2-Methyl-

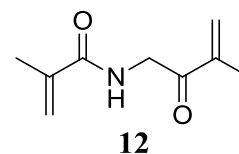


Figure 2.1: NAG.

N-(3-methyl-2-oxobut-3-enyl)acrylamide (Figure 2.1, NAG, **12**), a crosslinker composed of a methacrylamide and vinyl ketone group was synthesized and utilized

in traditional imprinting.⁵ This monomer showed better performance than NOBE when used in traditional imprinting, and the authors suggested it increased selectivity in MIPs due to the length reduction of NAG versus NOBE, which allowed it to form a more close-fitting binding site, combined with its rigidity.

The alteration of polymerizable groups that was previously studied for traditional imprinting can also be applied to the One Monomer Molecularly Imprinted Polymer (OMNiMIP) technique, which was described in Chapter 1. Tailoring new crosslinkers for improved selectivity of OMNiMIPs is important as this approach can uptake a larger amount of template in the pre-polymer complex (and consequently the binding site) leading to more binding sites and better selectivity when compared to traditional imprinting. Designing and synthesizing monomers for the OMNiMIP technique that could enhance selectivity further by altering the polymerizable groups was one of the goals of this project. Derivatives of NOBE that examine the roles of methacrylate, acrylate, or acrylamide groups in molecular imprinting were investigated. These monomers were polymerized by photo-initiated radical polymerization and were subsequently tested as OMNiMIP chromatographic stationary phases for selective binding of a single enantiomer. Although NAG has shown to form more selective MIPs than NOBE during traditional imprinting, it has not been utilized as the crosslinker for OMNiMIP imprinting. NOBE has been previously used and has been shown to form highly selective OMNiMIPs; thus, NOBE was enlisted as the control.⁴ As mentioned in Chapter 1, the design of NOBE incorporates a methacrylate and methacrylamide group. This combination of the methacrylate and methacrylamide groups in NOBE is important to achieve solubility of the monomer in the pre-polymer porogen (i.e. solvent) and to provide hydrogen bonding interactions between the monomer and print molecule. During the photo-initiated radical polymerization using NOBE, it

is anticipated that the methacrylate component will polymerize first, followed by the methacrylamide component. It is expected that both monomeric units polymerize quickly because both form stable tertiary radicals (radical stability is as follows tertiary > secondary > primary > methyl); however, it is probable that the methacrylate radical forms before the methacrylamide radical because the amide portion is more likely to participate in resonance and stabilize the radical less.

Improvements on the original OMNiMIP polymerizable groups began with the synthesis of the monomer 2-acrylamidoethyl acrylate, **13** (Figure 2.2). The design features of **13** include

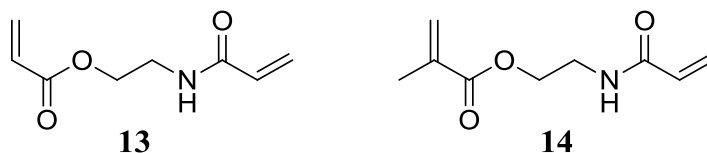


Figure 2.2: 2-acrylamidoethyl acrylate (**13**) and 2-acrylamidoethyl methacrylate, (**14**).

an acrylate and an acrylamide group differing from NOBE (**1**) only at the polymerizable ends to isolate the effects of changing the type of polymerizable groups. Here, the acrylate component is anticipated to polymerize before than the acrylamide group. This is attributed to the resonance participation of the acrylamide group slowing down the polymerization process, whereas the acrylate has a smaller competing resonance effect. Overall, it is expected that 2-acrylamidoethyl acrylate will polymerize moderately slower than NOBE because both sides of this molecule will form secondary radicals, opposed to the more stable tertiary radicals that NOBE generates.

2-acrylamidoethyl methacrylate, **14** was another compound designed and synthesized to study the effects of polymerization rates of OMNiMIPs (Figure 2.2.) The design of **14** also kept the NOBE (**1**) structure intact, keeping the same number of ester and amide groups for solubility and hydrogen bonding, and differed only by the polymerizable groups so that selectivity based

on changes of these groups could be studied. It is anticipated that 2-acrylamidoethyl methacrylate will have a similar polymerization pattern to 2-acrylamidoethyl acrylate with regard to which side of the compound polymerizes first. Here, the methacrylate will polymerize much faster than the acrylamide group. This is attributed to both the greater radical stability of the methacrylate portion as well as the competing effect of the amide group participating in resonance. The outcome of this phenomena means that relatively long stretches of linear polymers/oligomers will form initially as the methacrylate polymerizes, leaving the acrylamido group pendant. The slower polymerizing acrylamido group will start to form the crosslinks afterward, including both covalent and intermolecular hydrogen bonding of the amide groups.

The small alterations in the design features mentioned in regards to the crosslinkers 2-acrylamidoethyl acrylate (**13**) and 2-acrylamidoethyl methacrylate (**14**) are worthy to explore because the order in which polymerization of groups takes place could affect their ability to form more selective polymers as described previously when selectivity was improved in traditional imprinting using NAG.⁵ In the case of NAG, longer chains of linear polymer were formed first and crosslinking by the methacrylamide groups occurred subsequently, ultimately resulting in a superior imprinted polymer. The crosslinker NAG is described in further detail in section D and its ability to form a better selective OMNiMIP based on the cooperative effects of its polymerizable groups and the hydrogen bonding donor/acceptor proximity is discussed. Similar to the vinyl ketone forming before the methacrylamide in NAG, it is expected that **14** may improve OMNiMIPs because the methacrylate groups will likely form first, generating a linear polymer, followed by the acrylamide groups forming the crosslinked network analogous to the polymerization of NAG. Since molecule **14** incorporates an acrylamide instead of a methacrylamide group, a smaller impact of steric interference from the lack of an alpha methyl

group may be observed to some extent and may also lead to better selectivity of the MIP formed. It is expected that **14** will form a better imprinted polymer than crosslinker **13** because the design of crosslinker **13** reduces the rate of formation of both polymerizable groups compared to the groups in the NOBE structure and therefore will not form to the same extent a linear polymer first followed by the crosslinked network. The design of both **13** and **14** to some degree decreases the sterics of the crosslinkers, which may impact their solubility and hydrogen bonding capabilities and furthermore lead to the formation of OMNiMIPs with improved selectivity. Both **13** and **14** are expected to have improved solubility in the pre-polymer complex, which could lower phase separation during polymerization and lead to the formation of more selective binding sites. Another improvement towards selectivity that can transpire from reducing steric hindrance in both **13** and **14** is the increased ability of the crosslinker to wrap closely around the template; therefore forming a stronger hydrogen bond network between binding site and template.

The synthesis of NOBE (**1**), 2-acrylamidoethyl acrylate (**13**), and 2-acrylamidoethyl methacrylate (**14**) were all carried out using typical DCC/DMAP coupling procedures. The percent yields of the NOBE synthesis ranged from approximately 80% - 98%, with most reactions yielding above 90%. Percent yields of **13** and **14** were 43% and 53%, respectively. Although these percent yields were not as high as NOBE, they were not further optimized as the focus of these monomers was their use as crosslinkers for molecular imprinting.

B. Three-armed Crosslinkers

The crosslinking and number of selective sites on an OMNiMIP monomer influences its ability to form an imprinted polymer with high shape selectivity. One article showed that MIPs

prepared with crosslinkers containing three crosslinking appendages, such as pentaerythritol triacrylate, **15** and trimethylolpropane trimethacrylate (TRIM, **16**) performed better than ethylene glycol dimethylacrylate (EGDMA, **3**), which contains only two polymerizable appendages (Figure 2.3.)⁷ Here, the authors showed that the trifunctional crosslinkers in the molecularly imprinted polymer formulation for traditional imprinting resulted in MIPs exhibiting larger template load capacities and better chromatographic resolution.

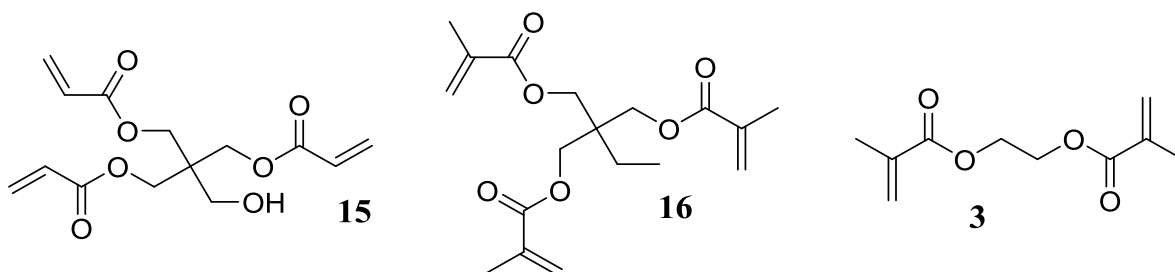


Figure 2.3: Structures of three and two armed crosslinkers.

The improvement in load capacity and resolution of the three armed crosslinkers was attributed to increased rigidity of the recognition site.⁸ An increase in the number of polymerizable groups may improve recognition of the template to the binding cavities by allowing a more rigid framework to form, which preserves the shape of the imprinted sites. While the change in the number of polymerizable groups on the crosslinker has been investigated for traditional imprinting, there has been no literature published to date using these crosslinking monomers for OMNiMIP imprinting. In this chapter, the synthesis of a new achiral 1, 3-dimethacrylamidopropan-2-yl methacrylate (**17**) and a chiral (*S*)-2,3-dimethacrylamidopropyl methacrylate (**18**) trifunctional crosslinker was completed and applied to OMNiMIP formation.

Crosslinker **17** contains three polymerizable groups, two being methacrylamide linkages and one methacrylate (Figure 2.4.) Not only is the increased number of polymerizable groups expected to form more rigid binding cavities than crosslinkers with two polymerizable groups,

the increased number of amide groups in comparison to NOBE is also expected to increase hydrogen bonding and lead to a more selective OMNiMIP. Three methacrylamide groups as opposed to two would provide an additional area for hydrogen bonding to occur. However, solubility of the crosslinker in the pre-polymerization porogen is expected to be poor because the molecule *N,N'*-(ethane-1,2-diyl)bis(2-methylacrylamide) (**2**), which contains two methacrylamide groups and zero methacrylate groups, is only soluble in polar porogens such as methanol, which would interfere with the hydrogen bonding interactions need to form the imprinted polymer.⁵

The design of the three-armed **18** also includes two methacrylamide groups and one methacrylate polymerizable group, and is also expected to increase rigidity due to the amount of polymerizable groups and magnify hydrogen bonding because of the extra methacrylamide group (compared to NOBE.) The difference between crosslinkers **17** and **18** is that molecule **18** is chiral (Figure 2.4) because it was synthesized from an amino acid derivative containing a stereocenter. The addition of a chiral center to this molecule may allow this crosslinker to complex to one enantiomer of the template stronger than the other enantiomer; therefore, each enantiomer should be imprinted individually and the selectivity of the resulting OMNiMIPs should be compared to determine which enantiomer lead to the polymer with better selectivity so that the better OMNiMIP can be compared to NOBE. Furthermore, the addition of a chiral center in **18** could also have an impact in imprinting racemic mixtures, a technique described in Chapter 3.

The syntheses of the two new trifunctional monomers, achiral 1,3-dimethacrylamidopropan-2-yl methacrylate (**17**) and chiral (*S*)-2,3-dimethacrylamidopropyl methacrylate (**18**), was completed. Crosslinker **17** was synthesized using DCC/DMAP to couple

MAA to the amino alcohol in 65% yield. Several approaches were attempted to synthesize molecule **18**. The first method comprised three steps, starting from malonic acid-mono ethyl ester. Amination of the malonic acid-mono ethyl ester followed by a LAH reduction, and finally a DCC/DMAP coupling reaction were completed. These steps afforded products that were difficult to separate on large scale; therefore, a new approach was deemed necessary. Starting from the salt (*S*)-2,3-bis((*tert*-butoxycarbonyl)amino)propanoic acid · dicyclohexylamine, **18** was successfully synthesized in three steps. After removal of the salt by extractions, a mixed anhydride was first formed by the addition of isobutyl chloroformate and NMM then reduction using sodium borohydride afforded the alcohol in 68% yield. Next, the BOC groups were removed using ethereal hydrogen chloride in quantitative yields. Lastly, DCC/DMAP was used to couple MAA to the three appendages to form molecule **18** with a 30% yield. The solubility of the three-armed crosslinkers and their ability to perform as OMNiMIP chromatographic stationary phases to imprint a single enantiomer was next analyzed and compared to the currently best performing OMNiMIP crosslinker, NOBE (*vide infra*.)

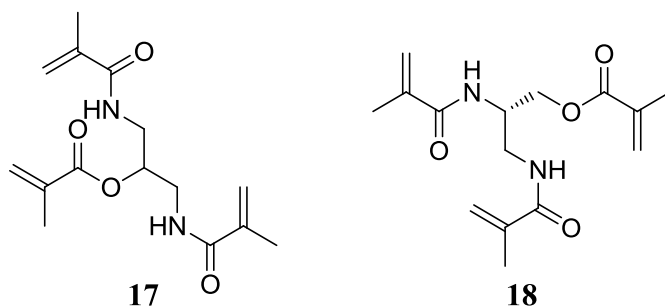


Figure 2.4: Three-armed crosslinkers for OMNiMIP imprinting.

C. Crosslinkers with Electron-withdrawing Groups

Another opportunity to improve the selectivity of non-covalently imprinted polymers is to strengthen the interactions of the template and monomer. One approach to strengthen these interactions is to increase the hydrogen bonding of template to the functional monomer.⁹ With this logic in mind, a new crosslinking monomer was designed to improve OMNiMIP imprinting by increasing the strength of the hydrogen bonding interactions between the monomer and template. Here, the addition of an electron withdrawing group (EWG) to the NOBE structure will make the amide functionality more acidic and therefore strengthen its participation in hydrogen bonding. The first crosslinker design incorporated CF₃ groups (illustrated in Figure 2.5) into the structure of NOBE, with its proposed synthesis starting from commercially available 2-(trifluoromethyl)acrylic acid. The synthesis of the trifluorinated crosslinker 2-(2-(trifluoromethyl)acrylamido)ethyl 2-(trifluoromethyl)acrylate has some literature precedent. In one article 2-(trifluoromethyl)acryloyl chloride was synthesized from 2-(trifluoromethyl)acrylic acid and was added to a primary alcohol to form an ester linkage.¹⁰ The success of this reaction led to the hypothesis that addition of 2-(trifluoromethyl)acryloyl chloride to ethanolamine (shown in the future work) could also be achieved; however, no significant amount of this

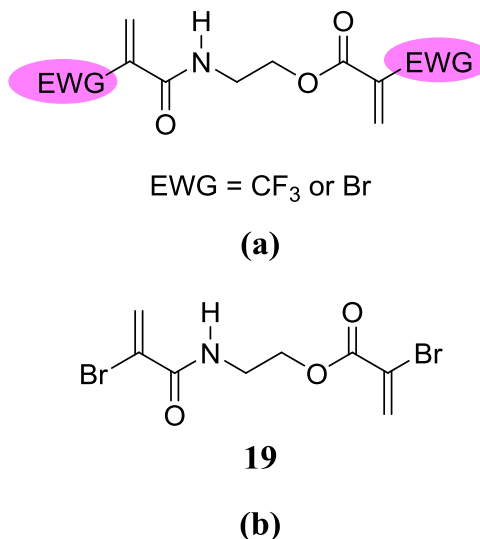


Figure 2.5: A general design placing electron-withdrawing groups on the ends of the structure of NOBE (a) and 2-(2-bromoacrylamido) ethyl 2-bromoacrylate, BrOBE (19, b).

material was synthesized. One explanation could be that the system was not completely free of water and hydrolysis occurred prior to formation of both the ester and amide.

Although the addition of CF_3 groups was an optimal design because of its size match in relation to the CH_3 groups that are found in NOBE, without significant amounts of material, this molecule was not tested as an OMNiMIP. While larger in atom size than carbon, bromine was chosen as the electron withdrawing group to be added to the structure of NOBE. Even though chlorine is smaller than bromine and would be a better design choice because it would create smaller steric interactions, the bromine starting material was more affordable at the time. The new crosslinker design puts Br on each end of the NOBE base structure, 2-(2-bromoacrylamido) ethyl 2-bromoacrylate (BrOBE, **19**.) This crosslinker design is predicted to promote stronger hydrogen bonding because the bromines will withdraw electron density, making the molecule more acidic. As electron density is shifted away from the amide, and the proton attached to the nitrogen of the amide becomes more acidic, the bond is weakened, and could allow for greater hydrogen bonding when in contact with template. The hydrogen bonding interactions of BrOBE with a BOC-Tyr template is shown in Figure 2.6. Here, it is expected that strong electron withdrawing appendages could strengthen hydrogen bonding and non-covalent imprinting.

BrOBE (**19**) was successfully synthesized in one step in quantitative yield. When only two equivalents of the bromo acrylic acid were used with both DCC/DMAP and DCC/HOBt, the yield was only ~10% or lower. When the amount of acid was increased to four equivalents, 100% of the theoretical yield of product was collected using DCC/DMAP. After synthesis, this monomer was imprinted with 5% L-BOC-Tyrosine. Polymerization was unsuccessful in the typical 13 x 100 mm tubes. In this case, crosslinked polymer formed only at the edge of the tube

and the inside was mostly “soft” polymer indicating that the material was not fully polymerized and furthermore not highly crosslinked.

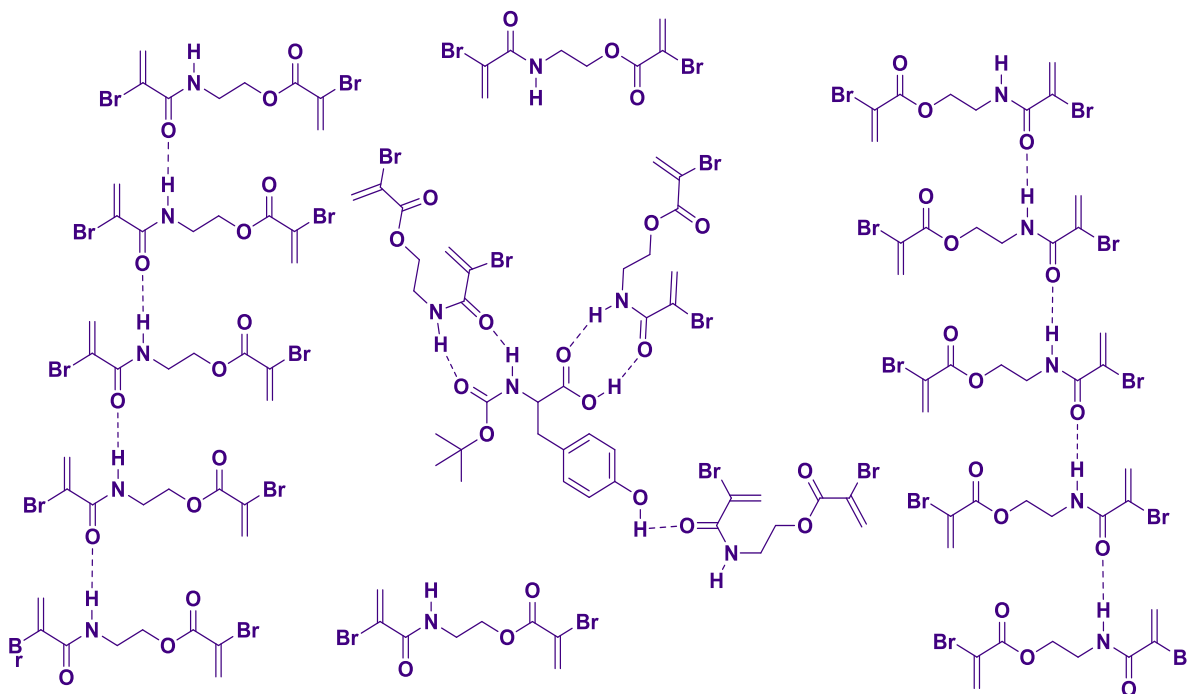


Figure 2.6: Hydrogen bonding interactions between the crosslinker BrOBE (19) and the template BOC-Tyr (7).

D. Crosslinkers with Hydrogen Bond Donor/Acceptor Proximity and Amide Content

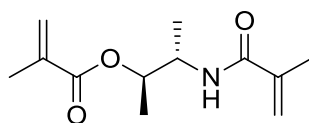
Another attempt to improve crosslinking monomers for OMNiMIP imprinting was to utilize a molecule that was previously demonstrated to be successful as a crosslinker with regard to traditional imprinting. The crosslinker 2-methyl-*N*-(3-methyl-2-oxobut-3-enyl)acrylamide (NAG, **12**), whose polymerizable groups were discussed previously, outperformed NOBE as a crosslinker in combination with the functional monomer methacrylic acid for separating enantiomers of both dansyl-phenylalanine and BOC-Tyrosine.⁵ The improvement in enantiomeric separation was attributed to the cooperative effects of the hydrogen bond donor and

acceptor being in closer proximity along with the increased amide content (in relation to the number of atoms in the molecule) of the crosslinker. Although this monomer did show excellent traditional imprinting results, it has never been tested as a crosslinking monomer for OMNiMIP imprinting. In this chapter NAG was synthesized and its ability to act as the sole monomer for OMNiMIP imprinting was evaluated by HPLC.

Starting from the Weinreb amide, NAG (**12**) was synthesized (Scheme 2.7.) After multiple attempts to synthesize molecule **12** on a gram scale, the highest yield achieved was 21% and this was obtained when the Grignard reagent was synthesized rather than purchased. Once synthesized, NAG was first polymerized using a photo-initiated radical polymerization protocol; however, the material afforded exhibited a “jelly” consistency indicating a low degree of double bond conversion. This material then was subjected to thermal polymerizations to cure the material, obtaining a solid material that could be ground and packed into HPLC columns.

E. Crosslinker with Stereochemical Rigidity

Piletsky and co-workers described the importance of rigidity in the formation of imprinted cavities through a series of experiments based on time lengths of polymerization.¹¹ In this article, the authors also explained that rigidity could influence the binding kinetics as well as the mobility of the print molecule into and out of the binding cavity; therefore, a balance of rigidity and mass transfer is essential. Thus, a hypothesis to improve the OMNiMIP imprinting



20

Figure 2.7: (2*R*,3*S*)-3-methacrylamidobutan-2-yl methacrylate (**20**).

technique is to increase polymer rigidity. One method to increase rigidity is to alter the present model compound, NOBE (**1**), by adding two relatively small alkyl groups to the spacer of the compound.

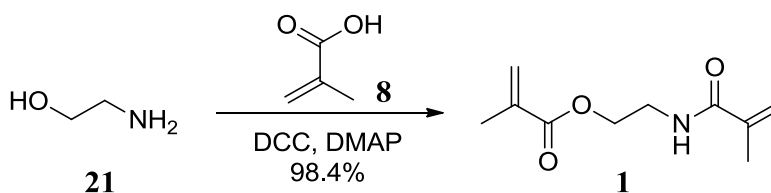
The introduction of two methyl groups, one to the alpha amido and one to the alpha ester position of NOBE was completed. This new molecule, (2*R*,3*S*)-3-methacrylamidobutan-2-yl methacrylate (Figure 2.7, **20**), incorporating the two methyl groups is predicted to cause the crosslinking monomer to twist in such a way that relieves the methyl-methyl repulsion. This configuration may cause a rigid framework that will lock into place and lead to better binding cavity formation. As pointed out in Chapter One, the addition of a small group, such as a methyl appendage at the alpha amido position of NOBE does not inhibit template binding.¹² It is anticipated that adding a second methyl group would continue to have a negligible effect on binding interactions and the reactivity of the polymerizable groups. The effects of this crosslinker on the imprinted polymer will be explored to determine if the rigidity from the locked-in twist of the crosslinking monomer will provide a better OMNiMIP imprinted cavity to form. Furthermore, this crosslinker is chiral with C₂ symmetry, which can improve chiral separations and be used for imprinting racemic molecules.

The synthesis of (2*R*,3*S*)-3-methacrylamidobutan-2-yl methacrylate (**20**) was successfully completed in 5 steps. Addition of trimethoxyethane to the stereochemically pure (2*R*,3*R*)-butane-2,3-diol afforded intermediate **35** in yields ranging from approximately 75-91%. Next, the addition of trimethylsilyl azide was completed. It should be noted that a color change from gold to red occurs when molecule (**37**) is synthesized. The highest yield for this reaction was 43%. The next two reactions, the de-protection of the alcohol followed by the reduction of the azide to the amine, were completed without purification by column chromatography and the

crude products were used to continue the synthesis. The final step involved a DCC/DMAP coupling reaction of the amino alcohol to MAA to afford the final product (2*R*,3*S*)-3-methacrylamidobutan-2-yl methacrylate (**20**.) Although this molecule has been successfully synthesized, a larger amount of material needs to be synthesized in order to study this molecule as a crosslinker for OMNiMIP imprinting, and this is ongoing research to be completed in the Spivak research group.

2.2 Experimentals

A. Crosslinkers with Alteration of Polymerizable Groups

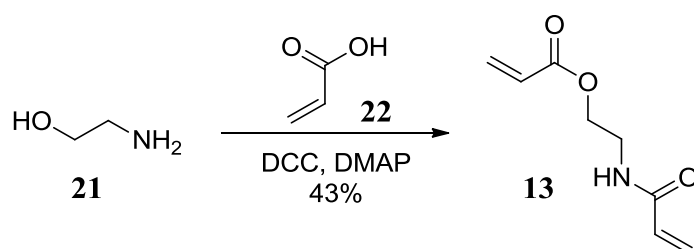


Scheme 2.1: Synthesis of NOBE (**1**).

2-methacrylamidoethyl methacrylate (NOBE, **1**):

NOBE (**1**) was synthesized according to a published protocol.¹³ In a 500 mL roundbottom, ethanolamine (**21**, 4.017 g, 0.0658 mol) and 225 mL DCM were cooled to 0°C. DMAP (1.6374 g, 0.0134 mol) and MAA (**8**, 12.6523 g, 0.147 mol) were added, followed by DCC (29.1370 g, 0.141 mol). The mixture was slowly warmed to room temperature and stirred for 2 days. The DCU was filtered off by vacuum filtration and the organic solution was washed with 1 N HCl (aq) (3 x 100 mL) and sat. NaHCO₃ (aq) (7 x 100 mL.) The organic layer was dried over MgSO₄ and the solvent evaporated to yield an oil (**1**, 12.7621 g, 98.4% yield.) ¹H NMR (CDCl₃, 400 MHz) δ ppm 6.41 (1H, br, NH), 6.06 (1H, s), 5.64 (1H, s), 5.54 (1H, s), 5.27-

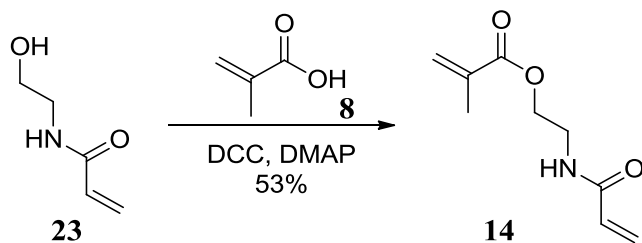
5.25 (1H, d, $J = 8$ Hz), 4.25-4.22 (2H, t, $J = 6$ Hz), 3.58-3.54 (2H, q), 1.90 (3H, s), 1.88 (3H, s.)
 ^{13}C NMR (CDCl_3 , 100MHz) δ ppm 168.46, 167.65, 139.78, 135.94, 126.20, 119.76, 63.36, 39.22, 18.58, 18.29.



Scheme 2.2: Synthesis of 2-acrylamidoethyl acrylate (13).

2-acrylamidoethyl acrylate (13):

The synthesis of 2-acrylamidoethyl acrylate (13) was adapted from a known literature procedure.¹⁴ Ethanolamine (21, 1.0 mL, 0.0166 mol) in 100 mL DCM was cooled to 0°C. Acrylic acid (22, 2.5 mL, 0.036 mol) and DMAP (0.081 g, 0.0036 mol) in 25 mL was added to the amino alcohol solution. After 10 min, DCC (7.5 g, 0.036 mol) in 25 mL DCM was added dropwise. The mixture was slowly allowed to cool to room temperature and was stirred for 3 days. After filtration of DCU, extractions using 1 N HCl (aq) (2 x 75 mL) and saturated NaHCO_3 (aq) (3 x 75 mL) were completed. The organic layer was dried over MgSO_4 and was filtered. After evaporation, the crude product was purified by column chromatography using 50/50 to 75/25 EtOAc/Hexanes to yield a yellow oil (13, 1.2009 g, 43%.) ^1H NMR (CDCl_3 , 400 MHz) δ ppm 6.50 (1H, br), 6.38 (dd, $J = 17.3, 1.3$ Hz, 1H), 6.24 (dd, $J = 17.1, 1.5$ Hz, 1H), 6.18 – 6.00 (m, 2H), 5.82 (dd, $J = 10.4, 1.4$ Hz, 1H), 5.60 (dd, $J = 10.2, 1.6$ Hz, 1H), 4.25 (t, $J = 5.4, 5.4$ Hz, 2H), 3.60 (q, $J = 5.5, 5.5, 5.5$ Hz, 2H.) ^{13}C NMR (CDCl_3 , 100MHz) δ ppm 166.17, 165.82, 131.40, 130.61, 127.90, 126.58, 63.15, 38.73.

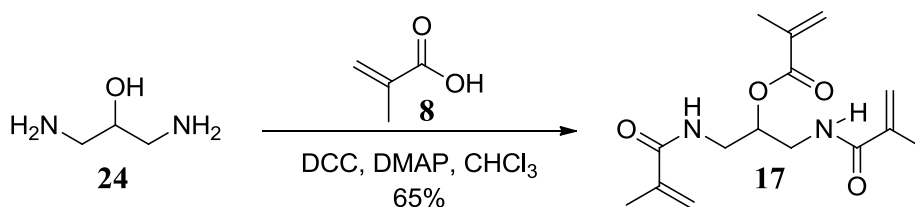


Scheme 2.3: Synthesis of 2-acrylamidoethyl methacrylate (**14**).

2-acrylamidoethyl methacrylate (**14**):

Hydroxyethyl acrylamide (**23**, 2.1172 g, 0.018 mol) in 75 mL DCM was cooled to 0°C. Methacrylic acid (**8**, 1.9054 g, 0.022 mol) and DMAP (4.8 mg, 0.039 mmol) in 25 mL DCM was added. DCC (4.46 g, 0.022 mol) in 25 mL DCM was added after 5 minutes and the reaction was stirred 2 days. After filtration of DCU, extractions using 0.5 N HCl (aq) (4 x 75 mL) and saturated NaHCO₃ (aq) (4 x 75 mL) were completed. The organic layer was dried over MgSO₄ and was filtered. After evaporation, the crude product was purified by column chromatography using 50/50 EtOAc/hexanes to afford 1.7830 g, 53% yield product (**14**.) ¹H NMR (CDCl₃, 400 MHz) δ ppm 6.27 (dd, *J* = 17.0, 1.5 Hz, 1H), 6.17 – 6.04 (m, 3H), 5.65 (t, *J* = 8 Hz, *J* = 8 Hz, 1H), 5.58 (t, *J* = 4 Hz, *J* = 4 Hz, 1H), 4.27 (t, *J* = 5.4, 5.4 Hz, 2H), 3.64 (q, *J* = 5.5, 5.5, 5.5 Hz, 2H), 1.93 (s, 3H). ¹³C NMR (CDCl₃, 100MHz) δ ppm 167.54, 165.73, 135.93, 130.61, 126.72, 63.38, 60.39, 38.95, 18.26.

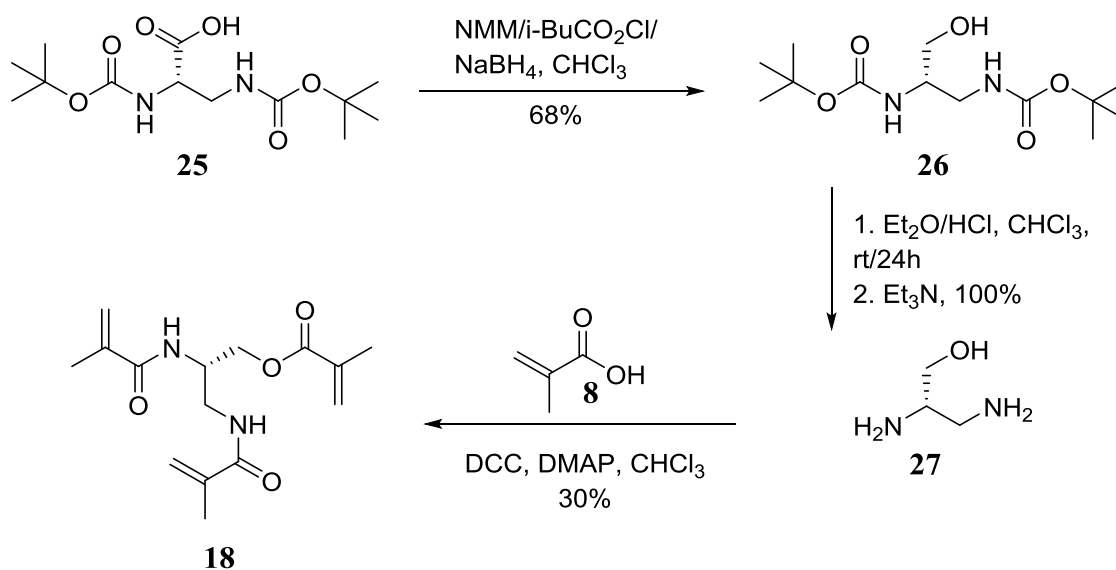
B. Three-armed Crosslinkers



Scheme 2.4: Synthesis of 1,3-dimethacrylamidopropan-2-yl methacrylate (**17**).

1,3-dimethacrylamidopropan-2-yl methacrylate (**17**):

1,3-diaminopropan-2-ol (**24**, 2.0231 g, 0.02245 mol) was dissolved in 50 mL CHCl_3 and was cooled to 0°C . MAA (**8**, 6.66 mL, 0.0785 mmol) and DMAP (0.9619 g, 7.87 mmol) in 30 mL chloroform was cooled then added to the amino alcohol solution. DCC (14.8973 g, 0.0722 mol) was added and the mixture was allowed to stir for 3.5 days. The DCU was filtered off and the organic layer was washed with 1 N HCl (aq) (4 x 150 mL) then sat. NaHCO_3 (aq) (4 x 150 mL). The organic layer was dried over MgSO_4 and was filtered. After solvent evaporation, the crude product was purified by column chromatography using 75/25 EtOAc/hexanes to yield 4.2835 g, 65% yield product (**17**.) ^1H NMR (CDCl_3 , 400 MHz) δ ppm 6.88 (br, 2H), 6.10 (s, 1H), 5.77 (s, 2H), 5.88 (s, 1H), 5.36 (s, 2H), 4.99-4.93 (m, 1H), 3.62-3.34 (m, 4H), 1.97 (s, 6H), 1.90 (s, 3H). ^{13}C NMR (CDCl_3 , 100MHz) δ ppm 169.14, 166.69, 139.54, 135.85, 126.56, 120.29, 71.47, 39.16, 18.61, 18.24. IR ν_{max} 3271.25, 1710.61, 1654.16, 1617.30, 1540.77, 1181.65, 1077.50.



Scheme 2.5: Synthesis of (*S*)-2,3-dimethacrylamidopropyl methacrylate (**18**).

(*S*)-di-tert-butyl (3-hydroxypropane-1,2-diyl)dicarbamate (**26**):

In a 250 mL roundbottom flask, (*S*)-2,3-bis((tert-butoxycarbonyl)amino)propanoic acid (**25**, 2.9006 g, 9.5 mmol) in 45 mL dry chloroform was cooled to 0°C. NMM (1.2 mL, 10.45 mmol) was added dropwise to the solution and the mixture was allowed to cool. Isobutylchloroformate (1.36 mL, 10.45 mmol) was added dropwise and the reaction mixture was stirred for 15 minutes. NaBH₄ (1.0824 g, 28.5 mmol) was added. Methanol (90 mL) was added dropwise over 15 minutes and the reaction mixture was allowed to stir for an additional 40 minutes then 18 mL 1 N HCl (aq) was added. H₂O was added and the product was extracted using chloroform (4 x 50 mL). The combined organic layer was washed with 1 N HCl (aq) (1 x 100 mL), H₂O (1 x 100 mL), sat. NaHCO₃ (aq) (1 x 100 mL), then H₂O (1 x 100 mL.) The organic layer was dried over MgSO₄, filtered, and the solvent evaporated. Column chromatography using 50/50 EtOAc/hexanes was used to purify the crude product to afford 1.8927 g, 68% product (**26**.) ¹H NMR (CDCl₃, 400 MHz) δ ppm 5.17-5.11 (br, 2H), 3.75 (m, 1H), 3.73-3.53 (m, 2H), 3.32-3.21 (m, 2H), 1.44 (s, 9H). ¹³C NMR (CDCl₃, 100MHz) δ ppm 157.74, 155.80, 80.30, 79.61, 61.59, 52.31, 40.22, 28.37, 28.30.

(*S*)-2,3-diaminopropan-1-ol (**27**):

(*S*)-di-tert-butyl (3-hydroxypropane-1,2-diyl)dicarbamate (**26**, 1.834 g, 6.3 mmol) was stirred in 1.55 M ethereal HCl (81.5 mL, 0.126 mol, 20 eq) overnight. Triethylamine was added to neutralize the solution. After solvent evaporation, the de-protected product (**27**) was obtained in quantitative yields. ¹H NMR (CDCl₃, 400 MHz) δ ppm 4.24 (br, 1H), 4.01 (m, 1 H), 3.45 (m, 1H), 2.90 (m, 2 H), 1.63 (m, 3H), 1.44 (m, 2 H). ¹³C NMR (CDCl₃, 100MHz) δ ppm 60.71, 49.82, 38.31.

(*S*)-2,3-dimethacrylamidopropyl methacrylate (**18**):

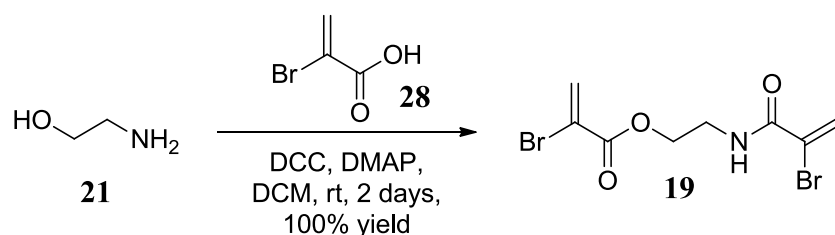
De-protected amino alcohol (**27**, 0.811 g, 9.0 mmol) was stirred in 100 mL chloroform. Et₃N (4 mL) was added dropwise to the suspension and the mixture became clear. The solution was cooled to 0°C. MAA (**8**, 2.7 mL, 31.5 mmol) and DMAP (0.3906 g, 3.2 mmol) in 15 mL chloroform was cooled then added dropwise to the alcohol solution. DCC (6.5762 g, 32.0 mmol) in 15 mL chloroform was cooled then added dropwise to the reaction mixture. The reaction mixture was allowed to slowly rise to room temperature and was stirred for 5 days. The DCU was filtered using vacuum filtration and the orange solution was washed with 1 N HCl (aq) (4 x 200 mL) then saturated NaHCO₃ (aq) (4 x 200 mL). The organic layer was dried over MgSO₄, filtered, and the solvent was evaporated. Purification by column chromatography using 75/25 EtOAc/hexane was performed on the crude product. Pure product (**18**, 0.8024 g) was obtained in 30% yield. ¹H NMR (CDCl₃, 400 MHz) δ ppm 7.11 (br, 1H), 6.76 (br 1H), 6.17 (s, 1H), 5.78 (s, 2H), 5.64 (s, 1H) 5.38-5.37 (d, 2H), 4.32 (s, 1H), 4.13-4.11 (m, 2H), 3.50-3.47 (m 2H), 1.73 (s, 3H), 1.71 (s, 3H), 1.70 (s, 3H). ¹³C NMR (CDCl₃, 100MHz) δ ppm 169.98, 168.99, 167.75, 139.11, 135.66, 130.92, 128.82, 126.80, 120.77, 63.27, 50.63, 41.19, 18.53, 18.46, 18.30.

Alteration of Polymerizable Groups and Three-armed Crosslinkers Polymer Preparation:

Monomer (1.5 g of **1**, **3**, **14**, **17**, or **18**) was added to the 13 x 100 mm glass tube with a solution of the print molecule L-BOC-Tyr (5%) dissolved in 1.5 mL acetonitrile. AIBN (1%) was added to the solution. Nitrogen was used to purge the sample for 5 minutes. After the sample was purged, the tube was capped and Teflon tape and Parafilm were used to seal the system. The tube was then inserted into a photoreactor apparatus where it was submerged in an ethylene glycol/H₂O bath to maintain the temperature and was exposed to a 450 W mercury arc

lamp surrounded by a borosilicate jacket for 8 hours. The polymer was then broken out of the tube and the template was removed by Soxhlet extraction for 2 days. The polymers were then ground and sized to 25-37 μm using U.S.A. Standard Testing Sieves. The sized polymer was then packed into 100 x 2.1 mm stainless steel columns and their imprinting abilities were analyzed by HPLC.

C. Crosslinkers with Electron-withdrawing Groups



Scheme 2.6: Synthesis of BrOBE (19).

2-(2-bromoacrylamido) ethyl 2-bromoacrylate (**19**):

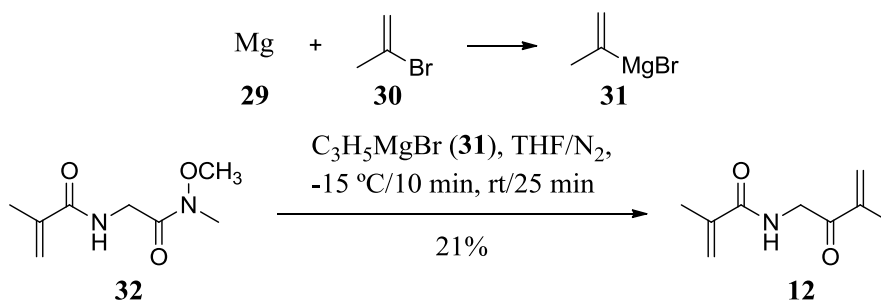
In a 100 mL round bottom, ethanolamine (**21**, 0.31 mL, 5.1 mmol) was dissolved in 12 mL DCM the solution was cooled to 0°C. Bromoacrylic acid (**28**, 3.0911 g, 20.5 mmol, 4 eq) and DMAP (46.1 mg, 0.4 mmol) were dissolved in 12 mL DCM was the solution was added dropwise to the amino alcohol solution. After 10 minutes, DCC (4.2358 g, 20.5 mmol, 4 eq) dissolved in 11 mL DCM was added to the reaction mixture by dropwise addition. The mixture was stirred at room temperature for 2 days. The DCU was filtered off and the DCM solution was washed with 1 N HCl (3 x 30 mL) (aq) and saturated NaHCO₃ (3 x 30 mL) (aq). The combined organic layers were dried over MgSO₄, and after filtration the solvent was evaporated. Column chromatography using 50/50 EtOAc/hexane was run and a colorless oil (**19**) was afforded in 100% yield. ¹H NMR (CDCl₃, 400 MHz) δ 7.08 (br, 1H), 6.90 (d, 1H, J= 4Hz), 6.88 (d, 1H, J=

4 Hz), 6.21 (d, 1H, J= 4 Hz), 6.0 (d, 1H, J= 4 Hz), 4.29-4.25 (t, 2H, J= 6 Hz), 3.62-3.55 (q, 2H).
¹³C NMR (CDCl₃, 100MHz) δ 161.86, 161.23, 131.46, 128.06, 122.37, 120.56, 64.76, 39.46.

2-(2-Bromoacrylamido) ethyl 2-bromoacrylate (19) Polymer Preparation:

Monomer (**19**, 0.5 g) was added to a NMR tube containing a solution of the template L-BOC-Tyr (5%) dissolved in 0.5 mL acetonitrile. AIBN (1%) was added and the solution was sonicated repeatedly for a few seconds to degas the pre-polymer complex while maintaining a room temperature solution. Nitrogen was flushed over the tube to remove air from the sample. The NMR tube was then capped and Teflon tape and Parafilm were used to seal the system. The tube was next inserted into a photoreactor where it was submerged in an ethylene glycol/H₂O bath to maintain the temperature during polymerization and the reaction mixture was exposed to a 450 W mercury arc lamp surrounded by a borosilicate jacket for 8 hours. The polymer was then broken out of the tube and the template was removed by Soxhlet extraction using methanol/acetic acid (90/10) for 2 days. The polymeric material was ground and sized to 20-37 μm using U.S.A. Standard Testing Sieves and packed into 100 x 2.1 mm stainless steel columns. The selectivity of the OMNiMIP chromatographic stationary phase was analyzed by HPLC.

D. Crosslinkers with Hydrogen Bond Donor/Acceptor Proximity and Amide Content



Scheme 2.7: Synthesis of NAG (12).

2-Methyl-N-(3-methyl-2-oxobut-3-enyl) acrylamide (NAG, **12**):

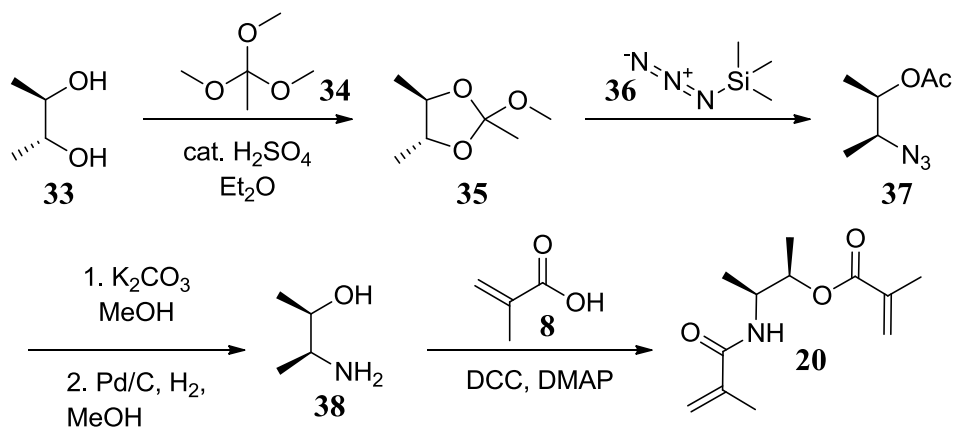
The synthesis of NAG was modified from a previous publication.⁵ Magnesium turnings (0.4099 g, 16.9 mmol, 1.9 eq) were oven dried overnight. After cooling under N₂, the Mg (**29**) was mashed. Dry THF (10 mL) was added followed by the addition of 2-bromopropene (**30**, 1.0709 g, 8.9 mmol). The colorless solution was refluxed for 30 minutes and became a gray/brown dirty dishwater color, indicating the formation of the isopropenyl magnesium bromide (**31**) in THF. The Weinreb amide (**32**, 0.6422 g, 3.4 mmol) in 5 mL THF was cooled to -5°C. Isopropenyl magnesium bromide (**31**) in THF (9.6 mL, 0.89 M, 2.5 eq) was added over five minutes and a white solid precipitated out. The mixture was allowed to slowly warm to room temperature and was stirred overnight for 18 hours. The reaction was quenched with saturated NH₄Cl (aq), and the THF was evaporated. Et₂O (50 mL) was added and the phases were separated. The organic phase was washed with brine (2 x 30 mL) and water (1 x 50 mL). The organic layer was dried over MgSO₄, filtered, and the solvent evaporated. Column chromatography was run on the yellow oil using 50/50 EtOAc/hexanes. A yellow oil (**12**, 121.7 mg, 21%) pure product based on NMR was collected. ¹H NMR (CDCl₃, 250 MHz) δ 6.76 (br, 1H), 6.07 (s, 1H), 5.89 (s, 1H) 5.78 (s, 1H), 5.36 (s, 1H), 4.51 (d, 2H, J = 4 Hz), 1.98 (s, 3H), 1.91 (s, 3H). ¹³C NMR (100 MHz, CDCl₃) δ 195.81, 168.16, 142.24, 139.11, 126.14, 120.31, 45.66, 18.51, 17.30.

NAG Imprint Polymerization:

NAG (**12**) was inserted into the photo reactor for 8 hours with 5% L-BOC-Tyr template, 1% AIBN initiator, and MeCN as the porogen. After photo-initiated radical polymerization, the afforded compound was a gel consistency with a small amount of solvent remaining at the top.

The gel was unable to be studied as a solid stationary phase for HPLC, so a curing step was required. The gel and solution was combined with an additional 25% template, 1% AIBN, and 3 mL MeCN. This mixture was purged with nitrogen for 5 minutes. The mixture (mostly an insoluble yellow opaque mixture) was allowed to equilibrate at room temperature (stirring occasionally) for one hour and was then brought to 80°C for ~8 hrs. The material became darker and harder, but was brittle. The material was then crushed and sonicated several times in attempt to homogenize the mixture. An additional 1% AIBN was added and the solution was purged with nitrogen and then was allowed to equilibrate for four hours before the heat was raised to 80°C for two days. This material was then ground and sized to 25-37µm using U.S.A. Standard Testing Sieves packed into a 50 x 2.1 mm HPLC column for analysis.

E. Crosslinker with Stereochemical Rigidity



Scheme 2.8: Synthesis of ((2*R*,3*S*)-3-methacrylamidobutan-2-yl methacrylate (**20**).

((4*R*,5*R*)-2-methoxy-2,4,5-trimethyl-1,3-dioxolane (**35**):

The synthesis of ((4*R*,5*R*)-2-methoxy-2,4,5-trimethyl-1,3-dioxolane (**35**) was adapted from a literature procedure.¹⁵ (2*R*,3*R*)-butane-2,3-diol (**33**, 1.2975 g, 0.014 mol) in 45 mL ether

was cooled to 0°C. Trimethoxyethane (**34**, 3.5 mL, 0.029 mol, 2 eq) followed by 38.4 μ L H₂SO₄ (aq) were added. The mixture was allowed to slowly warm to room temperature and was stirred overnight. Triethylamine (1.5 mL) was added to the colorless solution and this was poured into 75 mL saturated NaHCO₃ (aq), and the product was extracted with diethyl ether (3 x 30 mL.) After drying over MgSO₄ and evaporation of solvent, the crude colorless liquid (1.9158 g, 91% product (**35**)) was used in the next step without additional purification. ¹H NMR (CDCl₃, 400MHz) δ ppm 3.82-3.73 (m, 1H), 3.71-3.63 (m, 1H), 3.26 (s, 3H, OCH₃), 1.51 (s, 3H, CH₃), 1.29-1.27 (d, 3H), 1.23-1.21 (d, 3H). ¹³C NMR (100 MHz, CDCl₃) δ 120.84, 79.44, 78.97, 49.15, 23.42, 17.27, 16.81.

(2*R*,3*S*)-3-azidobutan-2-yl acetate (**37**):

(2*R*,3*S*)-3-azidobutan-2-yl acetate (**37**) was synthesized according to a prior report.¹⁵ (4*R*,5*R*)-2-methoxy-2,4,5-trimethyl-1,3-dioxolane (**35**, 2.4418 g 75%/wt product (contained trimethoxyethane (**34**)), 0.013 mol) and TMSN₃ (**36**, 4.3 mL, 0.033 mol) was heated at 60°C for four hours turning from a pale yellow to dark gold solution. The temperature was increased to 130°C and was stirred overnight. After evaporation, the dark red liquid was poured into water and was extracted using Et₂O (3 x 100 mL). The organic layer was dried over MgSO₄ and after filtration and evaporation, the crude product was purified by column chromatography (1/3 to 50/50 EtoAc/hexanes) to yield a yellow liquid (**37**, 0.8416 g, 43% yield) ¹H NMR (CDCl₃, 250MHz) δ ppm 4.75-4.69 (m, 1H), 3.73-3.70 (m, 1H), 2.06 (s, 3H, OAc), 1.19 (d, J = 12 Hz, 3H), 1.16 (d, J = 4 Hz, 3H). ¹³C NMR (100 MHz, CDCl₃) δ 170.88, 74.88, 69.87, 21.24, 18.98, 16.19. IR ν_{max} 2113.46 (s, azide), 1728.02 (s) cm⁻¹. HRMS (ESI-TOF): calcd for C₆H₁₁N₃O₂ (M)⁺: 157.0845.

(2*R*,3*S*)-3-azidobutan-2-ol:

The synthesis of (2*R*,3*S*)-3-azidobutan-2-ol was completed according to a prior publication.¹⁵ Methanol (50 mL) was added to (2*R*, 3*S*)-3-azidobutan-2-yl acetate (**37**, 0.7889 g, 5.02 mmol). K₂CO₃ (3.5158 g, 0.025 mmol, 5 eq) was added to the yellow solution and was stirred overnight at room temperature. The white solid was filtered off from the yellow solution. The MeOH was removed from the solution and the product was poured into water (20 mL) and extracted with Et₂O (3 x 20 mL.) The organic layer was dried over MgSO₄ and the solvent was evaporated to afford a gold liquid. A crude ¹H NMR showed formation of the product with some other material present. This crude product was used in the next step without further purification. ¹H NMR (CDCl₃, 250MHz) δ ppm 3.66-3.60 (m, 1H), 3.59-3.55 (m, 1H), 3.00 (br, 1H), 1.19 (d, J = 12 Hz, 3H), 1.16 (d, J = 4 Hz, 3H). ¹³C NMR (100 MHz, CDCl₃) δ 70.70, 62.65, 18.30, 13.79.

(2*R*,3*S*)-3-aminobutan-2-ol (**38**):¹⁵

The synthesis of (2*R*,3*S*)-3-aminobutan-2-ol (**38**) followed the method of a prior report.¹⁵ (2*R*,3*S*)-3-azidobutan-2-ol (0.3722 g, 3.2 mmol), 0.2020 g Pd/C, and 4 mL MeOH were stirred under a H₂ balloon at room temperature overnight. The reaction mixture was filtered through a celite cake twice and the filtrate was concentrated. Upon concentration, the mixture needed to be filtered through a celite cake again and was then completely concentrated yielding a pale gold colored oil. The crude product (**38**) was used in the next step without further purification. ¹H NMR (CDCl₃, 250MHz) δ ppm 3.68-3.59 (m, 1H), 2.93-2.81 (m, 1H), 1.86 (br, 3H, OH and NH₂), 1.09-1.07, d, 3H), 0.98-0.96 (d, 3H.)

(2*R*,3*S*)-3-methacrylamidobutan-2-yl methacrylate (**20**):

(2*R*,3*S*)-3-aminobutan-2-ol (**38**, 0.4047 g, 4.54 mmol crude product) in 50 mL DCM was cooled to 0°C. MAA (**8**, 0.8689 g, 10.1 mmol, 2.2 eq) was added slowly to the mixture. DMAP (139.9 mg, 1.15 mmol, 0.25 eq) was added and the temperature was allowed to equilibrate. DCC (2.0708 g, 10.0 mmol, 2.20 eq) was then added slowly. The mixture was allowed to slowly warm to room temperature and was stirred under argon for 2 days. The DCU was removed by vacuum filtration and the organic layer was washed with 1 N HCl (aq) (3 x 25 mL) and saturated NaHCO₃ (aq) (7 x 25 mL). The organic layer was dried over MgSO₄ and was filtered. After evaporation of solvent, column chromatography was run using EtOAc/hexanes (25/75 then 50/50) to elute the product. After evaporation, a colorless oil (**20**, 0.0847 g) was obtained. ¹H NMR (400 MHz, CDCl₃) δ 6.30 (br, 1H), 5.63 (s, 1H), 5.56 (s, 1H), 5.28 (s, 1H), 4.98 - 4.95 (m, 1H), 4.21 - 4.14 (m, 1H), 1.91 (s, 6H), 1.26 (d, *J* = 6.5 Hz, 3H), 1.15 (d, *J* = 6.8 Hz, 3H). ¹³C NMR (100 MHz, CDCl₃) δ 167.78, 167.27, 140.05, 136.27, 125.85, 119.49, 73.55, 48.73, 18.51, 18.22, 16.95, 14.69. IR ν_{\max} 1714.35, 1662.89, 1625.67, 1514.40. MS (ESI-TOF): calcd for C₁₂H₁₉NO₃ (M+H)⁺: 226.14; found 226.1434.

2.3 Results and Discussion of New Crosslinkers for Molecular Imprinting

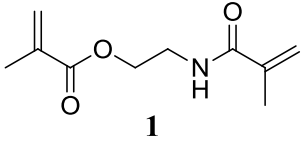
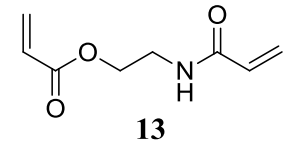
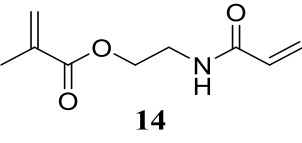
A. OMNiMIP Performance from Crosslinkers with Alteration of Polymerizable Groups

Once synthesized, crosslinkers **1**, **13**, and **14** were used to imprint L-BOC-Tyr using a photo-initiated radical polymerization technique. The OMNiMIPs formed using the crosslinkers 2-acrylamidoethyl acrylate (**13**) and 2-acrylamidoethyl methacrylate (**14**) were explored as HPLC stationary phases and their ability to separate BOC-Tyr enantiomers were compared to NOBE. For these trials, the particle size range and HPLC specifications were chosen to mimic

the conditions that were previously used to study NOBE.¹³ Herein, the OMNiMIP particles were ground using a mortar and pestle and sized to 25–37 μm using U.S.A. Standard Testing Sieves. NOBE and 2-acrylamidoethyl methacrylate (**14**) OMNiMIPs were packed into 100 x 2.1 mm stainless steel columns. Since a smaller amount of OMNiMIP was prepared from 2-acrylamidoethyl acrylate (**13**), this material was packed into a smaller 50 x 2.1 mm stainless steel column. Although the column sizes differed, the results were normalized by calculating the capacity factors (k') for all analytes evaluated.

For the HPLC analyses, all analytes were run in triplicate at room temperature under isocratic conditions with a 99% MeCN 1% acetic acid mobile phase at a 0.1 mL/min flow rate. The wavelength of detection for all experiments was 260 nm. The 1 mM BOC-tyrosine enantiomers were injected separately into the column so that effective separation factors (α') could be determined, and the total sample volume injected was 5 μL each. Acetone was used to determine the void volume so that the capacity factors (k') could be calculated according to Eq. 1.1. Results from the alteration of polymerizable groups are shown in Table 2.1. The α' for NOBE was determined to be 3.78 ± 0.4071 , while the α' for molecules **13** and **14** were determined to be 1.65 ± 0.0457 and 1.89 ± 0.0626 , respectively. All groups studied here were able to separate enantiomers of BOC-tyrosine, since all had α' greater than 1.0. The OMNiMIP stationary phase from NOBE performed better than 2-acrylamidoethyl methacrylate (**14**), and **14** performed better than 2-acrylamidoethyl acrylate (**13**).

Table 2.1: HPLC results for OMNiMIPs synthesized from the crosslinkers with alteration of polymerizable groups*.

Monomer	k'_D	k'_L	α'
 <p>1</p>	2.41 ± 0.0115	9.10 ± 0.979	3.78 ± 0.4071
 <p>13</p>	1.93 ± 0.05033	3.19 ± 0.0300	1.65 ± 0.0457
 <p>14</p>	1.97 ± 0.0577	3.73 ± 0.0577	1.89 ± 0.0626

*HPLC conditions: 25–37 μm particles; 100 x 2.1 (used for OMNiMIPs generated from **1** and **14**), 50 x 2.1 (used for OMNiMIP generated from **13**) column; mobile phase, MeCN/acetic acid (99:1); analytes (1mM BOC-L-tyrosine, 1 mM BOC-D-tyrosine, acetone (used to determine void volume)) were all detected at 260 nm; flow rate 0.1 mL/min; sample volume injected 5 μL .

The composition of the crosslinking monomer's polymerizable groups affected their polymerization and therefore OMNiMIP performance to separate chiral compounds. NOBE (**1**) contains a methacrylate and methacrylamide group. The methacrylate group polymerizes slightly faster than the methacrylamide group, forming a highly crosslinked rigid polymer with excellent imprinting towards BOC-Tyr. When compound **1** was studied as a stationary phase for HPLC, it was able to separate enantiomers of BOC-Tyr with a separation factor of 3.78 ± 0.4071 .

2-acrylamidoethyl acrylate (**13**) is comprised of acrylate and acrylamide groups and 2-acrylamidoethyl methacrylate (**14**) is composed of methacrylate and acrylamide groups, while

NOBE (**1**) contains methacrylate and methacrylamide groups. For several reasons, it was hypothesized that **13** and **14** may provide improved selectivity of the OMNiMIPs synthesized using these crosslinkers. For example, the structures of crosslinkers **13** and **14** are less sterically hindered and were anticipated to wrap more closely around the template when compared to **1**. These less sterically hindered crosslinkers were also expected to solubilize better than **1** in the pre-polymer complex, decreasing phase separation during the polymerization. Furthermore, the polymerizable group reactivity order, which consisted of **14** forming linear polymer first followed by crosslinking, which was previously shown to be successful for the crosslinker NAG in traditional imprinting, was also expected to improve the selectivity of the resulting OMNiMIPs; however, the imprinted polymers synthesized from crosslinkers **13** and **14** were subordinate to NOBE (**1**.)

The inferior performance of molecules **13** and **14** could be explained by the reactivity of the polymerizable groups negatively affecting the OMNiMIPs formed. As mentioned previously, secondary radicals are less stable than tertiary radicals and it is predicted that **13** will polymerize slower and be less reactive than **1** as it contains two end polymerizable groups that will form secondary radicals (both the acrylate and acrylamide) compared to two tertiary radicals from the methacrylate and methacrylamide groups of **1**. Molecule **14** will also not polymerize as quickly or be as reactive as compound **1**, but should polymerize marginally faster and be more reactive than compound **13** because **14** is comprised of a methacrylate group, which will form a tertiary radical and an acrylamide group that will form a secondary radical. The delay and lower reactivity of the crosslinkers **13** and **14** may result in early termination of the polymerization and form less crosslinked polymers. Polymers that are less crosslinked may have less structured selective binding sites, which would result in poor HPLC separation factors during the

OMNiMIPs analysis. The separation factor of compounds **13** and **14** are similar, $\alpha' = 1.65 \pm 0.0457$ and 1.89 ± 0.0626 respectively. Although these separation factors do show that these OMNiMIPs have the ability to be imprinted and can separate enantiomers of BOC-Tyr, they do not show any improvement to the original crosslinking monomer NOBE. With both polymerizable groups forming two stable tertiary radicals, crosslinker **1** performed the best followed by **14**, which contained groups that form one tertiary and one secondary radical. Finally, crosslinker **13** containing two polymerizable groups that form secondary radicals performed the worst. The order of performance suggests that the stability of the radical formed by the polymerizable groups of the crosslinkers plays a vital part in OMNiMIP formation.

B. Three-armed Crosslinkers

Two new crosslinkers with three polymerizable groups, (*S*)-2,3-dimethacrylamidopropyl methacrylate (**18**) and 1,3-dimethacrylamidopropan-2-yl methacrylate (**17**) were synthesized. Both **17** and **18** contain two methacrylamide groups that could participate in hydrogen bonding and one methacrylate group, and these crosslinkers differ only by the position of these groups. Crosslinker **18** was determined to be insoluble in acetonitrile, tetrahydrofuran, dimethylformamide, H₂O, and chloroform (common porogens) at 1 g/mL, a typical concentration for the photo-initiated radical polymerizations of imprinted polymers (Table 2.2.) The insolubility of crosslinker **18** prohibited its use as an OMNiMIP.

Crosslinker **17** was partially soluble in the polymerization solvent and was able to be tested as an OMNiMIP. The OMNiMIP resulting from the crosslinker 1,3-dimethacrylamidopropan-2-yl methacrylate (**17**) was analyzed by HPLC following a procedure similar to the analysis of NOBE presented previously and the results are shown in Table 2.2.

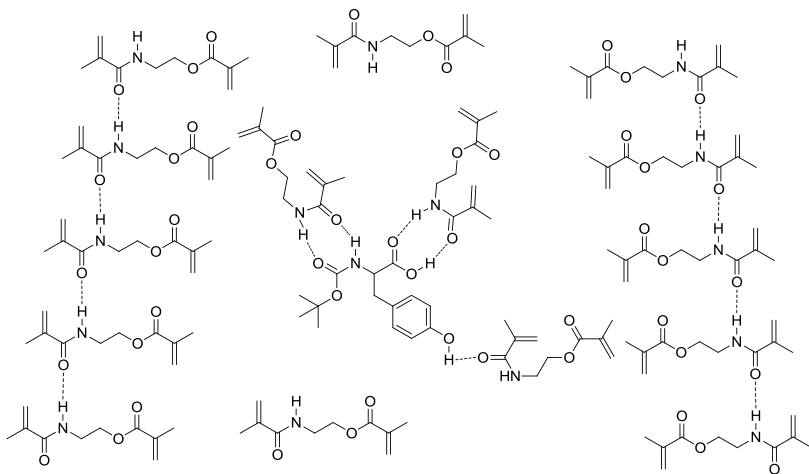
After optimization of chromatographic conditions, the best performance in selectivity was achieved using 1 mL/min as the flow rate. Although **17** was successful at separating enantiomers of BOC-Tyr ($\alpha' = 1.2$), it did not perform better than NOBE ($\alpha' = 3.78 \pm 0.4071$.)

Table 2.2: HPLC results of the OMNiMIPs synthesized from the three-armed crosslinkers* .

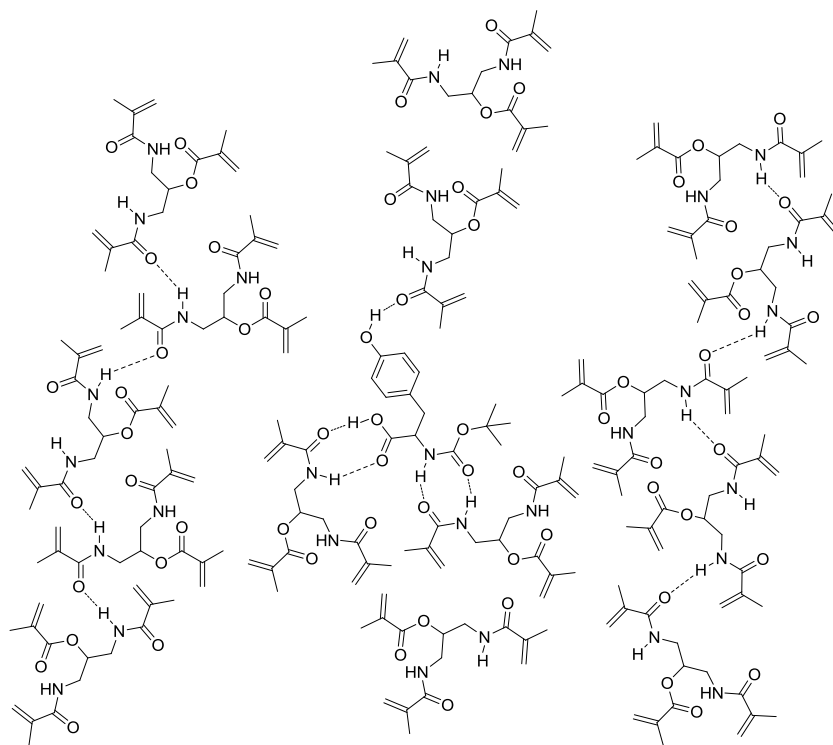
Monomer	k'_D	k'_L	α'
<p>17</p>	3.3	3.9	1.2
<p>18</p>	-	-	Not Soluble
<p>*HPLC conditions: 25–37 μm particle size; 100 x 2.1 column; MeCN/acetic acid (99:1) mobile phase; analytes (1mM BOC-L-tyrosine, 1 mM BOC-D-tyrosine, acetone (used to determine void volume)) were all detected at 260 nm; flow rate 1 mL/min; sample volume injected was 5 μL.</p>			

There are several possible reasons the additional amide appendage could have caused inferior (compared to NOBE) OMNiMIP selectivity, and an illustration of the predicted binding behavior is shown in Figure 2.8. Although three polymerizable groups are anticipated to form more rigid selective binding sites, this is only the case if all of the polymerizable groups react and if hydrogen bonding is not disrupted due to steric interactions. In the case of crosslinker **17**, the OMNiMIP could be negatively impacted because of the increased sterics (extra methacrylamide group compared to NOBE) of the crosslinker. Steric interference is increased in **17** compared to

NOBE because of the additional methacrylamide group. The trifunctional crosslinker will neither be able to stack to form the polymer backbone nor wrap around BOC-Tyr



(a)



(b)

Figure 2.8: Predicted binding behavior of NOBE (1) with itself and BOC-Tyr (a). Predicted binding behavior of a trifunctional crosslinker (17) with itself and BOC-Tyr (b).

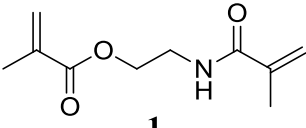
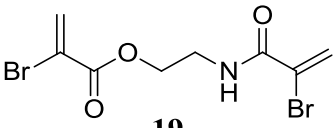
as compactly as in the case with NOBE; thus, **17** will form less structured binding cavities as shown in Figure 2.8. Another possible problem associated with the additional functional group is the risk of phase separation of the pre-polymer complex before the imprinted binding cavities are formed. Additionally, the extra methacrylamide group could cause more non-specific binding interactions to occur. These additional interactions would lower selectivity and may account for differences observed in the α' values seen between **17** and NOBE.

C. Crosslinkers with Electron-withdrawing Groups

HPLC analysis was conducted on the OMNiMIP synthesized from the new molecule BrOBE (**19**). The analysis was conducted in triplicate under the same conditions used for NOBE (**1**) mentioned previously, with the only difference being the particle size range of the two imprinted polymers. The NOBE polymer used was the typical size range 25-37 μm while 20-37 μm was used to analyze BrOBE (**19**). This small difference in size range is not expected to significantly impact the chromatographic results. The reason for the slightly larger size range for BrOBE (**19**) was due to the difficulty that arose with grinding **19** as it was a much “softer” polymer than NOBE. Despite the irregular consistency of the imprinted polymer formed, it was still packed onto an HPLC column for evaluation. With an increased backpressure when packing, the column containing this “soft” polymer was more difficult to fill than rigid crosslinked polymers. Once the packed column was put on the HPLC, the separation of L and D BOC-Tyr enantiomers was attempted. The results shown in Table 2.3 indicate that there was no separation of enantiomers by BrOBE ($\alpha' = 1.08 \pm 0.051$.) Having not even a partial separation of enantiomers indicated that there were no specific binding cavities formed. The lack of selective binding sites was not surprising as the “soft” polymer formed indicates poor crosslinking, and

therefore would not contain well structured binding sites needed for recognition. The “soft” nature of the polymer was attributed to a defective polymerization. This fault in the photo-initiated radical polymerization was attributed to the bromine affecting the polymerization by inhibition of the alkyl radicals.

Table 2.3: HPLC results for OMNiMIPs from the addition of EWG*.

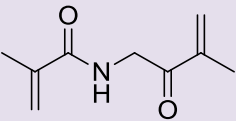
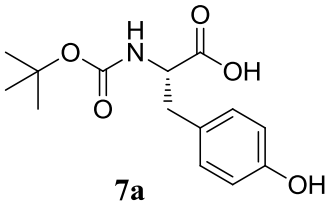
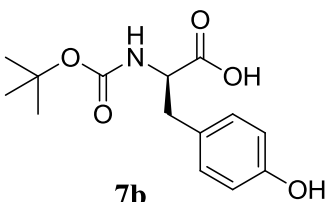
Monomer	k'_D	k'_L	α'
 <p>1</p>	2.41 ± 0.0115	9.10 ± 0.979	3.78 ± 0.4071
 <p>19</p>	0.062 ± 0.0023	0.057 ± 0.0017	1.08 ± 0.051

*HPLC conditions: particle size 25-37 (for OMNiMIP generated from **1**) and 20–37 μm (for OMNiMIP generated from **19**); 100 x 2.1 column; mobile phase, MeCN/acetic acid (99:1); analytes (1mM BOC-L-tyrosine, 1 mM BOC-D-tyrosine, acetone (to determine void volume)) were detected at 260 nm; flow rate 0.1 mL/min; sample volume injected 5 μL .

After using a two step method (photo-initiated radical polymerization followed by thermal curing) an OMNiMIP generated from the crosslinker (**12**) NAG was obtained and this OMNiMIP was analyzed by HPLC using two methods. The first method followed the same protocol as the one used to analyze NOBE and the results are shown in Table 2.4. The separation factor (α') for the NAG OMNiMIP was determined to be 2.39, indicating a good separation of BOC-Tyr enantiomers; however, this value is lower than the one obtained from imprinting NOBE (using only photo-initiated radical polymerization conditions.)

The successful results obtained using method one initiated further examination of the system. The second method used differed from the typical NOBE analysis. Here, the column

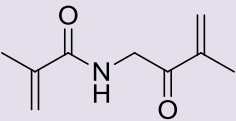
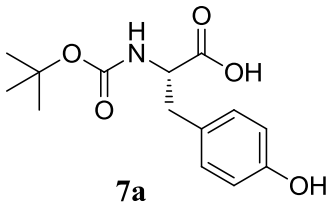
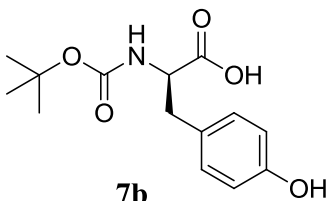
Table 2.4: HPLC results for the OMNiMIPs synthesized from NAG (100 x 2.1 mm column*).

 NAG, 12			
Analyte	RT (min)	k'	α'
1 mM L-BOC-Tyr  7a	35.39	9.79	2.39
1 mM D-BOC-Tyr  7b	16.74	4.10	
*HPLC conditions: 25-37 μm particle size; column size, 100 x 2.1 mm; 99/1 MeCN/AcOH mobile phase; flow rate: 0.1 mL/min; injected volume: 5 μL ; analytes (1mM BOC-L-tyrosine, 1 mM BOC-D-tyrosine, acetone (used to determine void volume)) were all detected at 260 nm.			

length was 50 x 2.1 mm instead of 100 x 2.1 and the flow rate was 0.2 mL/min as opposed to 0.1mL/min. This analysis also examined the analytes at 0.5 mM rather than the 1mM concentrations used during the analysis of NOBE. The results in Table 2.5 show similar enantiomeric selectivity as method 1 with the α' being 2.5. Again, this OMNiMIP generated

from the NAG (**12**) crosslinker was successful at separating enantiomers of BOC-Tyr, but did not improve the current NOBE system.

Table 2.5: HPLC results for the OMNiMIPs synthesized from NAG (50 x 2.1 mm column) ^{*}.

 NAG, 12			
Analyte	RT (min)	k'	α'
Acetone (void volume)	1.03	-	-
0.5 mM L-BOC-Tyr  7a	9.47	8.2	2.5
0.5 mM D-BOC-Tyr  7b	4.48	2.8	
[*] HPLC conditions: 25-37 μ m particle size; column size, 50 x 2.1 mm; 99/1 MeCN/AcOH mobile phase; flow rate: 0.2 mL/min; injected volume: 5 μ L; analytes (0.5 mM BOC-L-tyrosine, 0.5 mM BOC-D-Tyr, acetone (used to determine void volume)); were all detected at 260 nm.			

HPLC results (Table 2.4 and Table 2.5) using NAG as chromatographic stationary phase for enantiomeric separations showed that although it performs better as an OMNiMIP than many other crosslinking monomers, such as the trifunctional and altered polymerizable group monomers, it did not out perform NOBE at separating BOC-Tyr enantiomers. The lower

selectivity could be attributed to the formation of the polymer. Unlike the NOBE OMNiMIP, which was completely polymerized into a crosslinked network by photo-initiated radical polymerization, the NAG polymer did not photo polymerize as an OMNiMIP as effectively. The “jelly” nature of the NAG polymer that was formed from photo-initiated polymerization was not applicable for analysis on HPLC in its current state, so it was subsequently treated under thermal conditions. Although the polymer was hardened, it was not as selective as NOBE using only photo-initiated polymerization. It has been previously reported that imprinted polymers made by thermal polymerization do not imprint as well as those formed by photoradical polymerization due to the enhanced ability for the pre-polymer complex to form at lower temperatures.^{16,17} Thus, a more appropriate comparison of the crosslinkers NAG and NOBE would be to imprint both using a thermal polymerization technique.

2.4 New Crosslinking Monomers Overall Conclusions

Several attempts to improve OMNiMIPs by altering the crosslinking monomer have been explored. The use of two different types of polymerizable groups on a crosslinker; such as, with **13** and **14** did provide a successful system to separate enantiomers of BOC-Tyr ($\alpha' = 1.65 \pm 0.0457$ and 1.89 ± 0.0626 respectively); however, there was no improvement in selectivity in comparison to the model OMNiMIP system made from NOBE, which had an $\alpha' = 3.78 \pm 0.4071$. The outcomes of the radical stabilities of the crosslinkers when undergoing photo-initiated radical polymerization can explain why the OMNiMIPs synthesized from crosslinkers **13** and **14** did not perform as well as NOBE. For example, the stability of the radicals formed could negatively influence the rate of polymerization by causing a delay in the polymerization as well

as resulting in early termination of the polymerization, which in turn can affect polymer morphology and quality of binding sites.

The addition of polymerizable groups was also examined. Here, only molecule **17** was polymerized because the chiral trifunctional monomer **18** was insoluble in polymerization solvents. Although compound **17** did form an OMNiMIP that was selective for L-BOC-Tyr ($\alpha' = 1.2$), it did not improve selectivity of the OMNiMIP model. In this case, the sterics caused by the extra methacrylamide group may have negatively affected the polymer backbone by not enabling the crosslinker to stack. With fewer shape selective binding sites, the separation efficiency diminished. Also, the additional methacrylamide group may have increased non-specific binding interactions, which would also lower the separation effectiveness of the OMNiMIP towards BOC-Tyr.

The addition of electron withdrawing groups to the structure of the NOBE crosslinking monomer was partially investigated in an attempt to improve hydrogen bonding between the monomer and the template and lead to better imprinted cavities. However, crosslinker **19** did not lead to greater selectivity of the imprinted cavities ($\alpha' = 1.08 \pm 0.051$.) Here, bromine may have inhibited photo-initiated radical polymerization of the alkene groups of the crosslinker therefore leading to the formation of a “soft” polymer without shape selective binding sites.

In the case of NAG (**12**), the polymer had to be subjected to a two-step photo-initiated polymerization followed by thermal curing conditions in order to create a solid OMNiMIP that could be studied by HPLC. Although this polymer did have an α' as large as 2.5, it was still unable to outperform NOBE. This could be attributed to the additional harsh thermal polymerization conditions that were required to generate the NAG OMNiMIP. The new

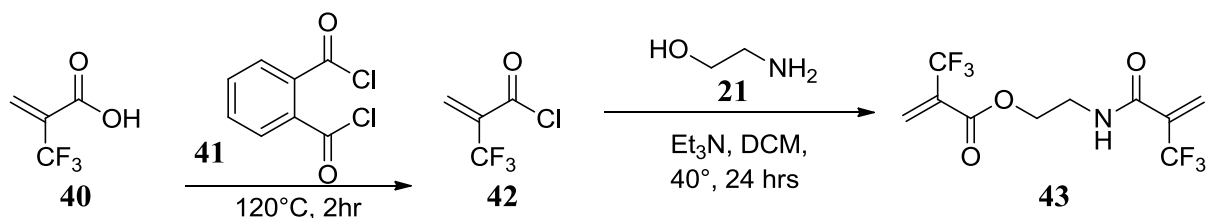
crosslinker **20** was successfully synthesized, but more material is required to test its ability to perform as a crosslinking monomer for OMNiMIP imprinting.

2.5 Future Work

Further work for the new three-armed crosslinker **17** can be explored for improvements in traditional imprinting. While the three-armed crosslinker did not improve OMNiMIP imprinting, it is anticipated that it may perform better in traditional imprinting. The problems of the three-armed monomer with overly dense crosslinking groups will decrease when a separate functional monomer (up to 50%) is added. These new systems can then be compared to traditional systems that utilize MAA as the functional monomer with TRIM as the crosslinker.

Designs for additional crosslinkers for OMNiMIP and traditional imprinting should also be explored. More crosslinkers containing electron withdrawing moieties to enhance hydrogen bonding should be examined. It was ultimately reasoned that the brominated NOBE derivative **19** failed to form a well-structured imprinted polymer because of its polymerization inhibition. Utilization of other electron withdrawing groups, such as CF_3 may provide the desired increase in hydrogen bonding without interfering with the polymerization of the OMNiMIP.

Literature precedent for the addition of phthalyl dichloride to 2-(trifluoromethyl)acrylic acid to form 2-(trifluoromethyl)acryloyl chloride followed by addition of a primary alcohol to form an ester is available.¹⁰ However, the addition of 2-(trifluoromethyl)acryloyl chloride to ethanolamine to form both ester and amide linkages has not yet been successfully achieved. Optimization of the conditions shown in Scheme 2.9 or a different synthetic route are required to generate the trifluorinated crosslinker 2-(2-(trifluoromethyl)acrylamido)ethyl 2-(trifluoromethyl)acrylate (**43**.)

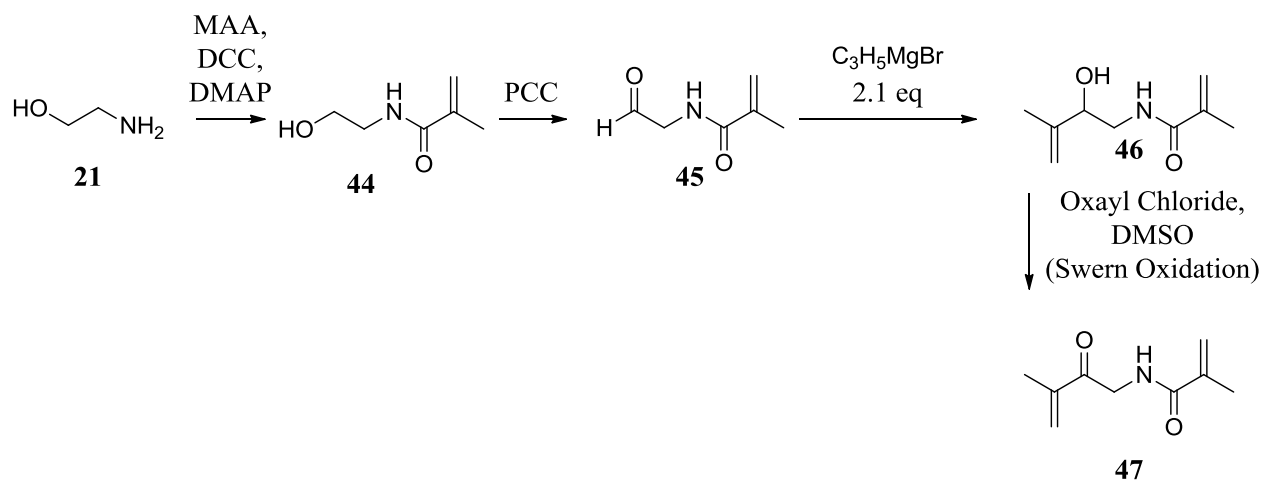


Scheme 2.9: Synthesis of the crosslinker 2-(2-(trifluoromethyl)acrylamido)ethyl 2-(trifluoromethyl)acrylate (43).

The nature of the OMNiMIP polymerizations should also further be explored. When comparing the selectivity of the imprinted material, NOBE has shown to be the best crosslinker for OMNiMIP imprinting synthesized by photo-initiated radical polymerizations reported thus far.^{4,13} When NOBE OMNiMIPs were made thermally, poor results were obtained. Obtaining efficient OMNiMIPs by thermal polymerization would have several advantages, such as elimination of the requirement of expensive photoreactor equipment or a radical initiator. Since NAG has shown success in OMNiMIP imprinting by utilization of a combination of photoradical and thermal polymerization it should be studied further using only thermal polymerization. Another study that should be explored is a combination of photoradical and thermal polymerizations to synthesize NOBE OMNiMIPs to determine if there are any improvements that can be made to its synthetic process. The combination of thermal and photo-initiated radical polymerization as well as the exclusively using thermal polymerizations in relation to selectivity can be compared between the NOBE and NAG OMNiMIPs.

With additional thermal polymerization studies being performed on OMNiMIPs synthesized from the NAG crosslinker, a higher yielding synthetic route to synthesize NAG should be developed. One alternative route to synthesize NAG is as follows: First couple methacrylic acid to the amine in the presence of DCC and DMAP. Next, oxidize the alcohol of **44** to the aldehyde using pyridinium chlorochromate (PCC) A Grignard reaction on the aldehyde

followed by a Swern oxidation with oxalyl chloride in DMSO will yield NAG as shown in Scheme 2.10. This synthesis is expected to be higher yielding and therefore more efficient as it has a simplified Grignard reaction than the previous approach to synthesize NAG.



Scheme 2.10: Synthesis of the crosslinker N-(3-methyl-2-oxobut-3-en-1-yl)methacrylamide (47).

2.6 References

1. Jenkins, A., Reactivity in conventional radical polymerization. *Chem. Listy* **2008**, *102*, 232-237.
2. Chan, G. Y. N.; Kambouris, P. A.; Looney, M. G.; Qiao, G. G.; Solomon, D. H., Approaches to the controlled formation of network polymers:: 2. Studies of hybrid crosslinking agents. *Polymer* **2000**, *41* (1), 27-34.
3. Sibrian-Vazquez, M.; Spivak, D. A., Characterization of molecularly imprinted polymers employing crosslinkers with nonsymmetric polymerizable groups. *Journal of Polymer Science Part A: Polymer Chemistry* **2004**, *42* (15), 3668-3675.
4. Sibrian-Vazquez, M.; Spivak, D. A., Molecular Imprinting Made Easy. *Journal of the American Chemical Society* **2004**, *126* (25), 7827-7833.
5. Sibrian-Vazquez, M.; Spivak, D. A., Enhanced Enantioselectivity of Molecularly Imprinted Polymers Formulated with Novel Cross-Linking Monomers. *Macromolecules* **2003**, *36* (14), 5105-5113.

6. Sibrian-Vazquez, M.; Spivak, D. A., Improving the Strategy and Performance of Molecularly Imprinted Polymers Using Cross-Linking Functional Monomers. *The Journal of Organic Chemistry* **2003**, *68* (25), 9604-9611.
7. Yan, H.; Row, K. H., Characteristic and synthetic approach of molecularly imprinted polymer. *Int. J. Mol. Sci.* **2006**, *7*, 155-178.
8. Kempe, M., Antibody-Mimicking Polymers as Chiral Stationary Phases in HPLC. *Analytical Chemistry* **1996**, *68* (11), 1948-1953.
9. Yu, C.; Mosbach, K., Insights into the origins of binding and the recognition properties of molecularly imprinted polymers prepared using an amide as the hydrogen-bonding functional group. *J Mol Recognit* **1998**, *11*, 69-74.
10. Hosoya, A.; Hamana, H.; Takani, A.; Narita, T., Synthesis and polymerization of novel fluoroalkyl 2-trifluoromethylacrylate possessing tetrahydrofuran moiety. *Journal of Polymer Science Part A: Polymer Chemistry* **2011**, *49* (23), 5129-5131.
11. Piletsky, S. A.; Mijangos, I.; Guerreiro, A.; Piletska, E. V.; Chianella, I.; Karim, K.; Turner, A. P. F., Polymer Cookery: Influence of Polymerization Time and Different Initiation Conditions on Performance of Molecularly Imprinted Polymers. *Macromolecules* **2005**, *38* (4), 1410-1414.
12. LeJeune, J.; Spivak, D., Chiral effects of alkyl-substituted derivatives of N,O-bismethacryloyl ethanolamine on the performance of one monomer molecularly imprinted polymers (OMNiMIPs). *Analytical and Bioanalytical Chemistry* **2007**, *389* (2), 433-440.
13. LeJeune, J. Design and Development of Chiral and Achiral Molecularly Imprinted Stationary Phases. Louisiana State University, Baton Rouge, 2010.
14. Sadykov, Z. M.; Mukhamediev, M. G.; Musaev, U. N., Synthesis of N-acryloyloxyethylacrylamide. *Russ. J. Org. Chem.* **2002**, *38*, 1204.
15. Detz, R. J.; Abiri, Z.; le Griel, R.; Hiemstra, H.; van Maarseveen, J. H., Enantioselective Copper-Catalysed Propargylic Substitution: Synthetic Scope Study and Application in Formal Total Syntheses of (+)-Anisomycin and (-)-Cytosazone. *Chemistry – A European Journal* **2011**, *17* (21), 5921-5930.
16. Yan, H.; Row, K., Characteristic and Synthetic Approach of Molecularly Imprinted Polymer. *International Journal of Molecular Sciences* **2006**, *7* (5), 155-178.
17. O'Shannessy, D. J.; Ekberg, B.; Mosbach, K., Molecular imprinting of amino acid derivatives at low temperature (0°C) using photolytic homolysis of azobisnitriles. *Analytical Biochemistry* **1989**, *177* (1), 144-149.

CHAPTER 3: RACEMIC AND SCALEMIC IMPRINTING

3.1 Introduction to Racemic and Scalemic Imprinting

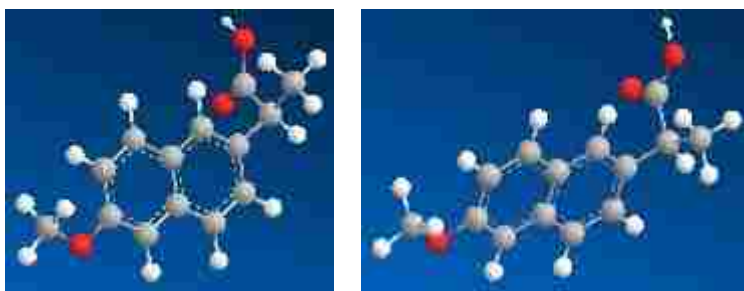
Approximately 50% of all pharmaceutical drugs used today are chiral molecules.¹ Therapeutic effects can be explored for each enantiomer of chiral molecules to determine their individual effectiveness in biological systems if incorporated into drugs. Each enantiomer of the chiral molecule may provide the same or different magnitudes of pharmaceutical benefits or toxic side effects. For example, one enantiomer could be active while the other is inactive, or one could be therapeutic while the other enantiomer is harmful.^{2,3,4} Which effects result from chiral molecules is dependent on the individual recognition and reaction of the enantiomer with the biological system.³ Although not all enantiomers will cause harmful side effects, having inactive forms will still increase the weight of the drug formulation and lower the amount of valuable medicine that can be loaded. Furthermore, the reason that enantiomers may behave differently in the body is due to

their differences in configuration.

While chiral molecules have the same molecular formula, the spatial arrangement of atoms

differs. For example, the

enantiomers 2-(6-methoxynaphthalen-2-yl) propanoic acid (a) and (-)-*R*-2-(6-methoxynaphthalen-2-yl) propanoic acid (b) are shown in



(a)

(b)

Figure 3.1: (+)-*S*-2-(6-methoxynaphthalen-2-yl) propanoic acid (a) and (-)-*R*-2-(6-methoxynaphthalen-2-yl) propanoic acid (b).

propanoic acid are shown in

Figure 3.1. Here, differences in spatial configurations cause differences in drug effectiveness.

The *S* enantiomer of 2-(6-methoxynaphthalen-2-yl) propanoic acid, also known as naproxen, is a

beneficial pharmaceutical used to treat fever and pain, while the *R* enantiomer causes harmful side effects.⁵

Another example of the importance of separating enantiomers is shown throughout asymmetric syntheses.^{6,7} Many reactions, such as S_N1 type reactions, can produce a racemic mixture of products.⁸ The ability to separate the chiral mixtures formed to obtain enantiopure products is crucial in the advancement of synthetic methods. Developing improved separation methods will not only simplify numerous purifications that are often required in multi-step syntheses, but new approaches will also allow mixtures of enantiomers that had previously been deemed inseparable to be separated.

As the importance of enantiomeric separations is growing, more techniques are being developed to isolate enantiomers.¹ Pirkle and other chiral affinity columns are often used to separate mixtures of enantiomers.^{9,10} Although these columns can be useful in separating enantiomers, there are many disadvantages. These columns often cost thousands of dollars. Also, the analytes that can be separated by these columns are very specific, requiring the purchase of many different chiral columns for use in multi-step syntheses.

Molecularly imprinted polymer columns are useful stationary phases for chromatography because they are made from inexpensive materials, straightforward to synthesize, and are tolerant to a range of conditions such as variable pH and temperature changes. Abundant with advantages, MIPs are not found overwhelmingly in the literature for chiral separations in large part because of a lack of templates used to synthesize them. Currently, almost all of the chiral imprinting papers published use a single enantiomer as the print molecule.^{11,12,13,14} Although imprinting a single enantiomer has applications in sensors and other recognition devices, its utility in preparative chromatographic separations of enantiomers is limited. The problem

associated with imprinting a single enantiomer is the requirement to have the enantiopure enantiomer in order to use it as a template for imprinting. If one was already able to isolate the print molecule needed to make the MIP, then synthesizing a chromatographic MIP column to isolate that enantiomer would not be as important.

Imprinting different molecules that have similar shapes and stereo-structures is one way MIPs have been synthesized to overcome the disadvantage of needing an enantiopure print molecule identical to the compound desired to be separated. Several papers have been published that use the cross-reactivities of similar compounds to separate racemic mixtures.^{15,16,17,18} In one paper, the authors imprinted similarly structured melamines (Figure 3.2) substituted with alkyl groups; such as, triethylmelamine (TEM, **48**), triisopropylmelamine (TPM, **49**), and tributylmelamine (TBM, **50**) to form recognition cavities for atrazine herbicides. It was important to use the cross-reactivities of the alkyl substituted melamines for selectivity of

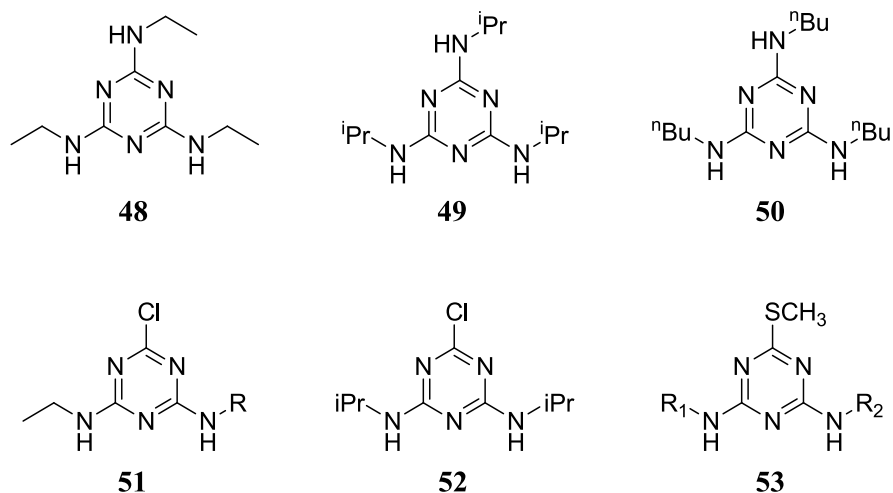


Figure 3.2: Structures of alkyl substituted melamines: triethylmelamine (48), triisopropylmelamine (49), tributylmelamine (50), atrazine (R= iPr) (51), simazine (R= Et) (51), cyanazine (R= C(CH₃)₂CN) (51), terbutylazine (R= tBu) (51), propazine (52), and ametryn (R₁= Et R₂= iPr) (53), prometryn (R₁= iPr R₂= iPr) (53), terbutryn (R₁= Et R₂= tBu) (53).

atrazine (Figure 3.2, **51**) and not atrazine itself because of concerns of template leaching interfering with quantitative measurements. In this study, MIPs synthesized using TEM as the template, in comparison to the other template molecules explored, had the best selectivity for atrazine. The better selectivity obtained using TEM was attributed to the smaller steric interferences caused by its smaller alkyl appendages. Furthermore, the cross-reactivity of TEM afforded binding cavities that most closely fit atrazine. Although it is possible to achieve selectivity for atrazine when imprinting a dummy molecule, its separation is less successful compared to imprinting the actual atrazine molecule.¹⁸

Another approach to separate racemic mixtures without using an enantiopure molecule as the template is to imprint a mixture of enantiomers. This technique eliminates the need to do cross-reactivity studies of multiple compounds with different molecular formulas while also eliminating enantiomer pre-isolation, which both enhance the efficacy of the MIP stationary phase for preparative chromatographic separations. Although this technique exists, only a handful of papers (discussed below) have been published in the past twenty years that attempt to imprint racemic mixtures, and there are currently no papers published on scalemic imprinting.^{19,20,21}

In 1998, the first reported racemic imprint was completed by Hosoya and co-workers.¹⁹ Here, the authors used (*S*)-(-)-*N*-methacryloyl-1-naphthylethylamine (Figure 3.3, **54**) as the

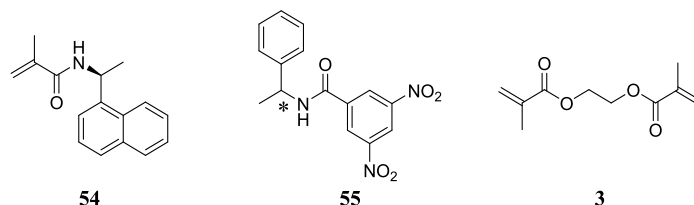


Figure 3.3: (*S*)-(-)-*N*-methacryloyl-1-naphthylethylamine (**54**), *N*-(3,5-Dinitrobenzoyl)- α -methylbenzylamine (**55**), and ethylene dimethacrylate (**3**).

chiral functional monomer and ethylene dimethacrylate (Figure 3.3, **3**) as the crosslinker to imprint a racemic mixture of N-(3,5-Dinitrobenzoyl)- α -methylbenzylamine (DNB (**55**), Figure 3.) In this case, the authors obtained a partial, but not baseline separation of DNB enantiomers using HPLC. Here, the authors only mention that the partial separation of DNB enantiomers is attributed to the more desirable interactions of the template and recognition cavity upon re-binding compared to the non-imprinted control, which showed no separation.

In a later paper by Torres et al., the authors imprinted a racemic mixture of bis[1-phenylethyl]amine (PEA) using the chiral functional monomer (*S*)-2-(2-methylacryloylamino)-3-phenyl propionic acid (MAPP)

and EGDMA as the crosslinker (Figure 3.4).²⁰

This paper also presented partial separation of enantiomers when the MIP was used as a chromatographic stationary phase for HPLC. In this case, the authors studied the mechanisms leading to enantiomeric separation through

computational studies of the template and functional monomer in the pre-polymer complex as well as adsorption isotherms of the imprinted

polymer and template. The results of the computational analysis of the pre-polymer complexes did not show any preference in binding of the functional monomer to either enantiomer. The authors' results from the binding isotherms showed that the small differences in the stability of

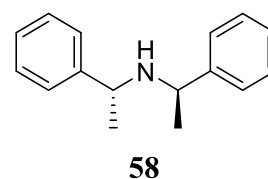
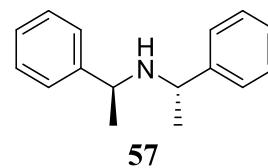
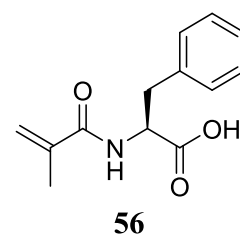
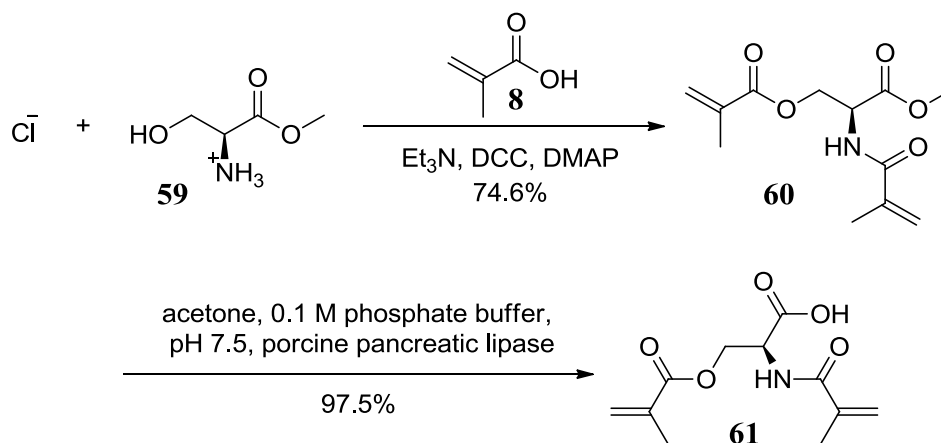


Figure 3.4: (*S*)-2-(2-methylacryloylamino)-3-phenyl propionic acid (**56**), *S*-bis[1-phenylethyl]amine (**57**), and *R*-bis[1-phenylethyl]amine (**58**).

the diastereomeric complexes of the template and functional monomer on the polymer's surface upon re-binding may be the cause of the observed enantioseparation.

A third publication briefly mentions the attempt to resolve enantiomers using an imprinted polymer made with a racemic print molecule.²¹ In this study, the sterics of OMNiMIP crosslinking monomers were first studied in the formation of OMNiMIPs that were imprinted with single enantiomers. (*S*)-2-methacrylamidopropyl methacrylate (L-NALA), the least sterically hindered chiral OMNiMIP which performed the best in single enantiomer imprinting, was used to attempt racemic imprinting. In this experiment, the chiral monomer was unable to generate a MIP that resolved enantiomers and had an $\alpha = 1.0$ indicating no selective recognition. Further studies of this crosslinking monomer as well as another chiral crosslinking monomer, 2-methacrylamido-3-(methacryloyloxy)propanoic acid (NOS, **61**), in regards to racemic imprinting are the topics of Chapter Three. The concept of imprinting a scalemic mixture, which has never been shown in the literature, is also presented using the L-NALA crosslinking monomer for OMNiMIP imprinting.

3.2 Experimentals: Syntheses of Crosslinking Monomers and OMNiMIP Polymerizations



Scheme 3.1: Synthesis of NOS (**61**).

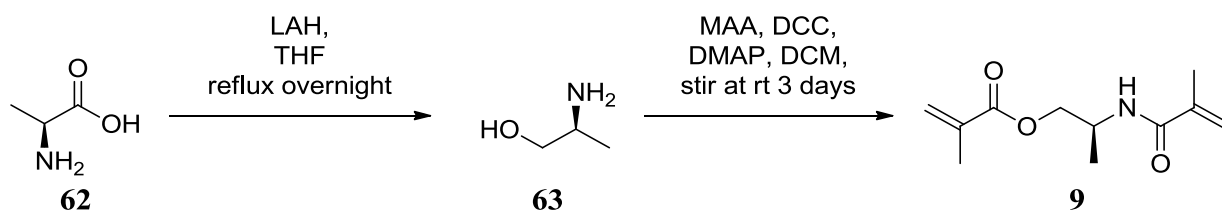
2-methacrylamido-3-methoxy-3-oxopropyl methacrylate (**60**):²²

L-Serine methyl ester hydrochloride (2.0230g, 13.0 mmol) in 100 mL DCM was cooled to 0°C. Et₃N (3.6 mL, 26.0 mmol) was added dropwise. In a separate roundbottom flask, MAA (2.2 mL, 26 mmol) and DMAP (0.3177 g, 2.6 mmol) in 25 mL dry DCM was cooled to 0°C. After both mixtures equilibrated to 0°C, the L-serine methyl ester hydrochloride solution was added to the MAA and DMAP solution. After 5 minutes, DCC (5.4083 g) in 25 mL DCM was added slowly. The reaction mixture was stirred at 0°C and was allowed to slowly cool to room temperature. The mixture stirred at room temperature for 5 days. The DCU was filtered off to give a yellow solution. The yellow solution was extracted with 0.5 M NaHCO₃ (aq) (2 x 75 mL) then 0.5 M sodium citrate (aq) (2 x 75 mL). The organic layer was dried over MgSO₄ and was filtered. Evaporation afforded the crude product as a yellow oil. Column chromatography using EtOAc/hexane (50/50) was used to purify the sample. The pure product (**60**) obtained was a yellow oil (2.4749 g) in 74.6% yield. ¹H NMR (CDCl₃, 400 MHz) δ ppm 6.70 (br, 1H), 6.08 (s, 1H), 5.76 (s, 1H), 5.60-5.59 (d, 1H J= 4Hz), 5.41 (s, 1H), 4.95-4.91 (m, 1H), 4.57-4.46 (m, 2H), 3.79 (s, 3), 1.98 (s, 3H), 1.91 (s, 3H). ¹³C NMR (CDCl₃, 100MHz) δ ppm 170.07, 167.92, 166.96, 139.17, 135.54, 126.57, 120.71, 64.08, 52.90, 52.09, 18.43, 18.20. IR ν_{max} 3365.33, 2956.86, 1724.59, 1668.25, 1626.80, 1521.83, 1163.51, 1019.28, 943.85.

2-methacrylamido-3-(methacryloyloxy)propanoic acid (**61**):²²

NOS-methyl ester (**60**, 1.3433 g, 5.3 mmol) was dissolved in 20 mL acetone in an amber bottle. 168 mL of 0.1 M phosphate buffer, pH 7.5, was added. Porcine pancreatic lipase EC 232-619-3087 (0.4267 g) was added and the mixture was sonicated for one minute. The reaction was rocked for 4 days at room temperature. 1 N HCl (aq) was added to acidify the mixture to pH

3, and it was extracted with EtOAc (4 x 100 mL.) The combined organic layers were dried with MgSO₄ and were filtered. After evaporation, the product (**61**, 1.2383 g) was collected in 97.5% yield. ¹H NMR (CDCl₃, 400 MHz) δ ppm 10.64 (br, 1H), 6.89-6.87 (d, 1H, J = 7.28 Hz), 6.08 (s, 1H), 5.78 (s, 1H), 5.58-5.57 (t, 1H, J = 1.42 Hz), 5.40 (s, 1H), 4.94-4.90 (m, 1H), 4.56-4.55 (d, 2H, J = 3.88 Hz), 1.95 (s, 3H), 1.89 (s, 3H). ¹³C NMR (CDCl₃, 100 MHz) δ ppm 171.71, 168.83, 167.18, 138.63, 135.48, 126.72, 121.61, 63.90, 52.26, 18.32, 18.13. IR ν_{max} 3401.69, 2959.39, 1717.91, 1653.46, 1623.43, 1539.49, 1166.75, 1021.11, 945.17. HRMS (ESI-TOF): C₁₁H₁₅NO₅ (M+Na)⁺: calcd for 264.0848; found 264.0685.



Scheme 3.2: Synthesis of L-NALA (9).

(*S*)-alaninol (**63**):²¹

Dry THF (200 mL) was cooled to 0°C. LAH (6.2820 g, 0.17 mol) was added and the temperature was allowed to equilibrate. *S*-alanine (9.8695 g, 0.11 mol) was added slowly. The mixture was refluxed overnight. Sat. potassium carbonate (aq) (20 mL) was added to quench the reaction. After vacuum filtration, the THF was removed to yield a colorless oil (4.5864 g, 55% yield.) ¹H NMR (CDCl₃, 400 MHz) δ ppm 3.55 (m, 1H), 3.23 (m, 1H), 3.01 (m, 1H), 2.01 (br, 3H), 1.06 (s, 3H). ¹³C NMR (CDCl₃, 100 MHz) δ ppm 68.27, 48.22, 20.09.

(*S*)-2-methacrylamidopropyl methacrylate (**9**):²¹

S-alaninol (**63**, 0.2626 g, 3.5 mmol) in 30 mL DCM was cooled to 0°C. MAA (0.6810 g, 7.9 mmol) and DMAP (0.1061 g, 0.87 mmol) were added and the temperature was allowed to equilibrate for 5 minutes. DCC (1.6317 g, 8.1 mmol) was added and the mixture was allowed to slowly warm to room temperature and was stirred for 3 days. After the DCU was filtered off, the material was washed with 1N HCl (aq) (3 x 20 mL) and sat. NaHCO₃ (aq) (4 x 20 mL). The combined organic layers were dried over MgSO₄ and the solvent was evaporated after filtration. Purification by column chromatography with 50/50 EtOAc/hexane was completed to yield 434.5 mg, 59% yield of (*S*)-2-methacrylamidopropyl methacrylate (**9**.) ¹H NMR (CDCl₃, 400 MHz) δ ppm 6.12 (s, 1H), 6.01 (br, 1H), 5.99 (s, 1H), 5.66 (s, 1H), 5.59 (s, 1H) 4, 4.39-4.36 (m, 1H), 4.16-4.09 (m, 2H), 1.94 (s, 6H), 1.24 (d, 3H, 4Hz). ¹³C NMR (CDCl₃, 100MHz) δ ppm 171.14, 167.89, 140.02, 135.93, 126.16, 119.51, 67.10, 44.89, 18.56, 18.27, 17.31.

Polymer Preparation:

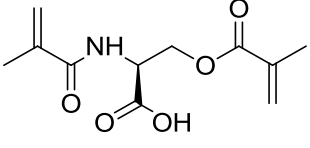
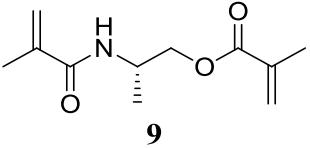
Crosslinking monomer (1 g, **61** or **9**) was added to the 13 x 100 mm glass tube with a solution of racemic 1,2-diphenyl ethylene-diamine (**61** templates) or racemic BOC-Tyr (**9** templates) (5%) dissolved in 1.3 mL acetonitrile to mimic conditions that were previously explored using single enantiomers.^{13, 22} AIBN (1%) was added to the solution and nitrogen was used to purge the sample for 5 minutes. The tube was then capped, and Teflon tape and Parafilm were used to seal the system. The tube was then inserted into a photoreactor apparatus where it was submerged in an ethylene glycol/H₂O bath to maintain the temperature and was exposed to a 450 W mercury arc lamp surrounded by a borosilicate jacket for 8 hours. The polymer was then broken out of the tube and the template was removed by Soxhlet extraction for 2 days. The

polymers were then ground and sized to 25-37 μm using U.S.A. Standard Testing Sieves and was packed into stainless steel columns and their selectivities were analyzed by HPLC.

3.3 Racemic and Scalemic Template Imprinting Results and Discussion

The performance of chiral OMNiMIPs synthesized using racemic templates was examined as stationary phases for HPLC. The results of the separation of enantiomers of 1, 2-diphenyl ethylene-diamine (**64** and **65**) and BOC-Tyr (**7**) when the analytes are studied individually using NOS and L-NALA as the crosslinking monomer in the OMNiMIP formulation is shown in Table 3.1. In the case of NOS, mobile phases composed of 90% MeCN

Table 3.1: Racemic Imprinting HPLC Results *

Templates:			
Monomer	k'_{64} ^(a) or D-BOC-Tyr ^(b)	k'_{65} ^(a) or L-BOC-Tyr ^(b)	α'
 <p>61 (a)</p>	0.34 ^(a)	0.55 ^(a)	1.6
 <p>9 (b)</p>	4.48 ^(b)	2.87 ^(b)	1.6

*HPLC conditions: 25–37 μm particles; 100 x 2.1 (a), 250 x 2.1 (b) columns; mobile phase, MeCN/acetic acid (90:10 (a), 99:1 (b)); analytes (1mM **64**, 1mM **65**, 1mM BOC-L-tyrosine, 1 mM BOC-D-tyrosine, acetone (used to determine void volume)) were all detected at 260 nm; flow rate 0.1 mL/min; sample volume injected 5 μL .

and 10% acetic acid (method 1) as well as 99% MeCN and 1% acetic acid (method 2) were studied. The analyses from both mobile phases resulted in the analytes eluting near the dead volume. Method 1 resulted in a small difference in capacity factors between the enantiomers whereas method 2 did not display any variation. The small capacity factors (k' 0.34 and 0.55) that were obtained on the NOS OMNiMIPs are not reliable because these values are not significantly different from the amount of error that may appear in these measurements. The selectivity factor for the OMNiMIP synthesized using L-NALA was determined to be 1.6 with capacity factors of 4.48 and 2.87 for the D and L enantiomers respectively. Here, the capacity factors larger than 1.0 acquired from the HPLC experiments using the L-NALA OMNiMIP are more reliable because each analyte eluted at a much later retention time than the void volume, indicating that it had better binding to the stationary phase and differed greatly from any error that may occur in the measurements.

The HPLC conditions for the OMNiMIP generated from L-NALA were thoroughly examined in an attempt to improve enantioseparation resolution of the analytes when they were run as a pair (Figure 3.5.) The effects of mobile phase polarity were first explored using 5 and 10% acetic acid in acetonitrile as the mobile phase; however, the ability to separate enantiomers of BOC-Tyr diminished. This is because the higher concentrations of acetic acid disrupted the ability of the analytes to bind well to the stationary phase, which forced the analytes to elute quickly from the chromatographic column and not separate from each other as indicated by the lower capacity factors in Figure 3.5. At 0.5 and 1% acetic acid in acetonitrile, the analytes were shown to have better resolution. The better selectivity is achieved because the acetic acid is not in a high enough concentration to disrupt the hydrogen bonding between the analyte and the imprinted polymer. Although there was a slightly better selectivity of enantiomers using 0.5%

acetic acid, 1% was chosen to proceed with the study because it provided a comparable separation with faster elution times.

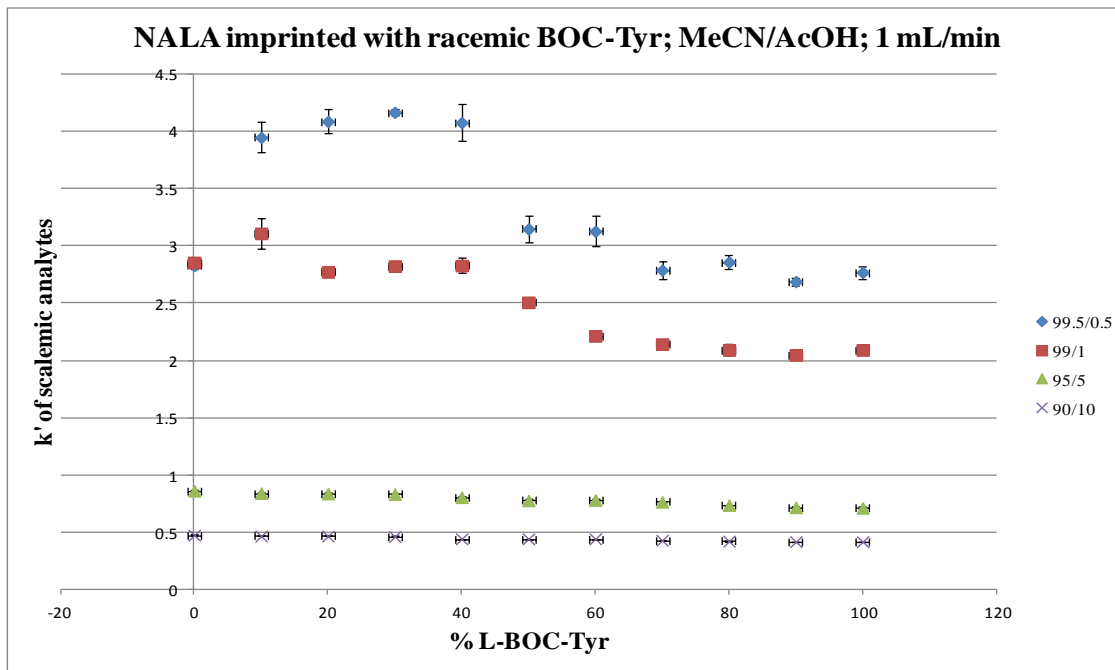


Figure 3.5: L-NALA imprinted with racemic BOC-Tyr (7) Mobile Phase Polarity Studies.

*HPLC conditions: particle size 25–37 μm ; column, 50 x 4.1; mobile phase, MeCN/acetic acid (99:1); analytes (1mM BOC-L-tyrosine, 1 mM BOC-D-tyrosine, acetone (used to determine void volume)) were all detected at 260 nm; flow rate 1 mL/min; the sample volume injected was 5 μL .

Next, the amount of imprinted packing material was increased in attempt to improve enantiomeric resolution. Columns with 100 x 2.1 mm, 50 x 4.1, and 250 x 2.1 mm dimensions were packed with the L-NALA OMNiMIP stationary phase. Although there was a small improvement in resolution using 2.5 times the imprinted material, the cost of requiring more imprinted material outweighed the benefit of the diminutive improved selectivity; therefore, it was decided that the 100 x 2.1 mm column size was sufficient to be used in further studies of the

racemic imprinted material. After optimization of conditions, the best selectivity achieved is shown by the chromatogram in Figure 3.6. Although baseline resolution is not achieved, it is comparable in resolution to the few imprinted systems that are presented in the literature (discussed previously.)

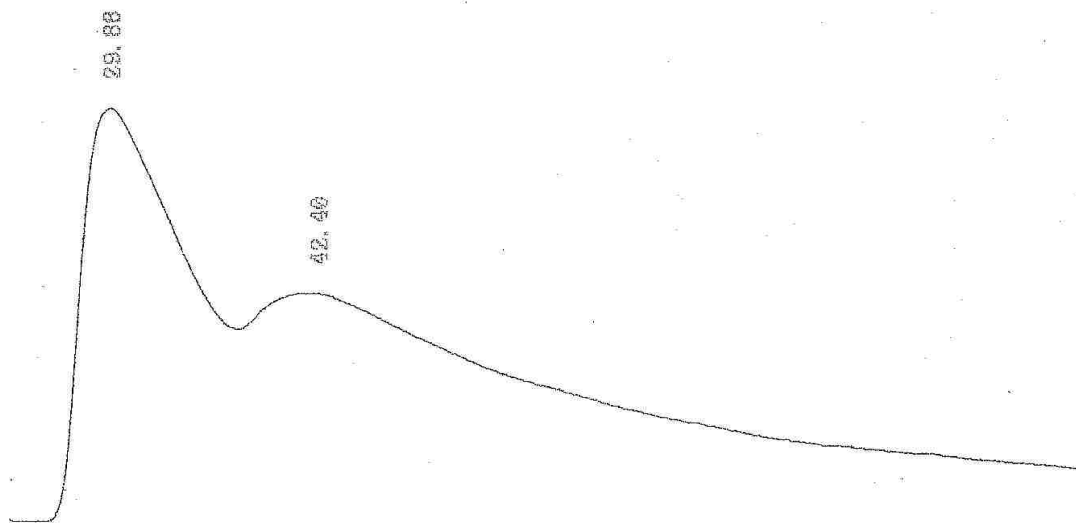


Figure 3.6: Chromatogram of racemic (7) imprinted polymer using L-NALA*.

*HPLC conditions: particle size 25–37 μm ; column, 250 x 2.1; mobile phase, MeCN/acetic acid (99:1); analytes (1mM Boc-L-tyrosine, 1 mM Boc-D-tyrosine, acetone (used to determine void volume)) were all detected at 260 nm; flow rate 0.1 mL/min; sample volume injected 5 μL .

After conditions were optimized, a cascade of scalemic analytes was tested on the L-NALA racemic OMNiMIP column (Figure 3.7) to determine if separation of scalemic analytes could be achieved and to determine the elution order. Partial separation was achieved for all scalemic analytes tested and the most retained enantiomer was determined to be D-BOC-Tyr. To explore reproducibility, nine additional OMNiMIPs were prepared using the crosslinking monomer L-NALA and the print molecule racemic BOC-tyrosine. These OMNiMIPs were also

evaluated by HPLC and the results showed that the elution order did not always favor the D enantiomer being most retained; therefore, while mixtures of enantiomers can be separated using this racemic imprinted system, the stereochemistry of the separated enantiomer must be determined.

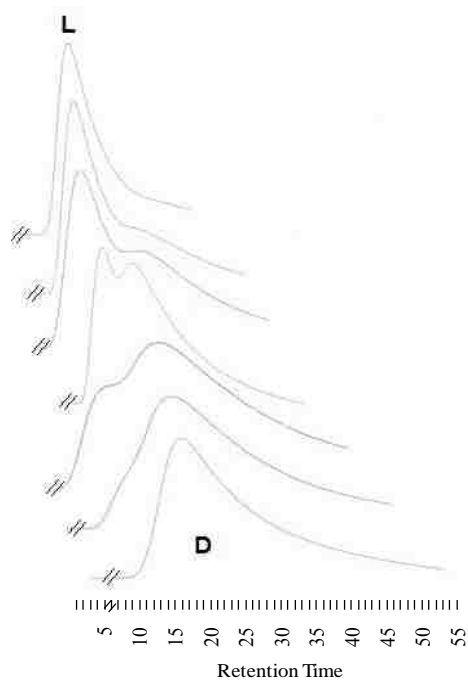


Figure 3.7: Scalemic analytes on L-NALA racemic imprinted polymer*.

*HPLC conditions: particle size 25–37 μm ; column, 100 x 2.1; mobile phase, MeCN/acetic acid (99:1); analytes (1mM Scalemic Mixtures of BOC-Tyrosine, acetone (used to determine void volume)) were all detected at 260 nm; flow rate 0.1 mL/min; sample volume injected 5 μL .

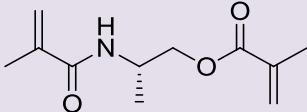
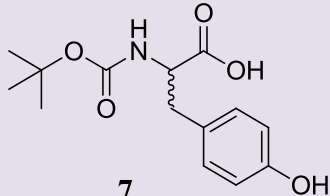
It should also be noted that the two peaks resulting from the chromatograms of analytes containing separated enantiomers are, in fact, the individual enantiomers and not just a complexation of the two enantiomers. This was validated not only by the cascade of chromatograms showing the ratios of peaks increasing and decreasing upon percentage changes

of enantiomer in the analytes, but also by NMR studies. According to a paper by Sellegren and Mosbach, ^1H NMR can be used to provide evidence for hydrogen bonding interactions between template and monomer in pre-polymer complex solutions.²³ In a similar manner, if complexes formed between the D and L enantiomers, they would also be expected to display differences in chemical shifts. Analysis by ^1H NMR was first carried out separately for D-BOC-Tyr (16 mg) in 0.5 mL acetonitrile and acetic acid (100/0 and 99/1) and L-BOC-Tyr in acetonitrile and acetic acid (100/0 and 99/1). The chemical shift results of the NH proton of single enantiomers of BOC-Tyr were then compared to spectra obtained for a racemic mixture of BOC-Tyr in both acetonitrile and acetic acid (100/0 and 99/1) and the spectra are shown in Appendix B. The differences in chemical shifts were ≤ 0.005 ppm in all cases when studied using 100% MeCN and ≤ 0.015 ppm in all cases when studied using 99/1 MeCN/AcOH. Since there was no significant change in the chemical shifts of the NH proton of the single enantiomer and racemic mixture of BOC-Tyr, it was concluded that a complex between the D and L BOC-Tyr enantiomers was not formed in the pre-polymer complex or the analyte solutions. As a comparison, the crosslinking monomer L-NALA (40 mg) and each enantiomer of the BOC-Tyr template (1:1 monomer:template and 1:2 monomer:template) were also studied (spectra are shown in Appendix B) in acetonitrile and acetic acid (100/0 and 99/1.) The NH protons shifted by at least 0.1 ppm in all cases, signifying that non-covalent interactions were present, thus the basis for the formation of imprinted sites in the polymer.

After successfully partially resolving BOC-Tyr enantiomers using racemic imprinting, scalemic mixtures as print molecules were explored using L-NALA as the crosslinker to synthesize OMNiMIPs. OMNiMIPs were imprinted with either 25% L-BOC-Tyr and 75% D-BOC-Tyr or 25% D-BOC-Tyr and 75% L-BOC-Tyr, and chromatographic evaluation revealed

that the polymers separated single enantiomers of BOC-Tyr with separation factor values of 1.7 and 1.5 respectively as shown in Table 3.2.

Table 3.2: Scalemic Imprinting HPLC Results*.

 9 (Crosslinker)			
 7 (Template)	k'_D	k'_L	α'
25% L 75% D	3.64	2.13	1.7
75% L 25% D	2.53	3.81	1.5

*HPLC conditions: particle size 25–37 μm ; column 100 x 2.1; mobile phase, MeCN/acetic acid (99:1); analytes (1mM BOC-L-tyrosine, 1 mM BOC-D-tyrosine, acetone (used to determine void volume)) were all detected at 260 nm; flow rate 0.1 mL/min; sample volume injected 5 μL .

The ability to separate mixtures of BOC-Tyr at different percentages of each enantiomer in the analyte was also studied. Figure 3.8 shows chromatograms obtained from the elution of several different analyte mixtures containing different percentages of enantiomers on the 25% L 75% D-BOC-Tyr OMNiMIP columns. Here, the chromatograms show the partial separation of BOC-Tyr enantiomers as different percentages of enantiomer in each analyte were tested. As expected, L-BOC-Tyr elutes quicker than D-BOC-Tyr on this chromatographic stationary phase because the template used contained 75% D-BOC-Tyr and 25% L-BOC-Tyr and in accord with chromatographic theory, molecules that fit into more binding sites will be retained longer.

Similarly, analyte mixtures were studied on the 25% D and 75% L-BOC-Tyr OMNiMIP columns. In this case, the L-BOC-Tyr analyte displayed a longer retention time compared to the D-BOC-Tyr because there were more chromatographic recognition sites accessible for the L enantiomer to specifically bind in comparison to those available to the D enantiomer.

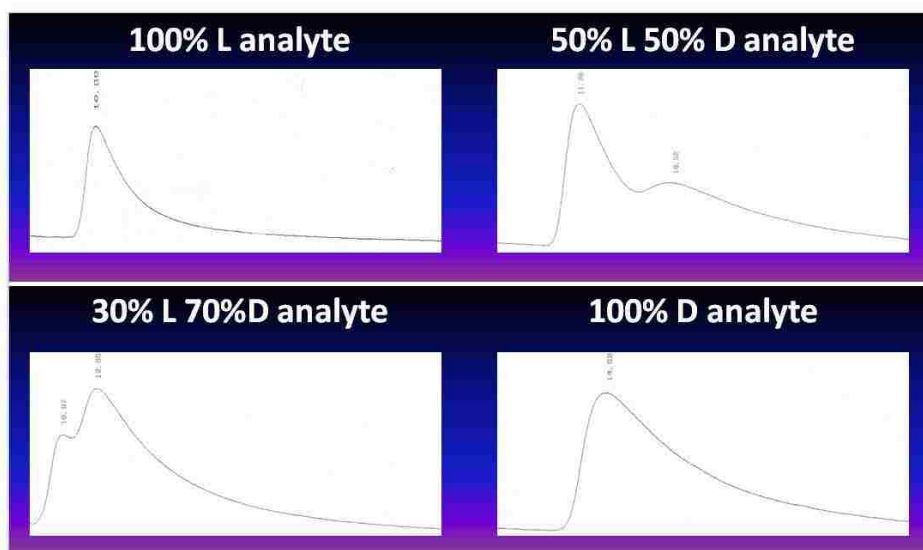


Figure 3.8: Scalemic Imprinted Chromatograms*.

*HPLC for **9** imprinted with 25% L 75% D BOC-Tyr; HPLC conditions: 25–37 μm particles; column 100 x 2.1; MeCN/acetic acid (99:1); analytes (1mM BOC-tyrosine analytes, acetone (used to determine void volume)) were detected at 260 nm; flow rate 0.1 mL/min; sample volume injected 5 μL .

The effects of temperature were also examined to determine if resolution of enantiomers could be improved on the scalemic imprinted columns. The columns were tested at 25°C, 40°C, and 55°C. As temperature was increased, the analytes tested eluted in a shorter amount of time as shown in Figure 3.9. Slight differences in resolution are due to the mass transfer changes that occur when temperature is increased. An increased temperature causes mass transfer to occur more quickly so that less time is needed for the analyte to equilibrate between the mobile phase and stationary phase. Although faster mass transfer equilibration can lead to a better resolution,

the increased temperature did not lead to any significant improvement in resolution. The lack of improvement can be attributed to increased longitudinal diffusion and these results are shown in Figure 3.9. Because there was no significant improvement of resolution achieved by increasing the temperature, all future studies were carried out at room temperature. Another important observation is the elution order of the enantiomers based on the HPLC column temperature. While the focus of this study was improvement of resolution by altering the temperature, it is interesting to note that the elution order may have changed when the temperature was raised from 40°C to 55°C as indicated by the chromatograms. Since a poor baseline was obtained for the chromatogram at 55°C, further studies would need to be completed to confirm that the elution order did in fact change.

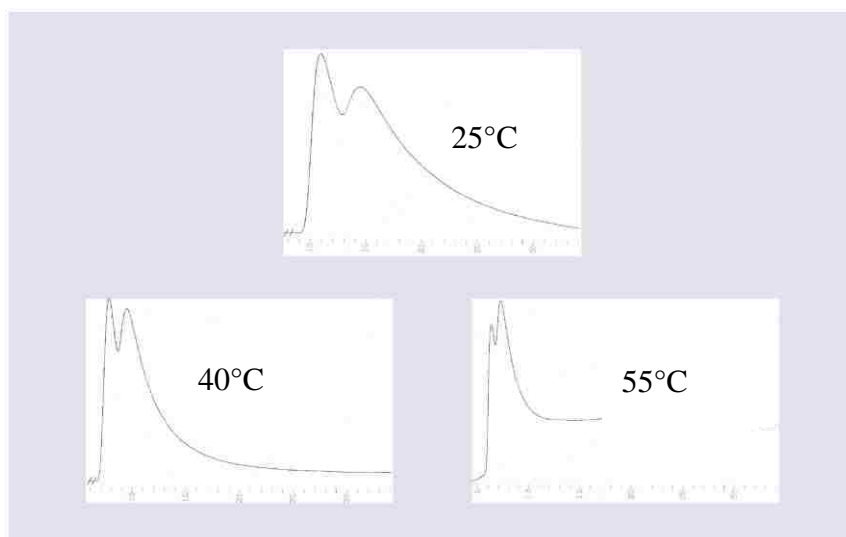


Figure 3.9: Temperature Experiments on 75% L and 25% D-BOC-Tyr Imprinted Columns.

*HPLC for monomer **9** imprinted with 75% L 25% D BOC-Tyr; HPLC conditions: particle size 25–37 μm ; column 100 x 2.1; mobile phase, MeCN/acetic acid (99:1); analytes (1mM racemic BOC-tyrosine analyte, acetone (used to determine void volume)) were all detected at 260 nm; flow rate 0.1 mL/min; sample volume injected 5 μL .

3.4 Racemic and Scalemic Imprinting Conclusions

Not only does imprinting racemic and scalemic templates allow MIPs to be useful stationary phases for preparative chromatographic separations, it also simplifies the overall general approach to imprinting polymers. As seen throughout Chapters 1 and 2, the simplification and improvement of chiral separations is an important and ongoing task for chromatographers using molecular imprinting worldwide. Using the OMNiMIP technique as opposed to the traditional non-covalent imprinting approach that utilizes a separate functional monomer and crosslinker was one way to make imprinting easier. The ability to imprint mixtures of enantiomers rather than an isolated enantiomer is another extremely important and useful approach that provides an exponentially wider range of chiral molecules to be separated using imprinted polymers.

Racemic imprinting using either L-NALA (**9**) or NOS (**61**) as the crosslinking monomers for synthesizing OMNiMIPs has shown partial separation of enantiomers. Both L-NALA and NOS OMNiMIPs showed selectivity when enantiomers were run individually on HPLC stationary phase. L-NALA was able to achieve a partial separation of enantiomers while NOS was completely unable to separate enantiomers when the analytes for HPLC contained various mixtures of BOC-Tyr enantiomers. Further studies using the monomer L-NALA to imprint scalemic mixtures were also investigated. In this study, imprinted polymers made using scalemic mixtures composed of 75% D-BOC-Tyr and 25% L-BOC-Tyr or 75% L-BOC-Tyr and 25% D-BOC-Tyr were used to study scalemic analytes. In both cases partial separation of enantiomers was achieved; and although baseline resolution would be optimal, a partial separation is still useful in chromatographic separations. For example, some enantiopure

material can be collected at the beginning and end of a HPLC run and the remaining mixture can be run again for further separations.

3.5 Racemic and Scalemic Imprinting Future Work

Further work studying the conditions during the photo-initiated radical polymerizations of L-NALA should be completed to determine which enantiomer becomes more selective during racemic imprinting. Studies that vary the temperature of the solution at -20°C to 20°C during polymerization should be examined to determine if these conditions alter the properties of the resulting racemic imprinted polymer. Once these conditions are evaluated, the optimum conditions for selective binding can be applied to scalemic imprinting. The optimized conditions could then be used to study different ratios of scalemic templates in the pre-polymer solution. The different ratios of scalemic templates evaluated by HPLC will show at what point resolution diminishes from the single imprinted molecule. This information will give valuable insight on the capacity of racemic and scalemic imprinting.

3.6 References

1. Sekhon, B. S., Enantioseparation of chiral drugs - an overview. *Int. J. PharmTech Res.* **2010**, 2, 1584-1594.
2. Davies NM, T. X., Importance of Chirality in Drug Therapy and Pharmacy Practice: Implications for Psychiatry. *Advances in Pharmacy* **2003**, 1 (3), 242–252.
3. Caldwell, J., The importance of stereochemistry in drug action and disposition. *J Clin Pharmacol* **1992**, 32, 925-9.
4. Caner, H.; Groner, E.; Levy, L.; Agranat, I., Trends in the development of chiral drugs. *Drug Discovery Today* **2004**, 9 (3), 105-110.

5. Yang, Y.; Su, B.; Yan, Q.; Ren, Q., Separation of naproxen enantiomers by supercritical/subcritical fluid chromatography. *Journal of Pharmaceutical and Biomedical Analysis* **2005**, *39* (3–4), 815-818.
6. Vegman, M.; Carmeli, S., Eight micropeptins from a *Microcystis* spp. bloom collected from a fishpond near Kibbutz Lehavot HaBashan, Israel. *Tetrahedron* **2013**, *69*, 10108-10115.
7. Bonney, K. J.; Braddock, D. C., A Unifying Stereochemical Analysis for the Formation of Halogenated C15-Acetogenin Medium-Ring Ethers From *Laurencia* Species via Intramolecular Bromonium Ion Assisted Epoxide Ring-Opening and Experimental Corroboration with a Model Epoxide. *J. Org. Chem.* **2012**, *77*, 9574-9584.
8. Guindon, Y.; Frenette, R.; Fortin, R.; Rokach, J., Direct synthesis of thio ethers from thiols and alcohols. *J. Org. Chem.* **1983**, *48*, 1357-9.
9. Dorsey, J. G.; Cooper, W. T.; Siles, B. A.; Foley, J. P.; Barth, H. G., Liquid Chromatography: Theory and Methodology. *Analytical Chemistry* **1998**, *70* (12), 591-644.
10. Görög, S.; Gazdag, M., Enantiomeric derivatization for biomedical chromatography. *Journal of Chromatography B: Biomedical Sciences and Applications* **1994**, *659* (1–2), 51-84.
11. Qin, L.; He, X.-W.; Li, W.-Y.; Zhang, Y.-K., Molecularly imprinted polymer prepared with bonded β -cyclodextrin and acrylamide on functionalized silica gel for selective recognition of tryptophan in aqueous media. *Journal of Chromatography A* **2008**, *1187* (1–2), 94-102.
12. Suedee, R.; Songkram, C.; Petmoreekul, A.; Sangkunakup, S.; Sankasa, S.; Kongyarit, N., Direct enantioseparation of adrenergic drugs via thin-layer chromatography using molecularly imprinted polymers. *Journal of Pharmaceutical and Biomedical Analysis* **1999**, *19* (3–4), 519-527.
13. Sibrian-Vazquez, M.; Spivak, D. A., Molecular Imprinting Made Easy. *Journal of the American Chemical Society* **2004**, *126* (25), 7827-7833.
14. Meador, D. S.; Spivak, D. A., Absolute Configuration Determination Using Enantiomeric Pairs of Molecularly Imprinted Polymers. *Organic Letters* **2014**, *16* (5), 1402-1405.
15. Matsui, J.; Fujiwara, K.; Takeuchi, T., Atrazine-selective polymers prepared by molecular imprinting of trialkylmelamines as dummy template species of atrazine. *Anal. Chem.* **2000**, *72*, 1810-1813.
16. Huang, B.-Y.; Chen, Y.-C.; Liu, C.-Y., An insight into the mechanism of CEC separation of template analogues on a norepinephrine-imprinted monolith. *J. Sep. Sci.* **2011**, *34*, 2293-2300.
17. Simon, R.; Collins, M. E.; Spivak, D. A., Shape selectivity versus functional group pre-organization in molecularly imprinted polymers. *Anal. Chim. Acta* **2007**, *591*, 7-16.

18. Matsui, J.; Miyoshi, Y.; Doblhoff-Dier, O.; Takeuchi, T., A molecularly imprinted synthetic polymer receptor selective for atrazine. *Anal. Chem.* **1995**, *67*, 4404-8.
19. Hosoya, K.; Shirasu, Y.; Kimata, K.; Tanaka, N., Molecularly Imprinted Chiral Stationary Phase Prepared with Racemic Template. *Analytical Chemistry* **1998**, *70* (5), 943-945.
20. Torres, J. J.; Gsponer, N.; Ramírez, C. L.; Vera, D. M. A.; Montejano, H. A.; Chesta, C. A., Experimental and theoretical studies on the enantioselectivity of molecularly imprinted polymers prepared with a chiral functional monomer. *Journal of Chromatography A* **2012**, *1266* (0), 24-33.
21. LeJeune, J.; Spivak, D., Chiral effects of alkyl-substituted derivatives of N,O-bismethacryloyl ethanolamine on the performance of one monomer molecularly imprinted polymers (OMNiMIPs). *Analytical and Bioanalytical Chemistry* **2007**, *389* (2), 433-440.
22. Sibrian-Vazquez, M.; Spivak, D. A., Improving the Strategy and Performance of Molecularly Imprinted Polymers Using Cross-Linking Functional Monomers. *The Journal of Organic Chemistry* **2003**, *68* (25), 9604-9611.
23. Sellergren, B.; Lepistoe, M.; Mosbach, K., Highly enantioselective and substrate-selective polymers obtained by molecular imprinting utilizing noncovalent interactions. NMR and chromatographic studies on the nature of recognition. *J. Am. Chem. Soc.* **1988**, *110*, 5853-60.

CHAPTER 4: EXPLORATION OF ABSOLUTE CONFIGURATION USING AN ENANTIOMERIC PAIR OF MOLECULARLY IMPRINTED POLYMERS

4.1 Introduction to the Determination of Absolute Configuration

In the mid 1800's, Louis Pasteur proposed that molecular asymmetry of molecules causes their ability to display distinct optical activity. In 1874, LeBel and van't Hoff further suggested that molecules possessed three-dimensional shapes, and that asymmetric molecules may rotate a plane of polarized light based on their spatial structure.^{1,2} Since the proposal of the tetrahedral structure of sp^3 hybridized carbons, the determination of which stereoisomer is present in a sample has been the subject of extensive research. The identification of absolute configuration (AC) is important in both academia and industry because molecules with different spatial features cause them to display various characteristics (e.g. the *S* enantiomer of thalidomide causes teratogenic effects while the *R* enantiomer acts as a sedative) as previously discussed in chapter three.^{3,4,5,6,7,8,9}

As an ongoing problem among scientists, the determination of absolute stereochemical configuration of compounds is continuously being developed using fundamental and technological approaches. There are several techniques that are currently employed to determine stereochemistry; such as, x-ray crystallography which can be used to directly determine absolute configuration from molecular 3-D structures. One large advantage of this method is that neither prior knowledge (e.g. binding strengths) nor both pairs of enantiomers is required to determine absolute configuration. However, a large drawback to this technique is that it requires the ability to form a crystal of the desired molecule and most compounds do not crystallize; therefore all oils and liquids are unable to be studied by this approach. In addition, the requirement of

expensive equipment and skilled technicians to perform the x-ray crystallographic experiments is a disadvantage.¹⁰

Another approach to determine absolute configuration is the Mosher method, which uses the chiral derivitizing agent α -methoxy- α -trifluoromethylphenylacetic acid (Figure 4.1) to react with alcohols and amines to determine their absolute configurations. The esters and amides produced from the derivatization reaction are then studied by NMR. The diastereomeric complexes

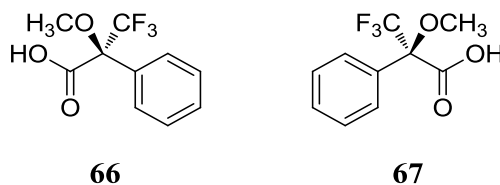


Figure 4.1: *S* (66) and *R* (67) α -methoxy- α -trifluoromethylphenylacetic acid (MTPA) (Mosher's acid).

display different ^1H and or ^{19}F NMR shifts for each diastereomer and these chemical shift differences allow the stereochemistry to be determined.¹¹ Although this method is reliable, it requires the synthesis or purchase of Mosher's acid, a nucleophile (e.g. $-\text{OAc}$ or $-\text{NH}_2$), and a synthetic step to perform the derivatization on each compound of interest. The required reactions using this reagent are similar for other chiral derivatization agents (when they are available), which makes these approaches disadvantageous.¹²

Vibrational circular dichroism (VCD) and Raman optical activity are two optical methods used to determine absolute configuration of molecules.^{13,14,15} In both cases vibrational energies cause a change in dipole moment. The square of the dipole moment change and its interactions with a magnetic component is proportionate to IR intensity in VCD. The interactions of the magnetic component that cause a change in polarizability are studied in optical activity and the square of these values is proportionate to Raman intensity.¹³ A large disadvantage of these methods is that the enantiomeric pair, known literature values, or computational analysis is required for comparison.

Recent papers published by Rychnovsky and co-workers explore another technique to determine absolute configuration, which they named competing enantioselective conversions (CEC).^{16,17,18,19,20} In these papers, the authors studied the rate of reaction between the molecule with unknown stereochemistry and each enantiomer of a chiral catalyst to determine the absolute stereochemistry. For example, both enantiomers of Birman's acylation catalyst homobenzotetramisole (HBTM (**68**), Figure 4.2) are used to determine the absolute configuration

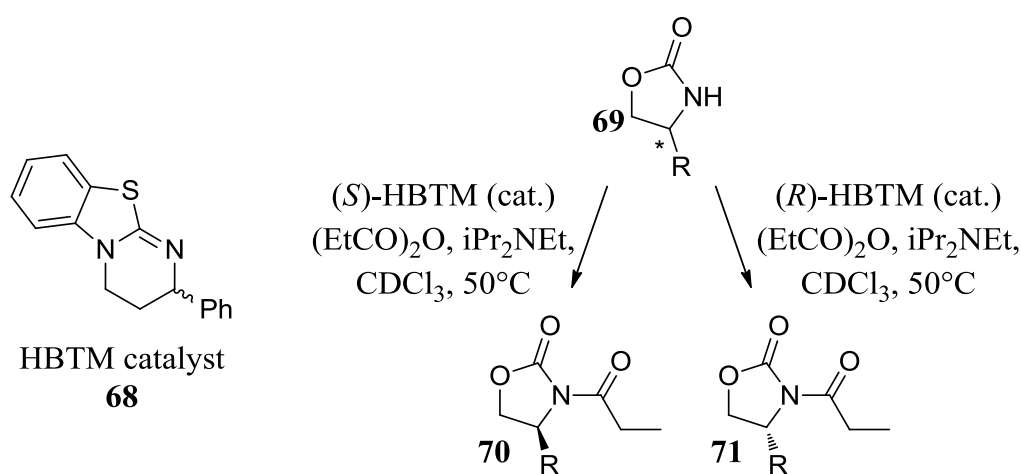


Figure 4.2: The catalyst homobenzotetramisole (HBTM) is used for CEC analysis. The molecule with the *R* group (alkyl group) forward reacts faster with the *S* catalyst compared to the *R* catalyst. The molecule with the *R* group (alkyl group) pointing backwards reacts faster with the *R* catalyst than the *S* catalyst. The difference in reaction rates of each enantiomer with the enantiomerically pure catalyst enables stereochemical determination.

of oxazolidinones and lactams.^{18,21} Advantages of this method are that only one enantiomer of the desired unknown compound is needed to determine its stereochemistry and this technique can be performed on a nanomolar scale. A great disadvantage to this approach however is the need to perform several reactions with the molecule containing unknown stereochemistry. First the molecule with unknown stereochemistry must be reacted with both enantiomers of the catalyst to determine the reactions rates. After the reaction rates with the catalyst are studied and

the absolute stereochemical configuration is determined, additional reactions are then required to convert the unknown molecule back to its original form if the product of the CEC analysis was not the desired overall product.

The use of chiral chromatography is another approach used to explore absolute configuration of molecules.^{22,23} Chiral chromatography has primarily been most useful for the separation of enantiomers and determination of % ee. With respect to AC determination, chiral chromatography has only been shown to identify stereochemistry when in combination with other analytical techniques or from examination of the elution order of each enantiomer with prior literature knowledge of their retention behaviors. In fact, a recent publication states, “Chiral chromatography will never be able to assign the absolute configuration of a single enantiomer without information about the retention of the second one. Therefore, it will not be possible to determine the absolute configuration of a single optically pure product...”.²² In Chapter Four, a solution to this conundrum is presented. The approach presented here uses molecularly imprinted polymer chiral stationary phases to determine absolute stereochemistry.²⁴ This method has several advantages, one being that it requires only one enantiomer for stereochemical determination, similar to Rychnovsky’s CEC approach, which also required only a single enantiomer. Unlike the CEC and other derivatization methods, the new MIP technique to determine AC has the advantage that it does not require any reactions to be executed on the enantiomer of interest. This method also does not require highly sophisticated instruments as with x-ray crystallography or any literature precedents for the molecule with unknown stereochemistry.

The goal of this project was to develop a new technique to determine the absolute configuration of organic molecules. This approach utilized two MIP stationary phase HPLC

columns, coined “DuoMIPs” to determine stereochemistry. Here, each MIP was imprinted with a generic template print molecule bearing either *R* or *S* stereochemistry. Analytes that include and differ from the print molecule were run on each enantiomeric DuoMIP column. The retention on each column was subsequently studied and the absolute configuration of the analyte was determined based on the energetic differences of the diastereomeric complexes formed between the analyte and the DuoMIPs. A mnemonic was also developed to aid in the understanding of the stereochemical determination. This new approach has the advantage that it only requires one enantiomer with unknown stereochemistry and does not require any reactions to be performed on the molecule of interest.

4.2 DuoMIP Design and Synthesis*

Due to larger uptake capacity and good recognition abilities, the OMNiMIP approach was selected to synthesize the DuoMIPs for exploration of AC determination. The crosslinking monomer along with the print molecule and its percentage in the polymer formulation were important design features examined. In most cases, NOBE was enlisted as the chemical crosslinking monomer for OMNiMIP imprinting. Another DuoMIP system was synthesized using the chiral monomer *S*-NALA with *R* or *S*-BOC-Tyr as the print molecules to study AC determination. NOBE DuoMIPs were synthesized using *R* or *S*-BOC-Tyr, *R* or *S*-BOC-Phe, *R* or *S*-BOC-Phe-OMe, or *R* or *S*-4-benzyl-2-oxazolidinone as the print molecules (Figure 4.3.) An

*Reprinted with permission from *Organic Letters* **2014** 16 (5), 1402-1405. Copyright 2014 American Chemical Society.

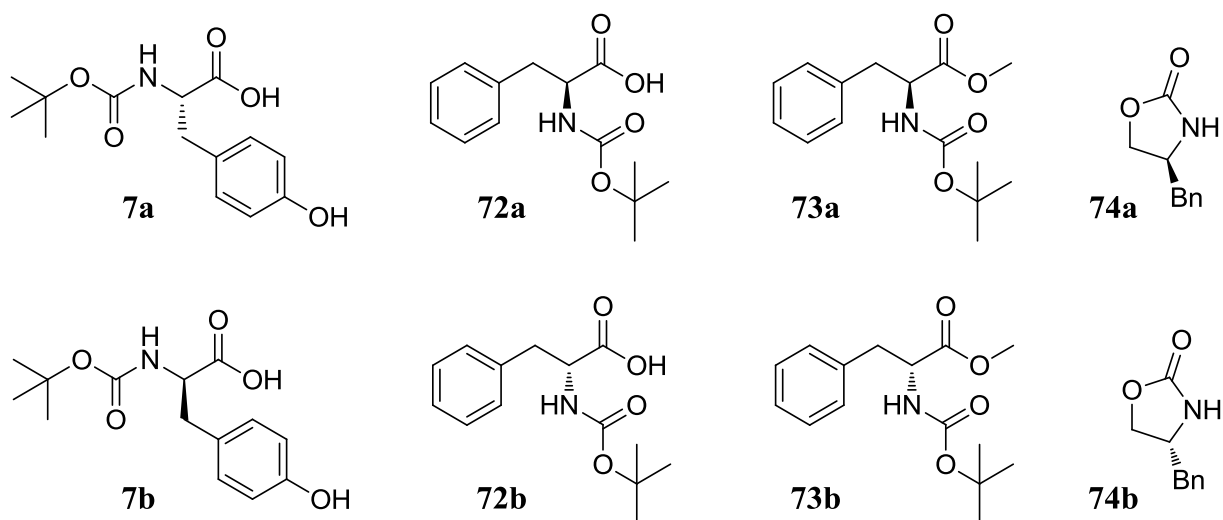
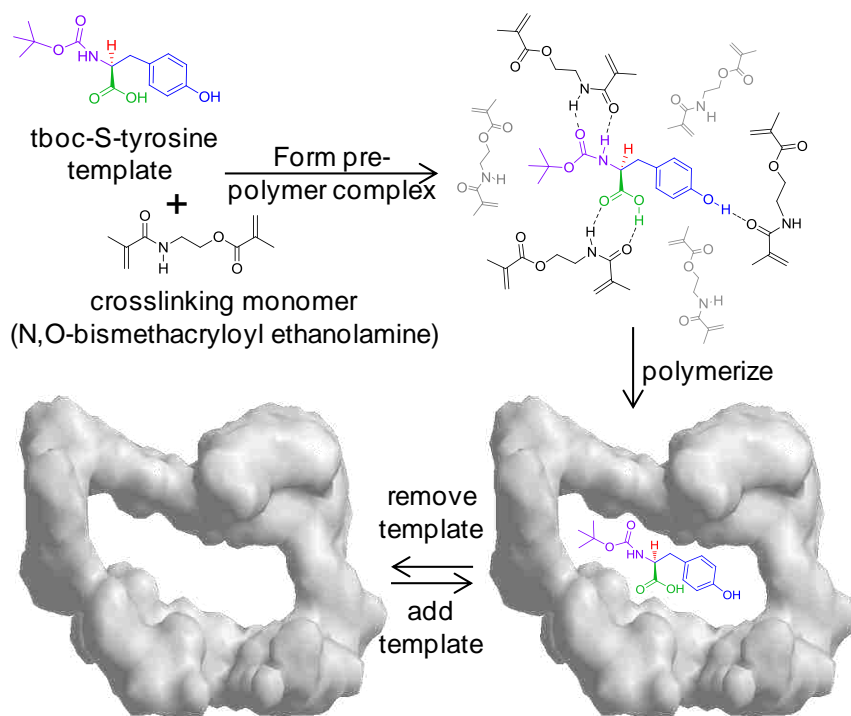


Figure 4.3: Structures of print molecules used for the DuoMIP syntheses: *S*-BOC-Tyr (7a), *R*-BOC-Tyr (7b), *S*-BOC-Phe (72a), *R*-BOC-Phe (72b), *S*-BOC-Phe-OMe (73a), *R*-BOC-Phe-OMe (73b), *S*-4-benzyl-2-oxazolidinone (74a) and *R*-4-benzyl-2-oxazolidinone (74b).

example of the synthesis of the *S*-MIP binding cavity of the DuoMIP system using NOBE as the crosslinking monomer and *S*-BOC-Tyr as the print molecule is illustrated in Scheme 4.1.



Scheme 4.1: Synthesis of the *S*-MIP of DuoMIP System

A simple mnemonic was developed to aid in the understanding of the DuoMIP system of AC determination (depicted in Figure 4.4.) Contributions by both hydrogen bonding and steric

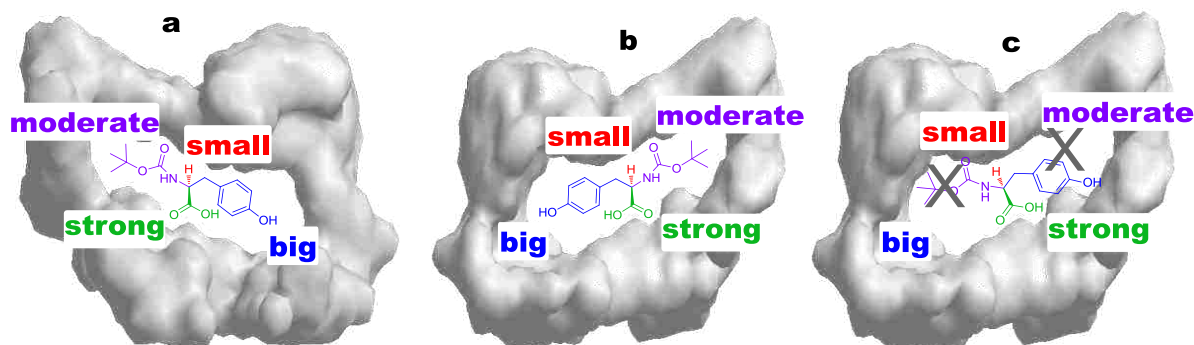


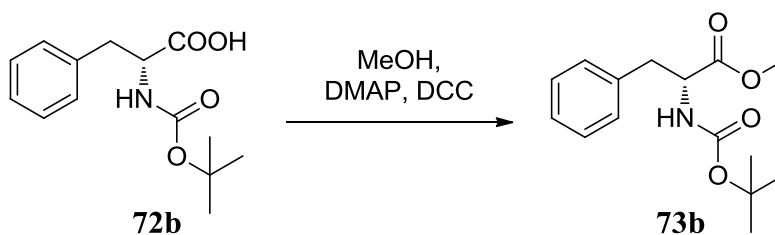
Figure 4.4: DuoMIP system. *S*-BOC-Tyr fits into the *S*-BOC-Tyr imprinted site (a), *R*-BOC-Tyr fits into the *R*-BOC-Tyr imprinted site (b), and *S*-BOC-Tyr does not fit into the *R*-BOC-Tyr imprinted site (c).

interactions are the key influences of this mnemonic. Labels such as strong, moderate, big, and small are used to describe these interactions. The stronger hydrogen bonding group is labeled “strong” and kept forward with respect to the plane of the page, and the weaker is labeled “moderate.” The hydrogen bonding groups are categorized to put the “stronger” in the carboxylate imprinted site and the weaker “moderate” group in the carbamate location. The label “big” denotes larger steric interactions and “small” labels the smaller steric interactions. It is also important to note that the BOC group is not categorized as “big” in spite of being large because of its distant position from the chiral center in the molecule. The BOC group and the stereocenter are three atoms apart and consequently has a smaller effect on enantiomeric stereodifferentiation compared to the aromatic group. Features of an analyte that do not fit the mnemonic and decrease interactions with the DuoMIP are labeled with an “X.” For example, c in Figure 4.4 illustrates the “big” aryl group poorly positioned in the “moderate” space and is labeled with an “X” to denote the lack of fit towards the mnemonic. In particular, this example

of the mnemonic illustrates the NOBE binding cavities of the DuoMIP system created with BOC-Tyr. As depicted, the *S*-BOC-Tyr fits into the *S*-BOC-Tyr imprinted site (Figure 4.4, a) and the *R*-BOC-Tyr fits into the *R*-BOC-Tyr imprinted site (Figure 4.4, b); while the *S*-BOC-Tyr does not fit into the *R*-BOC-Tyr imprinted site (Figure 4.4, c.) The better the fit into an imprinted site signifies better recognition between the analyte and the imprinted site. When the imprinted polymer is used as the stationary phase for HPLC, better binding is indicated by longer retention. Selective binding for molecules that match the mnemonic is the basis for absolute configuration determination, and a set of rules to ensure confidence in the determination has been devised (vide infra).

Synthesis

The NOBE crosslinker was synthesized according to the protocol in Chapter Two. All material used in the polymer formulation was purchased from Sigma-Aldrich and Chem-Impex, except D-BOC-Phe-OMe (**73b**), which was synthesized from the amino acid according to the protocol below (Scheme 4.2).



Scheme 4.2: Synthesis of D-BOC-Phe-OMe.

Synthesis of D-BOC-Phe-OMe (**73b**):

D-BOC-Phe-OH (**72b**, 0.5056 g, 1.9 mmol) was dissolved in 20 mL MeOH and cooled to 0°C. DMAP (30.0 mg, 0.25 mmol, 0.13 eq) was added and the solution was allowed to

equilibrate for 10 minutes. DCC (0.4554 g, 2.2 mmol, 1.15 eq) was added and the solution was slowly warmed to room temperature and stirred overnight. DCU was filtered off and methanol evaporated. The crude product was dissolved in DCM and washed with 0.5 N HCl (aq) (2 x 25 mL) and sat. NaHCO₃ (aq) (3 x 25 mL). The organic layer was dried over MgSO₄, filtered, and the solvent evaporated. The crude product was an oil containing a small amount of solid; by NMR it appeared to contain DCU, so it was filtered again. After drying under high vacuum for two hours, ¹H NMR showed a small amount of impurities remained. A preparatory plate was then run using 50/50 EtOAc/hexanes to afford pure D-BOC-Phe-OMe (**73b**.)

DuoMIP Polymer Formulation:

One example of a DuoMIP synthesis was depicted previously in Scheme 4.1. In all NOBE DuoMIP syntheses completed, the protocol was as follows: NOBE (3 g) was added to a solution of *R* or *S*-BOC-Tyr^a, *R* or *S*-4-benzyl-2-oxazolidinone^b, *R* or *S*-BOC-Phe^c, and *R* or *S*-BOC-Phe-OMe^d (4%^a, 5%^{a,b,c,d}, or 20%^a template) dissolved in 3 mL acetonitrile. AIBN (1%) was added to the solution and this was placed into a 13 x 100 mm glass tube. Nitrogen was used to purge each sample for 5 minutes. After the sample was purged, the tube was capped, and Teflon tape and Parafilm were used to seal the system. The tube was then inserted into a photoreactor apparatus where it was submerged in a H₂O bath to maintain room temperature and was exposed to a 450 W mercury arc lamp surrounded by a borosilicate jacket for 8 hours. The polymer was then broken out of the tube and the template was removed by Soxhlet extraction with methanol for 2 days. The polymers were then ground and sized to 25-37 μm using U.S.A. Standard Testing Sieves and were then packed into 100 x 2.1 mm stainless steel columns and their ability to determine absolute configuration were analyzed by HPLC.

4.3 Results and Discussion of NOBE DuoMIPs*

Each enantiomer of the DuoMIP stationary phases was packed into separate HPLC columns for AC analysis. The difference in retention of the analyte on each of the stationary phases was examined to determine AC. Since a clear difference in binding and selectivity was imperative to this analysis, a set of rules based on these factors were implemented to ensure confidence of the DuoMIP AC determination method. For this system, the capacity factors of the analytes must be greater than 1.0 because values larger than 1.0 indicate the ability of analytes to sufficiently bind the imprinted stationary phases for analysis. Significant binding is important for analysis as acknowledged in 1907 by Paul Ehrlich when he said, “Corpora non agunt nisi fixate,” which is translated to “Substances will not act if they do not bind.”²⁵

Another rule to provide confidence in the analysis of AC fixes the minimum value of a new term, the γ factor. To determine the γ values, the capacity factors of the analyte on each DuoMIP are compared. For analytes that fit the *S* imprinted cavity, the γ factor is defined as the capacity factor of that analyte obtained from the *S* imprinted column (k'_{SMIP}) divided by the capacity factor obtained from the *R* imprinted column (k'_{RMIP}). Conversely, the γ factor for analytes that selectively fit into the *R* imprinted cavities puts the k'_{RMIP} in the numerator and k'_{SMIP} is in the denominator as shown in (Eq. 4.1). For unknown analytes, the larger k' is positioned in the numerator and the smaller in the denominator. Based on similar limits employed by Rychnovsky and coworkers, minimum γ values of 1.2 were established to signify that the analyte's selectivity for one enantiomer of the imprinted polymers is significant beyond error to determine absolute configuration by the DuoMIP system.

*Reprinted with permission from *Organic Letters* **2014** 16 (5), 1402-1405. Copyright 2014 American Chemical Society.

$$\gamma = \frac{k'_{\text{SMIP}}}{k'_{\text{RMIP}}} \quad (\text{or } \gamma = \frac{k'_{\text{RMIP}}}{k'_{\text{SMIP}}}) \quad \text{Eq. 4.1}$$

The k' factor and γ values were used to evaluate all DuoMIPs synthesized, which included polymers made using 4%, 5%, and 20% *R* or *S*-BOC-Tyr as the print molecule. The DuoMIPs synthesized using 4% template displayed low separation factors compared to the DuoMIPs imprinted with higher percentages of template because there were less imprinted sites formed, and DuoMIPs imprinted with 5% BOC-Tyr template displayed partial success. As shown in Table 4.1, the absolute configuration could be determined for the analytes *S*-BOC-Tyr, *R*-BOC-Tyr, *S*-Z-Trp, *S*-Z-Ser, and *S*-2-phenyl glycinol based on the rules pertaining to capacity factor and γ values listed previously. *S*-Z-Phe, *R*-Z-Phe, *R*-Z-Trp, *S*-phenyl lactic acid, *S*-methoxy(trifluoromethyl)phenyl AcOH, *S*-phenyl butyric acid, *R*-phenyl butyric acid, *R*-phenyl butanol, *S*-chloro phenyl ethanol, *R*-chloro phenyl ethanol, *S*-binaphthol, and *R*-binaphthol did not meet the minimum k' and γ requirements required to determine AC, while the incorrect stereochemistry was determined in one case, *R*-Z-Ser.

Table 4.1: NOBE DuoMIPs imprinted with 5% *S*-BOC-Tyr or *R*-BOC-Tyr*

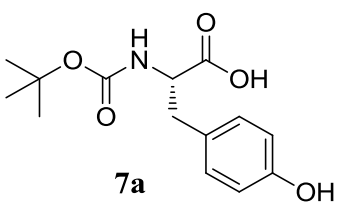
Analyte	k' on <i>R</i> column	k' on <i>S</i> column	γ
 <p>7a</p>	<i>S</i> -BOC-Tyr	1.8	5.6
			3.1

Table 4.1 NOBE DuoMIP imprinted with 5% *S*-BOC-Tyr or *R*-BOC-Tyr continued.

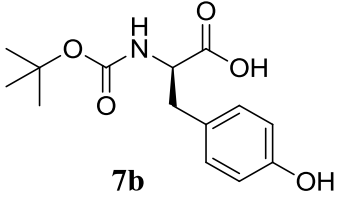
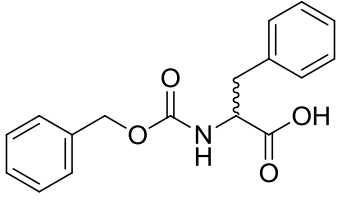
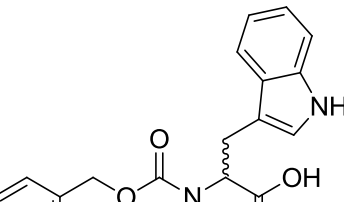
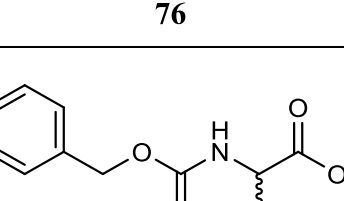
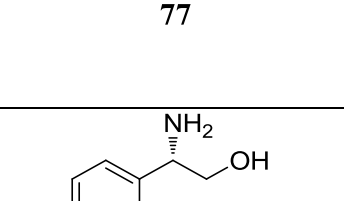
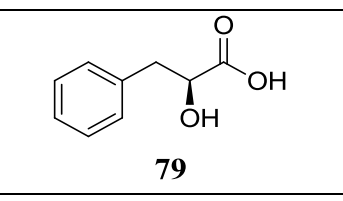
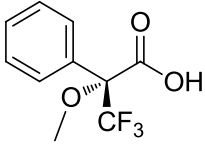
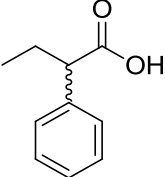
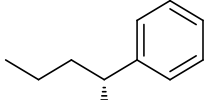
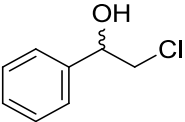
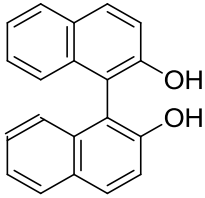
 <p>7b</p>	<i>R</i> -BOC-Tyr	6.9	1.8	3.8
 <p>75</p>	<i>S</i> -Z-Phe	0.6 ^a	0.9 ^a	1.5
	<i>R</i> -Z-Phe	0.7 ^a	0.6 ^a	1.2
 <p>76</p>	<i>S</i> -Z-Trp	1.2	1.6	1.3
	<i>R</i> -Z-Trp	1.4	1.4	1.0 ^b
 <p>77</p>	<i>S</i> -Z-Ser	1.3	1.5	1.2
	<i>R</i> -Z-Ser	1.3	1.5	1.2
 <p>78</p>	<i>S</i> -2-phenyl glycinol	2.2	4.0	1.8
 <p>79</p>	<i>S</i> -phenyl lactic acid	0.7 ^a	0.9 ^a	1.3

Table 4.1 NOBE DuoMIP imprinted with 5% *S*-BOC-Tyr or *R*-BOC-Tyr* continued.

 <p>80</p>	<i>S</i> -methoxy (trifluoro- methyl) phenyl AcOH	0.6 ^a	0.8 ^a	1.3
 <p>81</p>	<i>S</i> -phenyl butyric acid	0.3 ^a	0.3 ^a	1.0 ^b
	<i>R</i> -phenyl butyric acid	0.3 ^a	0.4 ^a	1.3
 <p>82</p>	<i>R</i> -phenyl butanol	0.1 ^a	0.1 ^a	1.0 ^b
 <p>83</p>	<i>S</i> -chloro phenyl ethanol	0.1 ^a	0.1 ^a	1.0 ^b
	<i>R</i> -chloro phenyl ethanol	0.1 ^a	0.1 ^a	1.0 ^b
 <p>84</p>	<i>S</i> -binaphthol	0.5 ^a	0.5 ^a	1.0 ^b
	<i>R</i> -binaphthol	0.5 ^a	0.5 ^a	1.0 ^b

*HPLC conditions: particle size, 25-37 μm; column size, 100 x 2.1 mm; flow rate: 99/1 MeCN/AcOH; 0.1 mL/min; injected volume: 5 μL; analytes/wavelength detection: 5 mM *S*-CBZ-Phe/260 nm, 5 mM *R*-CBZ-Phe/260 nm, 1 mM BOC-*S*-tyrosine/260 nm, 1 mM BOC-*R*-tyrosine/260 nm, 0.2 mM Cbz-*S*-tryptophan/260 nm, 0.2 mM Cbz-*R*-tryptophan/260 nm, 1 mM 0.2 mM (*R*)-(-)-1,1'-bi-2-naphthol/300 nm, 10 mM *S*-2-phenyl-glycinol/262 nm, 5 mM *S*-2-chloro-1-phenyl ethanol/262 nm, 5 mM *R*-2-chloro-1-phenyl ethanol/262 nm, 2 mM *S*-(+)-2-phenyl butyric acid/262 nm, 2 mM *R*-(-)-2-phenyl butyric acid/262 nm, 1 mM *S*-phenyl-lactic acid/262 nm, 1 mM *S*-methoxy (trifluoro-methyl) phenyl acetic acid/262 nm, 1 mM *R*-1-phenyl-

Table 4.1 NOBE DuoMIP imprinted with 5% *S*-BOC-Tyr or *R*-BOC-Tyr* continued.

CBZ- <i>S</i> -serine/260 nm, 1 mM CBZ - <i>R</i> -serine/260 nm, 0.2 mM (<i>S</i>)-(-)-1,1'-bi-2-naphthol/300 nm, 1-butanol/262 nm. ^a The k' does not meet the minimum binding requirements and cannot be used to determine AC. ^b The γ factor is lower than minimum criteria and cannot be used to determine AC.

The partial successes achieved from the NOBE DuoMIP system formed from imprinting 5% *R* or *S*-BOC-Tyr led to the development of another NOBE DuoMIP system where 20% BOC-Tyr template was chosen for the synthesis. It is important to note that the amount of template can be increased to 20% in this system as the OMNiMIP approach to imprinting was used.²⁶ OMNiMIPs allow a greater capacity of print molecule to be used because the polymer consists of 100% of the crosslinking monomer. The addition of a larger amount of template in the construction of the DuoMIPs led to the formation of a greater number of selective and strong binding imprinted cavities, which therefore led to a larger number of successful determinations of absolute configuration.

The results for the determination of AC using NOBE and 20% BOC-Tyr are shown in Table 4.2. Using the 20% imprinted DuoMIP system, the absolute configuration could be accurately determined for *S*-BOC-Tyr, *R*-BOC-Tyr, *S*-Z-Phe, *R*-Z-Phe, *S*-Z-Trp, *R*-Z-Trp, *S*-2-phenyl glycinol, *S*-phenyl lactic acid, and (*S*)-*N*-acetyl-tyrosine as each of these analytes exhibited capacity factors greater than 1.0 and γ values larger than 1.2. The AC of *S*-2-chloro-1-phenyl ethanol, *R*-2-chloro-1-phenyl ethanol, *R*-(-)-*O*-acetyl mandelic acid, *S*-(+)-2-phenyl butyric acid, *R*-(+)-2-phenyl butyric acid, *S*-nicotine, *R*-nicotine, *R*-phenyl butanol, *S*-1,1'-bi-2-naphthol, and *R*-1,1'-bi-2-naphthol could not be determined because these analytes had poor retention to the DuoMIPs (i.e. low k' values.) The AC of *S*-Z-Ser, *R*-Z-Ser, *S*-Naphthylethyl amine, and *R*-naphthylethyl amine were also could not be determined because, although each of these analytes displayed k' values larger than 1.0, the retention on both enantiomers of the

DuoMIPs were similar therefore their γ values were below the 1.2 minimum requirement. It is important to note that there were no incorrect assignments of stereochemistry when the k' and γ criteria for binding and selectivity were followed.

Table 4.2: NOBE DuoMIP imprinted with 20% *S*-BOC-Tyr or *R*-BOC-Tyr*.

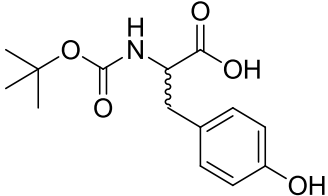
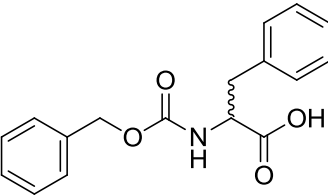
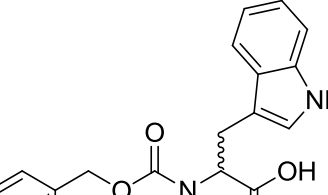
Analytes		k' on L-imprinted column	k' on D-imprinted column	γ
 7	<i>S</i> -BOC-Tyr	15.1	4.1	3.7
	<i>R</i> -BOC-Tyr	4.5	13.0	2.9
 75	<i>S</i> -Z-Phe	1.9	1.5	1.3
	<i>R</i> -Z-Phe	1.6	2.3	1.4
 76	<i>S</i> -Z-Trp	4.0	3.0	1.3
	<i>R</i> -Z-Trp	3.0	3.7	1.2

Table 4.2 NOBE DuoMIP imprinted with 20% *S*-BOC-Tyr or *R*-BOC-Tyr* continued.

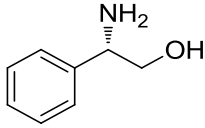
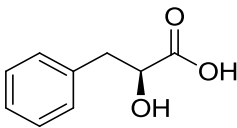
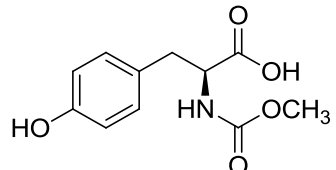
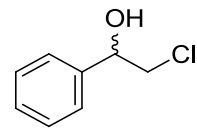
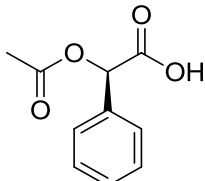
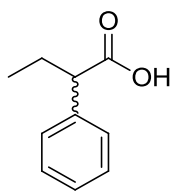
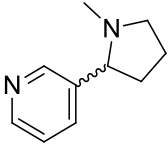
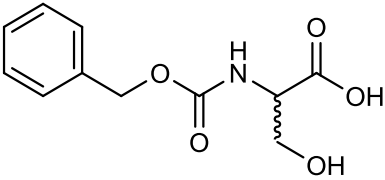
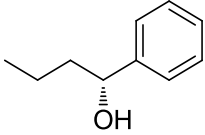
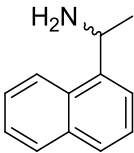
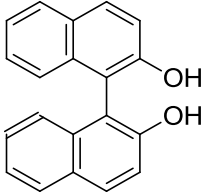
 <p>78</p>	<i>S</i> -2-Phenyl glycinol	5.1	3.2	1.6
 <p>79</p>	<i>S</i> -Phenyl lactic acid	1.8	1.4	1.3
 <p>85</p>	(<i>S</i>)- <i>N</i> -acetyl-tyrosine	11.2	6.5	1.7
 <p>83</p>	<i>S</i> -2-Chloro-1-phenyl ethanol	0.2 ^a	0.1 ^a	2.0
	<i>R</i> -2-Chloro-1-phenyl ethanol	0.2 ^a	0.1 ^a	2.0
 <p>86</p>	<i>R</i> -(-)- <i>O</i> -Acetyl mandelic acid	0.8 ^a	0.8 ^a	1.0 ^b
 <p>81</p>	<i>S</i> (+)-2-Phenyl butyric acid	0.5 ^a	0.5 ^a	1.0 ^b
	<i>R</i> (-)-2-Phenyl butyric acid	0.5 ^a	0.5 ^a	1.0 ^b

Table 4.2 NOBE DuoMIP imprinted with 20% *S*-BOC-Tyr or *R*-BOC-Tyr* continued.

 87	<i>S</i> -Nicotine	0.5 ^a	0.5 ^a	1.0 ^b
	<i>R</i> -Nicotine	0.5 ^a	0.6 ^a	1.2
 77	<i>S</i> -Z-Ser	2.7	2.5	1.1 ^b
	<i>R</i> -Z-Ser	2.7	2.5	1.1 ^b
 82	<i>R</i> -Phenyl butanol	0.2 ^a	0.1 ^a	2.0 ^b
 88	<i>S</i> -Naphthylethyl amine	3.4	3.4	1.0 ^b
	<i>R</i> -Naphthylethyl amine	3.4	3.1	1.1 ^b
 84	<i>S</i> -1,1'-bi-2-naphthol	0.9 ^a	0.8 ^a	1.1 ^b
	<i>R</i> -1,1'-bi-2-naphthol	0.9 ^a	0.8 ^a	1.1 ^b

*HPLC conditions: 25-37 μm particle; 100x2.1 mm column; 99/1 MeCN/AcOH; 0.1 mL/min; injected: 5 μL; analytes: 2.5 mM *S*-BOC-Tyr, 2.5 mM *R*-BOC-Tyr, 1 mM *S*-Z-Phe, 1 mM *R*-

Table 4.2 NOBE DuoMIP imprinted with 20% *S*-BOC-Tyr or *R*-BOC-Tyr continued

Z-Phe, 0.2 mM *S*-Z-Trp, 0.2 mM *R*-Z-Trp, 1 mM *S*-2-phenyl glycinol, 1 mM *S*-phenyl lactic acid, 1 mM (*S*)-*N*-acetyl-tyrosine, 5 mM *S*-2-Chloro-1-phenyl ethanol, 5 mM *R*-2-Chloro-1-phenyl ethanol, 1 mM *R*-(-)-*O*-Acetyl mandelic acid, 2 mM *S*-(+)-2-Phenyl butyric acid, 2 mM *R*-(-)-2-Phenyl butyric acid, 1 mM *S*-Nicotine, 1 mM *R*-Nicotine, 1mM *S*-Z-Ser, 1 mM *R*-Z-Ser, 1 mM *R*-Phenyl butanol, 1 mM *S*-naphthylethyl amine, 1 mM *R*-naphthylethyl amine, 0.2 mM *S*-1,1'-bi-2-naphthol, 0.2 mM *R*-1,1'-bi-2-naphthol. ^aThe k' does not meet the minimum binding requirements and therefore cannot be used γ factor calculation to determine AC. ^bThe γ value calculated is lower than minimum requirements and cannot be used to determine AC.

The mnemonic shown previously in Figure 4.4 can be extended to assist in the explanation of the AC determination of analytes that differ from the print molecule. For example, Figure 4.5 illustrates the analyte (*S*)-*N*-acetyl-tyrosine in the binding cavity of both the *S* and the *R*-MIP enantiomers of the DuoMIP system imprinted with BOC-Tyr. Here, (*S*)-*N*-acetyl-tyrosine fits into the *S*-MIP cavity (Figure 4.5, a), but does not show a good fit into the *R*-

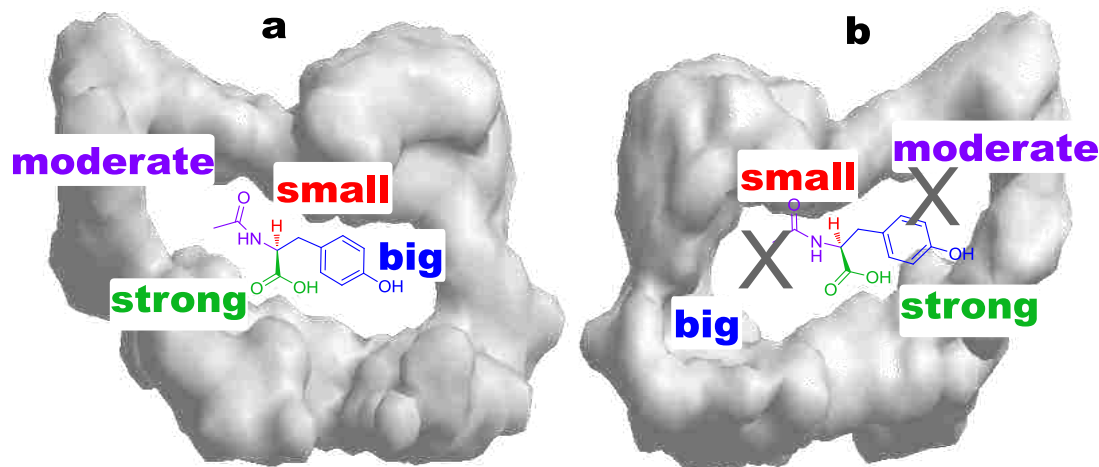


Figure 4.5: Absolute configuration analysis of (*S*)-*N*-acetyl-tyrosine absolute using the DuoMIP system imprinted with *S* (a) and *R* (b)-BOC-Tyr.

MIP cavity (Figure 4.5, b.) With the aid of the mnemonic, the analyte binding results from the chromatography analyses are better understood. When the analyte (*S*)-*N*-acetyl-tyrosine was eluted on both the *R* and the *S* imprinted DuoMIPs, it was retained longer on the *S* imprinted

column than the *R* imprinted column (Figure 4.6.) This difference in retention is due to the selectivity of (*S*)-*N*-acetyl-tyrosine in the binding cavity of each enantiomer of the DuoMIP system, and accounts for its ability to be useful for AC determination of unknown molecules.

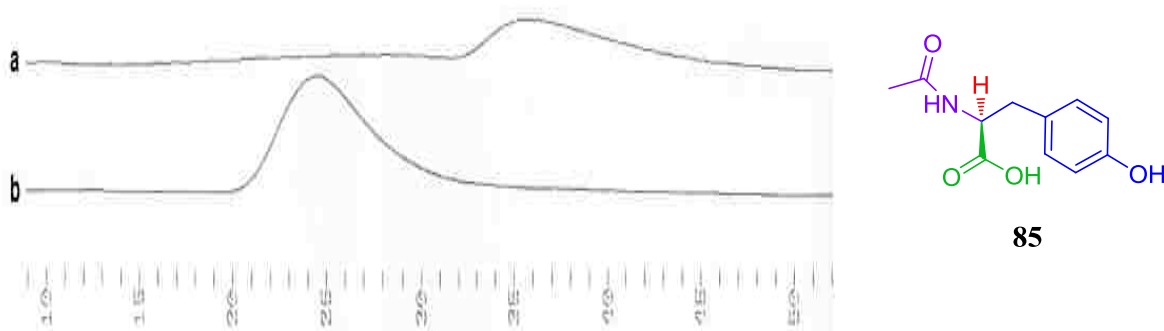


Figure 4.6: *S*-Acetyl-Tyr analyte (85) on NOBE imprinted with 20% *S*-BOC-Tyr (*S*-MIP)^a and *S*-Acetyl-Tyr analyte on NOBE imprinted with 20% *R*-BOC-Tyr (*R*-MIP)^b.

Figure 4.7 can be used to further aid in the understanding of the AC determination of non-amino acids using the mnemonic. Figure 4.7, a depicts that (*S*)-phenyllactic acid fits into the *S*-MIP enantiomer of the DuoMIP system; and Figure 4.7, b illustrates that (*S*)-phenyllactic acid exhibits a poor fit into the *R*-MIP enantiomer. This result correlates to the values shown in Table 4.2 where the k' was 1.8 on the *S*-MIP and 1.4 on the *R*-MIP with a γ value of 1.3. Figure 4.7, c portrays (*S*)-phenyl glycinol fitting into the *S*-MIP; and Figure 4.7, d shows that the same (*S*)-phenyl glycinol does not fit into the *R*-MIP binding cavity. These illustrations in the mnemonic also aid in understanding the experimental data in Table 4.2 where (*S*)-phenyl glycinol had a k' of 5.1 on the *S*-MIP and 3.2 on the *R*-MIP with a 1.6 γ value.

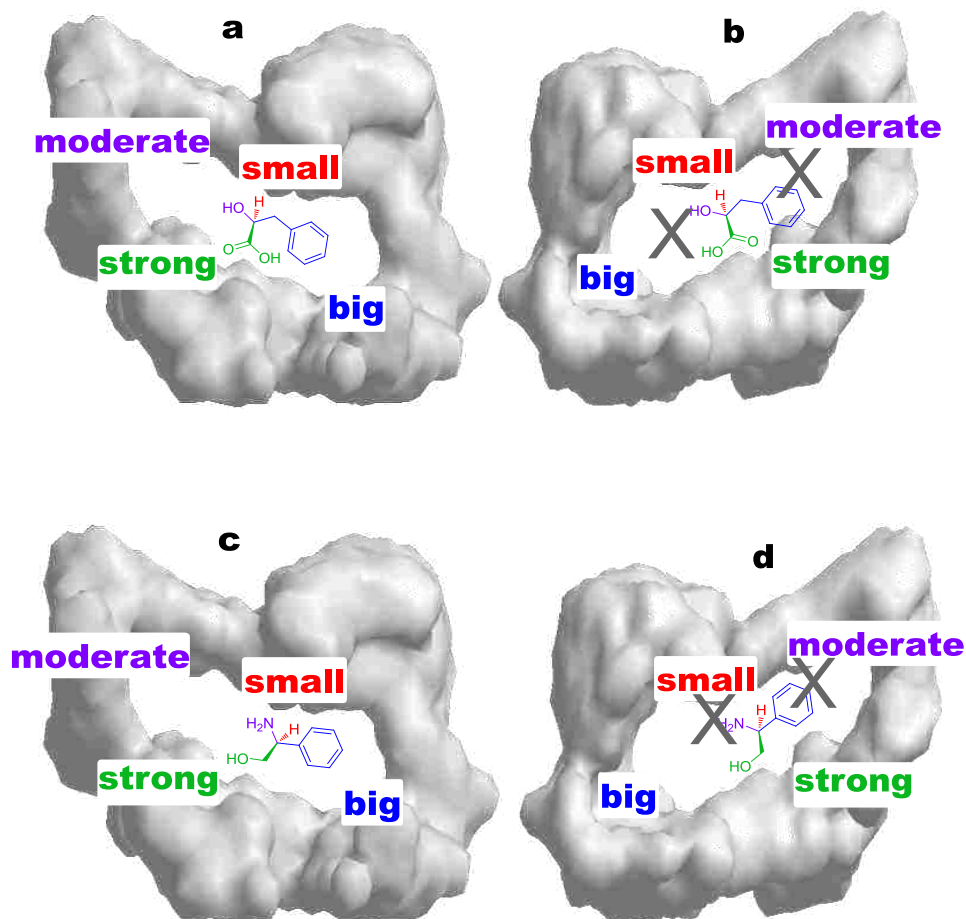


Figure 4.7: (*S*)-phenyllactic acid in the binding cavity of the NOBE OMNiMIP imprinted with 20% *S*-BOC-Tyr (a), (*S*)-phenyllactic acid in the binding cavity of the NOBE OMNiMIP imprinted with 20% *R*-BOC-Tyr (b), (*S*)-phenyl glycinol in the binding cavity of the NOBE OMNiMIP imprinted with 20% *S*-BOC-Tyr (c), and (*S*)-phenyl glycinol in the binding cavity of the NOBE OMNiMIP imprinted with 20% *R*-BOC-Tyr (d).

The NOBE DuoMIP system was studied further to demonstrate the importance of the hydrogen bonding and steric interactions in the DuoMIP design. NOBE DuoMIPs were synthesized using 5% *R* or *S*-4-benzyl-2-oxazolidinone as the print molecules. These templates were chosen as a means to compare the DuoMIP system directly to Rychnovsky's kinetic resolution methods where he studied the absolute configuration of oxazolidinones.¹⁸ For this system, nearly all of the k' and or γ values for each of the analytes were below the minimum

criteria required for confidence in AC determination. It is not surprising that these DuoMIPs could not be used to determine the absolute configuration of unknown analytes because these MIPs were not synthesized with a design that led to a distribution of strong hydrogen bonding and steric interactions around the chiral center significant for differentiating diastereomeric complex energies of the enantiomeric adsorbents and analyte as shown in Figure 4.8.

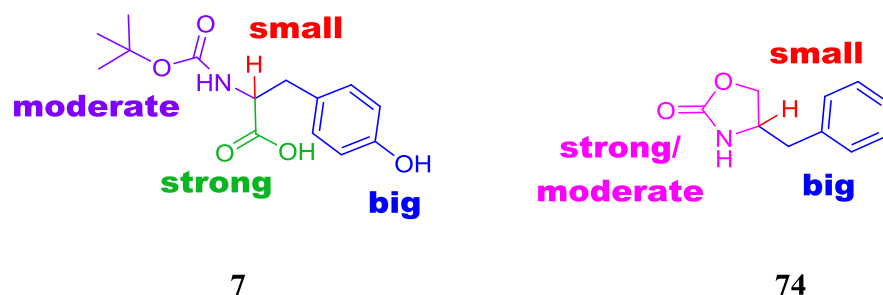


Figure 4.8: The “strong” and “moderate” hydrogen bonding groups and the “small” and “big” groups are illustrated for BOC-Tyr (7) and the “strong/moderate” group and the “small” and “big” groups are shown for 4-benzyl-2-oxazolidinone (74) print molecules.

Two other DuoMIP systems were subsequently synthesized with 5% *R* or *S*-BOC-Phe and *R* or *S*-BOC-Phe-OMe as the print molecules to further show the importance of the binding site formation in the determination of AC. The BOC-Phe DuoMIPs were used to determine the AC accurately for four analytes while the BOC-Phe-OMe DuoMIPs only accurately determined three AC examples as shown in Table 4.3. The BOC-Phe DuoMIPs determined AC for more analytes, and provided larger γ values indicating that the reliability of the BOC-Phe DuoMIP system was also better than the system based on the BOC-Phe-OMe. These results are not surprising as the BOC-Phe system that performed the best had a print molecule with a carboxylic acid as illustrated in Figure 4.9. The carboxylic acid group is important because it is a strong hydrogen bond donor. The strong hydrogen bond accounts for some of the recognition between the binding cavity of the DuoMIP adsorbents and the analytes studied by HPLC. Although there

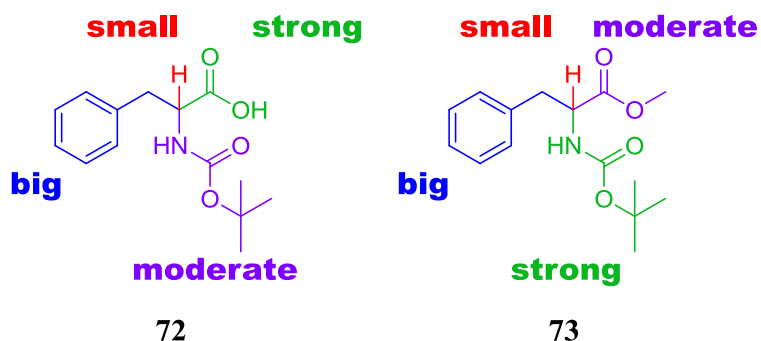


Figure 4.9: The “strong” and “moderate” hydrogen bonding groups and the “small” and big” groups are illustrated for BOC-Phe (72) and BOC-Phe-OMe (73).

were some successes by these DuoMIPs it should be noted that the AC of *S*-Z-Ser on the BOC-Phe DuoMIPs and *R*-Z-Trp and *R*-Z-Ser on the BOC-Phe-OMe were incorrectly identified. These results show that there are further difficulties to the DuoMIP system formed with BOC-Phe and BOC-Phe-OMe, which might be overcome by using a larger amount of template (20%) as in the case of the BOC-Tyr systems.

Table 4.3: NOBE DuoMIPs imprinted with BOC-Phe or BOC-Phe-OMe templates* .

Analyte	γ from BOC-Phe imprinted columns	γ from BOC-Phe-OMe imprinted columns
<p>7</p>	<i>S</i> -BOC-Tyr	1.1 ^b
	<i>R</i> -BOC-Tyr	1.1 ^b
<p>73</p>	<i>S</i> -BOC-Phe-OMe	n/a
	<i>R</i> -BOC-Phe-OMe	n/a

Table 4.3: NOBE DuoMIPs imprinted with BOC-Phe or BOC-Phe-OMe templates* continued.

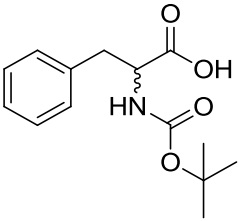
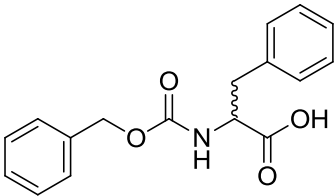
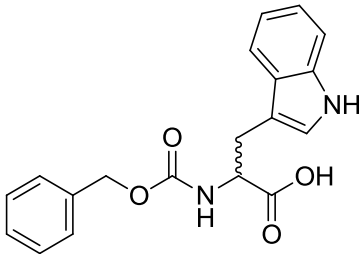
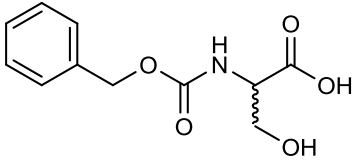
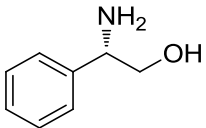
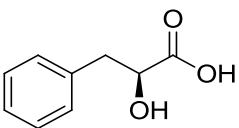
 <p>72</p>	<i>S</i> -BOC-Phe	1.6 ^a	n/a ^c
	<i>R</i> -BOC-Phe	1.2 ^{a,b}	n/a ^c
 <p>75</p>	<i>S</i> -Z-Phe	1.2 ^a	1.0 ^{a,b}
	<i>R</i> -Z-Phe	1.6 ^a	1.2 ^a
 <p>76</p>	<i>S</i> -Z-Trp	1.1 ^b	1.3
	<i>R</i> -Z-Trp	1.1 ^b	1.3 ^d
 <p>77</p>	<i>S</i> -Z-Ser	1.3 ^d	1.2
	<i>R</i> -Z-Ser	1.1 ^b	1.3 ^d
 <p>78</p>	<i>S</i> -2-phenyl glycinol	1.4	1.1 ^b
 <p>79</p>	<i>S</i> -phenyl lactic acid	1.4 ^a	1.1 ^{a,b}

Table 4.3 NOBE DuoMIPs imprinted with BOC-Phe or BOC-Phe-OMe templates* continued.

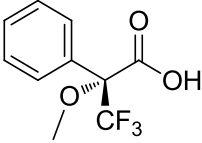
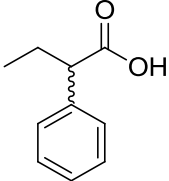
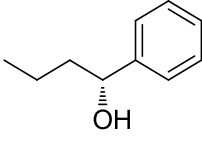
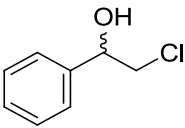
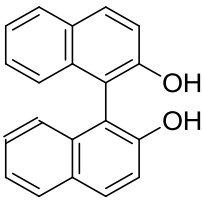
 <p>80</p>	<p><i>S</i>-methoxy(trifluoroethyl)phenylAcOH</p>	<p>1.7</p>	<p>1.1^b</p>
 <p>81</p>	<p><i>S</i>-phenyl butyric acid</p>	<p>1.5</p>	<p>1.0^{a,b}</p>
	<p><i>R</i>-phenyl butyric acid</p>	<p>1.7^a</p>	<p>1.0^{a,b}</p>
 <p>82</p>	<p><i>R</i>-phenyl butanol</p>	<p>1.3^a</p>	<p>1.0^{a,b}</p>
 <p>83</p>	<p><i>S</i>-chloro phenyl ethanol</p>	<p>2.6^a</p>	<p>1.0^{a,b}</p>
	<p><i>R</i>-chloro phenyl ethanol</p>	<p>2.0^a</p>	<p>1.0^{a,b}</p>
 <p>84</p>	<p><i>S</i>-binaphthol</p>	<p>1.0^{a,b}</p>	<p>1.0^{a,b}</p>
	<p><i>R</i>-binaphthol</p>	<p>1.0^{a,b}</p>	<p>1.0^{a,b}</p>

Table 4.3 NOBE DuoMIPs imprinted with BOC-Phe or BOC-Phe-OMe templates* continued.

*HPLC conditions: 25-37 μm particles; 100 x 2.1 mm column; 99/1 MeCN/AcOH; 0.1 mL/min; injected 5 μL ; 1 mM BOC-*S*-tyrosine/260 nm, 1 mM BOC-*R*-tyrosine/260 nm, 5 mM *S*-BOC-Phe-OMe/260 nm, 5 mM *R*-BOC-Phe-OMe/260 nm, 1 mM BOC-*S*-Phe/260 nm, 1 mM BOC-*R*-Phe/260 nm, 5 mM *S*-CBZ-Phe/260 nm, 5 mM *R*-Z-Phe/260 nm, 0.2 mM *Z*-*S*-tryptophan/260 nm, 0.2 mM *Z*-*R*-tryptophan/260 nm, 1 mM *Z*-*S*-serine/260 nm, 1 mM *Z*-*R*-serine/260 nm, 10 mM *S*-2-phenyl-glycinol/262 nm, 1 mM *S*-phenyl-lactic acid/262 nm, 1 mM *S*-methoxy (trifluoro-methyl) phenyl acetic acid/262 nm, mM *S*-(+)-2-phenyl butyric acid/262 nm, 2 mM *R*-(-)-2-phenyl butyric acid/262 nm, 1 mM *R*-1-phenyl-1-butanol/262 nm, 5 mM *S*-2-chloro-1-phenyl ethanol/262 nm, 5 mM *R*-2-chloro-1-phenyl ethanol/262 nm, 0.2 mM (*S*)-(-)-1,1'-bi-2-naphthol/300 nm, 0.2 mM (*R*)-(-)-1,1'-bi-2-naphthol/300 nm. ^a k' and ^b γ do not meet criteria and cannot be used to determine AC. ^cValues not available are listed as n/a. ^dAC was incorrect.

4.4 Exploration of a Chiral OMNiMIP for AC Analysis

The exploration of a chiral monomer for synthesizing DuoMIPs was also studied and compared to NOBE DuoMIPs. Here, L-NALA was chosen as the chiral crosslinking monomer because its structure only differs from NOBE by a single methyl group in the position alpha to the amide group (Figure 4.10.) As shown in Table 4.4, AC could correctly be identified for *S*-

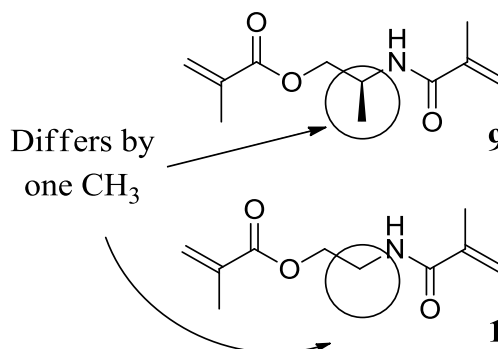


Figure 4.10: The structure of L-NALA (9) differs from NOBE (1) by one methyl group in the alpha amido position.

BOC-Tyr, *R*-BOC-Tyr, *R*-Z-Trp, *R*-Z-Ser, *S*-phenyl glycinol and (*S*)-*N*-acetyl tyrosine.

Although there were some successes using L-NALA as the crosslinking monomer for the

DuoMIP synthesis it was decided that the ease of preparation and results of the NOBE DuoMIP system is the most effective for AC determination thus far.

Table 4.4: L-NALA DuoMIP system imprinted with *R* or *S*-BOC-Tyr* .

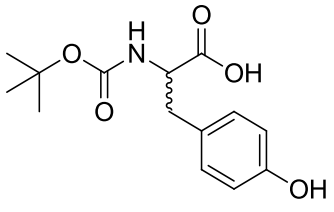
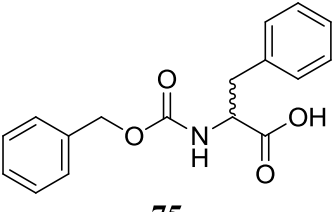
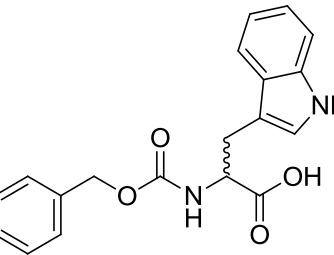
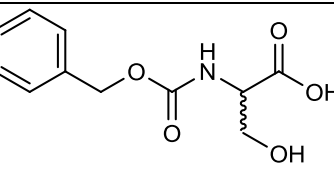
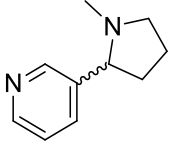
Analytes		k'on L-MIP	k'on D-MIP	γ
 7	<i>S</i> -BOC-Tyr	10.9	2.5	4.4
	<i>R</i> -BOC-Tyr	2.1	5.3	2.4
 75	<i>S</i> -Z-Phe	0.9 ^a	1.0 ^a	1.1 ^b
	<i>R</i> -Z-Phe	0.7 ^a	1.0 ^a	1.4 ^a
 76	<i>S</i> -Z-Trp	1.5	1.6	1.1 ^b
	<i>R</i> -Z-Trp	1.3	1.7	1.3
 77	<i>S</i> -Z-Ser	1.4	1.5	1.1 ^b
	<i>R</i> -Z-Ser	1.2	1.5	1.3
 87	<i>S</i> -Nicotine	0.3 ^a	0.3 ^a	1.0 ^{a,b}
	<i>R</i> -Nicotine	0.3 ^a	0.3 ^a	1.0 ^{a,b}

Table 4.4 L-NALA DuoMIP system imprinted with *R* or *S*-BOC-Tyr* continued.

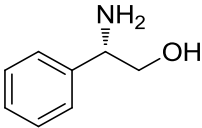
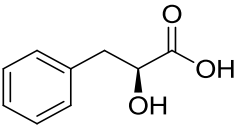
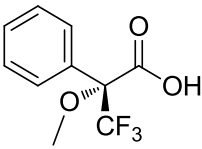
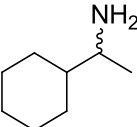
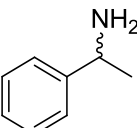
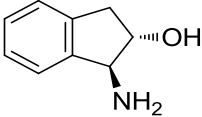
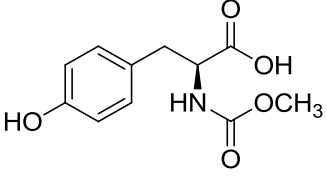
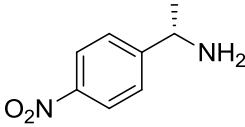
 78	<i>S</i> -2-phenyl glycinol	2.5	3.1	1.2
 79	<i>S</i> -phenyl lactic acid	0.8 ^a	1.0	1.3 ^a
 80	<i>S</i> -methoxy trifluoro methyl phenyl acetic acid	1.9	2.0	1.0 ^b
 89	<i>S</i> -Cyclohexylethylamine	2.4	2.2	1.1 ^b
	<i>R</i> -Cyclohexylethylamine	2.3	2.3	1.0 ^b
 90	<i>S</i> -methyl benzylamine	2.8	2.6	1.1 ^b
	<i>R</i> -methyl benzylamine	2.7	2.7	1.0 ^b
 91	<i>S,S</i> -trans amino indanol	4.4	4.7	1.1 ^b

Table 4.4 L-NALA DuoMIP system imprinted with *R* or *S*-BOC-Tyr* continued.

 <p style="text-align: center;">85</p>	(<i>S</i>)-N-Acetyl-Tyrosine	4.9	4.0	1.2
 <p style="text-align: center;">92</p>	<i>S</i> -methyl nitro benzyl amine	2.5	2.4	1.0 ^b
<p>*HPLC conditions: particle size, 25-37 μm; column size, 100 x 2.1 mm; flow rate: 0.1 mL/min, 99/1 MeCN/AcOH mobile phase; injected volume: 5 μL; 260 nm wavelength detection, analytes: 1 mM <i>S</i>-BOC-Tyr, 1 mM <i>R</i>-BOC-Tyr, 1 mM <i>S</i>-Z-Phe, 1 mM <i>R</i>-Z-Phe, 0.2 mM <i>S</i>-Z-Trp, 0.2 mM <i>R</i>-Z-Trp, 1 mM <i>S</i>-Z-Ser, 1 mM <i>R</i>-Z-Ser, 1 mM <i>S</i>-2-phenyl glycinol, 1 mM <i>S</i>-phenyl lactic acid, 1 mM <i>S</i>-methoxy trifluoro methyl phenyl acetic acid, 1 mM, 1 mM <i>S</i>-Nicotine, 1 mM <i>R</i>-Nicotine, 1 mM <i>S</i>-Cyclohexylethylamine, 1 mM <i>R</i>-Cyclohexylethylamine, 1 mM <i>S</i>-methyl benzyl amine, 1 mM <i>R</i>-methyl benzyl amine, 1 mM <i>S,S</i>-trans amino indanol, 1 mM (<i>S</i>)-N-Acetyl-Tyrosine, 1 mM <i>S</i>-methyl nitro benzyl amine. ^aThe <i>k'</i> does not meet the criteria and cannot be used to determine AC. ^bThe γ value is lower than criteria and cannot be used to determine AC.</p>				

4.5 Absolute Configuration Determination Conclusions

As shown throughout the many approaches to determine absolute configuration in the literature, the determination of stereochemistry is an ongoing important research topic. Current methods encompass numerous drawbacks; such as, the requirement of multiple reactions or derivatizations, need for prior literature values, computational studies, or both enantiomers for comparison; and therefore, methodological improvements are needed in the determination of absolute stereochemistry of compounds. In Chapter Four, a new technique, the DuoMIP method, was developed as another solution to the AC determination quandary. DuoMIP systems were synthesized from the crosslinking monomers NOBE and L-NALA using OMNiMIP imprinting. The importance of a large template loading in the polymer formulation was demonstrated as the

best performance in relation to AC determination was when 20% (as compared to 4 and 5% template) *R* or *S*-BOC-Tyr was used as the print molecules with NOBE as the crosslinker. In this case, each enantiomeric adsorbent of the DuoMIP system contained a greater number of recognition cavities formed from the strong hydrogen bonding and steric interactions. The binding affinity ($k' \geq 1$) and selectivity ($\gamma \geq 1.2$) of the unknown analyte with each enantiomer of the DuoMIP system allowed the correct AC determination of a series of molecules.

4.6 Absolute Configuration Future Work

Further studies synthesizing NOBE DuoMIPs for AC determination should be completed with different print molecules (including non-amino acid derivatives), such as *R* and *S*-phenyl glycinol. Optimizing the cross-reactivity of the template and series of analytes studied could broaden the scope of the DuoMIP system for absolute configuration determinations. Other crosslinkers for the creation of DuoMIPs synthesized using OMNiMIP and traditional imprinting approaches should also be examined. For example, the crosslinker NAG (**12**) introduced in Chapter 2 could be used to imprint *R* and *S*-Z-Trp by traditional and OMNiMIP imprinting and evaluation of these polymers as DuoMIPs can be studied by HPLC. In addition to OMNiMIP and traditional imprinting, other chromatographic stationary phases could also be studied to gain knowledge in the dual column method of AC determination. Pirkle or other chiral separation columns can be purchased or synthesized and tested to see if they too can be used in a dual system for determination of AC.

4.7 References

1. Drayer, D. E., The early history of stereochemistry: from the discovery of molecular asymmetry and the first resolution of a racemate by pasteur to the asymmetrical chiral carbon of van't Hoff and Le Bel. *Drugs Pharm. Sci.* **2012**, *211*, 1-6.
2. Hoff, J. H. v. t. A suggestion looking to the extension into space of the structural formulas at present used in chemistry. And a note upon the relation between the optical activity and the chemical constitution of organic compounds. <http://www.chemteam.info/Chem-History/Van%27t-Hoff-1874.html> (accessed October 31, 2013).
3. Caldwell, J., The importance of stereochemistry in drug action and disposition. *J Clin Pharmacol* **1992**, *32*, 925-9.
4. Caner, H.; Groner, E.; Levy, L.; Agranat, I., Trends in the development of chiral drugs. *Drug Discovery Today* **2004**, *9* (3), 105-110.
5. Yang, Y.; Su, B.; Yan, Q.; Ren, Q., Separation of naproxen enantiomers by supercritical/subcritical fluid chromatography. *Journal of Pharmaceutical and Biomedical Analysis* **2005**, *39* (3-4), 815-818.
6. Vegman, M.; Carmeli, S., Eight micropeptides from a *Microcystis* spp. bloom collected from a fishpond near Kibbutz Lehavot HaBashan, Israel. *Tetrahedron* **2013**, *69*, 10108-10115.
7. Prasad, K. R.; Gutala, P., Total Synthesis and Determination of the Absolute Configuration of 5,6-Dihydro- α -pyrone Natural Product Synargentolide B. *J. Org. Chem.* **2013**, *78*, 3313-3322.
8. Bonney, K. J.; Braddock, D. C., A Unifying Stereochemical Analysis for the Formation of Halogenated C15-Acetogenin Medium-Ring Ethers From *Laurencia* Species via Intramolecular Bromonium Ion Assisted Epoxide Ring-Opening and Experimental Corroboration with a Model Epoxide. *J. Org. Chem.* **2012**, *77*, 9574-9584.
9. Eriksson, T.; Bjorkman, S.; Hoglund, P., Clinical pharmacology of thalidomide. *Eur. J. Clin. Pharmacol.* **2001**, *57*, 365-376.
10. Flack, H. D.; Bernardinelli, G., The use of X-ray crystallography to determine absolute configuration. *Chirality* **2008**, *20*, 681-690.
11. Dale, J. A.; Dull, D. L.; Mosher, H. S., α -Methoxy- α -trifluoromethylphenylacetic acid, a versatile reagent for the determination of enantiomeric composition of alcohols and amines. *The Journal of Organic Chemistry* **1969**, *34* (9), 2543-2549.
12. Louzao, I.; Seco, J. M.; Quinoa, E.; Riguera, R., ¹³C NMR as a general tool for the assignment of absolute configuration. *Chem. Commun. (Cambridge, U. K.)* **2010**, *46*, 7903-7905.

13. Tam, C. N.; Bour, P.; Keiderling, T. A., An Experimental Comparison of Vibrational Circular Dichroism and Raman Optical Activity with 1-Amino-2-propanol and 2-Amino-1-propanol as Model Compounds. *J. Am. Chem. Soc.* **1997**, *119*, 7061-7064.
14. Freedman, T. B.; Cao, X.; Dukor, R. K.; Nafie, L. A., Absolute configuration determination of chiral molecules in the solution state using vibrational circular dichroism. *Chirality* **2003**, *15*, 743-58.
15. Gussem, E. D.; Bultinck, P.; Feledziak, M.; Marchand-Brynaert, J.; Stevens, C. V.; Herrebout, W., Vibrational Circular Dichroism versus Optical Rotation Dispersion and Electronic Circular Dichroism for diastereomers: the stereochemistry of 3-(1[prime or minute]-hydroxyethyl)-1-(3[prime or minute]-phenylpropanoyl)-azetidin-2-one. *Physical Chemistry Chemical Physics* **2012**, *14* (24), 8562-8571.
16. Wagner, A. J.; Rychnovsky, S. D., Kinetic Analysis of the HBTM-Catalyzed Esterification of an Enantiopure Secondary Alcohol. *Organic Letters* **2013**, *15* (21), 5504-5507.
17. Miller, S. M.; Samame, R. A.; Rychnovsky, S. D., Nanomole-Scale Assignment of Configuration for Primary Amines Using a Kinetic Resolution Strategy. *Journal of the American Chemical Society* **2012**, *134* (50), 20318-20321.
18. Perry, M. A.; Trinidad, J. V.; Rychnovsky, S. D., Absolute Configuration of Lactams and Oxazolidinones Using Kinetic Resolution Catalysts. *Org. Lett.* **2013**, *15*, 472-475.
19. Wagner, A. J.; David, J. G.; Rychnovsky, S. D., Determination of Absolute Configuration Using Kinetic Resolution Catalysts. *Organic Letters* **2011**, *13* (16), 4470-4473.
20. Wagner, A. J.; Rychnovsky, S. D., Determination of Absolute Configuration of Secondary Alcohols Using Thin-Layer Chromatography. *The Journal of Organic Chemistry* **2013**, *78* (9), 4594-4598.
21. Birman, V. B.; Li, X., Homobenzotetramisole: An Effective Catalyst for Kinetic Resolution of Aryl-Cycloalkanols. *Org. Lett.* **2008**, *10*, 1115-1118.
22. Roussel, C.; Rio, A. D.; Pierrot-Sanders, J.; Piras, P.; Vanthuyne, N., Chiral liquid chromatography contribution to the determination of the absolute configuration of enantiomers. *Journal of Chromatography A* **2004**, *1037* (1-2), 311-328.
23. Aboul-Enein, H. Y., High-performance liquid chromatographic enantioseparation of drugs containing multiple chiral centers on polysaccharide-type chiral stationary phases. *Journal of Chromatography A* **2001**, *906* (1-2), 185-193.
24. Meador, D. S.; Spivak, D. A., Absolute Configuration Determination Using Enantiomeric Pairs of Molecularly Imprinted Polymers. *Organic Letters* **2014**, *16* (5), 1402-1405.
25. Klotz, I. M., Ligand-Receptor Complexes: Origin and Development of the Concept. *Journal of Biological Chemistry* **2004**, *279* (1), 1-12.

26. Meng, A. C.; LeJeune, J.; Spivak, D. A., Multi-analyte imprinting capability of OMNiMIPs versus traditional molecularly imprinted polymers. *Journal of Molecular Recognition* **2009**, 22 (2), 121-128.

CHAPTER 5: SYNTHESIS OF A NEW CHIMERIC ANTIOXIDANT

5.1 Introduction to Diseases Associated with Oxidative Stress

According to the Global Action Plan published by the World Health Organization in 2013, it was estimated that over 17 million deaths were caused by cardiovascular disease in 2008 and that number is expected to exceed 25 million by the year 2030.¹ Increasing mortality due to cardiovascular disease is a worldwide problem that has escalated research attention.² Research has shown that the development of cardiovascular disease as well as neurodegenerative diseases such as Alzheimer's and Parkinson's are linked to oxidative damage *in vivo*.^{3,4} In particular, oxidative damage in arteries leads to atherosclerosis, a major origin of cardiovascular disease.⁵ The early stages of atherosclerosis have been associated with free radical oxidation of low density lipoproteins (LDLs), which occurs on the lipid and or protein portions of the lipoprotein.^{6,7} The uptake of oxidized LDLs (ox-LDLs) by macrophages leads to foam cell formation in the subendothelial space. The accumulation of these foam cells results in plaque formation in the arterial intima and thus triggers atherosclerosis (Figure 5.1).^{8,9}

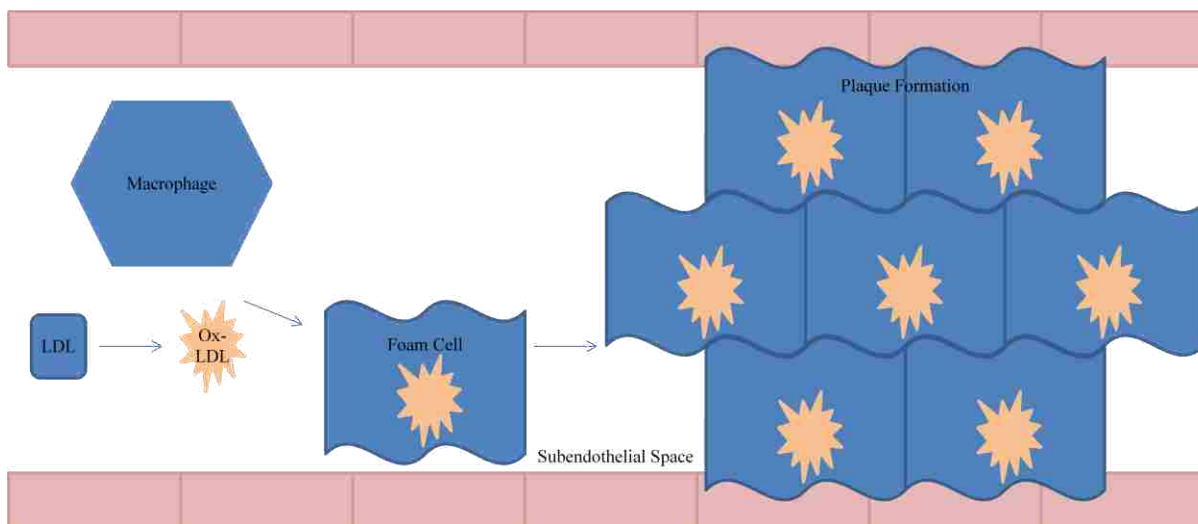


Figure 5.1: Diagram of Atherosclerosis development.

One approach to minimize atherosclerosis and other diseases that are caused by oxidative stress is to reduce or eliminate the free radical species formed in the body.¹⁰ There are numerous antioxidant molecules that have been shown to reduce oxidative damage.¹¹ These antioxidants can be categorized based on the environments that they thrive in, either lipophilic or hydrophilic. For example, vitamin E is a term used to describe a group of eight lipophilic antioxidant molecules, which include four tocopherols and four tocotrienols (Figure 5.2). The structural features of the tocopherols and tocotrienols differ only by the unsaturated double bonds found in

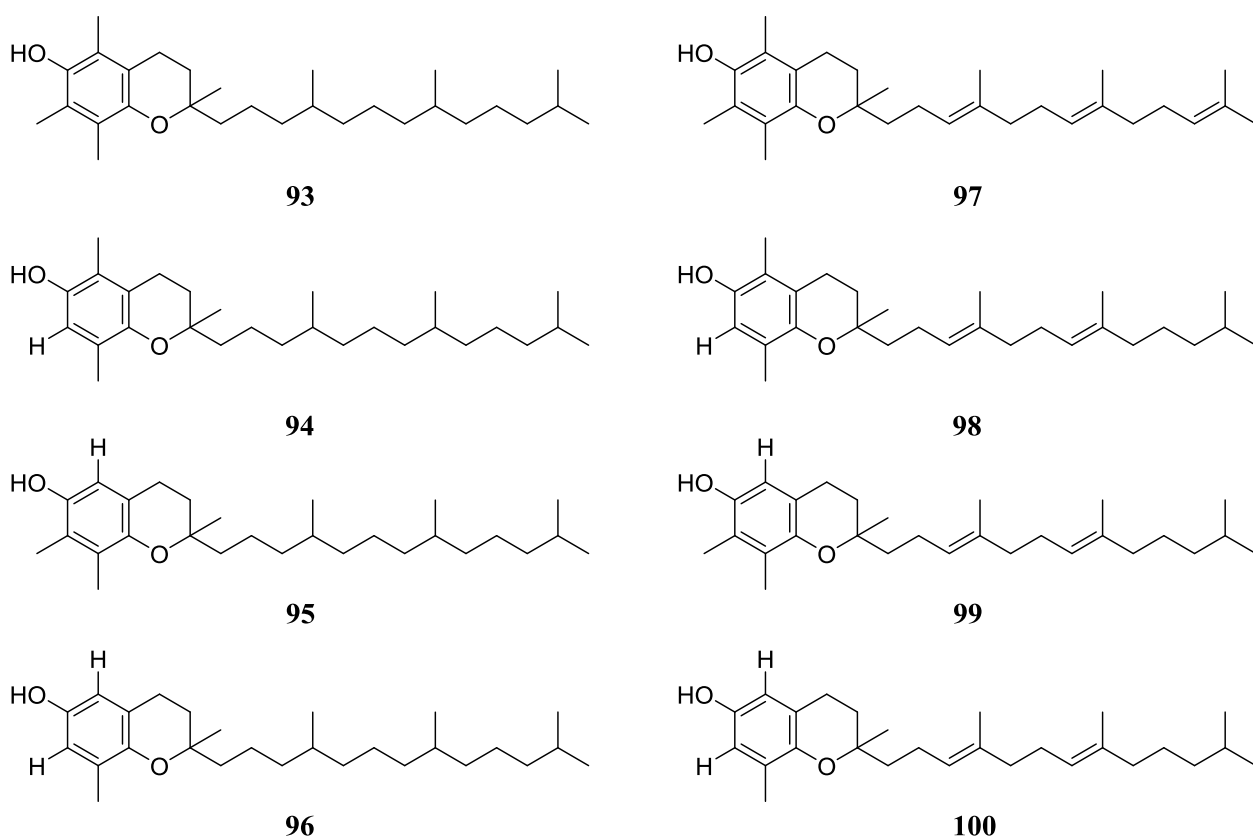


Figure 5.2: Structures of vitamin E molecules: α -tocopherol (93), β -tocopherol (94), γ -tocopherol (95), δ -tocopherol (96), α -tocotrienol (97), β -tocotrienols (98), γ -tocotrienols (99), and δ -tocotrienols (100).

the latter. The variations among the individual molecules in each category are distinguished by the methyl groups attached on the benzene ring.

The subtle structural differences of these antioxidants dictate how recognition and antioxidant activity occurs. For example, the methyl appendage arrangement on the benzene ring of α -tocopherol is specifically recognized by the 32 kDa α -tocopherol transferase protein (α -TTP).^{12,13} After recognition by the transferase protein, α -TOC is transported into lipoproteins and is further transported to tissues.¹⁴ Here, the lipophilic α -tocopherol antioxidant is able to inhibit oxidation of the lipid portion of LDLs.^{15,16,17} A limitation to this antioxidant molecule and many other lipophilic molecules is its inability to penetrate hydrophilic media. For instance, although lipophilic molecules are successful at oxidation inhibition in the lipid portion of LDLs, they are unable to prevent oxidation in hydrophilic apolipoproteins; such as, Apo B-100.^{16,17}

Another category of antioxidants consists of hydrophilic molecules. In a similar manner, hydrophilic antioxidants such as vitamin C (**101**), carnosine (**102**), and folic acid (**103**) are successful at prevention of oxidative stress in hydrophilic environments as represented in the cell cytosol and blood plasma (Figure 5.3).^{18,19,20,21} While these antioxidants are equipped to reduce oxidation in hydrophilic media, they are unable to sufficiently enter into hydrophobic environments. The inability of hydrophilic molecules to infiltrate the hydrophobic regions makes them incapable of therapeutic activity in these environments.

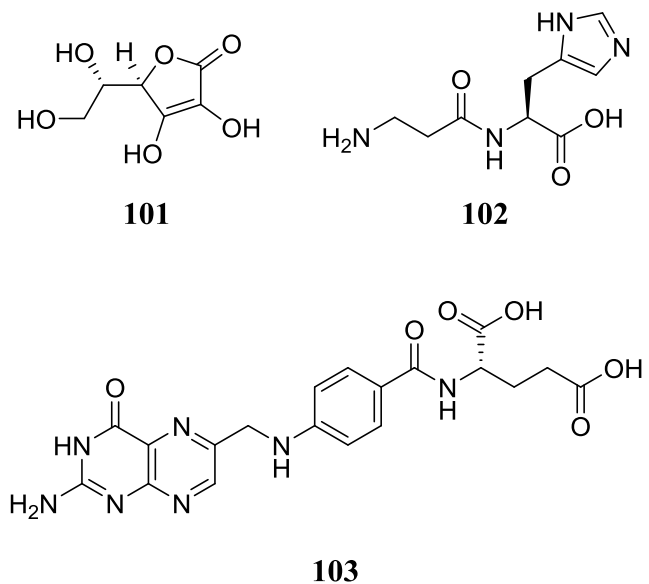
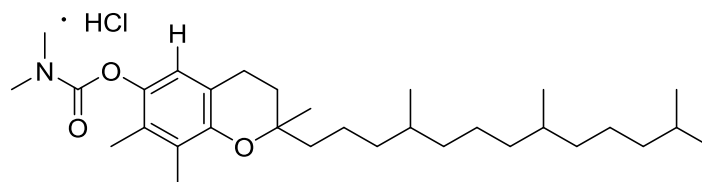
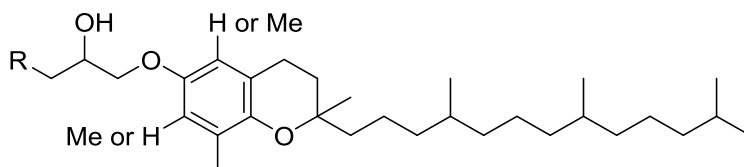


Figure 5.3: Structures of hydrophilic antioxidant molecules: vitamin C (101), carnosine (102), and folic acid (103).

The failure to gain access to both hydrophobic and hydrophilic regions simultaneously in biological environments is a problem addressed in the literature. For example, conjugation of lipophilic vitamin E with other moieties to improve water solubility has been accomplished.^{22,23,24} Takata and co-workers derivatized an isomer of vitamin E to form a water-soluble molecule (Figure 5.4, **104**). Ogata describes a series of derivatives containing several different amino acids attached to the hydroxyl group on tocopherol, which make these isomers of vitamin E also water-soluble (Figure 5.4, **105**).²⁵ In these examples, once the derivatives permeate the hydrophilic environment, they can hydrolyze to form the original vitamin E



104



R= cysteine, taurine, aminobutyric acid, glutathione, aspartic acid, and glutamic acid

105

Figure 5.4 Water-soluble vitamin E derivatives.

structure. Although these vitamin E derivatives can enter hydrophilic media, a problem that arises from these analogues and others that utilize the hydroxyl group of vitamin E is the loss of recognition by α -TTP while the hydrophilic moiety is attached since the OH appendage is an area of key enzymatic recognition.²⁶ Until hydrolysis to free the hydroxyl group is achieved, strong recognition by α -TTP is not accomplished. This reduction in recognition results in the reduced ability to penetrate LDLs through the α -TTP mechanism and consequently the molecules do not achieve antioxidant activity in both hydrophilic and lipophilic regions of LDLs

at the same time. To address this conundrum, the design and synthesis of a novel chimeric antioxidant that leaves the hydroxyl group intact is discussed throughout Chapter 5. Here, the introduction of carnosine, a hydrophilic moiety, to the lipophilic antioxidant α -tocopherol at the end of the phytol chain is synthetically accomplished, and the rate of radical inhibition examined using a 1,1-diphenyl-2-picrylhydrazyl (DPPH) assay.^{27,28}

5.2 VECAR Design

Vitamin E Carnosine (VECAR, **106**) was designed to provide both lipophilic and hydrophilic antioxidant moieties in a single chimeric molecule. There are three main regions of the VECAR structure that impart its unique lipophilic and hydrophilic abilities (Figure 5.5).²⁷

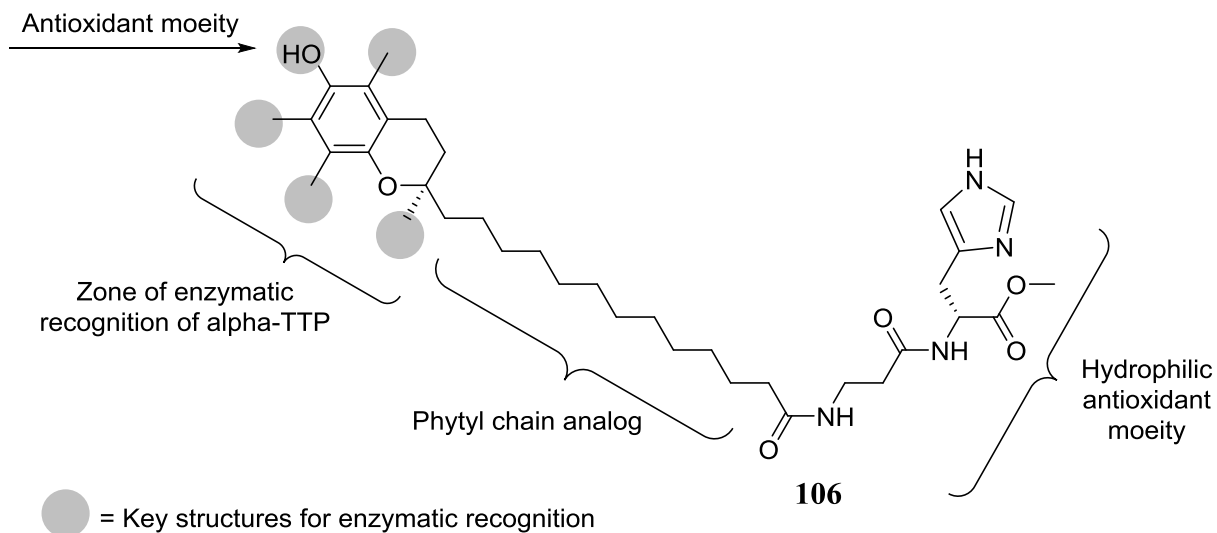


Figure 5.5 VECAR (106) design.

The left hand portion of VECAR keeps the chromanol ring of α -tocopherol intact as it encompasses key zones of enzymatic recognition by α -TTP as identified by Meier et al.²⁶ Meier and co-workers generated crystal structures of α -TTP and used computational studies to identify that the hydroxyl and methyl groups on the chromanol ring are important recognition sites

between the enzyme and α -toc. The authors determined that the hydroxyl groups participate in hydrogen bonding with the serine and valine moieties of α -TTP's binding pocket while the methyl appendages interact through van der Waals forces.

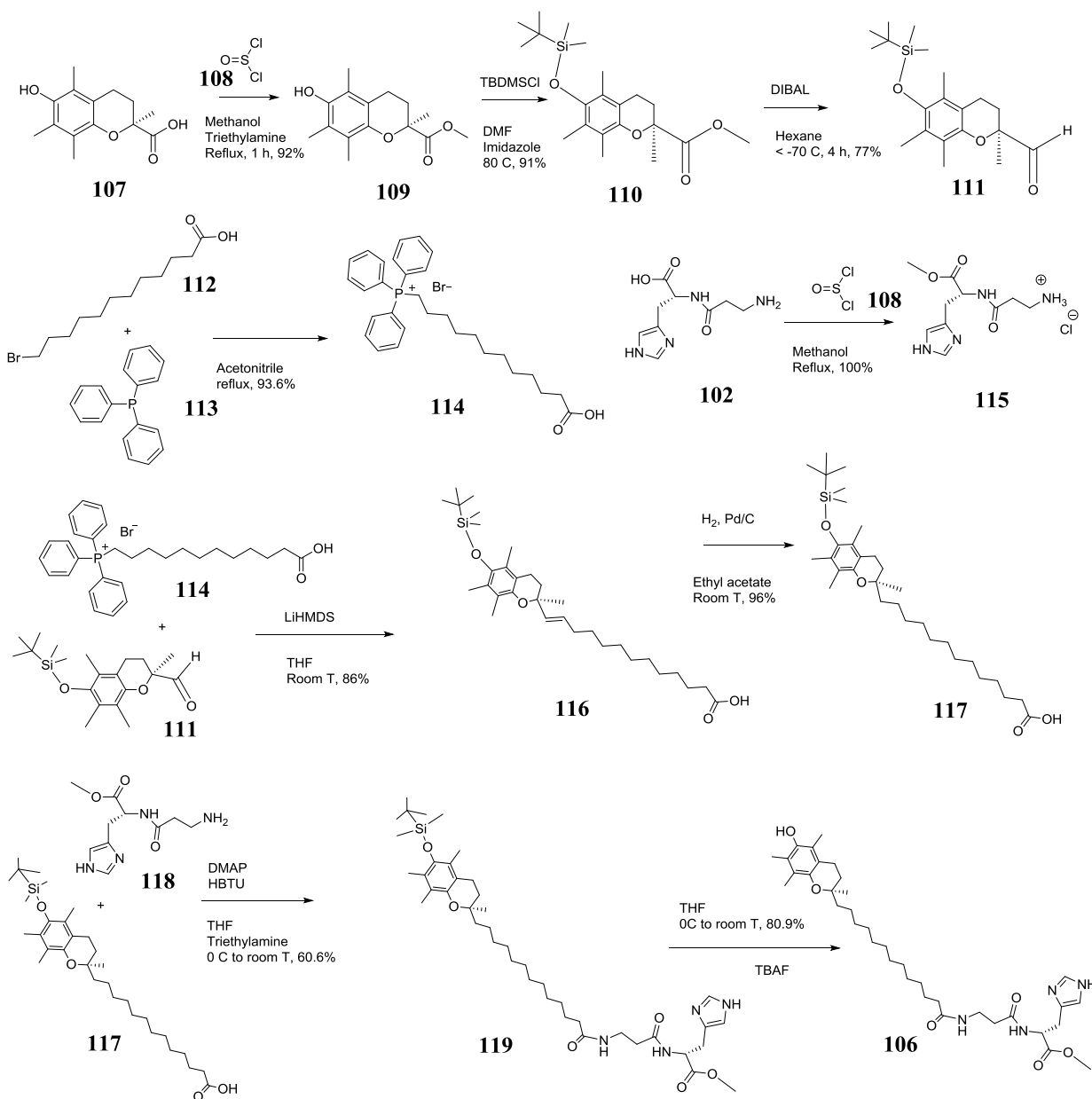
Another region of design importance is the middle section, the phytyl chain, of VECAR. Diplock and co-workers performed *in vivo* studies on rats to examine phytyl chain features. They determined that the length of the phytyl chain was important as shown when they decreased ($n \leq 11$) or increased ($n \geq 16$) the number of carbons and the effectiveness of the derivative diminished.²⁹ For these reasons, the length of VECAR's phytyl chain is retained to 12 carbons so that hydrophobic interactions within the binding pocket are maintained. The methyl appendages found on the phytyl chain of α -toc are removed in the design of VECAR to afford a more simplistic synthesis. Precedents for the elimination of the methyl groups on the phytyl tail without decreased α -TTP recognition arise from prior research reported in the literature.^{26,30} Ingold et al., completed a rat curative myopathy assay, which studied the pyruvate kinase activity in plasma to show that the removal of methyl groups in the 4', 8', and 12' positions do not hinder α -TTP recognition *in vivo*.³⁰ Studies completed by Diplock and co-workers have also shown the insignificance of the 4', 8', and 12' methyl appendages.²⁹

The last design segment is the right hand portion of VECAR, which contains the hydrophilic moiety attached to the end of the phytyl tail. Unlike many systems that couple molecules to the hydroxyl group of vitamin E, carnosine is a unique antioxidant to be coupled to the phytyl chain end. This conjugation is anticipated to provide antioxidant activity to more universal regions *in vivo* while maintaining its ability to be recognized by α -TTP for transfer into LDLs. Recent publications by Atkinson and co-workers have explored the synthesis of vitamin E analogues conjugated to fluorescent markers and studied their pathways in cells; for example

the vitamin E derivatives incorporating dipyrrometheneboron difluoride (BODIPY) and 7-nitrobenz-2-oxa-1,3-diazole (NBD) at the end of the phytyl chain.^{13,31} The successful recognition obtained by α -TTP suggests the possibility that alterations at the phytyl chain end will not affect cellular uptake. Although lipophilic molecules have been attached to the phytyl tail, a hydrophilic antioxidant moiety has not been explored; thus, the addition of carnosine, a hydrophilic dipeptide, has been chosen for the chimeric VECAR design. Kohen and co-workers have shown that the imidazole moiety of carnosine is important for its antioxidant mechanism.³² Through their studies, they concluded that the proton on the nitrogen in the imidazole ring as well as on the carbon directly next to the ring were involved in the antioxidant activity; therefore, leaving the imidazole portion of carnosine intact was crucial for the VECAR design.

5.3 VECAR Synthesis and Experimentals

The synthesis of the chimeric antioxidant vitamin E carnosine is depicted in Scheme 5.1. The overall synthesis comprised nine total steps, with seven being linear and had an overall yield of 26.1%. Protocols for several intermediates were based on the prior work of Lei and Atkinson.³³ The introduction of stereochemistry in the molecule arises from the commercially available starting material *S*-Trolox™ (**107**). At first, the synthesis of **109** was completed following a literature protocol using methanol and *p*-toluenesulfonic acid to esterify *S*-Trolox™ (**107**), which led to typical yields of about 50%.³³ To optimize the conditions for the esterification of *S*-Trolox™ (**107**), the protocol was changed to use thionyl chloride (**108**) instead of *p*-toluenesulfonic acid and the yields of **109** were improved to 83-92%.



Scheme 5.1 VECAR (106) Synthesis.

After esterification of *S*-Trolox™ (**107**), the addition of the TBDMS protecting group to form the ester molecule containing a protected hydroxyl group (**110**) was high yielding; 91% yield was typical after purification. Reduction of the ester (**110**) with DIBAL-H generated the aldehyde (**111**.) The purification of the aldehyde (**111**) from the ester (**110**) was not trivial. The

retention of the aldehyde and ester on chromatographic columns is very similar and separation of these molecules required gradient elution as well as multiple purifications in some cases. Avoiding formation of the ester is the key for improved yields and easier purification and this can be accomplished by using DIBAL-H and the aldehyde product free from all water contaminants. After optimization, the aldehyde (**111**) was synthesized in 77% yield and was used subsequently in a Wittig reaction. In a separate pot, 12-bromododecanoic acid (**112**) and triphenylphosphine (**113**) were reacted to form the phosphonium salt (**114**) in high yields, 93.6% at optimum.

The Wittig reaction proceeded as expected and the red ylide (**114**) solution turned yellow upon addition of the aldehyde (**111**) to form the unsaturated molecule (**116**) with typical yields of about 86%. The alkene of molecule **117** was reduced using H₂ and Pd/C. This reaction often required filtering multiple times through a celite cake, but was still high yielding with typical yields above 95%. The first several attempts to couple carnosine to molecule **117** were unsuccessful and this was attributed to the insolubility of carnosine in the reaction solvents that were explored (methanol, acetonitrile, THF, and DMF.) To improve solubility of carnosine, the carnosine methyl ester was synthesized (**115**.) Thionyl chloride (**108**) was used to convert carnosine (**102**) to the methyl ester salt (**115**), which upon addition of Et₃N formed the carnosine methyl ester (**118**) in quantitative yields. The addition of carnosine methyl ester **118** to **117** was not a trivial synthetic step. Multiple attempts using DCC and HOBt to perform the coupling were unsuccessful because many impurities were formed and separation from the desired product **119** was difficult. The formation of a mixed anhydride using isobutyl chloroformate and NMM were also unsuccessful as the desired product was not formed. Finally, **118** and **117** were coupled using HBTU and DMAP yielding the protected VECAR molecule (**119**) in yields above

50%, 60.6% at optimal after purification by reverse phase chromatography. The protecting group was then removed from **119** using TBAF, and after purification by reverse phase chromatography, VECAR (**106**) was obtained in 80.9% yield at optimal.

(*S*)-methyl 6-hydroxy-2,5,7,8-tetramethylchroman-2-carboxylate (**109**):²⁷

Commercially available *S*-Trolox™ (Sigma-Aldrich) (**107**, 3.04 g, 12.1 mmol) was dissolved in 25 mL dry methanol. Triethylamine (2.4 mL, 17.0 mmol) was added to the solution and the reaction mixture stirred for 15 minutes at 0°C. Thionyl chloride (**108**, 1.06 mL, 14.6 mmol, 1.2 eq) was added to the mixture and this was stirred at 0°C for 10 additional minutes. The solution was refluxed at 70°C for 1 hour. After completion of the reaction, the solution was cooled to room temperature and was purged with nitrogen to remove any thionyl chloride that remained. After solvent evaporation, the brown solid was recrystallized from 75 mL methanol to afford white crystals (**109**, 2.95 g, 92%). ¹H (CDCl₃, 400 MHz) δ 4.31 (br, 1H, OH), 3.69 (s, 3H, OCH₃), 2.68 (m, 2H), 2.45 (m, 1 H), 2.20 (s, 3H), 2.16 (s, 3H), 2.07 (s, 3H), 1.87 (m, 1H), 1.62 (s, 3H, CH₃). ¹³C NMR (CDCl₃, 100MHz) δ 174.53, 145.52, 145.31, 122.56, 121.30, 118.45, 116.87, 77.03, 52.38, 30.63, 25.45, 20.97, 12.21, 11.84, 11.26. IR ν_{max} 3527.61, 2989.30, 2926.84, 1738.34, 1454.75, 1193.27, 1113.77 cm⁻¹. MS (ESI-TOF): calcd for C₁₅H₂₀NaO₄ (M+Na)⁺: 287.1260; found: 287.1241.

(*S*)-methyl-6-(tert-butyldimethylsilyloxy)-2,5,7,8-tetramethylchroman-2-carboxylate (**110**):^{33,27}

Tert-butyldimethylsilyl chloride (1.081g, 7.2mmol) and imidazole (1.339 g, 19.7 mmol) was added to a solution of (*S*)-methyl-6-hydroxy-2,5,7,8-tetramethylchroman-2-carboxylate (**109**, 1.254 g, 4.7 mmol) in 10 mL dry dimethylformamide (10 mL). The reaction mixture was

stirred under argon in an oil bath for 5 hours at 85°C until no starting material (**109**) was detected by TLC. The mixture was poured into brine (100 mL) and was extracted with ethyl acetate (4 X 50 mL). The organic extracts were combined and dried over magnesium sulfate followed by solvent evaporation to afford a light yellow colored oil. Purification of the crude product was completed using column chromatography on silica gel using the mobile phase CH₂Cl₂:hexane (3:1) to yield 1.62 g (91%) white solid product (**110**). ¹H (CDCl₃, 400 MHz) δ ppm 3.66 (s, 3H, OCH₃), 2.57 (m, 2H), 2.44 (m, 1H), 2.15 (s, 3H), 2.11 (s, 3H), 2.02 (s, 3H), 1.88 (m, 1H), 1.60 (s, 3H), 1.04 (s, 9H), 0.11 (s, 6H). ¹³C NMR (CDCl₃, 100MHz) δ ppm 174.55, 145.90, 144.81, 126.14, 123.48, 122.70, 117.06, 77.02, 52.30, 30.58, 26.11, 25.41, 21.07, 18.62, 14.34, 13.39, 12.00, -3.28, -3.34. IR ν_{max} 2957.55, 2928.25, 2856.92, 1746.92, 1464.01, 1260.53, 1110.79 cm⁻¹. MS (ESI-TOF): calcd for C₂₁H₃₄NaO₄Si (M+Na)⁺: 401.2124; found 401.2171.

(*S*)-6-(tert-butyldimethylsilyloxy)-2,5,7,8-tetramethylchroman-2-carbaldehyde (**111**):^{33,27}

Compound **110** (3.282 g, 8.67 mmol) in 35 mL dry hexane was cooled to -75°C in a dry ice/ acetone bath. Diisobutylaluminum hydride, DIBAL-H, (1.0 M in hexane, 16 mL, 16 mmol) was added dropwise through a syringe maintain a temperature below -70°C. After 2 hours, 25 mL methanol was added and stirred for 15 minutes. The reaction vessel was lifted from the dry ice/acetone bath and was allowed to slowly warm to -28°C. Upon warming 15 mL water was added to the solution. The solution was then poured into brine (100 mL) and was extracted with hexane/ethyl acetate (2:1) (4 X 100 mL). After the organic layers were combined and dried over magnesium sulfate, the solvent was evaporated. Purification of the crude product by column chromatography using 1:1 to 3:1 CH₂Cl₂:hexane led to 2.33 g product (**111**, 77% yield.) ¹H (CDCl₃, 400 MHz) δ ppm 9.63 (s, 1H), 2.55 (m, 2H), 2.27 (m, 1H), 2.17 (s, 3H), 2.12 (s, 3H),

2.02 (s, 3H), 1.82 (m, 1H), 1.39 (s, 3H), 1.05 (s, 3H), 0.12 (s, 6H). ^{13}C NMR (CDCl_3 , 100MHz) δ ppm 204.91, 145.56, 145.13, 126.50, 123.89, 122.84, 117.62, 80.28, 27.93, 26.08, 21.62, 20.49, 18.60, 14.35, 13.38, 12.06, -3.31, -3.34. IR ν_{max} 2928.40, 2857.11, 2799.65, 1741.47, 1463.23, 1255.44, 1101.77, 836.53 cm^{-1} . MS (ESI-TOF): calcd for $\text{C}_{20}\text{H}_{33}\text{O}_3\text{Si}$ ($\text{M}+\text{H}$) $^+$: 349.2199; found 349.2023.

11-carboxyundecyl)triposponium bromide (**114**):^{33,27}

12-bromododecanoic acid (**112**, 1.66 g, 5.9 mmol) was dissolved in 13 mL dry acetonitrile when heated and stirred. Triphenylphosphine (**113**, 1.637 g, 6.2 mmol) and 13 mL dry acetonitrile were heated and stirred, and this solution was added to the 12-bromododecanoic/MeCN solution and the reaction mixture was refluxed overnight. After cooling, the solvent was evaporated. The resulting crystals were dissolved in 14 mL DCM and transferred to an Erlenmeyer flask. Toluene (40 mL) was added to the dissolved crystals and the solution was stirred and heated. After the solution was cooled, the phosphonium salt was allowed to slowly crystallize and was removed by filtration, yielding 3.01 g (**114**, 93.6%). ^1H NMR (CDCl_3 , 400 MHz) δ ppm 7.76-7.67 (m, 9H), 7.67-7.27 (m, 6H), 3.56-3.51 (m, 2H), 2.28 (t, 2H, $J = 7.42$ Hz), 1.53-1.45 (m, 6H), 1.17-1.11 (m, 12H). ^{13}C NMR (CDCl_3 , 100 MHz) δ ppm 177.51, 135.11, 135.09, 133.61, 133.51, 130.61, 130.48, 118.60, 117.75, 34.50, 30.37, 30.21, 29.09, 29.07, 28.97, 28.94, 28.81, 24.73, 22.88, 22.52, 22.48, 22.39. IR ν_{max} 2925.16, 2848.82, 1715.11, 1436.26, 1113.18 cm^{-1} . MS (ESI-TOF): calcd for $\text{C}_{30}\text{H}_{39}\text{BrO}_2\text{P}$ ($\text{M}+\text{H}-\text{Br}$) $^+$: 461.2831; found 461.2332.

(*S,E*)-13-(6-(tert-butyldimethylsilyloxy)-2,5,7,8-tetramethylchroman-2-yl)tridec-12-enoic acid
(**116**):^{33,27}

The phosphonium salt (**114**) (2.50 g, 11.5 mmol) was dissolved in 40 mL dry THF under argon at room temperature. LiHMDS in THF (1 M in THF, 16.5 mL, 11.5 mmol) was added by dropwise addition to the phosphonium salt (**114**) solution and the red ylide was stirred under argon for 2 hours. A solution of the aldehyde (**111**, 1.45 g) in 8 mL dry THF was added dropwise to the reaction vessel and a color change from red to pale yellow was observed. After the suspension was stirred for 3 additional hours, the reaction was quenched with 80 mL saturated NH₄Cl (aq) and 80 mL water. Extractions were completed with ethyl acetate, and the organic extracts were combined and dried over magnesium sulfate. After solvent evaporation, the crude product was triturated with cold hexane to remove the triphenylphosphine oxide. Next, the hexane was evaporated and the crude product was purified using column chromatography with ethyl acetate:hexane (1:1) mobile phase yielding 1.90 g (**116**, 86%). ¹H NMR (CDCl₃, 400 MHz) δ ppm 5.33-5.31 (m, 2H), 2.55-2.53 (m, 2H), 2.36-2.33 (m, 2H), 2.11 (s, 3H), 2.10 (s, 3H), 2.08-2.01 (m, 2H), 2.04 (s, 3H), 1.65-1.62 (m, 2H), 1.47 (s, 3H), 1.29-1.22 (m, 16H) 1.05 (s, 9 H), 0.12 (s, 6H). ¹³C NMR (CDCl₃, 100MHz) δ ppm 179.99, 146.06, 144.13, 133.26, 132.49, 125.77, 123.46, 122.42, 117.83, 75.52, 34.04, 33.40, 29.97, 29.54, 29.42, 29.23, 29.05, 27.97, 27.23, 26.09, 24.67, 21.27, 18.58, 14.34, 13.40, 12.17, -3.35. IR ν_{max} 2927.02, 2855.11, 1709.96, 1462.79, 1254.07, 1090.75, 837.25 cm⁻¹. MS (ESI-TOF): calcd for C₃₂H₅₄O₄Si (M)⁺: 530.3791; found 530.3740.

(*R*)-13-(6-(tert-butyldimethylsilyloxy)-2,5,7,8-tetramethylchroman-2-yl)tridecanoic acid
(**117**):^{33,27}

116 (0.95 g, 3.67mmol) was dissolved in 85 mL ethyl acetate, and Pd/C (0.505 g) was added. A syringe connected to a balloon containing hydrogen was added to the reaction vessel and was stirred at room temperature for 18 hours. After the mixture was filtered through a celite cake and the solvent evaporated, an oil (**117**) was collected. Trace amounts of Pd/C were removed by column chromatography using the mobile phase hexane:ethyl acetate (4:1), yielding **117** (0.91 g 96%.) ¹H NMR (CDCl₃, 400 MHz) δ ppm 2.60 (t, 2H, J= 7.40), 2.40 (t, 2H, J= 6.28), 2.16 (s, 3H), 2.13 (s, 3H), 2.11 (s, 3H), 1.79-1.92 (m, 2H), 1.59-1.70 (m, 4H), 1.47-1.53 (m, 2H), 1.32 (br, 16H), 1.28 (s, 3H), 1.11 (s, 9H), 0.18 (s, 6H). ¹³C NMR (CDCl₃, 100MHz) δ ppm 180.52, 145.97, 144.10, 125.86, 123.52, 122.72, 117.52, 77.31, 39.66, 34.18, 31.60, 30.26, 29.71, 29.68, 29.52, 29.33, 29.14, 26.18, 24.74, 23.88, 23.70, 20.97, 18.65, 14.39, 13.47, 12.01, - 3.29. IR ν_{\max} 2928.58, 2853.19, 1711.92, 1252.43, 1087.10, 836.06 cm⁻¹. MS (ESI-TOF): calcd for C₃₂H₅₆O₄Si (M+H)⁺: 533.4026; found 533.4011.

Carnosine Methyl Ester Dihydrochloride (**115**):^{34,27}

Carnosine (**102**) (602.9 mg, 2.7 mmol) was suspended in 24 mL anhydrous methanol and was cooled to 0°C. Thionyl chloride (**108**, 0.25 mL, 3.3 mmol) was added to the reaction by dropwise addition and reaction mixture was stirred at 0°C for 10 additional minutes. Next, the solution was heated and refluxed for 1 hour at 75°C. After the reaction mixture was cooled to room temperature, the solvent was evaporated to afford **115** in quantitative yield. **115** was utilized in the next step without subsequent purification. ¹H NMR ((CD₃)₂SO) δ 9.04 (s, 1H), 8.89-8.87 (d, 1 H), 8.09 (br, 3H), 7.49, (s, 1H), 4.62-4.56 (m, 1H), 3.65 (s, 3H), 3.19-3.05 (m,

2H), 2.92 (br, 2H), 2.57 (t, 2H, J= 6.82). ^{13}C NMR (DMSO, 100MHz) δ ppm 171.36, 170.15, 134.06, 129.33, 117.50, 52.71, 52.01, 35.38, 32.31, 26.23. IR ν_{max} 3417.02, 3138.25, 1737.08, 1660.26, 1624.71. MS (ESI-TOF): calcd for $\text{C}_{10}\text{H}_{17}\text{ClN}_4\text{O}_3$ (M-H) $^+$: 275.0911; found 275.0912.

(*R*)-methyl-2-(3-(13-((*R*)-6-((tert-butyl)dimethylsilyl)oxy)-2,5,7,8-tetramethylchroman-2-yl)tridecanamido)propanamido)-3-(1H-imidazol-4-yl)propanoate (**119**).^{35,36,37,38,27}

117 (840 mg, 1.59 mmol), carnosine-methyl ester hydrochloride (**115**) (662 mg, 2.39 mmol), DMAP (19 mg, 0.16 mmol), and triethylamine (1.67 mL, 5 eq) were added to 13.4 mL anhydrous DMF. After the reaction solution was cooled to 0°C, HBTU (721 mg, 1.9 mmol) dissolved in anhydrous 3 mL DMF was added drop wise. The reaction mixture was stirred at 0°C for an additional 20 minutes and was then allowed to slowly warm to room temperature where it was allowed to stir overnight. After solvent evaporation under high vacuum, the crude product was dissolved in chloroform and washed with water. The organic layer was collected and the solvent was evaporated. Purification of the crude product was completed using 300 Å reverse phase silica gel (C_{18}). The C_{18} was prepared by taking 100 mg silica gel and suspending it in 500 mL toluene. Octadecyltrichlorosilane (C_{18} , 21 ml, 0.52 mol) was added to the suspension drop wise. After 10 min, triethylamine (28 ml, 4 equiv.) was added and the suspension was refluxed at 125°C for 24 hours. Next, toluene (1 L), DCM (1 L), ethyl acetate (1 L), and methanol (4 L) were used to wash the synthesized C_{18} silica. Finally, the C_{18} reversed phase silica was dried under high vacuum. Chromatography using the C_{18} reversed phase silica and a methanol:water (7:3) mobile phase afforded **119** (0.62 g, 60.6%). ^1H NMR (MeOD) δ 7.58 (s, 1H), 6.87 (s, 1H), 4.69-4.66 (m, 1H), 3.72 (s, 3H), 3.41-3.37 (m, 2H), 3.12-2.96 (m, 2H), 2.54

(t, 2H, J = 6.62 Hz), 2.41 (t, 2H, J = 6.66 Hz), 2.15 (t, 2H, J = 7.60 Hz), 2.07 (s, 3H), 2.03 (s, 3H; s, 3H), 1.82-1.71 (m, 2H), 1.57 (m, 3H), 1.44 (m, 3H), 1.26 (br, 16H), 1.20 (s, 3H), 1.04 (s, 9H), 0.10 (s, 6H). ^{13}C NMR (MeOD, 100MHz) δ ppm 176.30, 173.64, 173.46, 147.22, 145.32, 136.37, 126.56, 124.42, 123.52, 118.68, 75.51, 54.10, 52.76, 40.31, 37.11, 36.82, 36.36, 32.81, 31.20, 30.74, 30.63, 30.46, 30.33, 26.94, 26.68, 24.57, 24.22, 21.84, 19.50, 14.86, 13.91, 12.26, -3.07. IR ν_{max} 3446.06, 2927.19, 2854.43, 1733.62, 1716.69, 1683.57, 1652.84, 1646.99, 1256.82, 1090.42, 837.37 cm^{-1} . MS (ESI-TOF): calcd for $\text{C}_{42}\text{H}_{70}\text{N}_4\text{O}_6\text{Si}$ (M+H) $^+$: 755.5134; found 755.5127.

(*R*)-methyl-2-(3-(13-((*R*)-6-hydroxy-2,5,7,8-tetramethylchroman-2-yl)tridecanamido)propanamido)-3-(1H-imidazol-4-yl)propanoate, VECAR (**106**):²⁷

119 (255 mg) was dissolved in 10 mL dry THF. TBAF (2.9 mL of a 1 M THF solution) was added drop wise via a syringe and the solution was stirred at room temperature for 1.5 hours. After the THF was evaporated, the crude product was taken up in 200 mL chloroform and the solution was washed three times with water. The crude product was purified using column chromatography on 60 Å reverse phase silica gel by gradient elution with methanol:water (30/70) and methanol:water:ammonium hydroxide (8:1:1) as the mobile phases. The first two fractions eluted were impurities and finally the pure VECAR was obtained in the last fraction, yielding **106** (175 mg, 80.9%). ^1H (MeOD, 400 MHz) δ 7.68 (s, 1H), 6.89 (s, 1H), 4.69-4.65 (m, 1H), 3.69 (s, 3H), 3.39-3.34 (m, 2H), 3.12-2.95 (m, 2H), 2.57 (t, 2H, J = 6.9Hz), 2.39 (t, 2H, J = 6.7Hz), 2.14 (t, 2H, J = 3.6Hz), 2.11 (s, 3H), 2.07 (s, 3H), 2.03 (s, 3H), 1.79-1.72 (m, 2H), 1.59-1.53 (m, 3H), 1.43-1.39 (m, 3H), 1.27-1.26 (br, 16H), 1.19 (s, 3H). ^{13}C NMR (MeOD, 100MHz) δ ppm 176.43, 173.70, 173.36, 146.74, 136.25, 124.42, 122.99, 122.06, 118.26, 75.42, 53.99,

52.81, 40.22, 37.11, 36.85, 36.38, 32.99, 31.21, 30.71, 30.61, 30.44, 30.31, 29.87, 26.96, 24.58, 24.15, 21.77, 12.80, 12.02, 11.83. IR ν_{\max} 3445.78, 2962.90, 2928.89, 2854.65, 1733.63, 1652.73, 1646.86, 1260.60, 1083.82, 844.71 cm^{-1} . MS (ESI-TOF): calcd for $\text{C}_{36}\text{H}_{56}\text{N}_4\text{O}_6$ $(\text{M}+\text{H})^+$: 641.4278; found 641.4293.

VECAR (**106**) Antioxidant Activity:

The antioxidant activity of VECAR was examined *in vitro* using a 1,1-diphenyl-2-picrylhydrazyl (DPPH) assay. DPPH (**120**) is a molecule containing a stable free radical and this stability allows for its use in assays (Figure 5.6.)³⁹ To

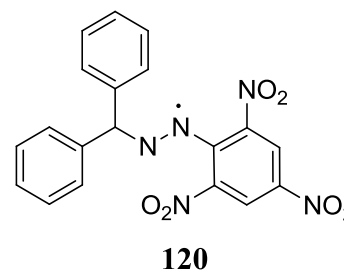


Figure 5.6 The structure of DPPH (120).

determine antioxidant performance, the ability of an antioxidant to scavenge the free radical of DPPH is analyzed spectroscopically. The purple DPPH radical turns to pale yellow when the radical is quenched. The antioxidant activity of VECAR was studied by Astete following a protocol employed by Luo and co-workers.^{27,28} Here, a 0.4 mM DPPH in methanol stock solution was prepared and stored at -20°C in the absence of light. An acetic acid in water mixture was used to dilute the sample to 1 mL maintaining a pH of 3.5. The sample was then added to the diluted DPPH solution attaining 0.1 mM DPPH and a 2 mL total sample volume, keeping the ratio of water to methanol at 1/1 v/v. Pure methanol and 1 mL water (pH = 3.5) were used to prepare the blank and the controls were made using 1 mL DPPH/methanol solution and 1 mL water (pH = 3.5.) After equilibrating for 30 mins, the absorptions of solutions at five different concentrations (0.01, 0.0125, 0.015, 0.02, and 0.025 mM) were taken at 518 nm in triplicate using a Geminys 6

spectrophotometer (Thermo Scientific, Waltham, MA). The percent inhibition was calculated according to Eq. 5.1.

$$\% \text{ change in activity} = 100 * \frac{\text{Abs}_{\text{control}} - \text{Abs}_{\text{sample}}}{\text{Abs}_{\text{control}}} \quad \text{Eq. 5.1}$$

A plot of the inhibition percentages versus the concentration of the antioxidant sample is shown in Figure 5.7 and the linear regressions were used to determine the moment that 50% DPPH was reduced by the antioxidant (the IC₅₀ value.) It was determined that the IC₅₀ values for VECAR (**106**) and α-tocopherol (**93**) were 24.9±1.4 μM and 24.4±1.5 μM respectively. These values for VECAR (**106**) and α-tocopherol (**93**) are essentially identical and verify that there was no loss of antioxidant activity *in vitro*. The retention of antioxidant activity shown by the DPPH assay was expected because the main component of vitamin E carnosine (**106**) is α-tocopherol (**93**) and both molecules contain the free hydroxyl functional group that is able to function as an antioxidant. To test whether the antioxidant activity is improved in LDLs by the addition of the carnosine moiety, studies will be performed *in vivo*.

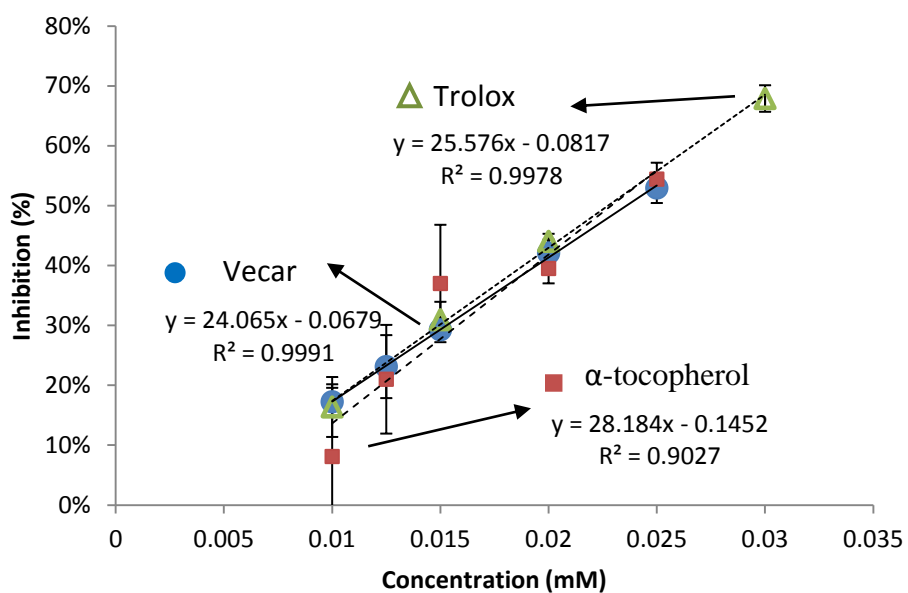


Figure 5.7 DPPH Assay used to determine the inhibition values.

5.4 VECAR Conclusion

A chimeric antioxidant, vitamin E carnosine (**106**), was successfully designed and synthesized, and its antioxidant activity was compared to α -toc *in vitro*. Three important regions were accounted for in the VECAR design; the chromanol ring, the phytyl tail, and the hydrophilic tail end. Two essential design features were to keep the chromanol ring intact and to use a 12 carbon tail to maintain the key regions of recognition by α -TTP. To accomplish this, 9 total, 7 linear synthetic steps were required. In the first synthetic step, thionyl chloride was used to convert the carboxylic acid of commercially available *S*-Trolox (**107**) to the methyl ester in 92% yield. *Tert*-Butyldimethylsilyl chloride (TBDMS-Cl) was used to protect the hydroxyl group of compound **107** in 91% yield. The resulting ester (**109**) was reduced to the aldehyde (**111**) in 77% yield using diisobutylaluminum hydride (DIBAL-H). Triphenylphosphine (**113**) and 12-bromododecanoic acid (**112**) were refluxed to form the phosphonium salt (**114**, 93.6% yield) for the Wittig reaction with compound **116** (86% yield). H₂ in the presence of Pd/C was used to hydrogenate the alkene resulting in **117** in 96% yield. After several failed attempts to attach carnosine directly to the carboxylic acid end of compound **117**, it was determined that the carnosine methyl ester (**118**) should be formed. Carnosine (**102**) was converted to the methyl ester salt (**115**) in quantitative yields using thionyl chloride. After the addition of triethylamine, the carnosine methyl ester (**118**), which was more soluble in the coupling reaction than the prior acid moiety was coupled to **117** using HBTU to generate compound **119** in 60.6% yield. The TBDMS protecting group of **119** was removed to yield the final product, VECAR (**106**), in 80.9% yield (26.1% overall yield) using TBAF. The final product (**106**) was studied using a DPPH assay which showed that VECAR and α -toc had nearly identical antioxidant activities,

and therefore, it was determined that there was no loss of antioxidant activity of the chimeric molecule *in vitro*.

5.5 VECAR Future Work

Further studies will be completed to examine the antioxidant activity of VECAR (106.) At this time, only a DPPH assay was used to determine if the antioxidant activity of VECAR through the chromanol ring was maintained in comparison to α -tocopherol. While this is important to show that there is no loss in antioxidant activity, the efficacy of the α -tocopherol transport system needs to be studied in biological systems. *In vivo* studies will be used to compare the uptake and bioavailability of VECAR to α -toc using an animal model. Once accessibility of VECAR in an animal model is shown, further results on its utility in prevention of atherosclerosis and other diseases caused by oxidative damage will be acquired.

5.6 References

1. World Health Organization, W. H. O. Global action plan for the prevention and control of noncommunicable diseases 2013-2020. <http://www.who.int/iris/handle/10665/94384#sthash.1ddcKrsp.dpuf>.
2. Psarros, C.; Lee, R.; Margaritis, M.; Antoniadis, C., Nanomedicine for the prevention, treatment and imaging of atherosclerosis. *Maturitas* **2012**, *73*, 52-60.
3. Halliwell, B., Oxidative stress and neurodegeneration: where are we now? *J. Neurochem.* **2006**, *97*, 1634-1658.
4. Young, I. S.; Woodside, J. V., Antioxidants in health and disease. *J Clin Pathol* **2001**, *54*, 176-86.
5. Cai, A.; Zheng, D.; Qiu, R.; Mai, W.; Zhou, Y., Lipoprotein-associated phospholipase A2 (Lp-PLA(2)): a novel and promising biomarker for cardiovascular risks assessment. *Dis Markers* **2013**, *34*, 323-31.

6. Yuan, X. M.; Brunk, U. T.; Olsson, A. G., Effects of Iron- and Hemoglobin-Loaded Human Monocyte-Derived Macrophages on Oxidation and Uptake of LDL. *Arteriosclerosis, Thrombosis, and Vascular Biology* **1995**, *15* (9), 1345-1351.
7. Ursini, F.; Davies, K. J. A.; Maiorino, M.; Parasassi, T.; Sevanian, A., Atherosclerosis: another protein misfolding disease? *Trends in Molecular Medicine* **2002**, *8* (8), 370-374.
8. Morel, D.; DiCorleto, P.; Chisolm, G., Endothelial and smooth muscle cells alter low density lipoprotein in vitro by free radical oxidation. *Arteriosclerosis, Thrombosis, and Vascular Biology* **1984**, *4* (4), 357-364.
9. Esterbauer, H.; Dieber-Rotheneder, M.; Striegl, G.; Waeg, G., Role of vitamin E in preventing the oxidation of low-density lipoprotein. *The American Journal of Clinical Nutrition* **1991**, *53* (1), 314S-321S.
10. Theriault, A.; Chao, J.-T.; Wang, Q.; Gapor, A.; Adeli, K., Tocotrienol: a review of its therapeutic potential. *Clin. Biochem.* **1999**, *32*, 309-319.
11. Shetti, N.; Patil, R., Antioxidants: its beneficial role against health damaging free radical. *World J. Sci. Technol.* **2011**, *1*, 46-51.
12. Moure, A.; Cruz, J. M.; Franco, D.; Domínguez, J. M.; Sineiro, J.; Domínguez, H.; José Núñez, M. a.; Parajó, J. C., Natural antioxidants from residual sources. *Food Chemistry* **2001**, *72* (2), 145-171.
13. Zhang, W.; Frahm, G.; Morley, S.; Manor, D.; Atkinson, J., Effect of Bilayer Phospholipid Composition and Curvature on Ligand Transfer by the α -Tocopherol Transfer Protein. *Lipids* **2009**, *44* (7), 631-641.
14. Blatt, D. H.; Leonard, S. W.; Traber, M. G., Vitamin e kinetics and the function of tocopherol regulatory proteins. *Nutrition* **2001**, *17* (10), 799-805.
15. Noguchi, N.; Niki, E., [51] Apolipoprotein B protein oxidation in low-density lipoproteins. In *Methods in Enzymology*, Lester, P., Ed. Academic Press: 1994; Vol. Volume 233, pp 490-494.
16. Fuller, C. J.; Agil, A.; Lender, D.; Jialal, I., Superoxide production and LDL oxidation by diabetic neutrophils. *J Diabetes Complications* **1996**, *10*, 206-10.
17. Mashima, R.; Yoshimura, S.; Yamamoto, Y., Reduction of Lipid Hydroperoxides by Apolipoprotein B-100. *Biochem. Biophys. Res. Commun.* **1999**, *259*, 185-189.
18. McClements, D. J.; Decker, E. A., Lipid Oxidation in Oil-in-Water Emulsions: Impact of Molecular Environment on Chemical Reactions in Heterogeneous Food Systems. *Journal of Food Science* **2000**, *65* (8), 1270-1282.

19. Mishra, R.; Bisht, S. S., Antioxidants and their characterization. *J. Pharm. Res.* **2011**, *4*, 2744-2746.
20. Rehman, A.; Collis, C. S.; Yang, M.; Kelly, M.; Diplock, A. T.; Halliwell, B.; Rice-Evans, C., The effects of iron and vitamin C co-supplementation on oxidative damage to DNA in healthy volunteers. *Biochem. Biophys. Res. Commun.* **1998**, *246*, 293-298.
21. Cooke, M. S.; Evans, M. D.; Mistry, N.; Lunec, J., Role of dietary antioxidants in the prevention of in vivo oxidative DNA damage. *Nutr. Res. Rev.* **2002**, *15*, 19-41.
22. Chen, W.; Park, S. K.; Yu, W.; Xiong, A.; Sanders, B. G.; Kline, K., Synthesis and screening of novel vitamin E derivatives for anticancer functions. *European Journal of Medicinal Chemistry* **2012**, *58* (0), 72-83.
23. Takata, J.; Hidaka, R.; Yamasaki, A.; Hattori, A.; Fukushima, T.; Tanabe, M.; Matsunaga, K.; Karube, Y.; Imai, K., Novel d- γ -tocopherol derivative as a prodrug for d- γ -tocopherol and a two-step prodrug for S- γ -CEHC. *Journal of Lipid Research* **2002**, *43* (12), 2196-2204.
24. Elnagar, A. Y.; Wali, V. B.; Sylvester, P. W.; El Sayed, K. A., Design and preliminary structure-activity relationship of redox-silent semisynthetic tocotrienol analogues as inhibitors for breast cancer proliferation and invasion. *Bioorg Med Chem* **2010**, *18* (2), 755-68.
25. Ogata, K.; Nakao, H. C. T. Tocopherol derivatives. EP683164A1, 1995.
26. Meier, R.; Tomizaki, T.; Schulze-Briese, C.; Baumann, U.; Stocker, A., The Molecular Basis of Vitamin E Retention: Structure of Human α -Tocopherol Transfer Protein. *Journal of Molecular Biology* **2003**, *331* (3), 725-734.
27. Astete, C. E.; Songe Meador, D.; Spivak, D.; Sabliov, C., Synthesis of Vitamin E-Carnosine (Vecar): New Antioxidant Molecule with Potential Application in Atherosclerosis. *Synthetic Communications* **2012**.
28. Luo, X.-D.; Basile, M. J.; Kennelly, E. J., Polyphenolic Antioxidants from the Fruits of *Chrysophyllum cainito* L. (Star Apple). *J. Agric. Food Chem.* **2002**, *50*, 1379-1382.
29. Diplock, A. T.; Xu, G.; Yeow, C.; Okikiola, M., Relationship of tocopherol structure to biological activity, tissue uptake, and prostaglandin biosynthesis. *Ann. N. Y. Acad. Sci.* **1989**, *570*, 72-84.
30. Ingold, K. U.; Burton, G. W.; Foster, D. O.; Hughes, L., Is methyl-branching in α -tocopherol's tail important for its in vivo activity? Rat curative myopathy bioassay measurements of the vitamin E activity of three 2RS-n-alkyl-2,5,7,8-tetramethyl-6-hydroxychromans. *Free Radical Biol. Med.* **1990**, *9*, 205-10.

31. West, R.; Panagabko, C.; Atkinson, J., Synthesis and Characterization of BODIPY- α -Tocopherol: A Fluorescent Form of Vitamin E. *J. Org. Chem.* **2010**, *75*, 2883-2892.
32. Kohen, R.; Yamamoto, Y.; Cundy, K. C.; Ames, B. N., Antioxidant activity of carnosine, homocarnosine, and anserine present in muscle and brain. *Proc. Natl. Acad. Sci. U. S. A.* **1988**, *85*, 3175-3179.
33. Lei, H.; Atkinson, J., Synthesis of Phytol- and Chroman-Derivatized Photoaffinity Labels Based on α -Tocopherol. *J. Org. Chem.* **2000**, *65*, 2560-2567.
34. Abdo, M.-R.; Joseph, P.; Boigegrain, R.-A.; Liautard, J.-P.; Montero, J.-L.; Koehler, S.; Winum, J.-Y., Brucella suis histidinol dehydrogenase: Synthesis and inhibition studies of a series of substituted benzylic ketones derived from histidine. *Bioorg. Med. Chem.* **2007**, *15*, 4427-4433.
35. Zhao, M.; Bi, L.; Bi, W.; Wang, C.; Yang, Z.; Ju, J.; Peng, S., Synthesis of new class dipeptide analogues with improved permeability and antithrombotic activity. *Bioorg. Med. Chem.* **2006**, *14*, 4761-4774.
36. Wu, G.; Liu, J.; Bi, L.; Zhao, M.; Wang, C.; Baudy-Floc'h, M.; Ju, J.; Peng, S., Toward breast cancer resistance protein (BCRP) inhibitors: design, synthesis of a series of new simplified fumitremorgin C analogues. *Tetrahedron* **2007**, *63*, 5510-5528.
37. Montalbetti, C. A. G. N.; Falque, V., Amide bond formation and peptide coupling. *Tetrahedron* **2005**, *61*, 10827-10852.
38. Sudo, Y.; Wada, T., Characteristics of octadecylsilylated silica gels end-capped by high-temperature silylation. *Journal of Chromatography A* **1998**, *813* (2), 239-246.
39. Apak, R.; Gorinstein, S.; Bohm, V.; Schaich, K. M.; Ozyurek, M.; Guclu, K., Methods of measurement and evaluation of natural antioxidant capacity/activity (IUPAC Technical Report). *Pure Appl. Chem.* **2013**, *85*, 957-998.

APPENDIX A: SPECTRA FOR CHAPTER TWO

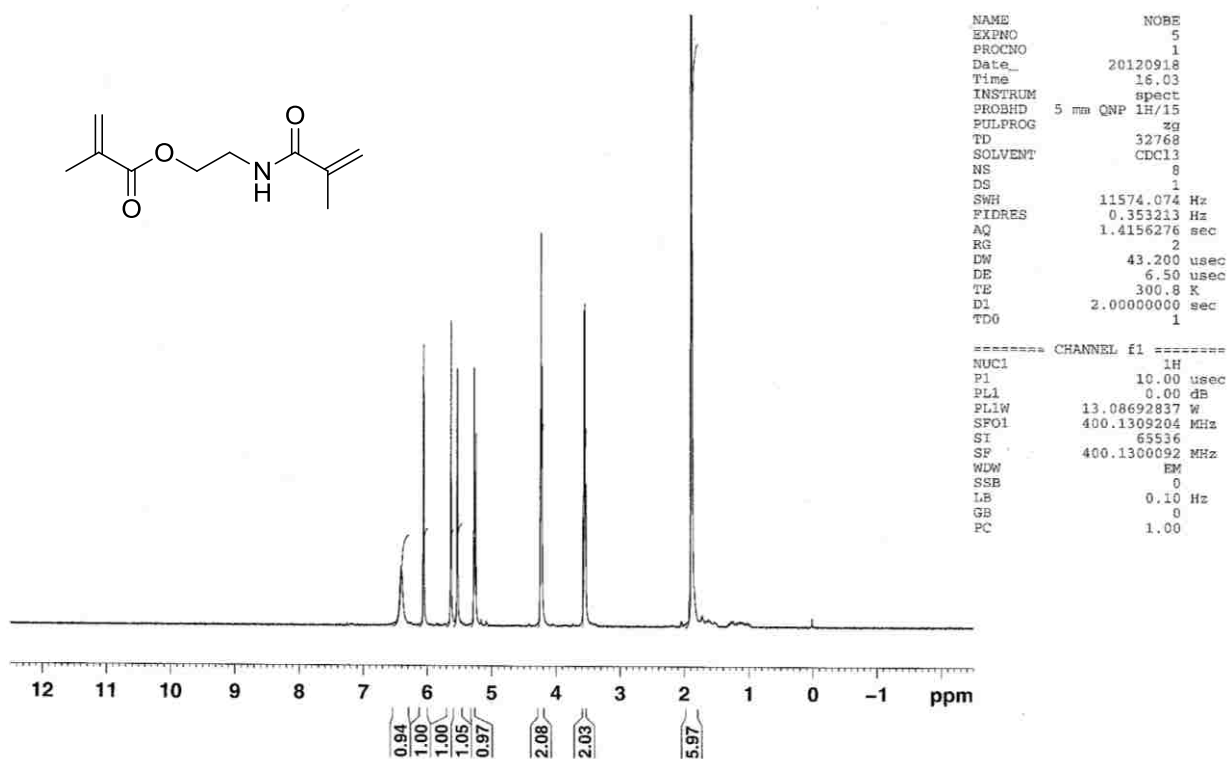


Figure A1: 2-methacrylamidoethyl methacrylate (NOBE (1)) ¹H NMR.

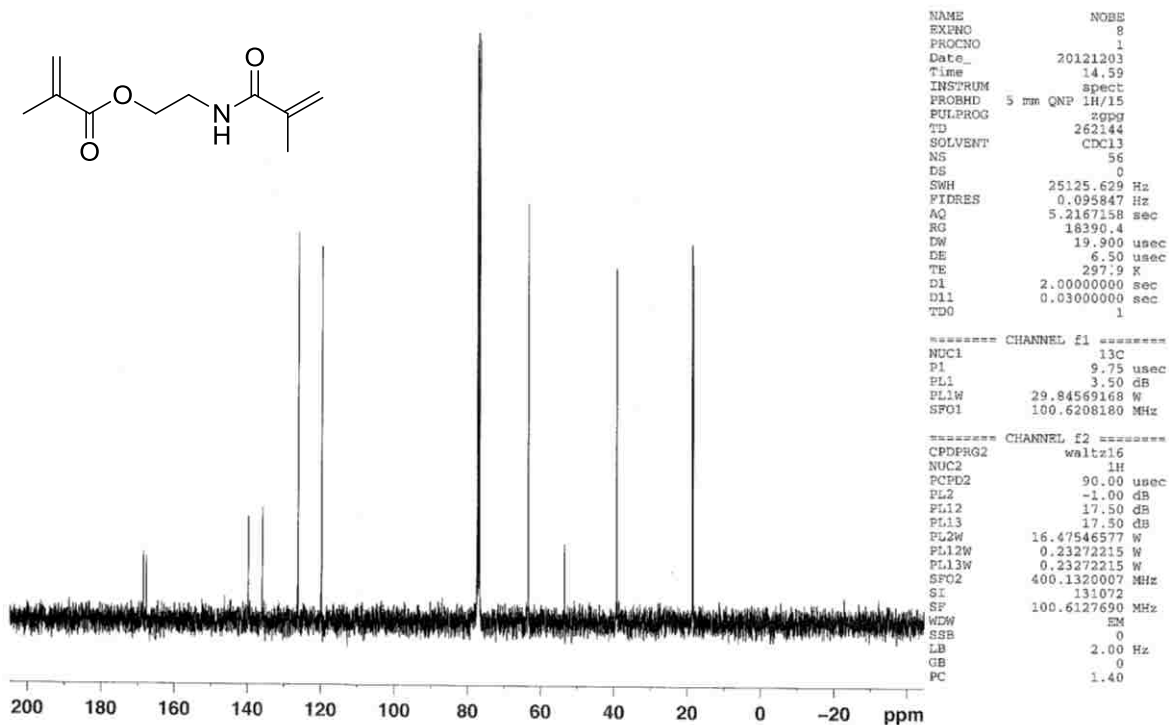


Figure A2: 2-methacrylamidoethyl methacrylate (NOBE (1)) ¹³C NMR.

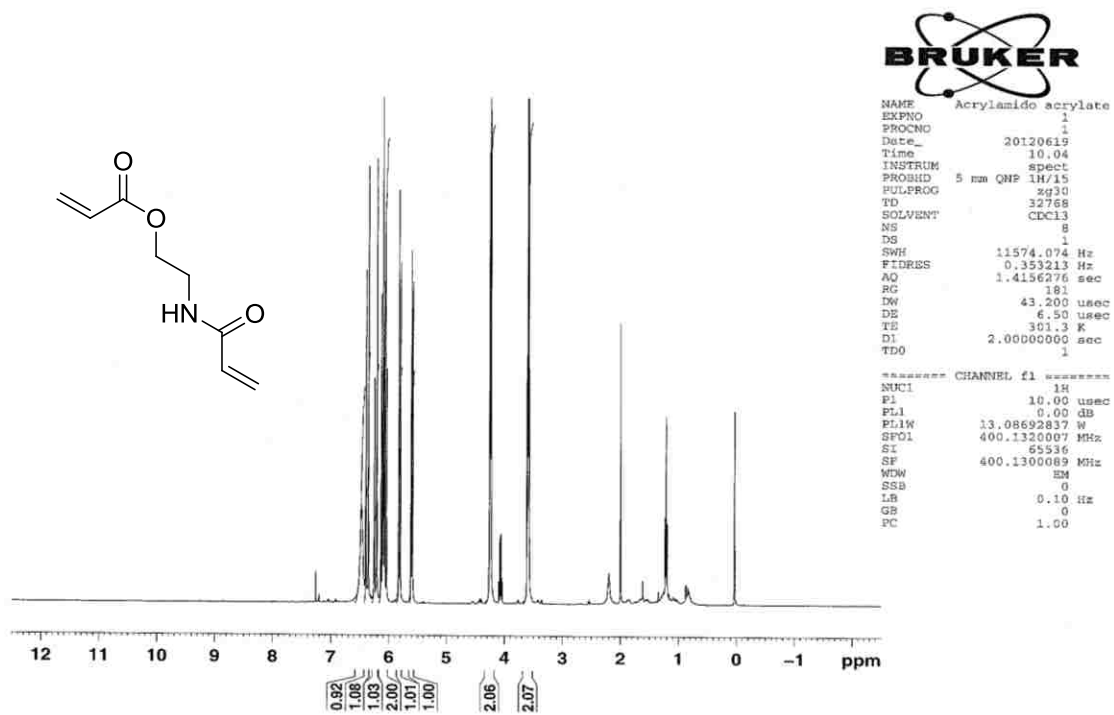


Figure A3: 2-acrylamidoethyl acrylate (13) ¹H NMR.

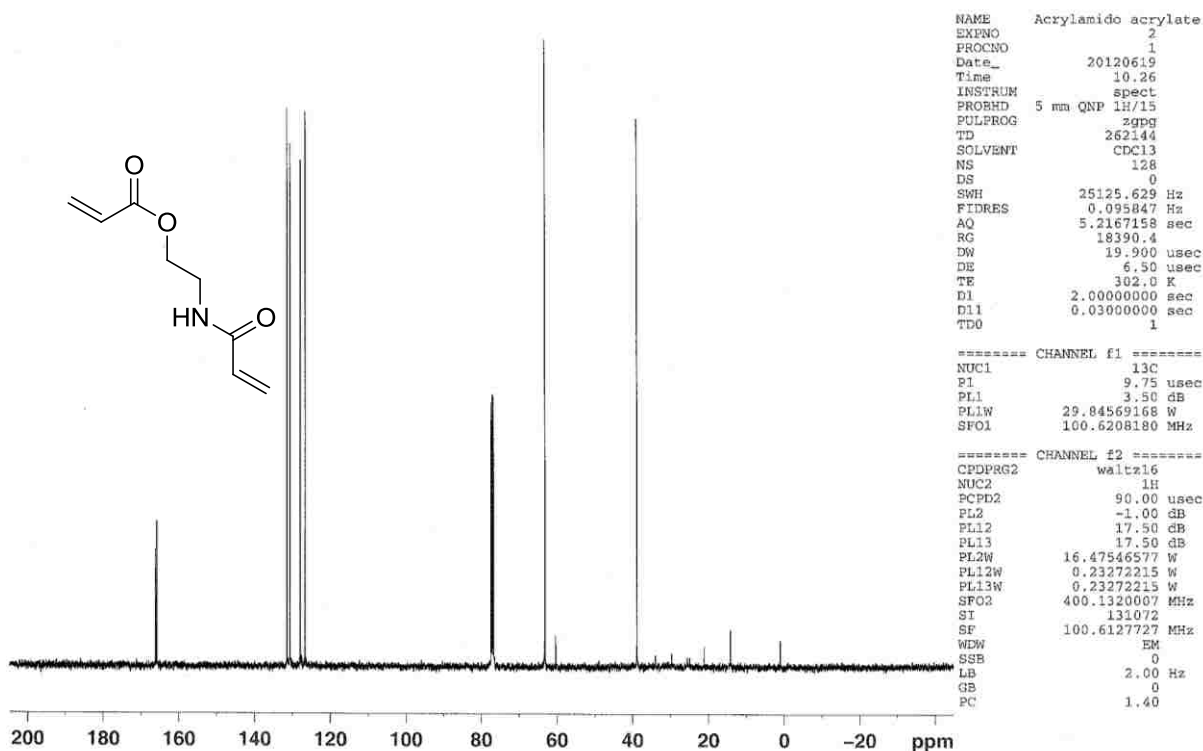


Figure A4: 2-acrylamidoethyl acrylate (13) ¹³C NMR.

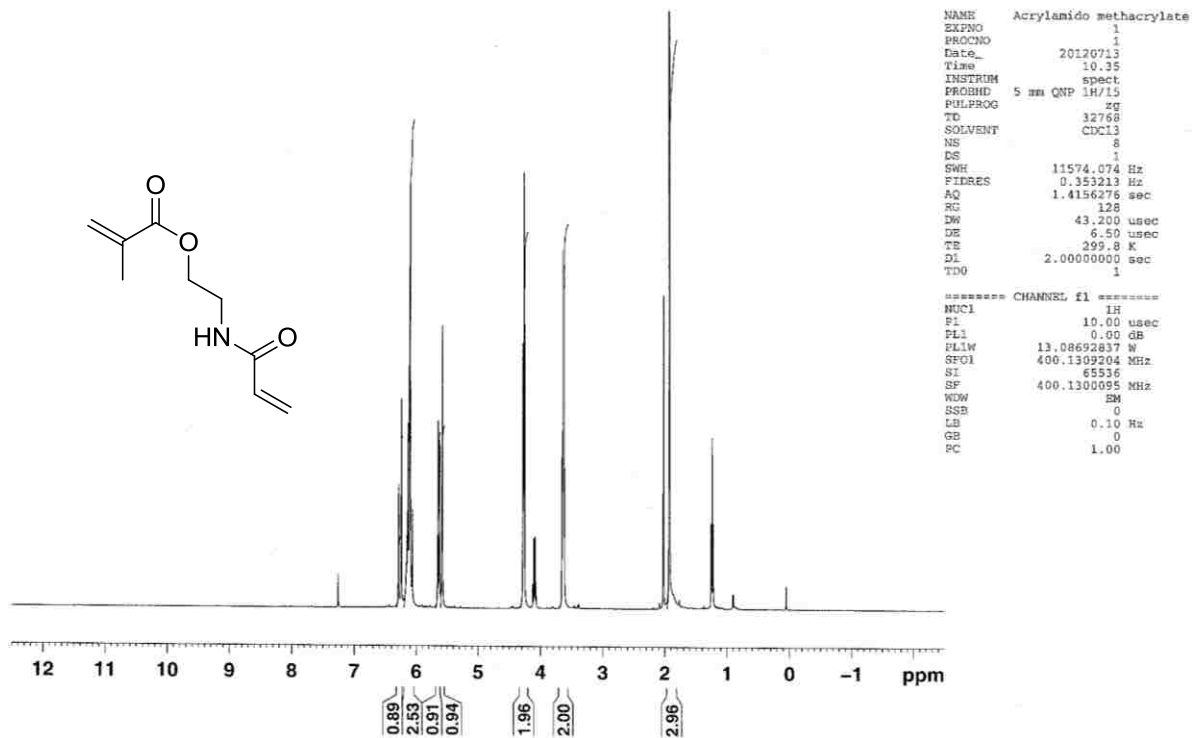


Figure A5: 2-acrylamidoethyl methacrylate (14) ¹H NMR.

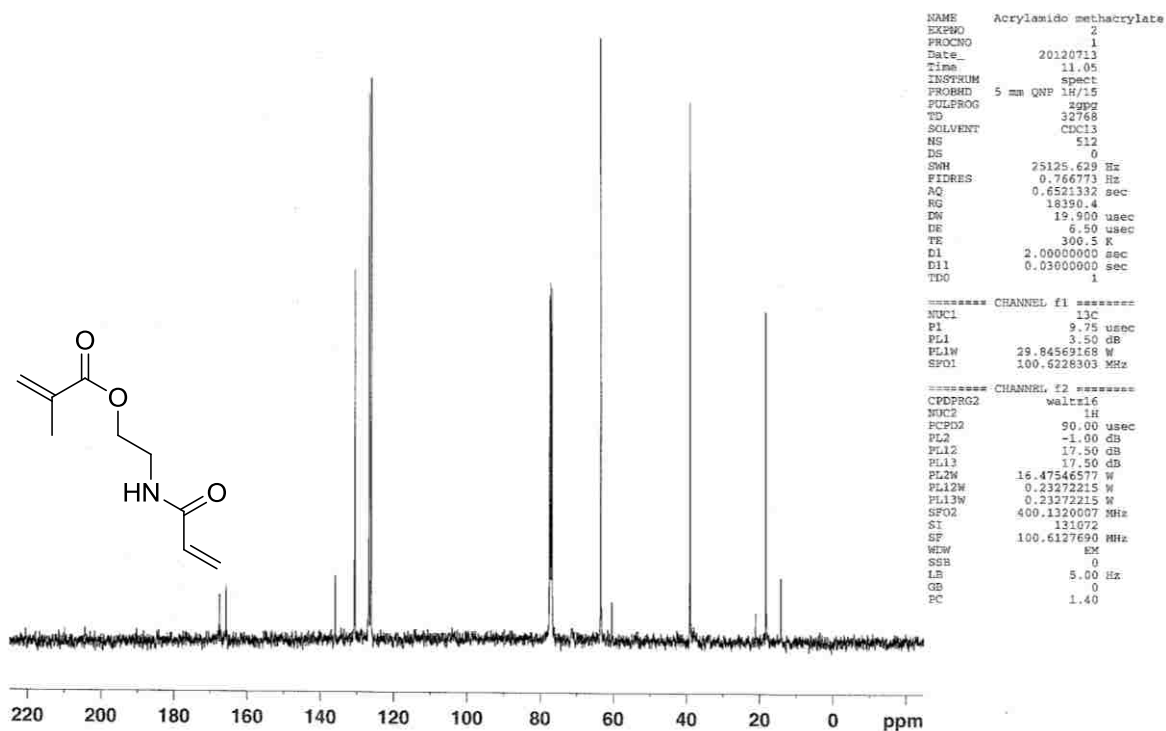


Figure A6: 2-acrylamidoethyl methacrylate (14) ¹³C NMR.

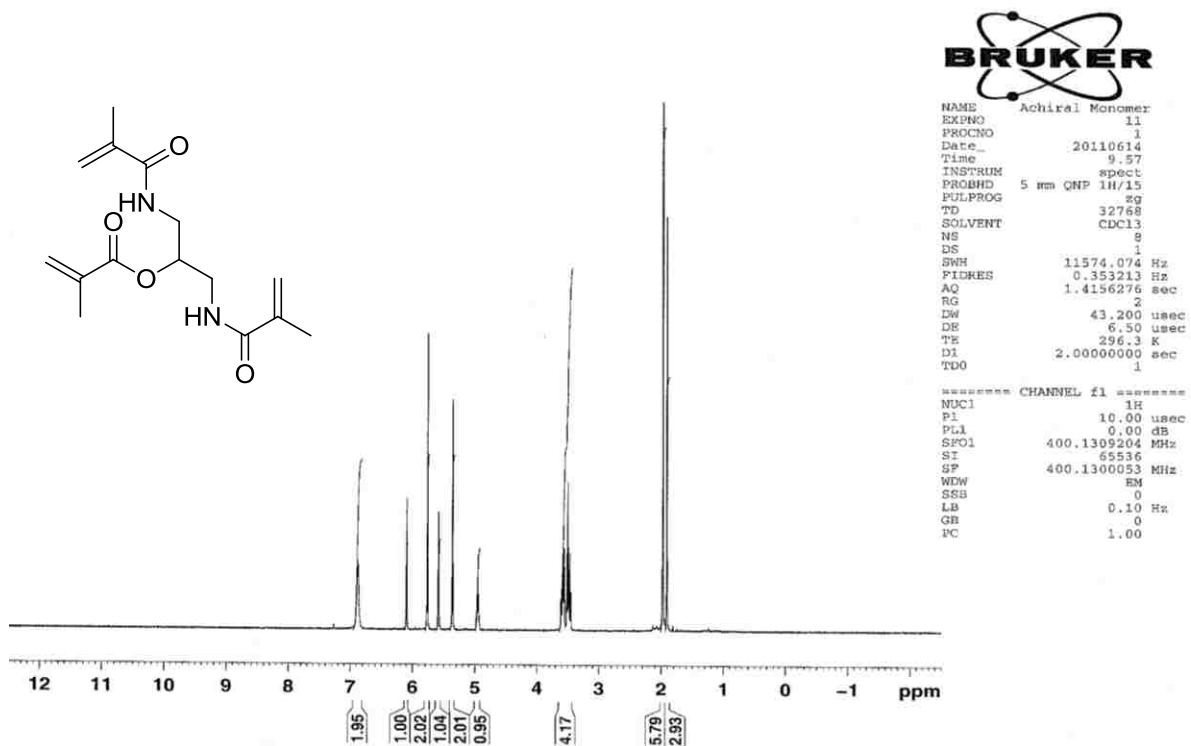


Figure A7: 1,3-dimethacrylamidopropan-2-yl methacrylate (17) ^1H NMR.

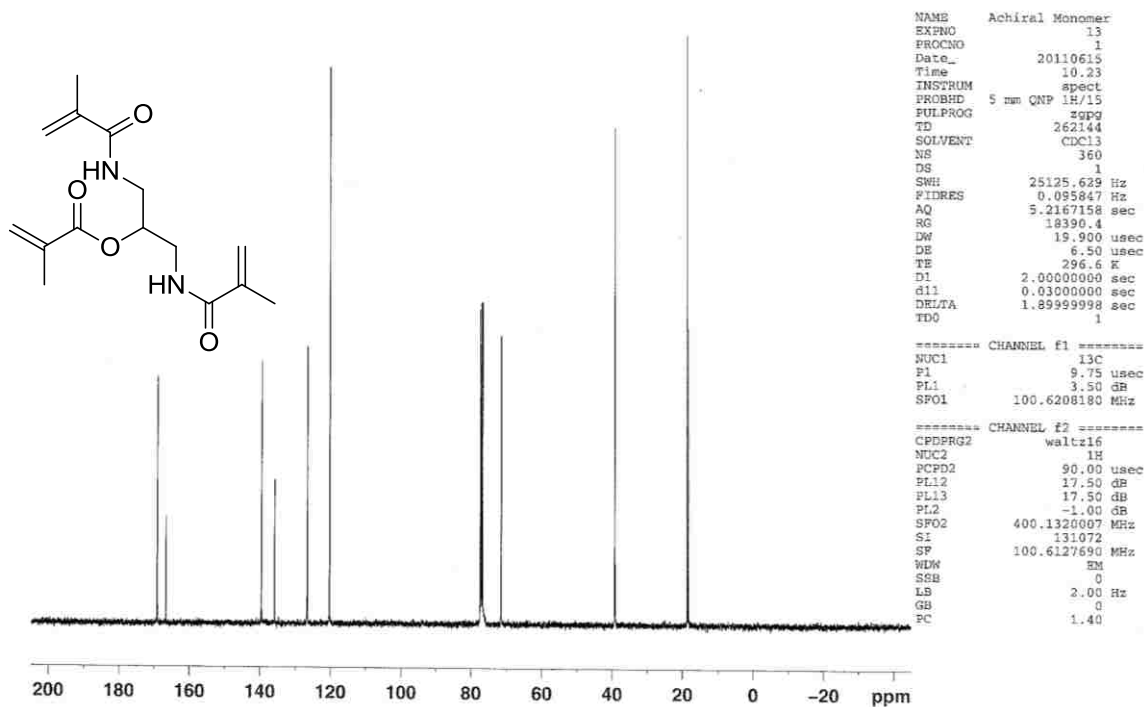


Figure A8: 1,3-dimethacrylamidopropan-2-yl methacrylate (17) ^{13}C NMR.

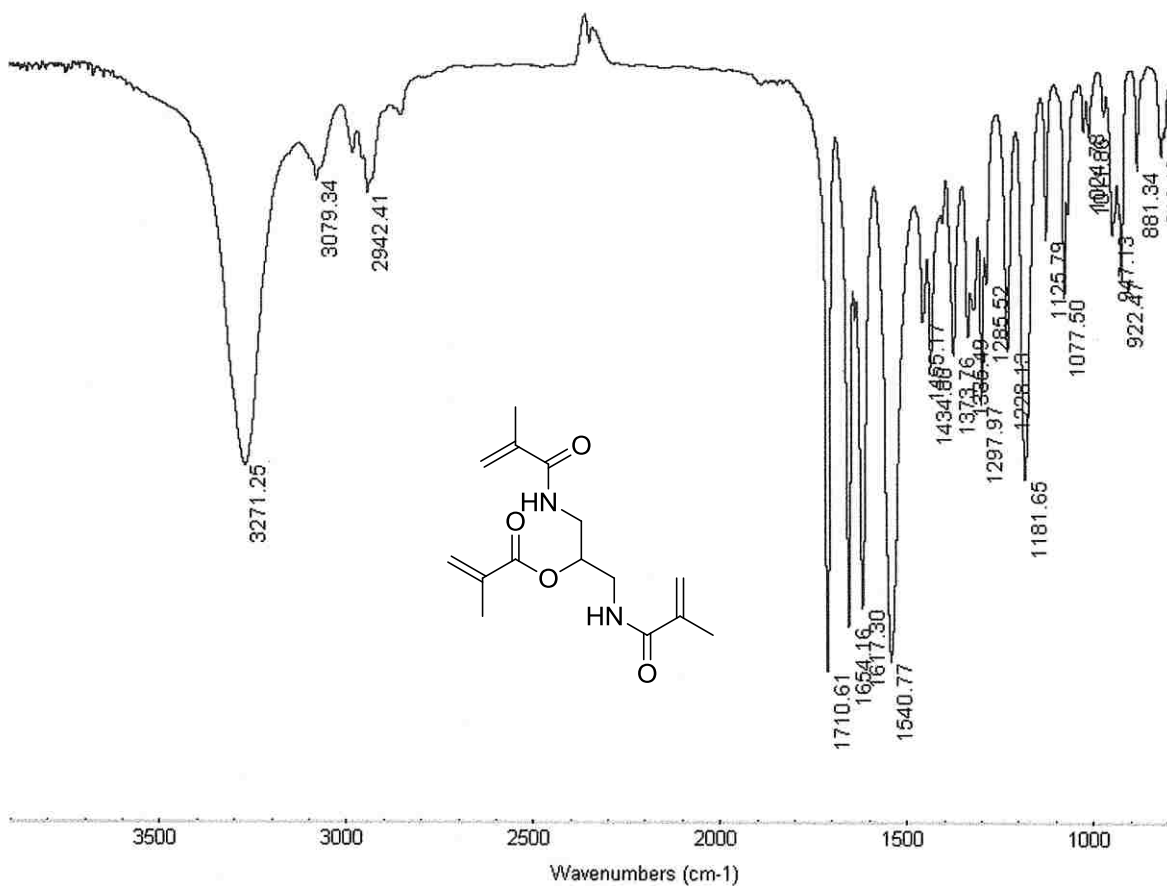


Figure A9: 1,3-dimethacrylamidopropan-2-yl methacrylate (17) IR.

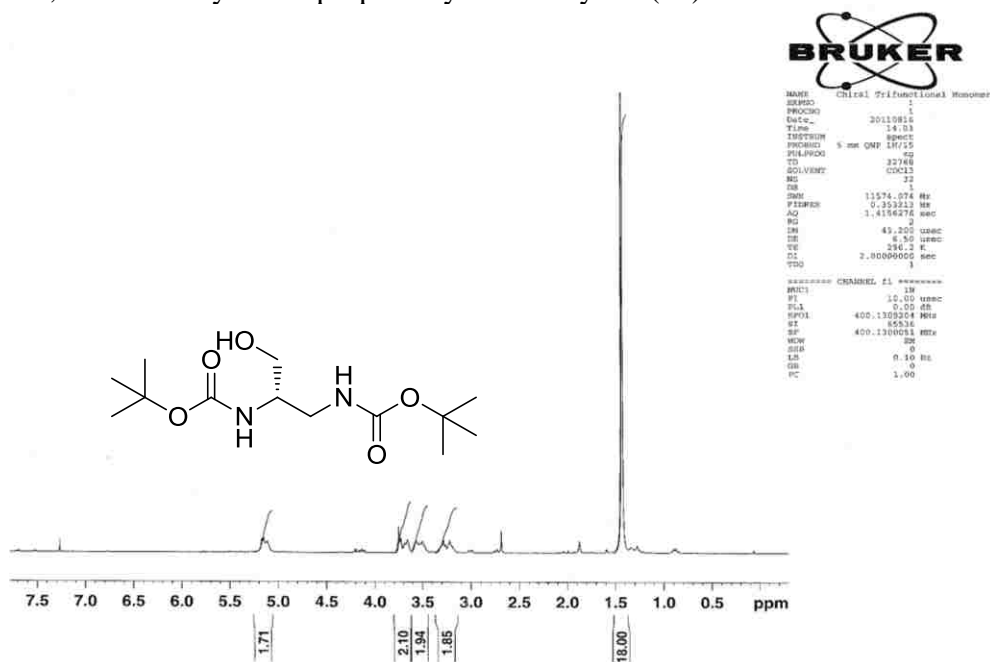


Figure A10: (S)-di-tert-butyl (3-hydroxypropane-1,2-diyl)dicarbamate (26) ¹H NMR.

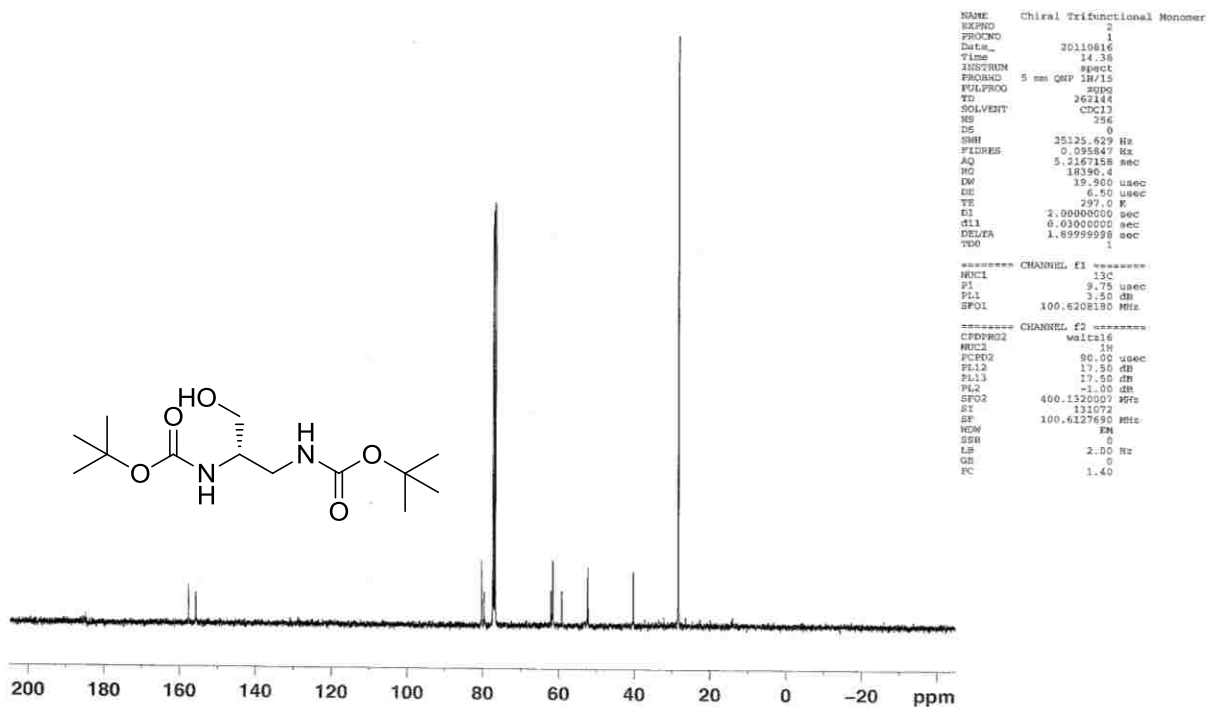


Figure A11: (S)-di-tert-butyl (3-hydroxypropane-1,2-diyl)dicarbamate (26) ¹³C NMR.

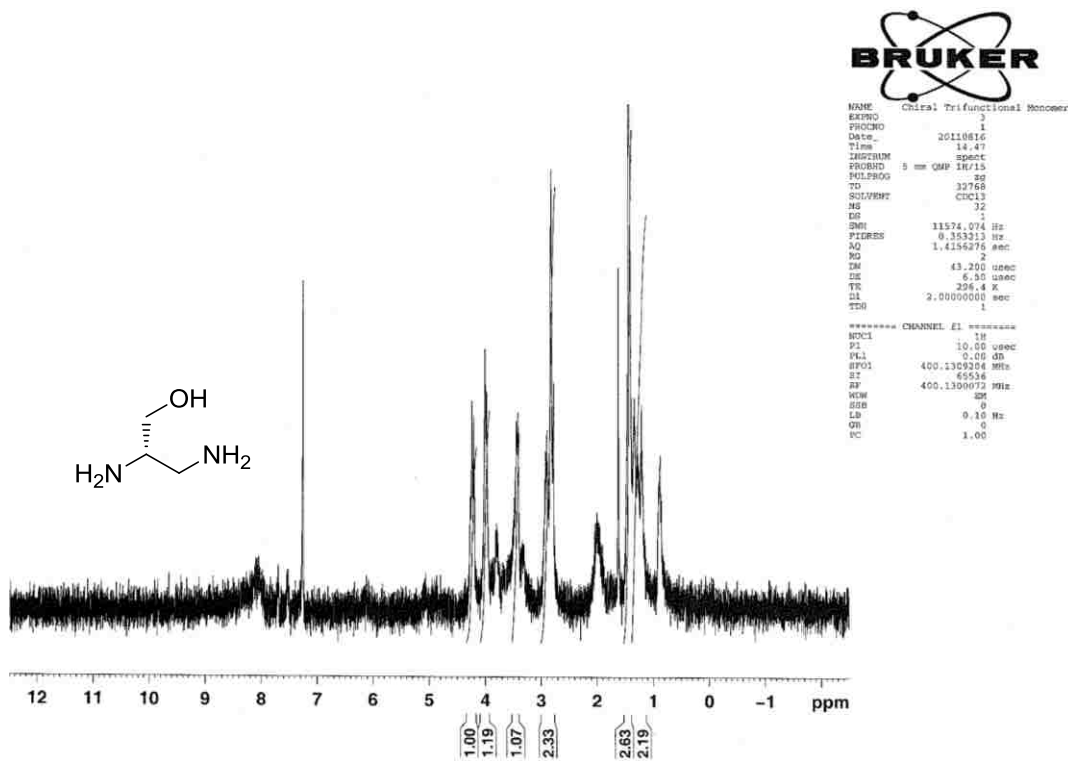


Figure A12: (S)-2,3-diaminopropan-1-ol (27) ¹H NMR.

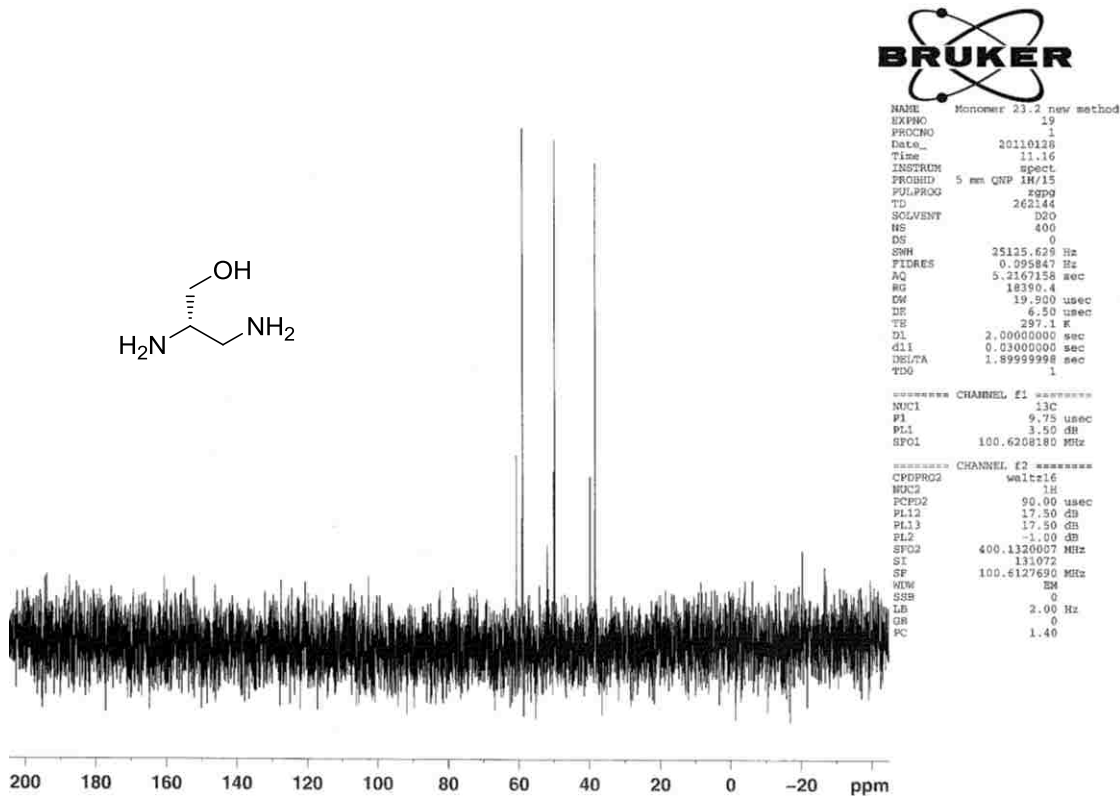


Figure A13: (*S*)-2,3-diaminopropan-1-ol (27) ^{13}C NMR.

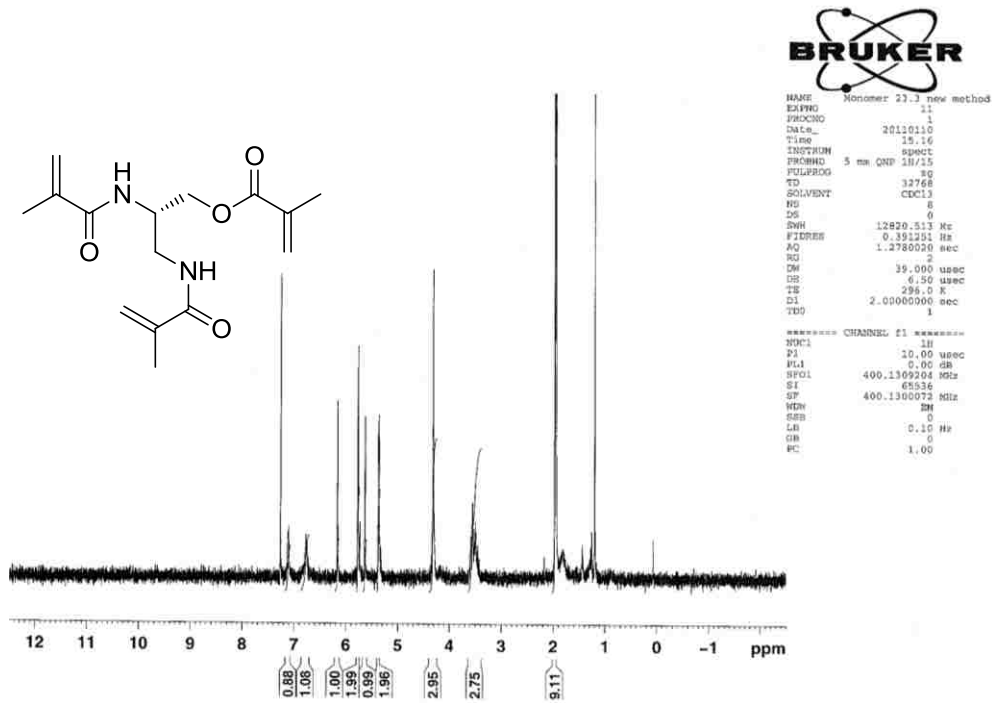


Figure A14: (*S*)-2,3-dimethacrylamidopropyl methacrylate (18) ^1H NMR.

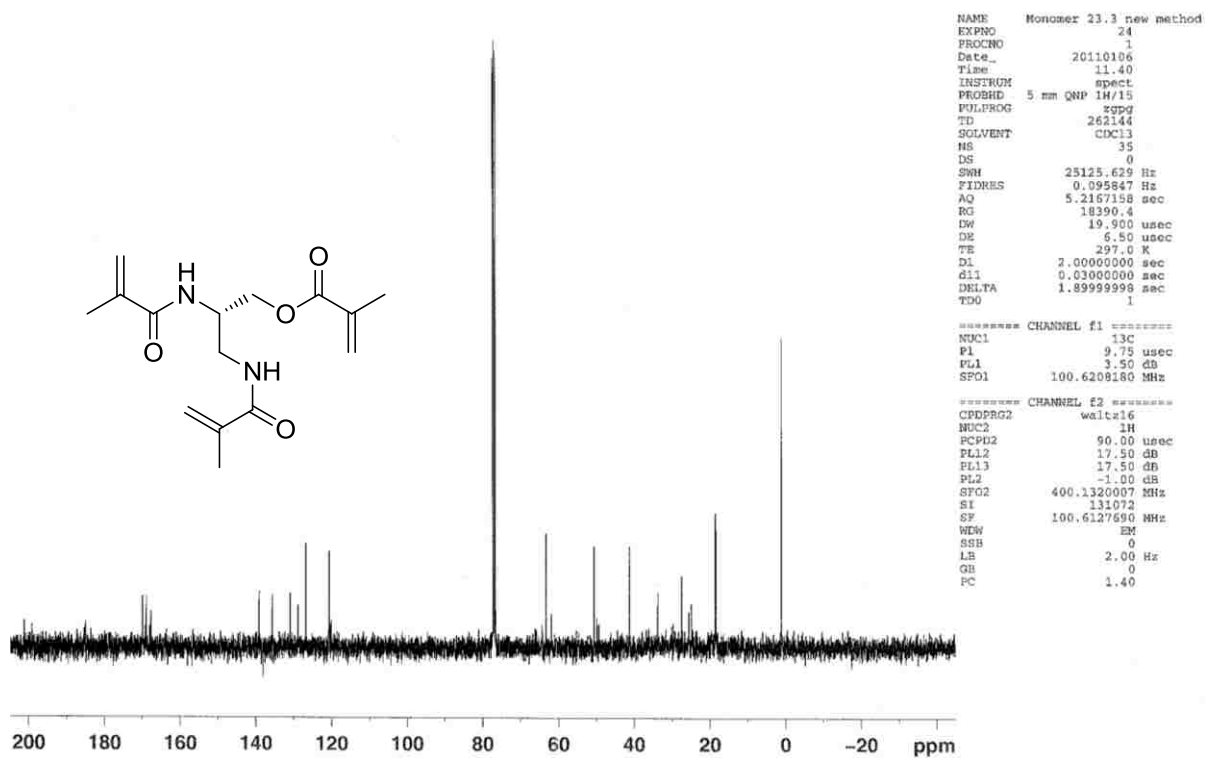


Figure A15: (S)-2,3-dimethacrylamidopropyl methacrylate (18) ^{13}C NMR.

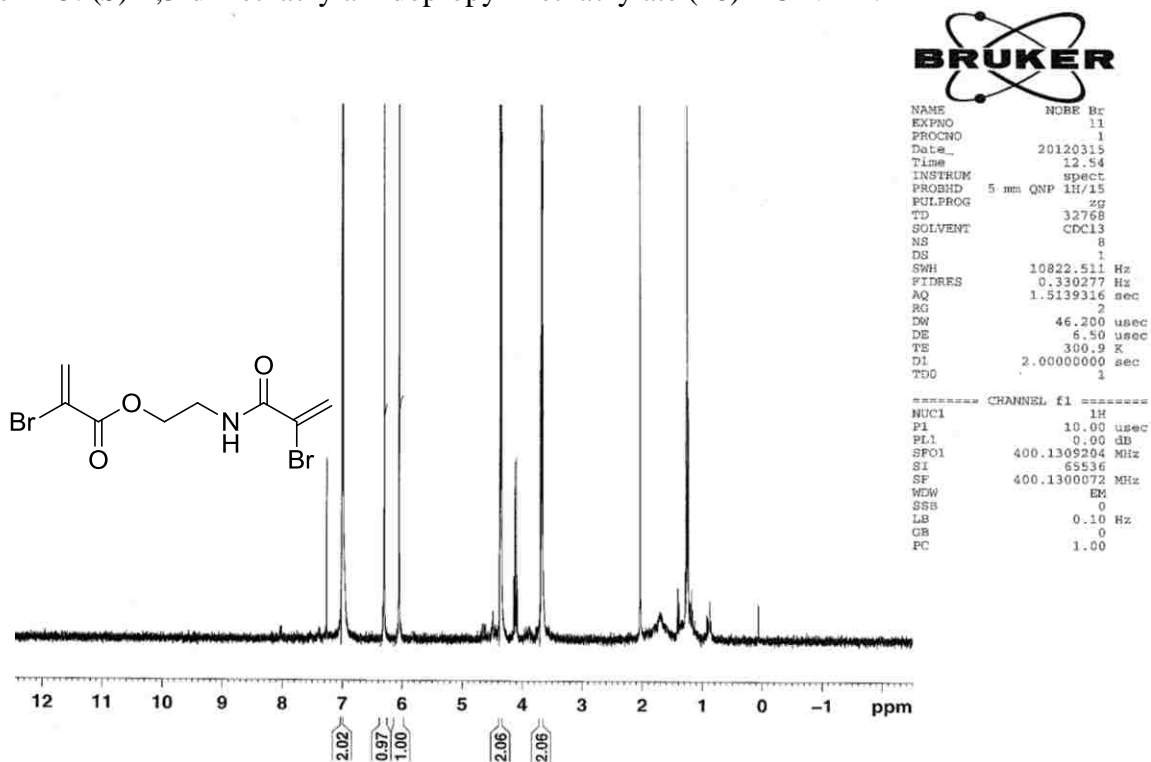


Figure A16: 2-(2-bromoacrylamido)ethyl 2-bromoacrylate (19) ^1H NMR.

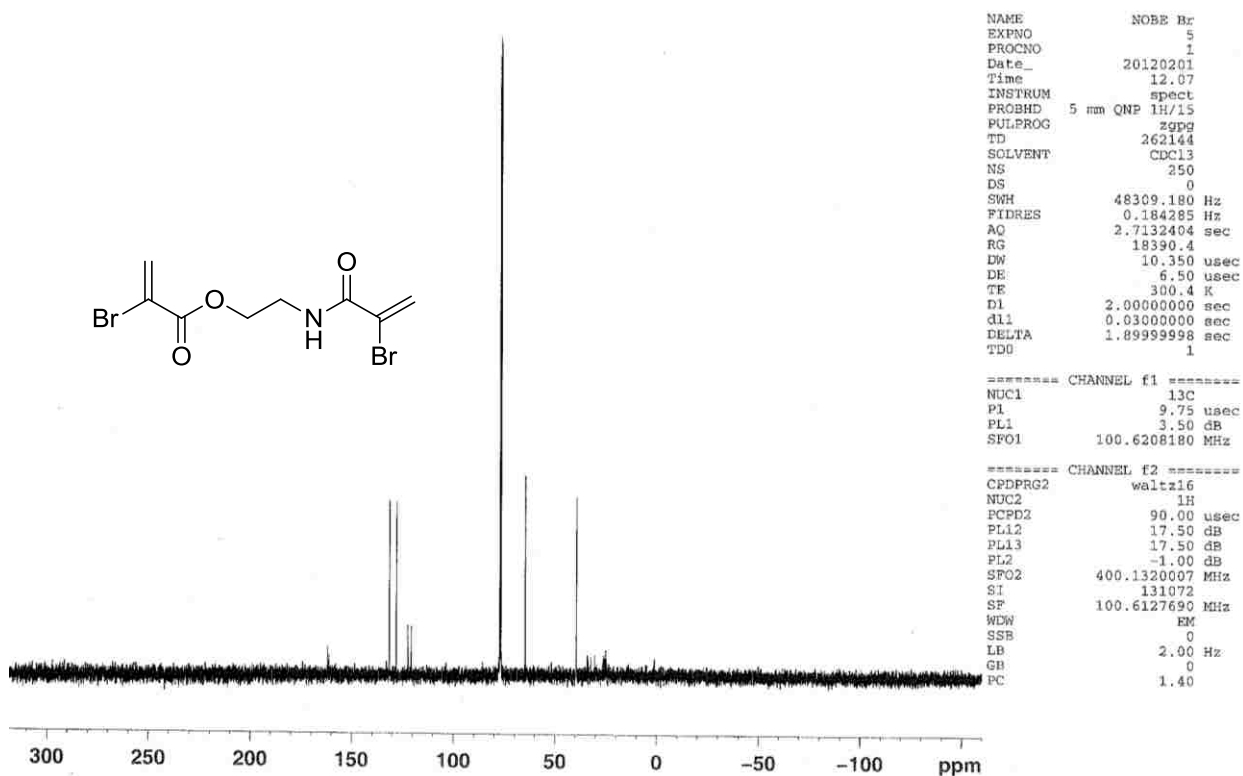


Figure A17: 2-(2-bromoacrylamido)ethyl 2-bromoacrylate (19) ¹³C NMR.

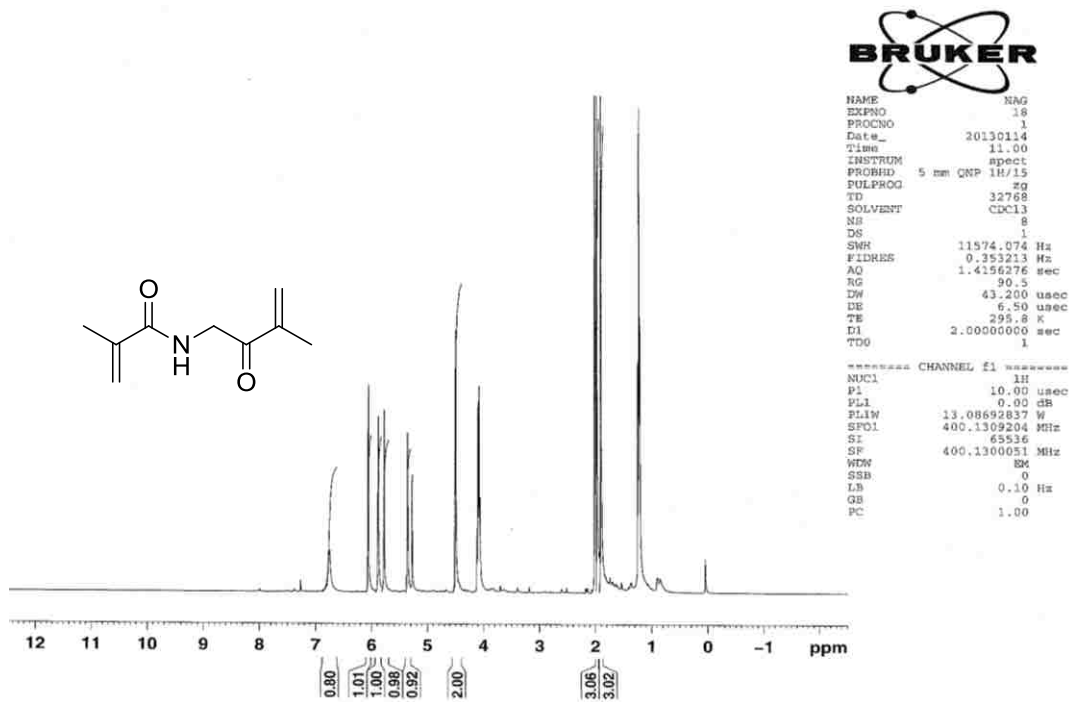


Figure A18: N-(3-methyl-2-oxobut-3-en-1-yl)methacrylamide (NAG (12)) ¹H NMR.

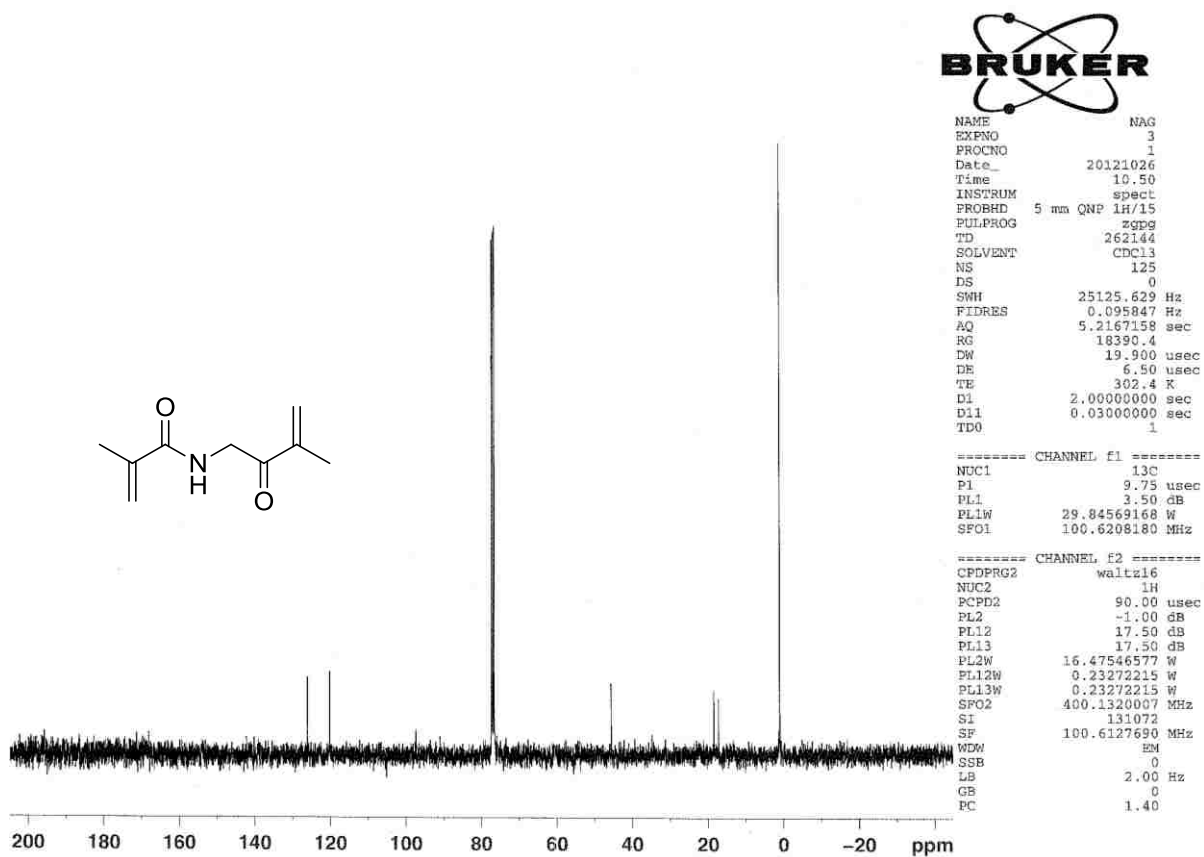


Figure A19: N-(3-methyl-2-oxobut-3-en-1-yl)methacrylamide (NAG (12)) ^{13}C NMR.

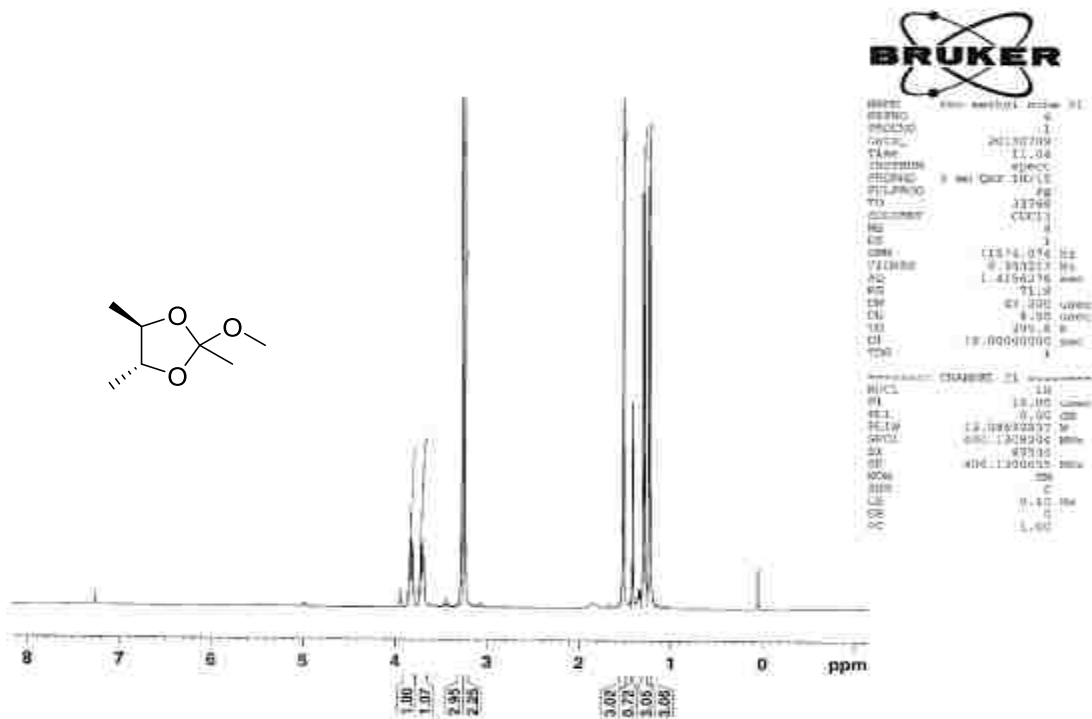


Figure A20: (4R,5R)-2-methoxy-2,4,5-trimethyl-1,3-dioxolane (35) ^1H NMR.

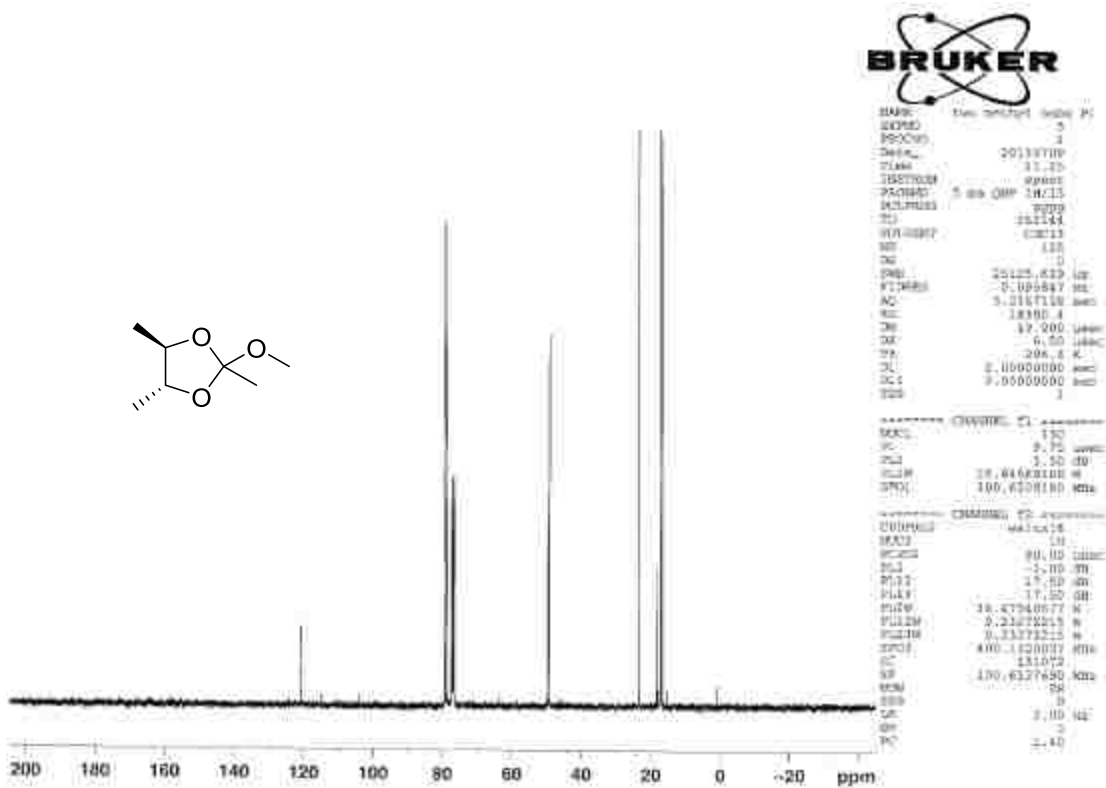


Figure A21: (4R,5R)-2-methoxy-2,4,5-trimethyl-1,3-dioxolane (35) ^{13}C NMR.

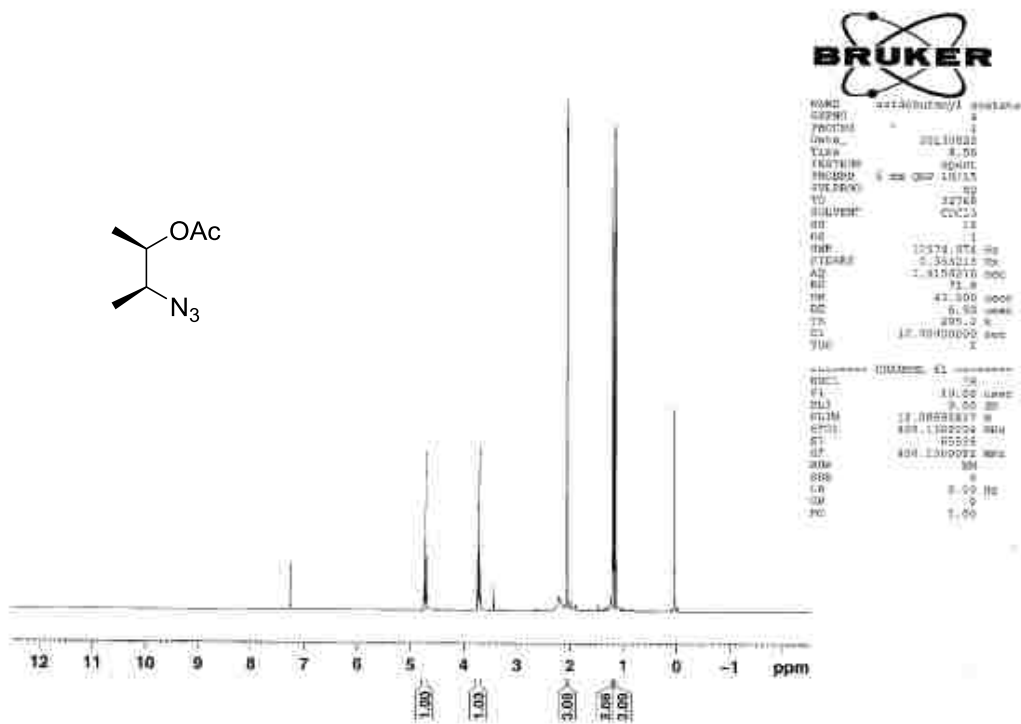


Figure A22: (2R,3S)-3-azidobutan-2-yl acetate (37) ^1H NMR.

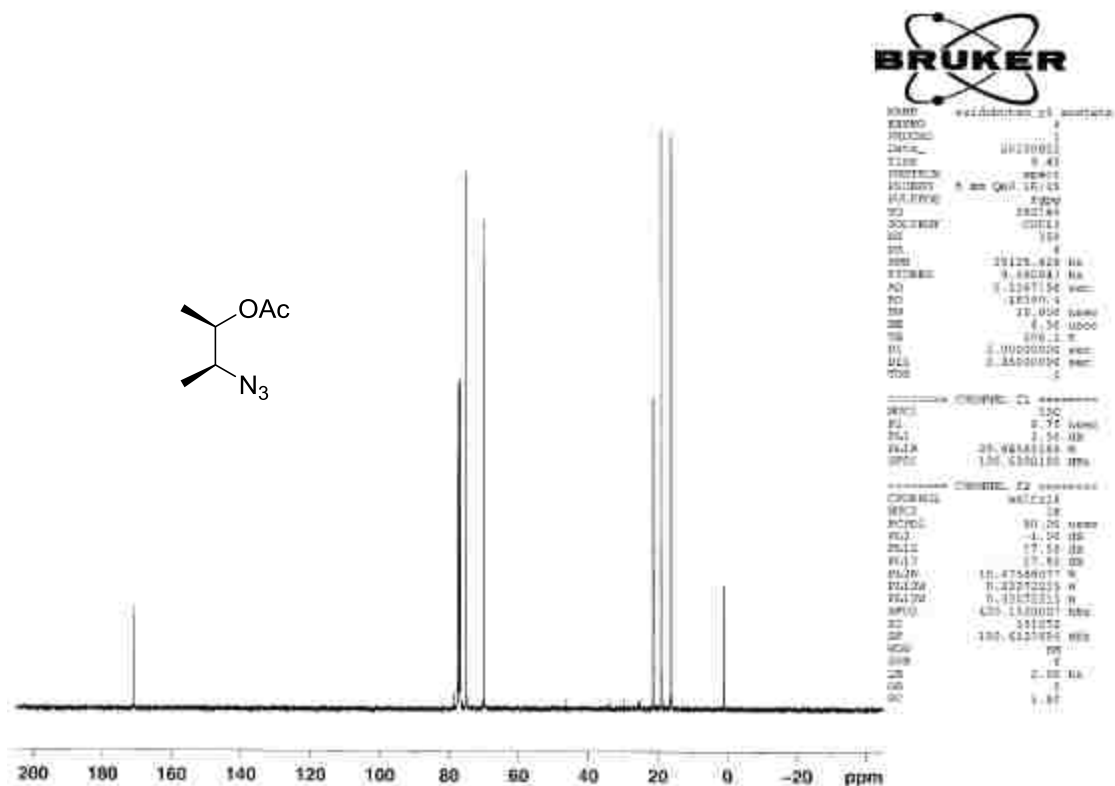


Figure A23: (2*R*,3*S*)-3-azidobutan-2-yl acetate (37) ^{13}C NMR.

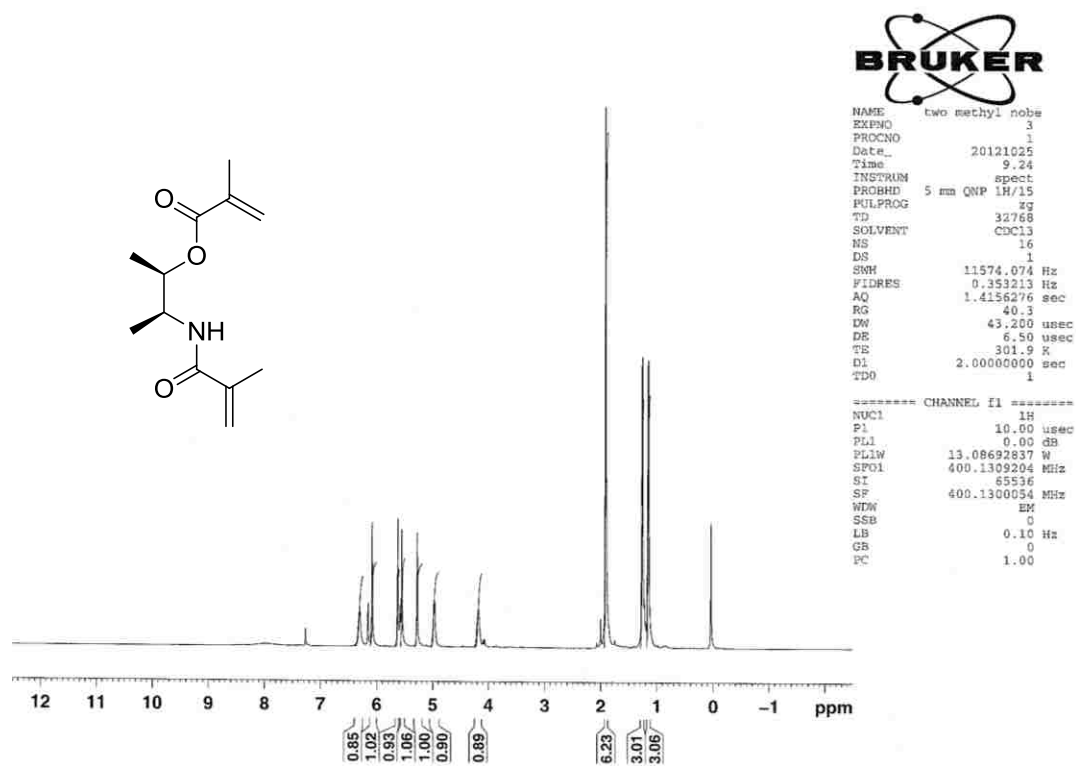


Figure A24: (2*R*,3*S*)-3-methacrylamidobutan-2-yl methacrylate (20) ^1H NMR.

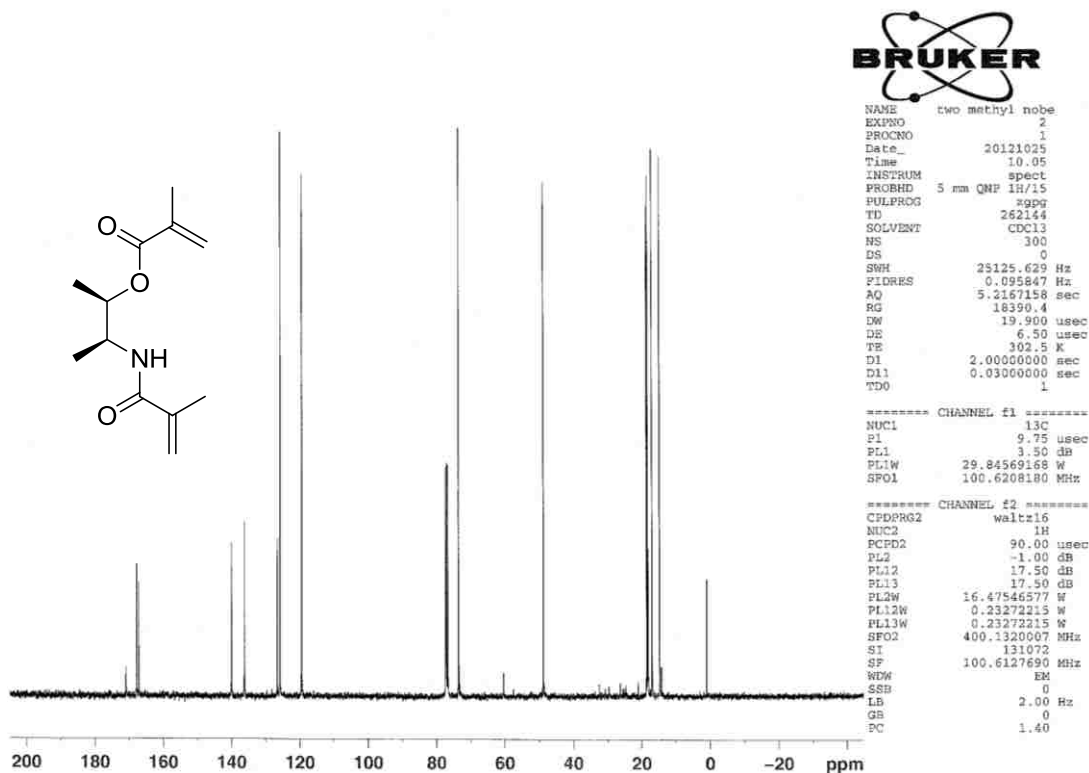


Figure A25: (2R,3S)-3-methacrylamidobutan-2-yl methacrylate (20) ^{13}C NMR.

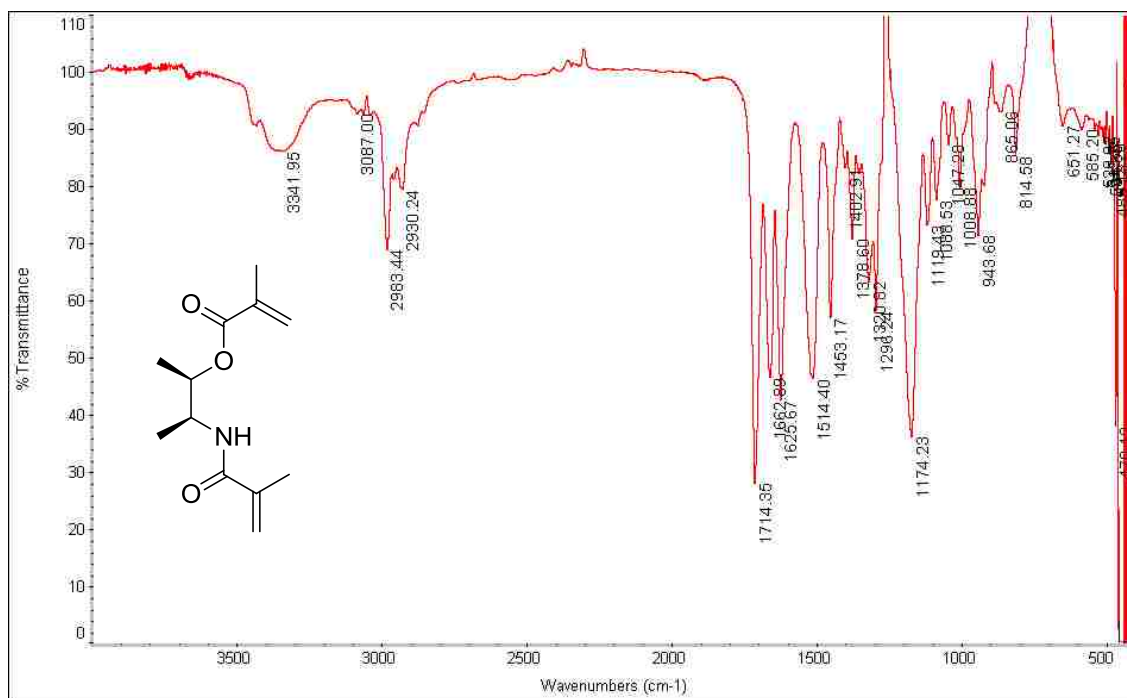


Figure A26: (2R,3S)-3-methacrylamidobutan-2-yl methacrylate (20) IR.

Chromatograms. The following chromatograms of the selected were analyzed at different chart speeds making them appear to be different sizes; however, all chromatograms were normalized in size with respect to time using the void volume (D_v)

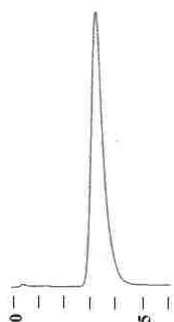


Figure A27: Acetone used to determine D_v for OMNiMIPs synthesized with NOBE (1.)

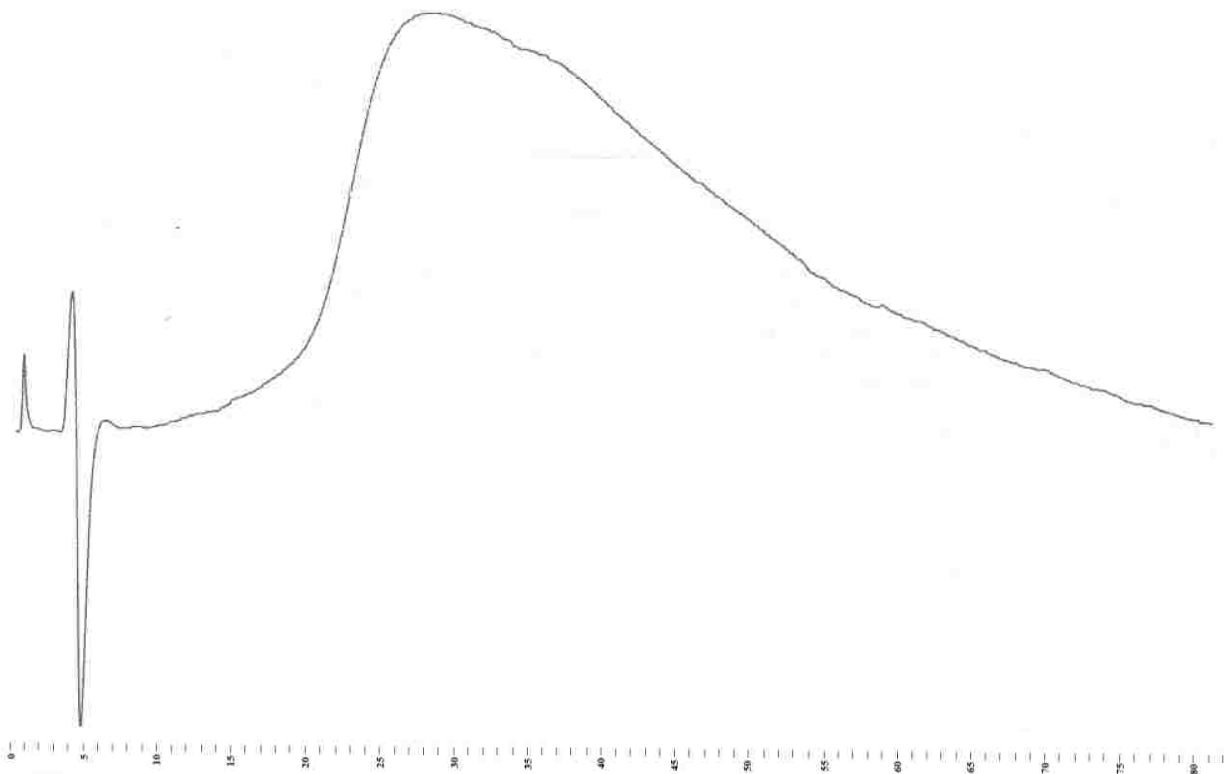


Figure A28: 1 mM L-BOC-Tyr on the OMNiMIP synthesized from NOBE (1.)

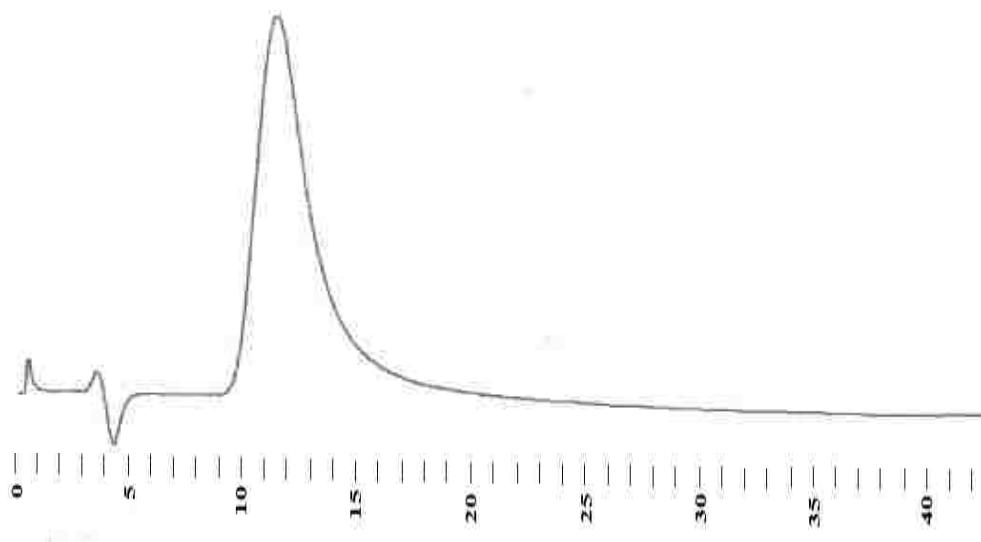


Figure A29: 1 mM D-BOC-Tyr on the OMNiMIP synthesized from NOBE (1.)

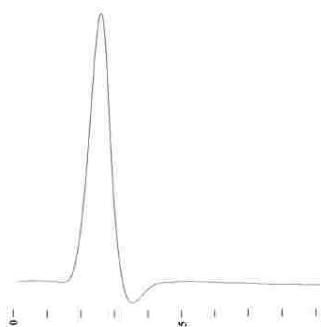


Figure A30: Acetone used to determine D_V for OMNiMIPs synthesized with 2-acrylamidoethyl acrylate (13.)

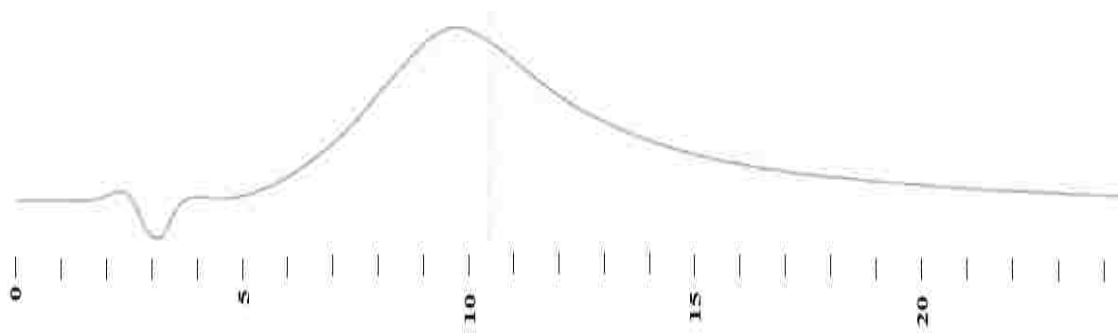


Figure A31: 1 mM L-BOC-Tyr on the OMNiMIP synthesized from 2-acrylamidoethyl acrylate (13.)

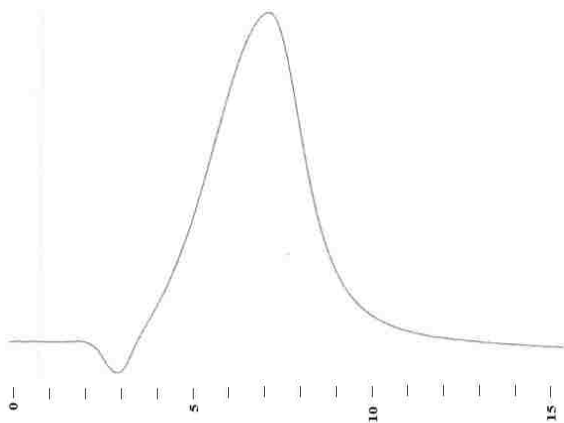


Figure A32: 1 mM D-BOC-Tyr on the OMNiMIP synthesized from 2-acrylamidoethyl acrylate (13.)

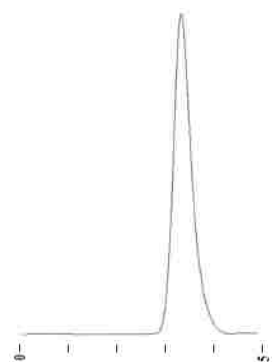


Figure A33: Acetone used to determine D_V for OMNiMIPs synthesized with 2-acrylamidoethyl methacrylate (14.)

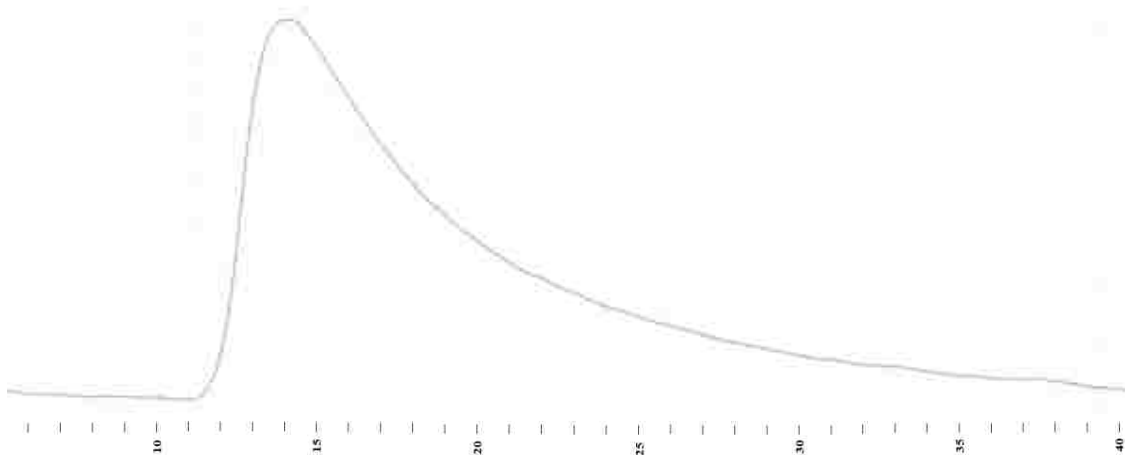


Figure A34: 1 mM L-BOC-Tyr on the OMNiMIP synthesized from 2-acrylamidoethyl methacrylate (14.)

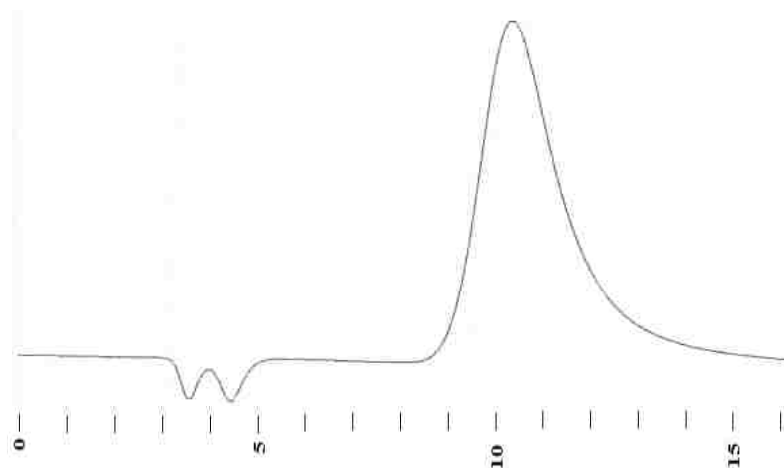


Figure A35: 1 mM D-BOC-Tyr on the OMNiMIP synthesized from 2-acrylamidoethyl methacrylate (14.)

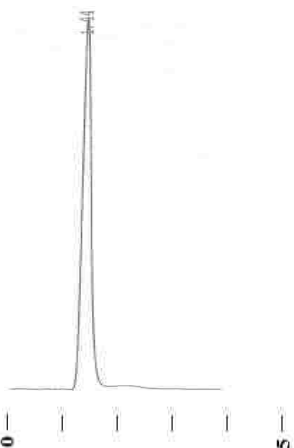


Figure A36: Acetone used to determine D_V for OMNiMIPs synthesized with 1,3-dimethacrylamidopropan-2-yl methacrylate (17.)

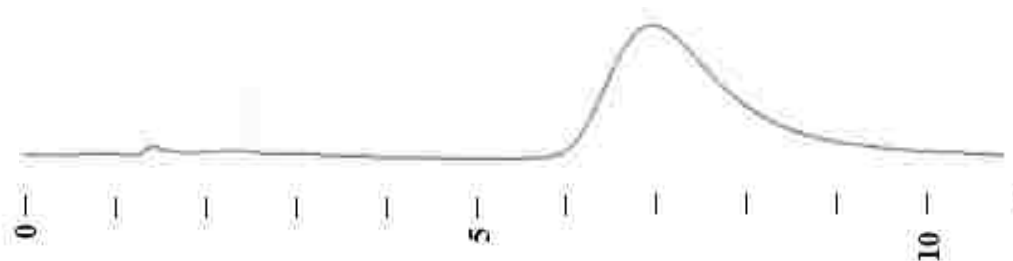


Figure A37: 1 mM L-BOC-Tyr on the OMNiMIP synthesized from 1,3-dimethacrylamidopropan-2-yl methacrylate (17.)

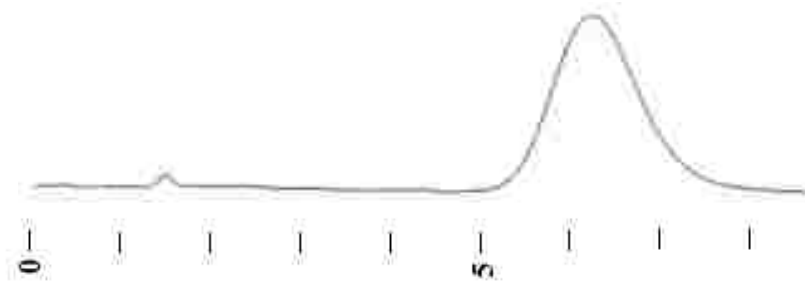


Figure A38: 1mM D-BOC-Tyr on the OMNiMIP synthesized from 1,3-dimethacrylamidopropan-2-yl methacrylate (17.)

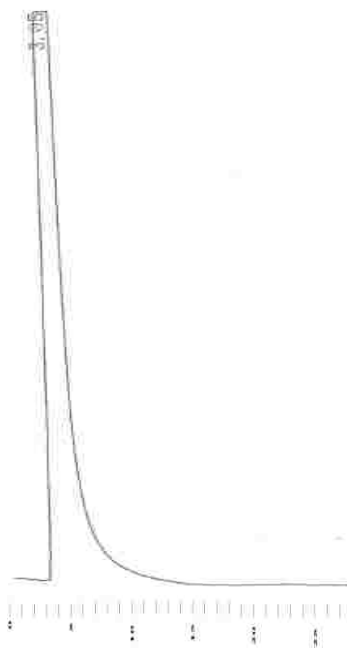


Figure A39: 1mM L-BOC-Tyr on the OMNiMIP synthesized from BrOBE (19) ($D_V = 3.0$.)

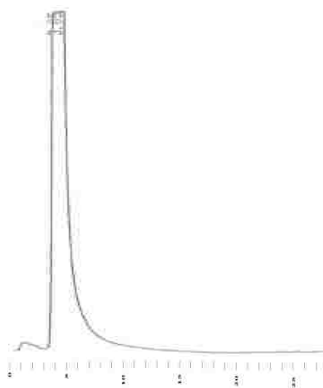


Figure A40: 1mM D-BOC-Tyr on the OMNiMIP synthesized from BrOBE (19) ($D_V = 3.0$.)

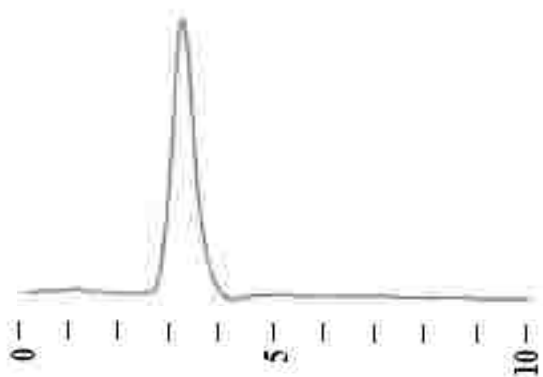


Figure A41: Acetone used to determine D_V (0.1 mL/min) for OMNiMIPs synthesized with NAG (12.)

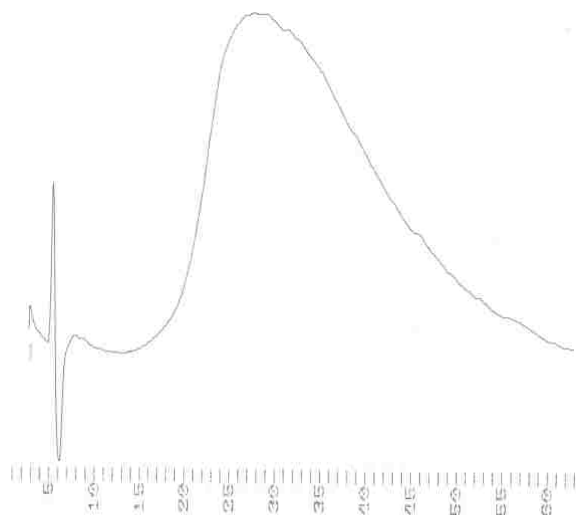


Figure A42: 1 mM L-BOC-Tyr (0.1 mL/min) on the OMNiMIP synthesized from NAG (12.)

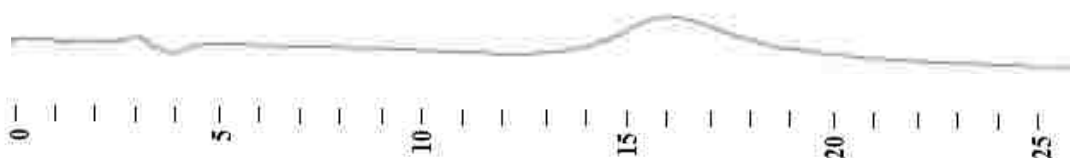


Figure A43: 1 mM D-BOC-Tyr (0.1 mL/min) on the OMNiMIP synthesized from NAG (12.)

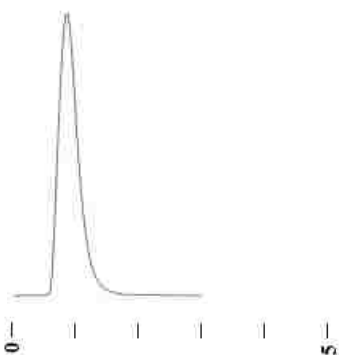


Figure A44: Acetone used to determine D_V (0.2 mL/min) for OMNiMIPs synthesized with NAG (12.)



Figure A45: 0.5 mM L-BOC-Tyr (0.2 mL/min) on the OMNiMIP synthesized from NAG (12.)

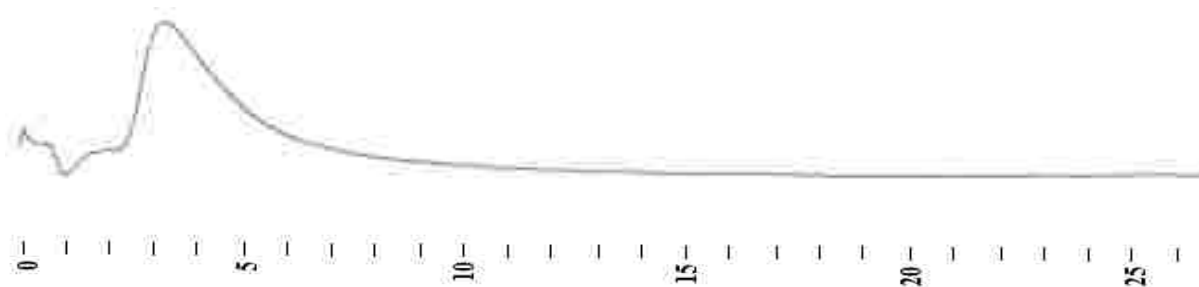


Figure A46: 0.5 mM D-BOC-Tyr (0.2 mL/min) on the OMNiMIP synthesized from NAG (12.)

APPENDIX B: SPECTRA FOR CHAPTER THREE

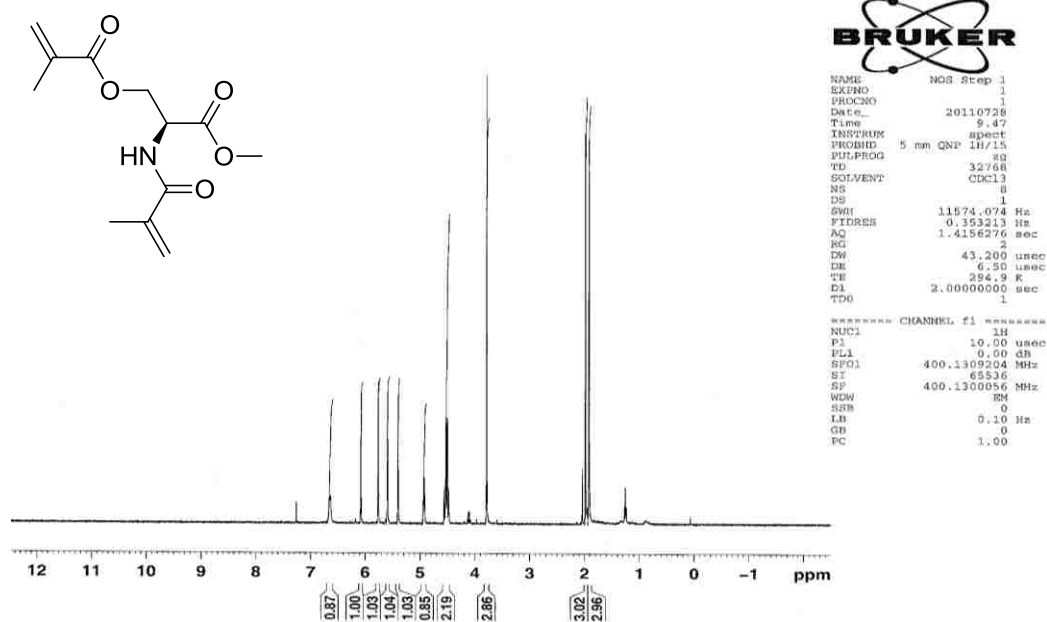


Figure B1: 2-methacrylamido-3-methoxy-3-oxopropyl methacrylate (NOS Step 1) ^1H NMR.

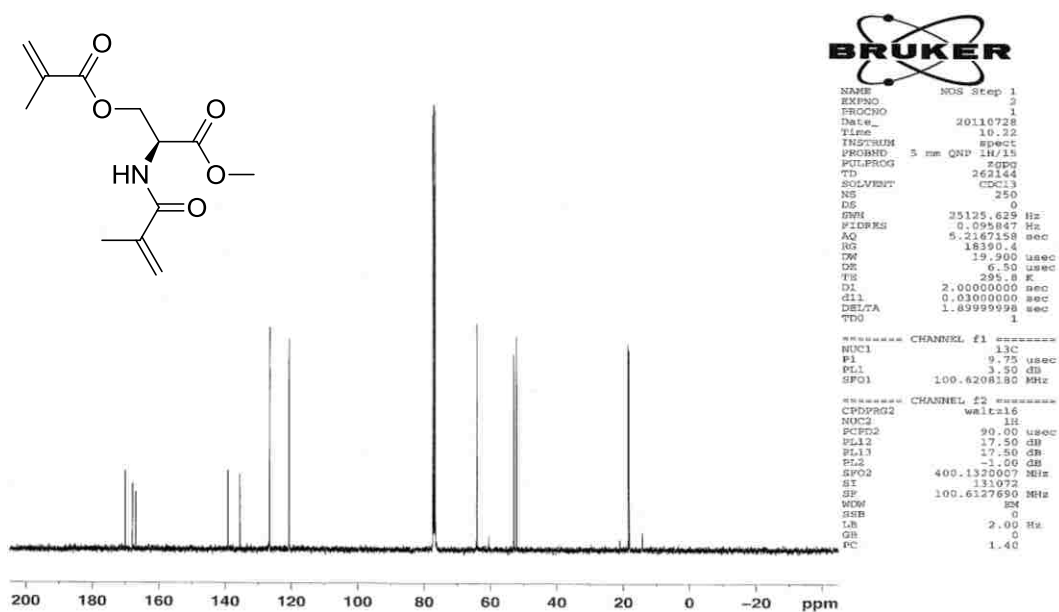


Figure B2: 2-methacrylamido-3-methoxy-3-oxopropyl methacrylate (NOS Step 1) ^{13}C NMR.

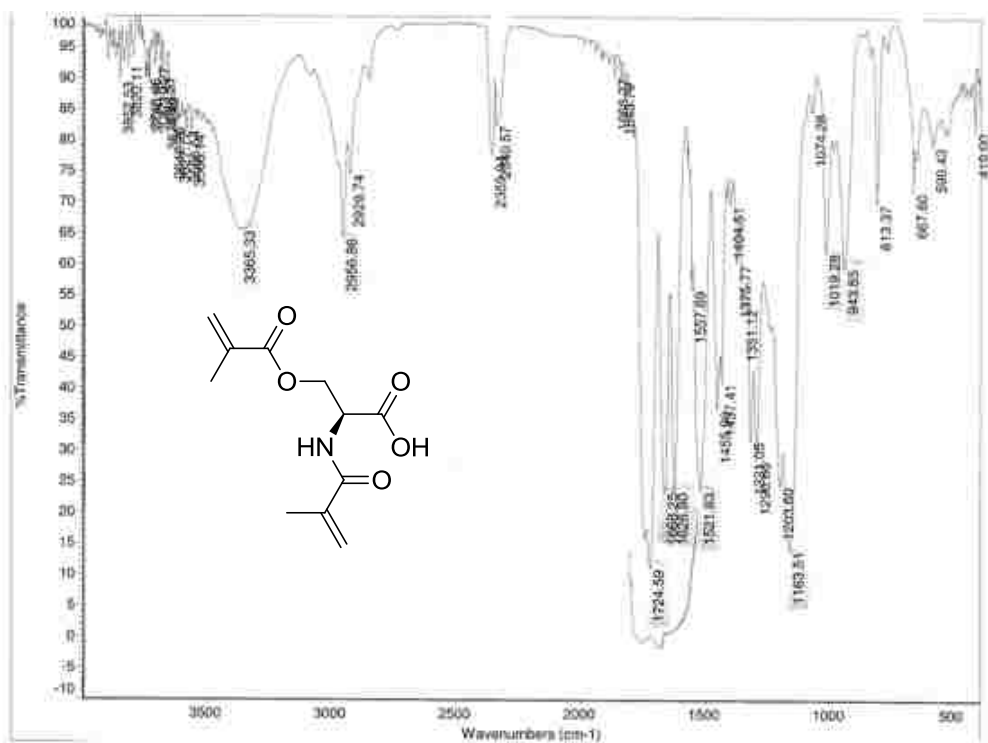


Figure B3: 2-methacrylamido-3-methoxy-3-oxopropyl methacrylate (NOS Step 1) IR.

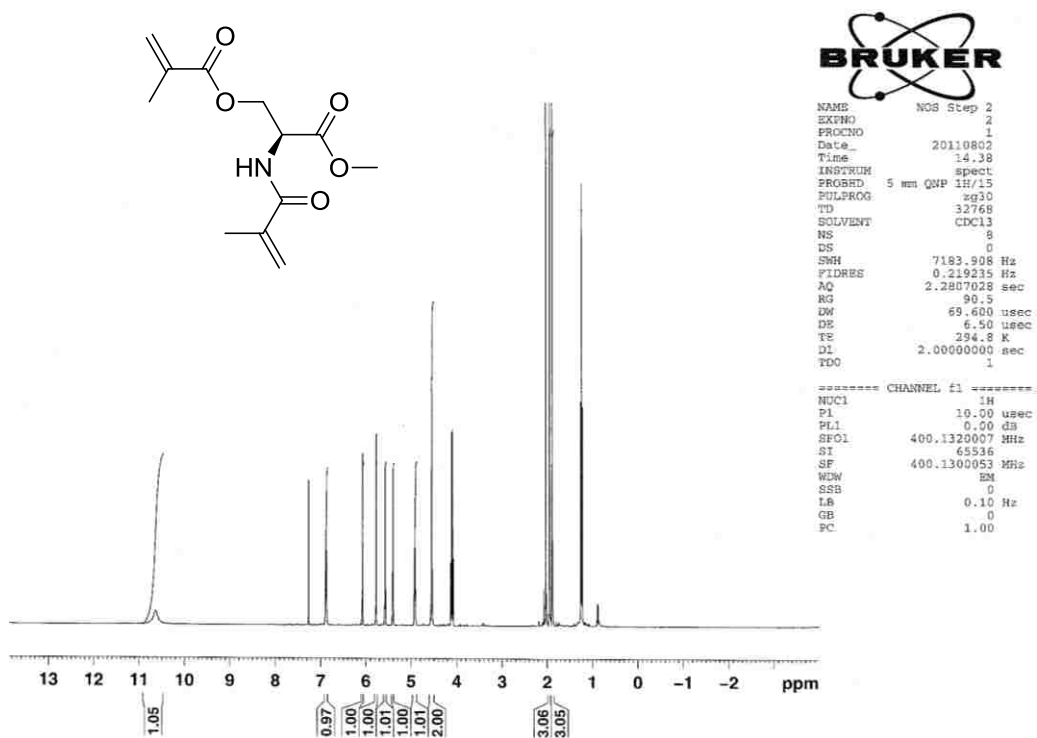


Figure B4: 2-methacrylamido-3-(methacryloyloxy)propanoic acid (NOS) ¹H NMR.

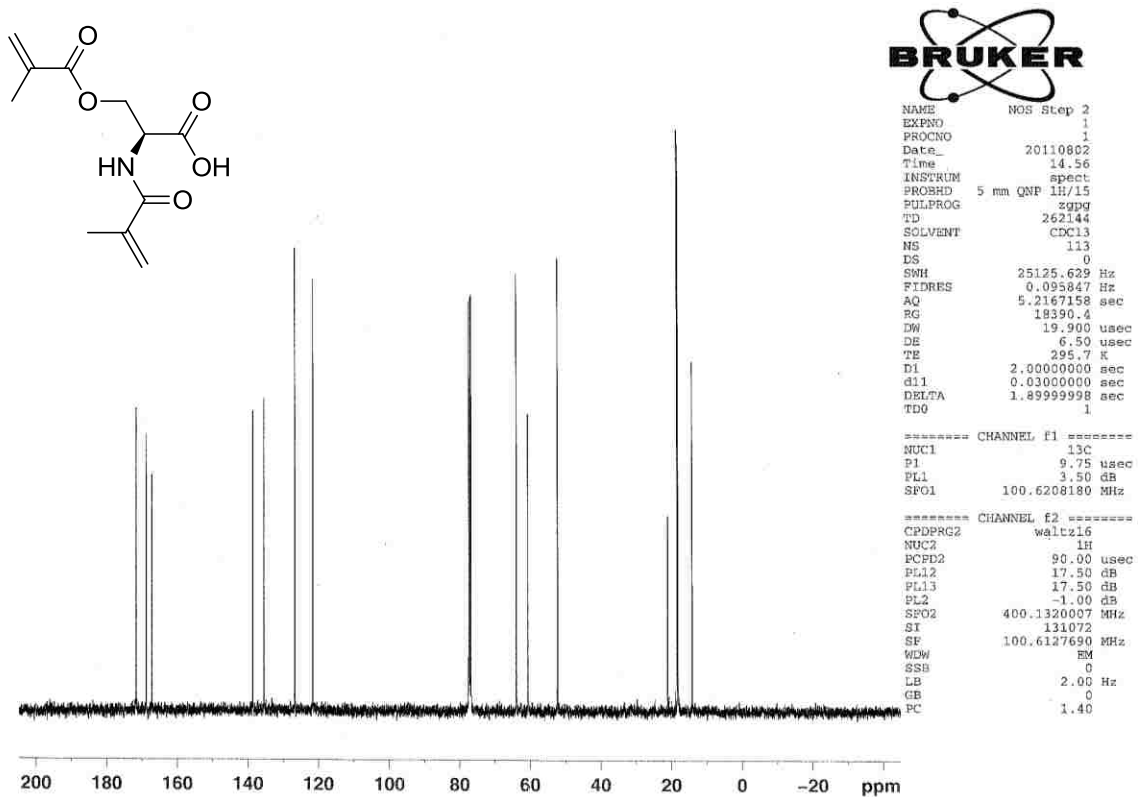


Figure B5: 2-methacrylamido-3-(methacryloyloxy)propanoic acid (NOS) ^{13}C NMR.

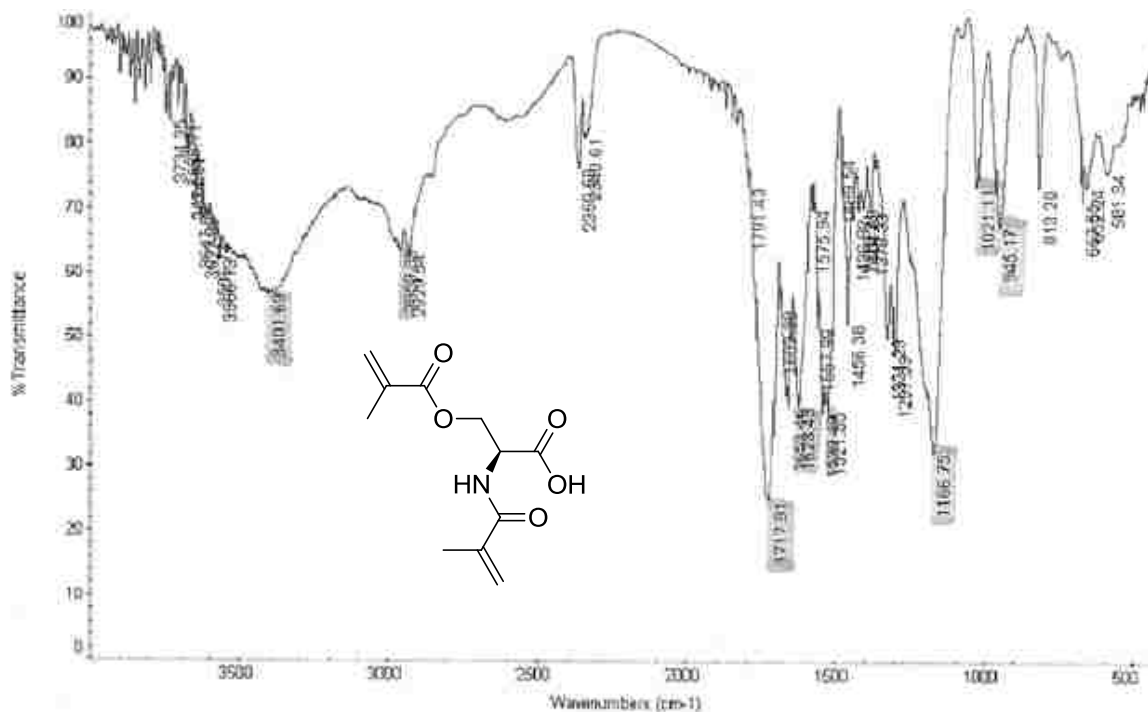


Figure B6: 2-methacrylamido-3-(methacryloyloxy)propanoic acid (NOS) IR.

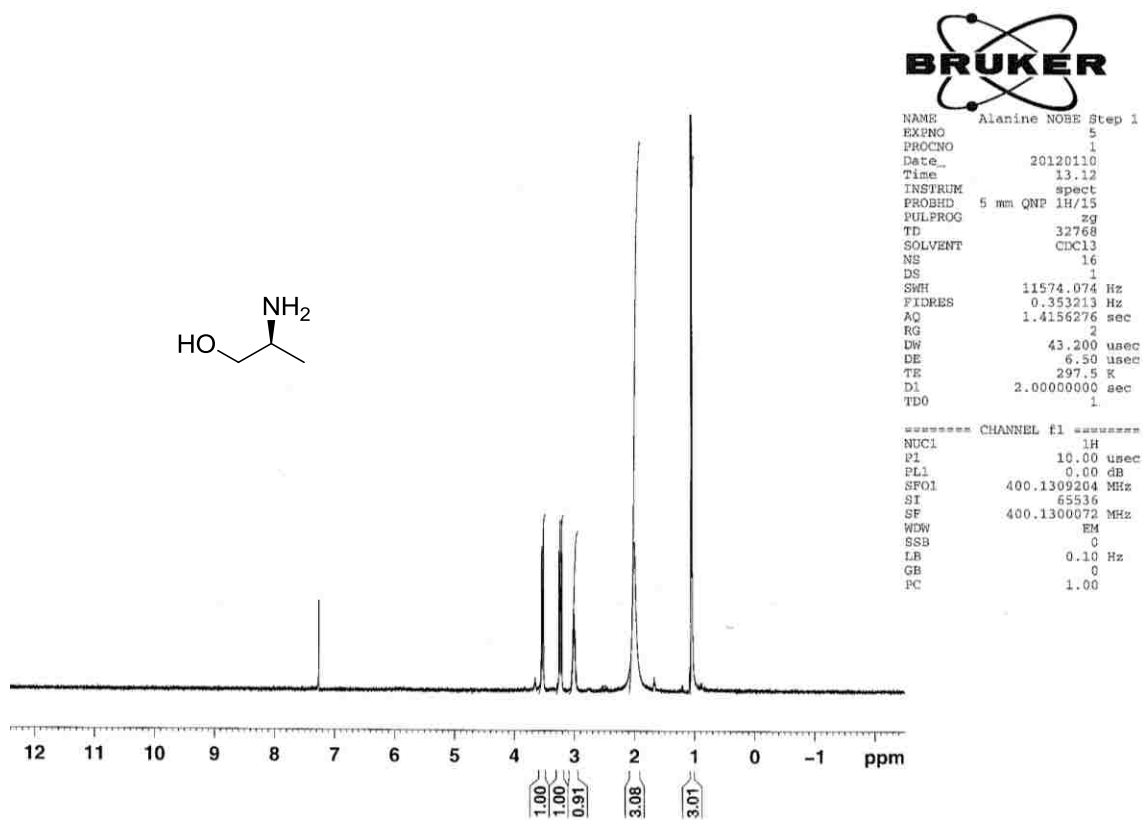


Figure B7: *S*-alaninol ¹H NMR.

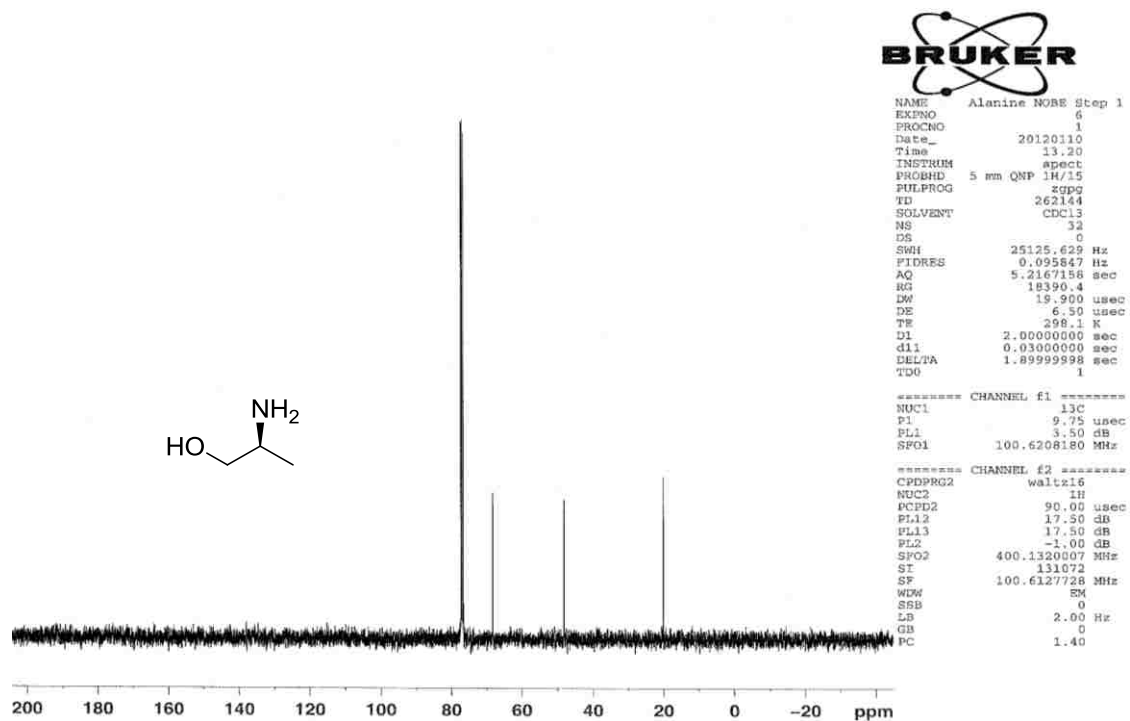


Figure B8: *S*-alaninol ¹³C NMR.

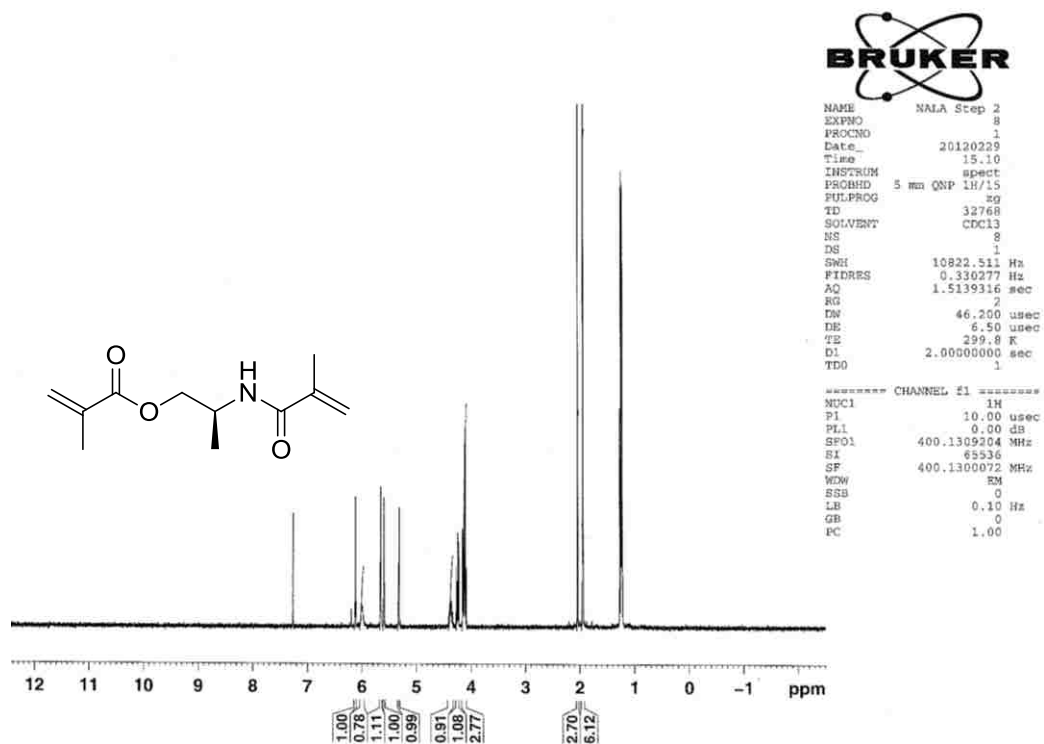


Figure B9: (*S*)-2-methacrylamidopropyl methacrylate (L-NALA) ¹H NMR.

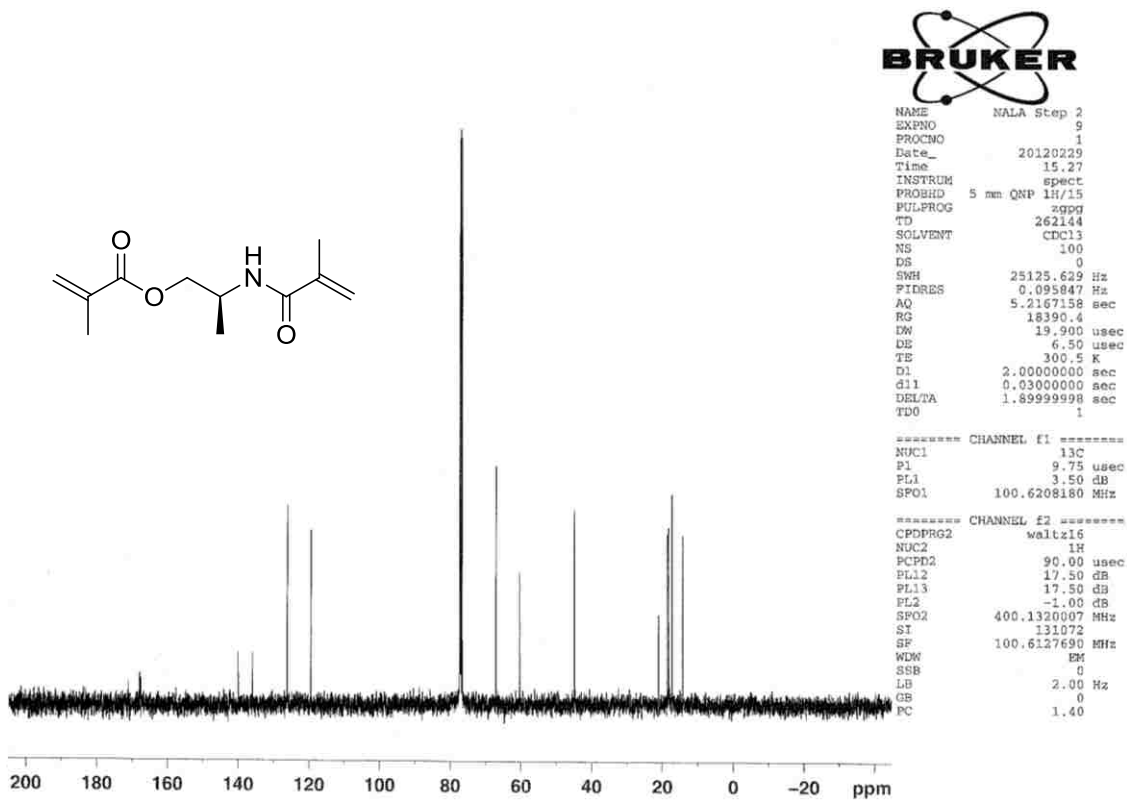


Figure B10: (*S*)-2-methacrylamidopropyl methacrylate (L-NALA) ¹³C NMR.

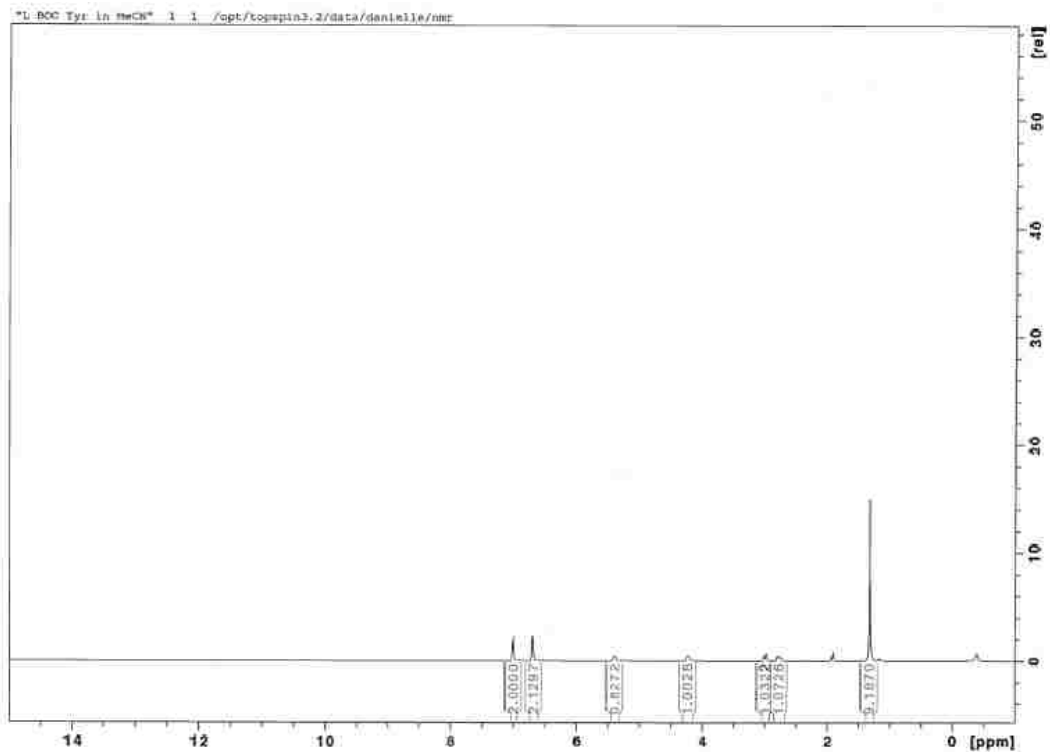


Figure B11: L-BOC-Tyrosine in 100% MeCN ^1H NMR.

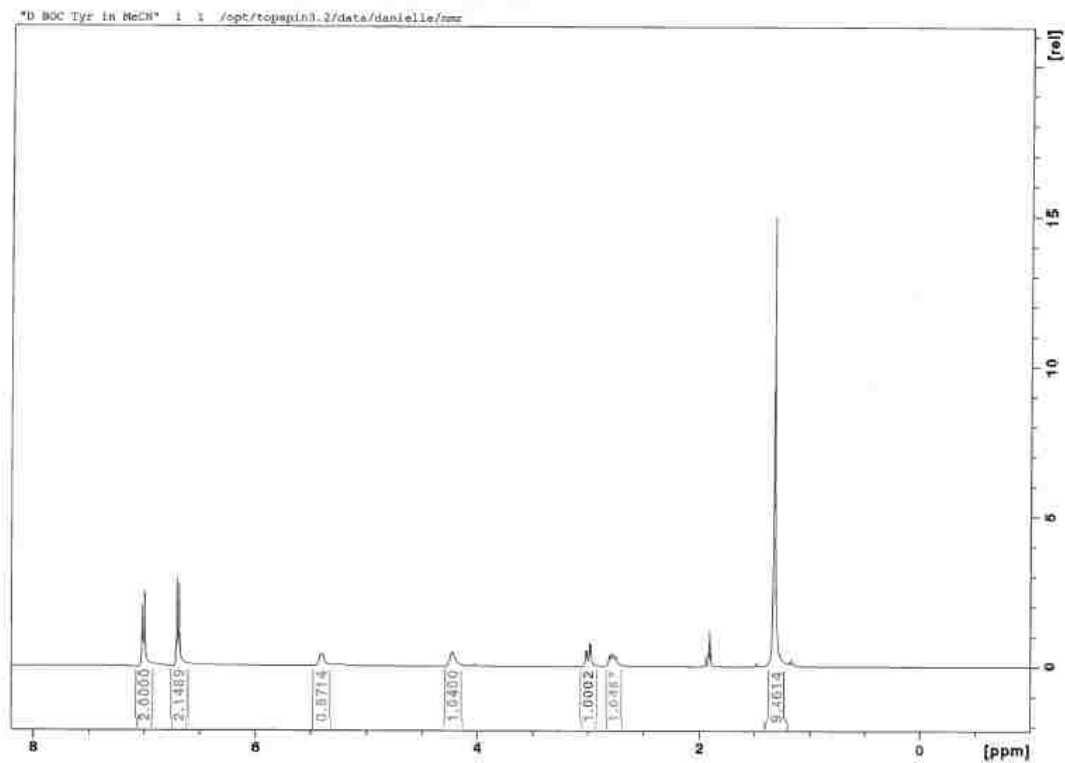


Figure B12: D-BOC-Tyrosine in 100% MeCN ^1H NMR.

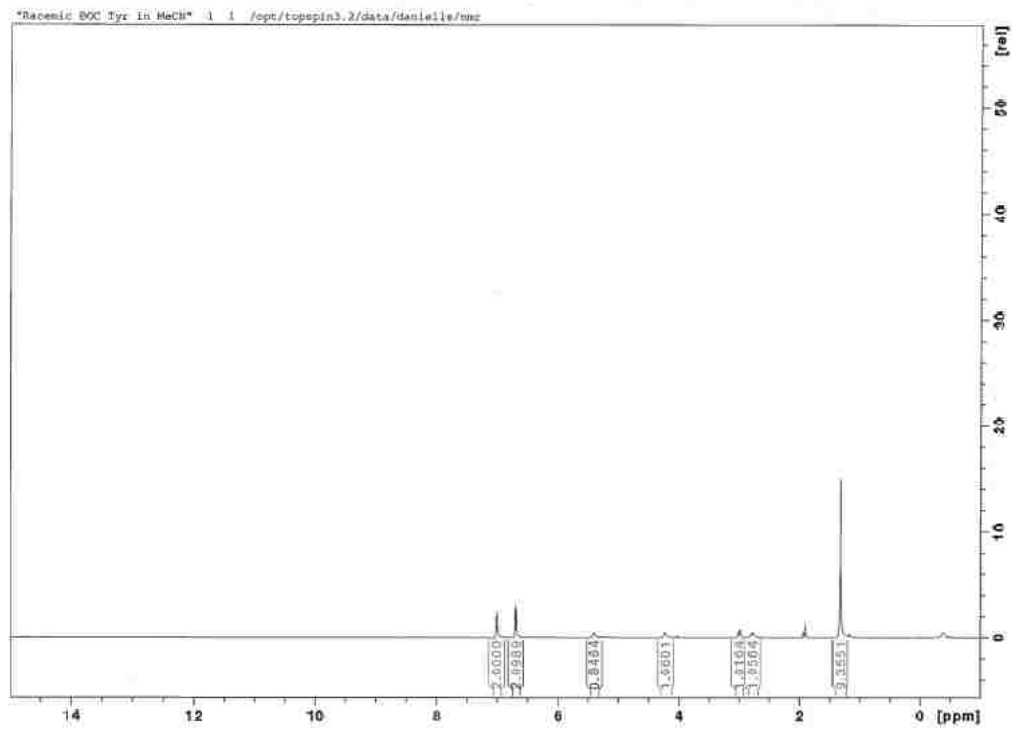


Figure B13: Racemic-BOC-Tyrosine in 100% MeCN ^1H NMR.

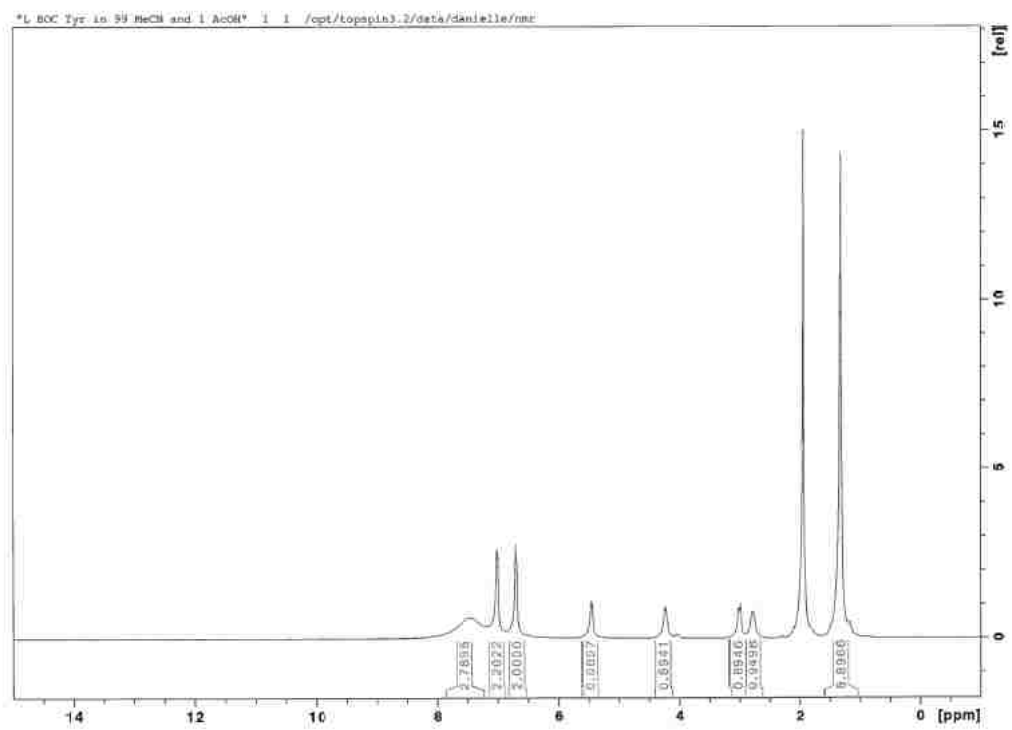


Figure B14: L-BOC-Tyrosine in 99% MeCN 1% AcOH ^1H NMR.

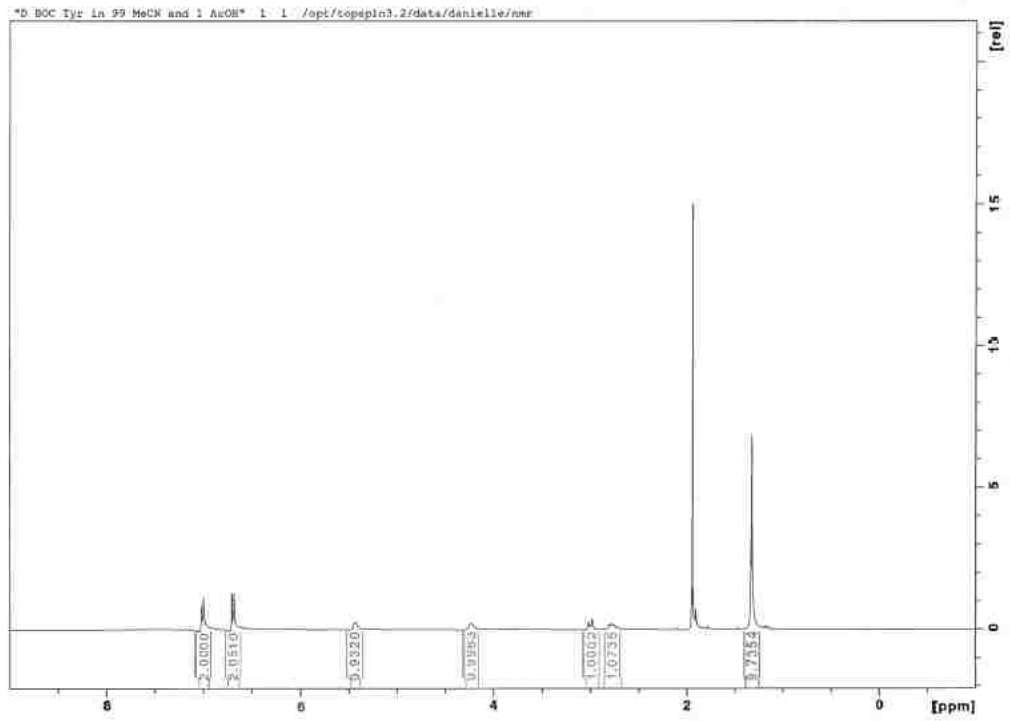


Figure B15: D-BOC-Tyrosine in 99% MeCN 1% AcOH ^1H NMR.

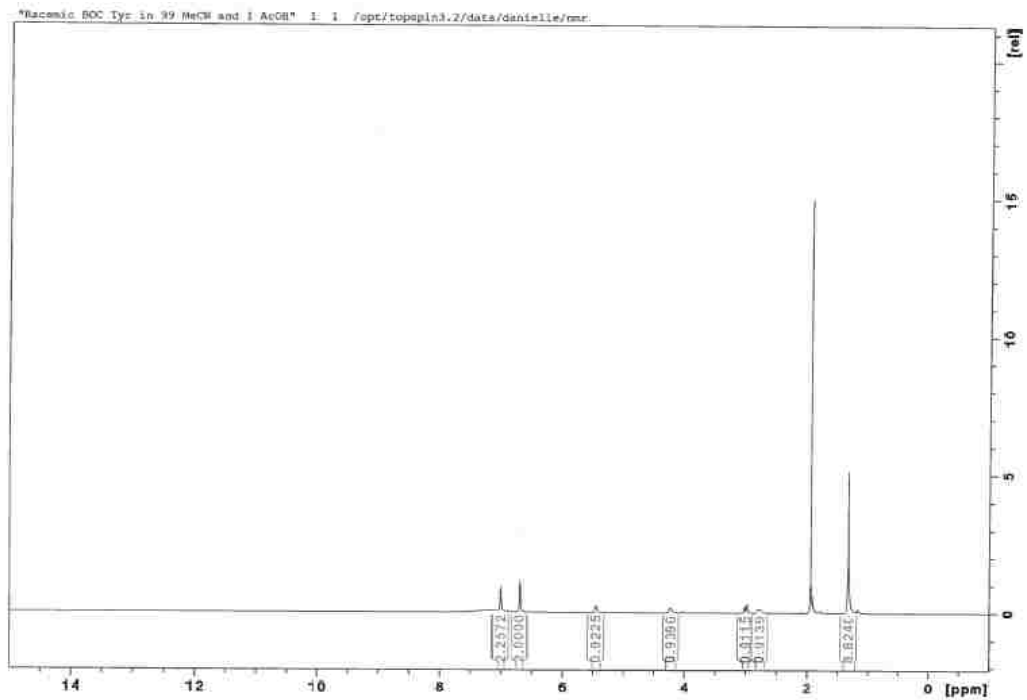


Figure B16: Racemic-BOC-Tyrosine in 99% MeCN 1% AcOH ^1H NMR.

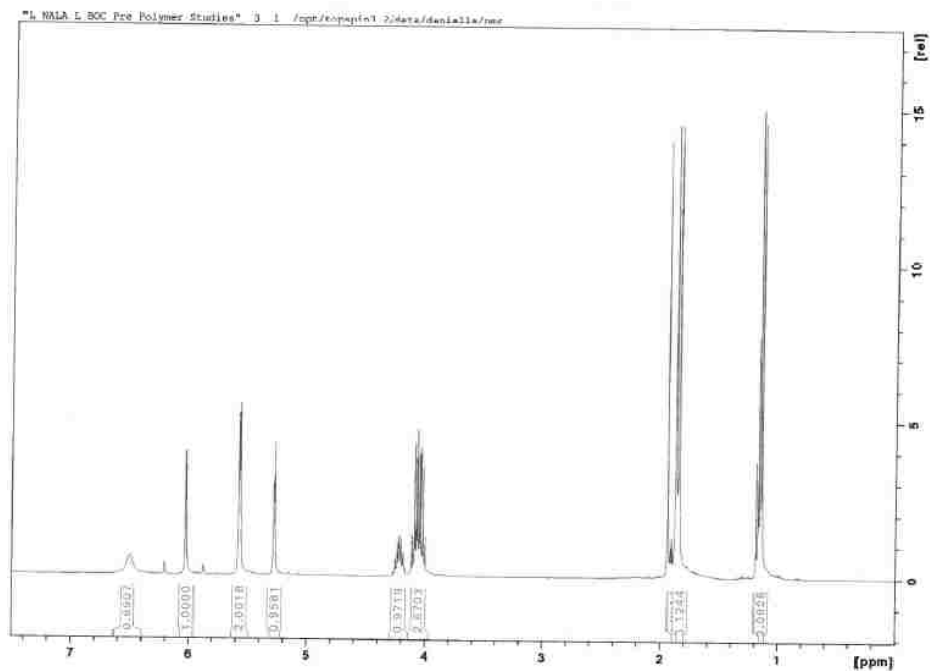


Figure B17: L-NALA in MeCN ^1H NMR.

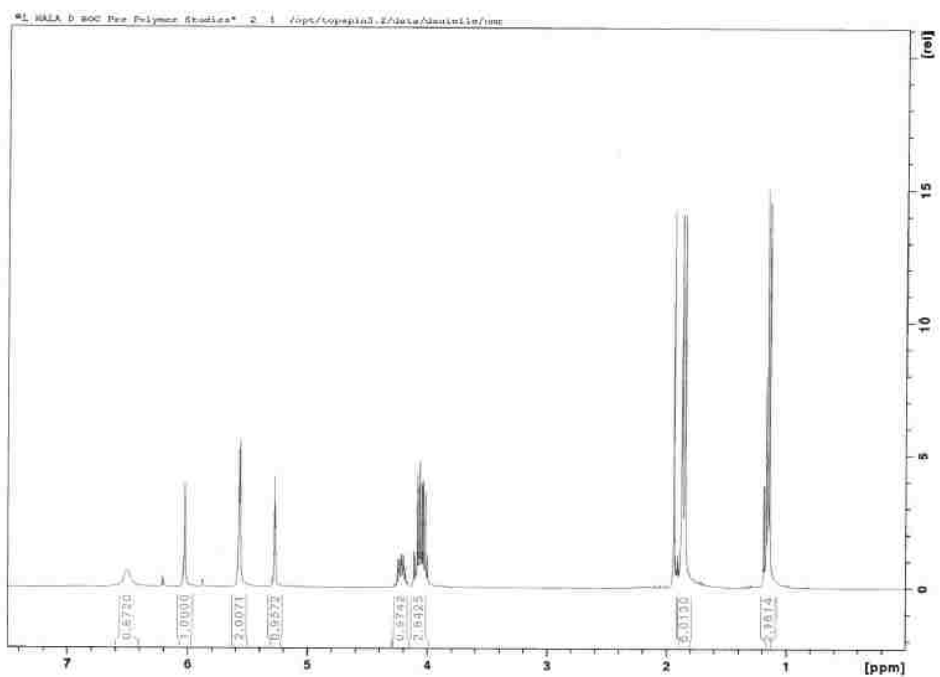


Figure B18: D-NALA in MeCN ^1H NMR.

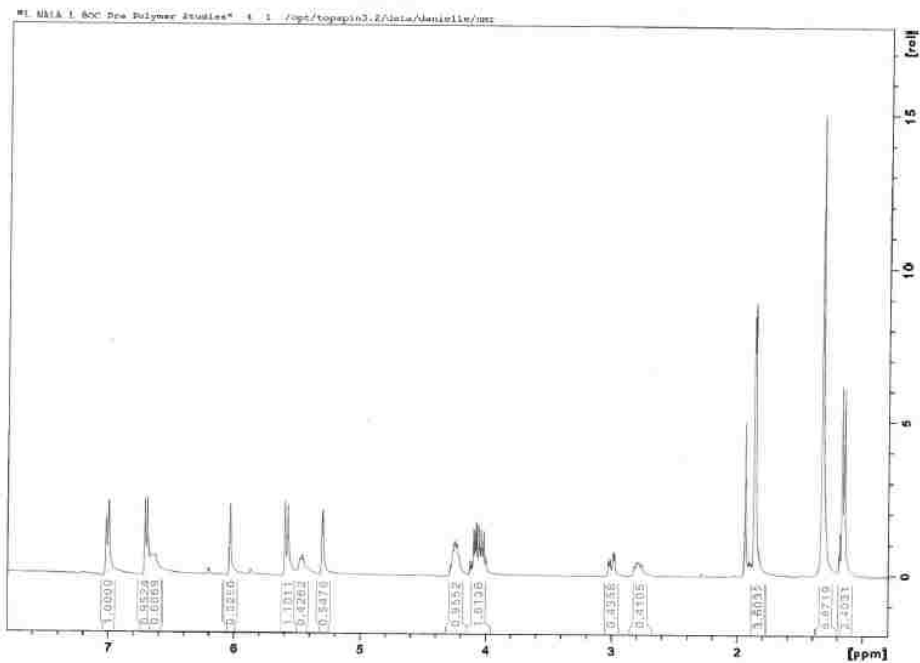


Figure B19: L-NALA and L-BOC-Tyr (1:1) in MeCN ^1H NMR.

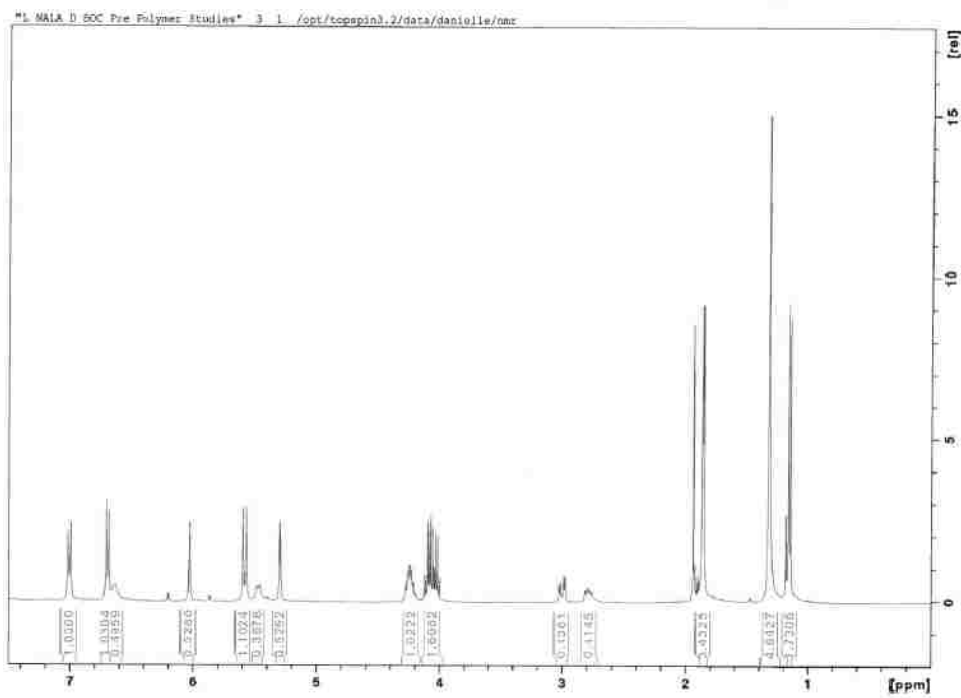


Figure B20: L-NALA and D-BOC-Tyr (1:1) in MeCN ^1H NMR.

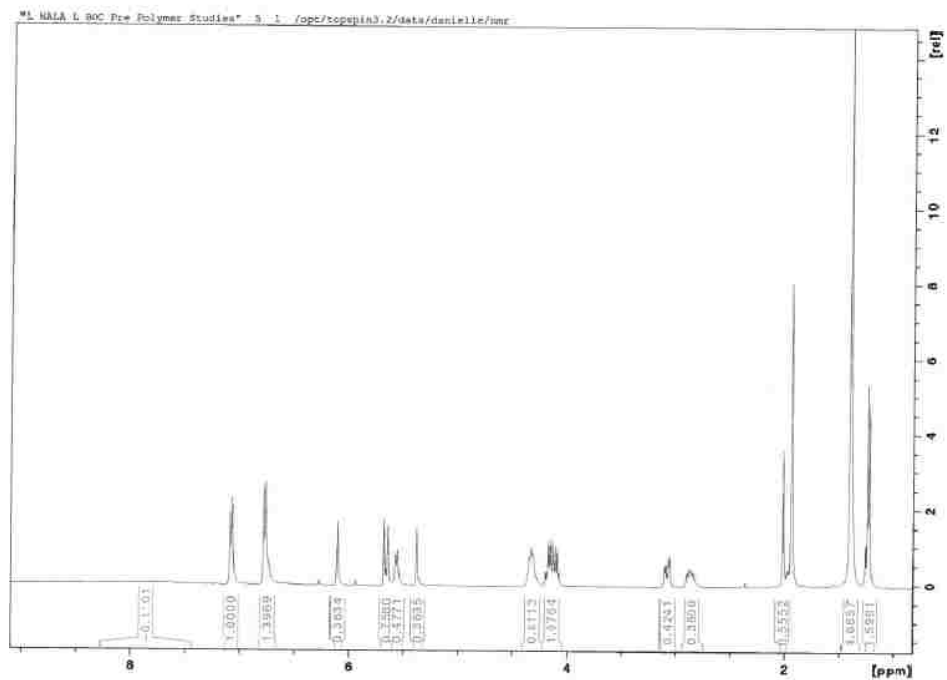


Figure B21: L-NALA and L-BOC-Tyr (1:2) in MeCN ^1H NMR

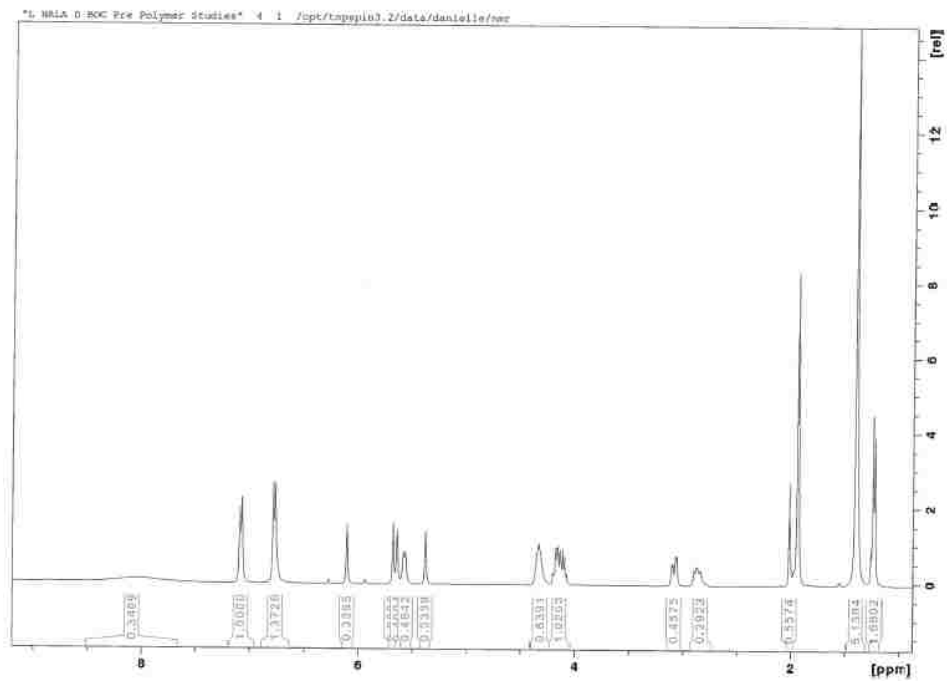


Figure B22: L-NALA and D-BOC-Tyr (1:2) in MeCN ^1H NMR.

Chromatograms. The following chromatograms of the selected were analyzed at different chart speeds making them appear to be different sizes; however, all chromatograms were normalized in size with respect to time using the void volume (D_v)

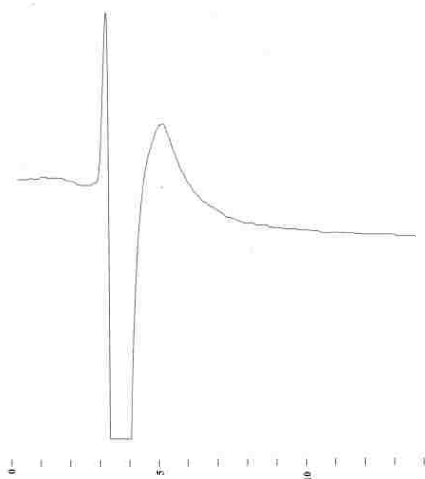


Figure B23: 1 mM *S,S* 1,2-diphenyl ethylene-diamine on the OMNiMIP synthesized from NOS.

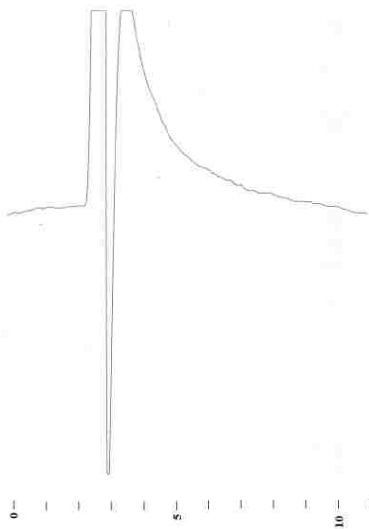


Figure B24: 1 mM *R,R* 1,2-diphenyl ethylene-diamine on the OMNiMIP synthesized from NOS.

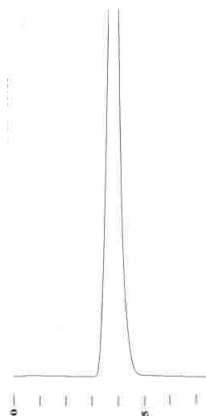


Figure B25: Acetone used to determine D_V (100 x 2.1 mm column) for OMNiMIPs synthesized with L-NALA (9.)

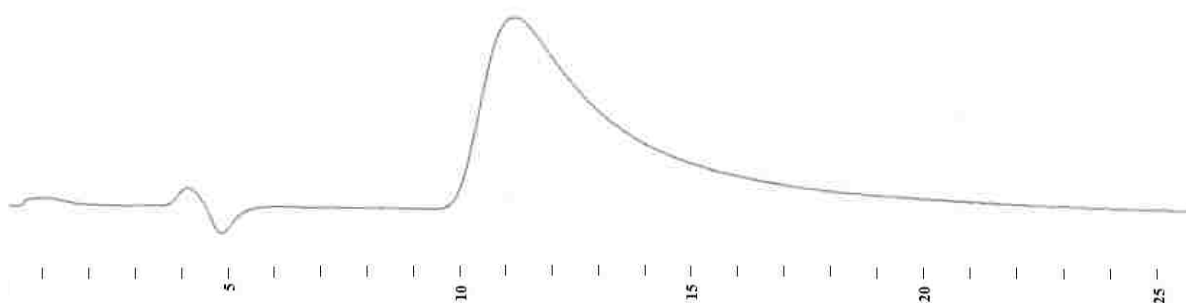


Figure B26: 1 mM L-BOC-Tyr on the OMNiMIP (100 x 2.1 mm column) synthesized with L-NALA (9.)

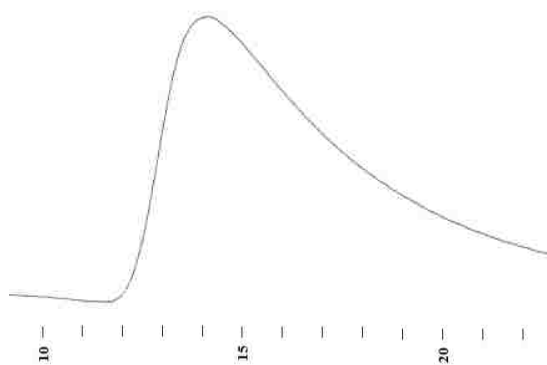


Figure B27: 1 mM D-BOC-Tyr on the OMNiMIP (100 x 2.1 mm column) synthesized with L-NALA (9.)

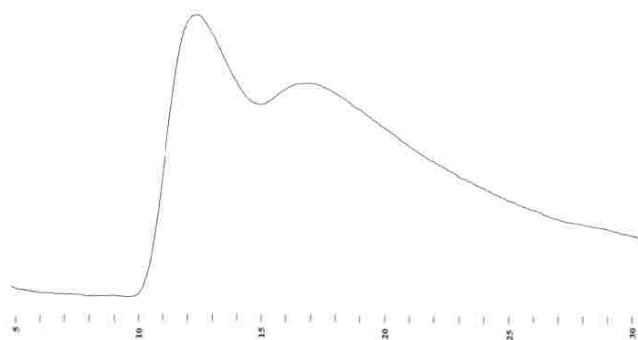


Figure B28: 0.5 mM racemic-BOC-Tyr on the OMNiMIP (100 x 2.1 mm column) synthesized with L-NALA (9.)

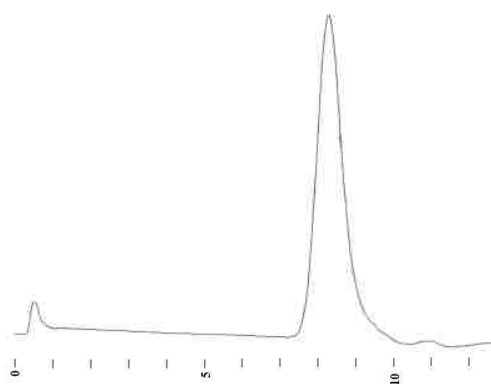


Figure B29: Acetone used to determine D_V (250 x 2.1 mm column) for OMNiMIPs synthesized with L-NALA (9.)

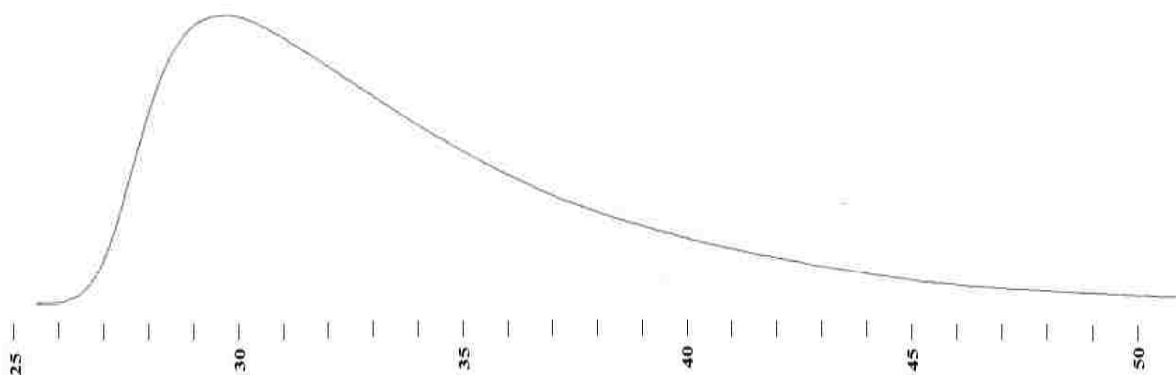


Figure B30: 1 mM L-BOC-Tyr on the OMNiMIP (250 x 2.1 mm column) synthesized with L-NALA (9.)

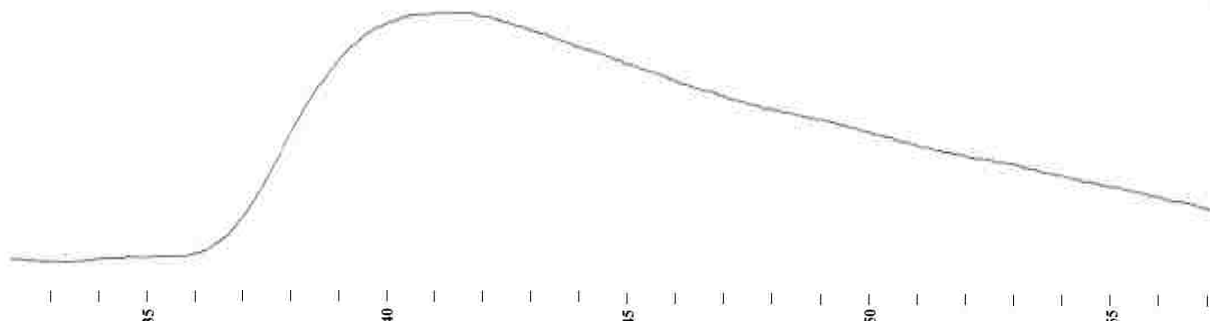


Figure B31: 1 mM D-BOC-Tyr on the OMNiMIP (250 x 2.1 mm column) synthesized with L-NALA (9.)

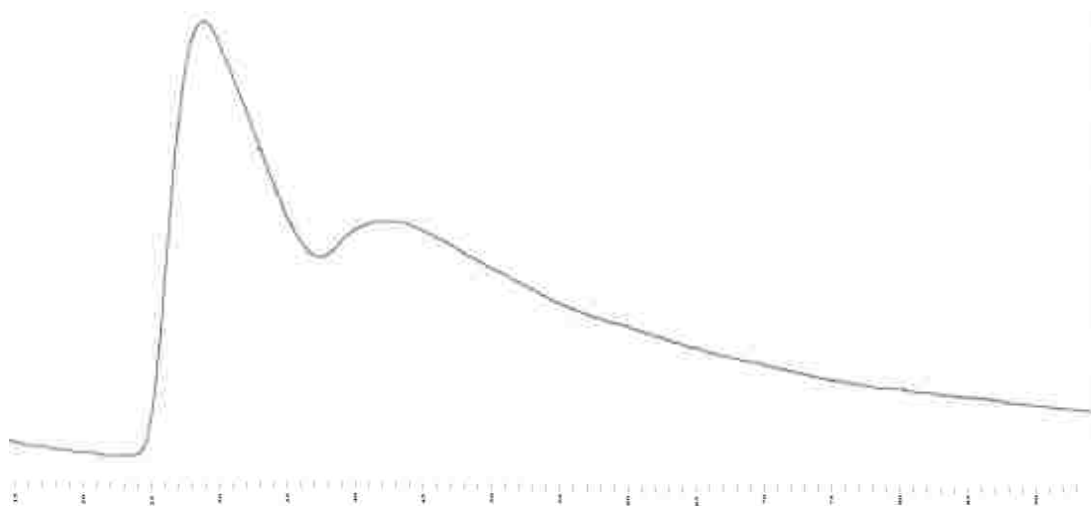


Figure B32: 1 mM racemic-BOC-Tyr on the OMNiMIP (250 x 2.1 mm column) synthesized with L-NALA (9.)

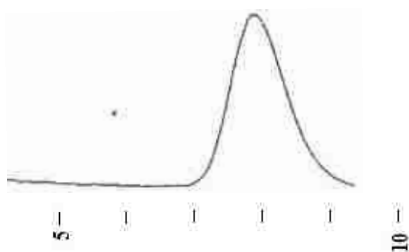


Figure B33: Acetone used to determine D_V (50 x 4.1 mm column) for OMNiMIPs synthesized with L-NALA (9.)

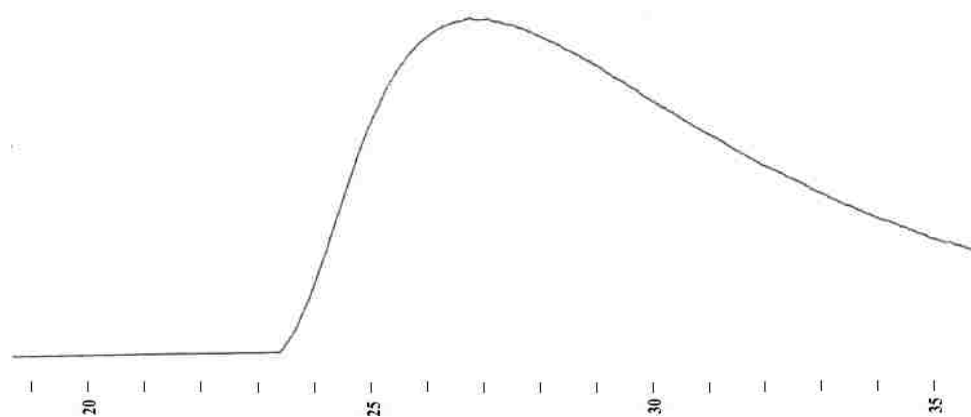


Figure B34: 1 mM L-BOC-Tyr on the OMNiMIP (50 x 4.1 mm column) synthesized with L-NALA (9.)

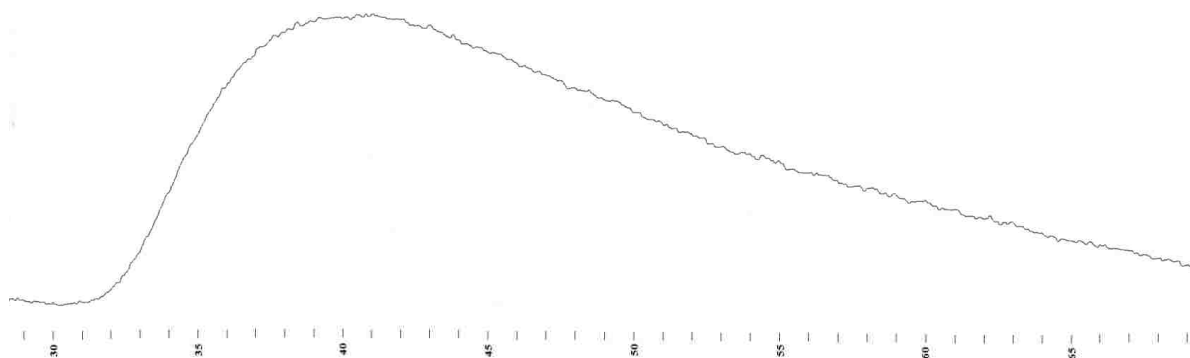


Figure B35: 1 mM D-BOC-Tyr on the OMNiMIP (50 x 4.1 mm column) synthesized with L-NALA (9.)

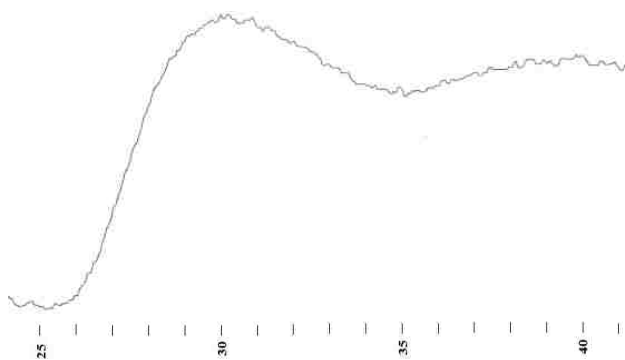


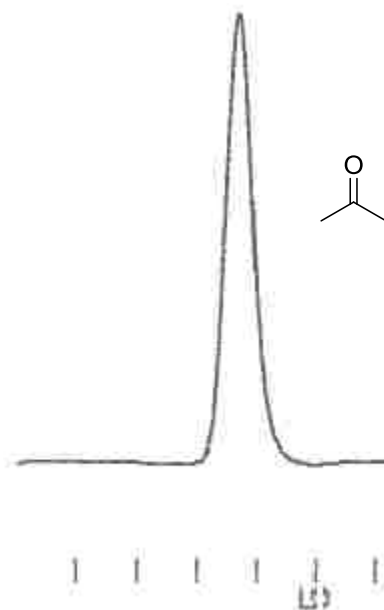
Figure B36: 1 mM racemic-BOC-Tyr on the OMNiMIP (50 x 4.1 mm column) synthesized with L-NALA (9.)

APPENDIX C: CHROMATOGRAMS FOR CHAPTER FOUR

Select chromatograms reprinted with permission from *Organic Letters* **2014** *16* (5), 1402-1405.

Copyright 2014 American Chemical Society.

Acetone on the 20% *R*-BOC-Tyr imprinted column ($D_v = 3.61$.)



Acetone on the 20% *S*-BOC-Tyr imprinted column ($D_v = 3.23$.)

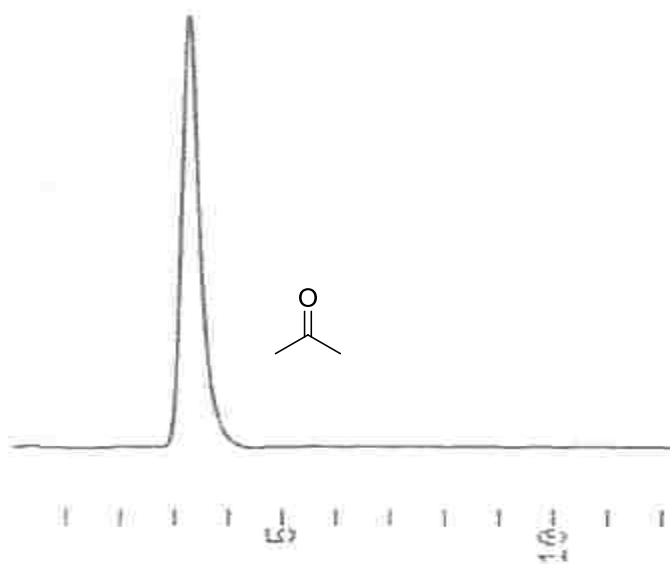
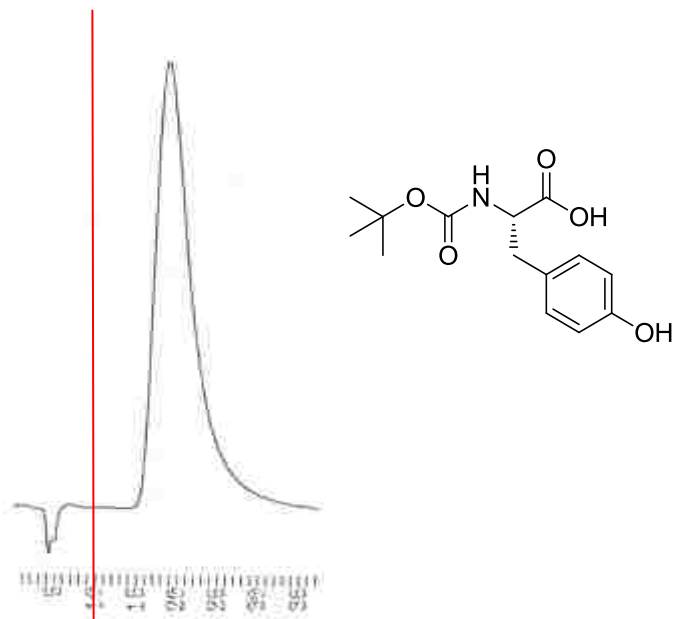


Figure C1: Void volume (D_v) determined by acetone.

Chromatograms. The following figures compare the chromatograms of selected analytes from the list in Table 1 on the DuoMIPs. In some cases, the chromatograms were analyzed at different chart speeds making them appear to be different sizes; however, all chromatograms were normalized in size with respect to time and calibrated to the red line.

2.5 mM *S*-BOC-Tyr (7a) on the 20% *R*-BOC-Tyr imprinted column ($D_v = 3.61$)



2.5 mM *S*-BOC-Tyr (7a) on the 20% *S*-BOC-Tyr imprinted column ($D_v = 3.23$)

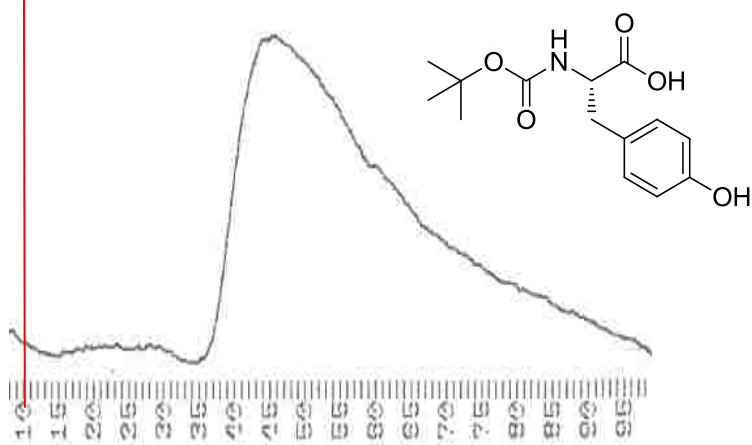
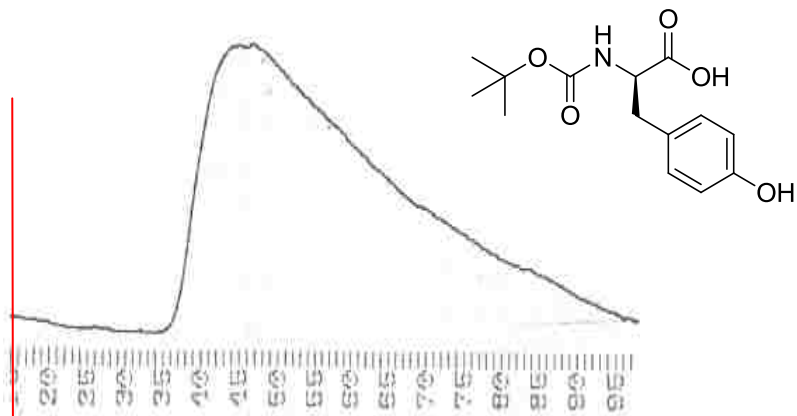


Figure C2: *S*-BOC-Tyr (7a) on the DuoMIPs.

2.5 mM *R*-BOC-Tyr (7b) on the 20% *R*-BOC-Tyr imprinted column ($D_v = 3.61$)



2.5 mM *R*-BOC-Tyr (7b) on the 20% *S*-BOC-Tyr imprinted column ($D_v = 3.23$)

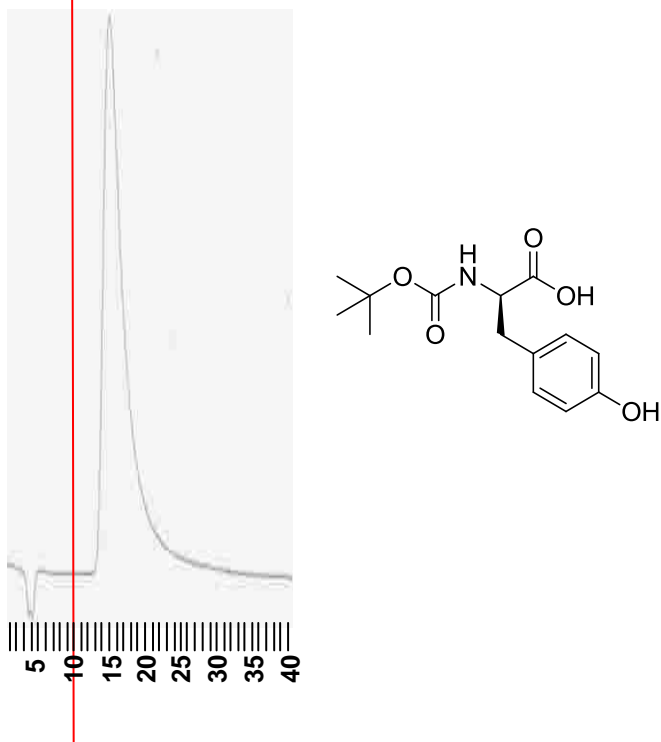
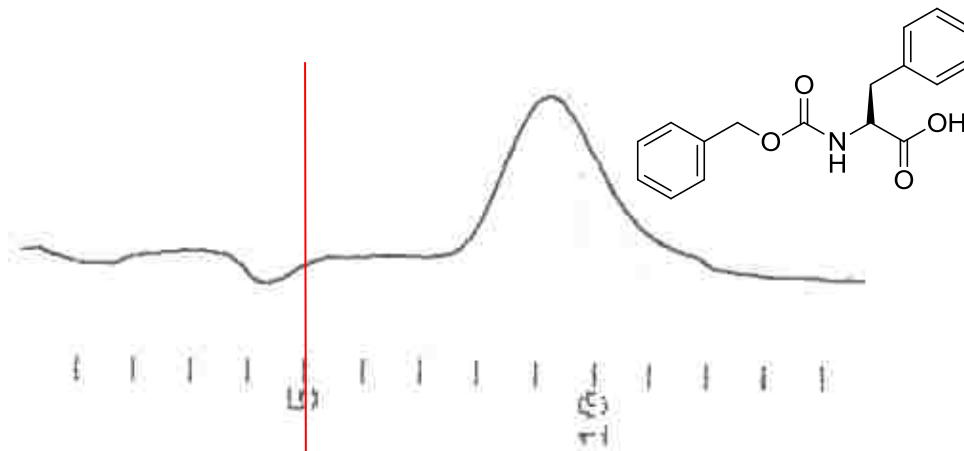


Figure C3: *R*-BOC-Tyr (7b) on the DuoMIPs.

Important Note: Although the retention time on the *R*-MIP is higher, the k' of the analyte on the *S*-MIP is higher, as shown in Table 1. This is due to the difference in dead volume values. Thus, AC is still accurately accounted for.

1 mM *S*-Z-Phe (75a) on the 20% *R*-BOC-Tyr imprinted column ($D_v = 3.61$)



1 mM *S*-Z-Phe (75a) on the 20% *S*-BOC-Tyr imprinted column ($D_v = 3.23$)

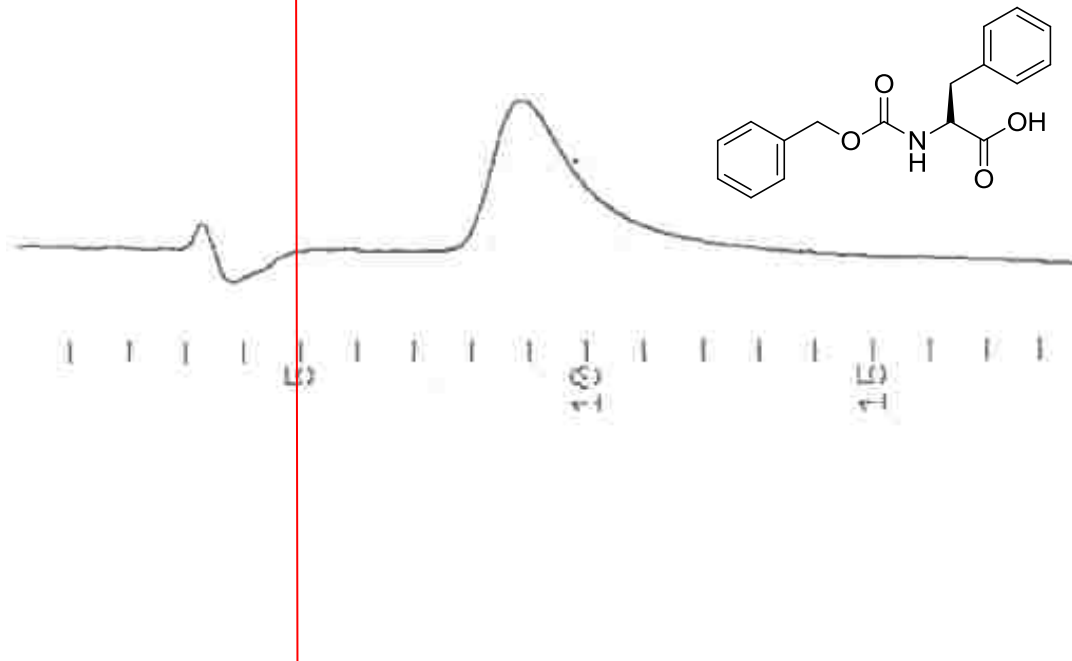
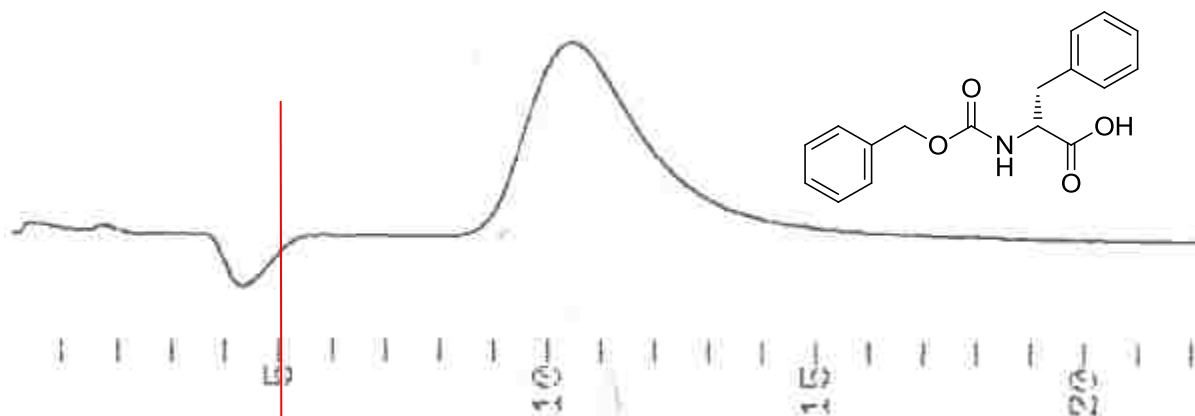


Figure C4: *S*-Z-Phe (75a) on the DuoMIPs.

1 mM *R*-Z-Phe (75b) on the 20% *R*-BOC-Tyr imprinted column ($D_v = 3.61$)



1 mM *R*-Z-Phe (75b) on the 20% *S*-BOC-Tyr imprinted column ($D_v = 3.23$)

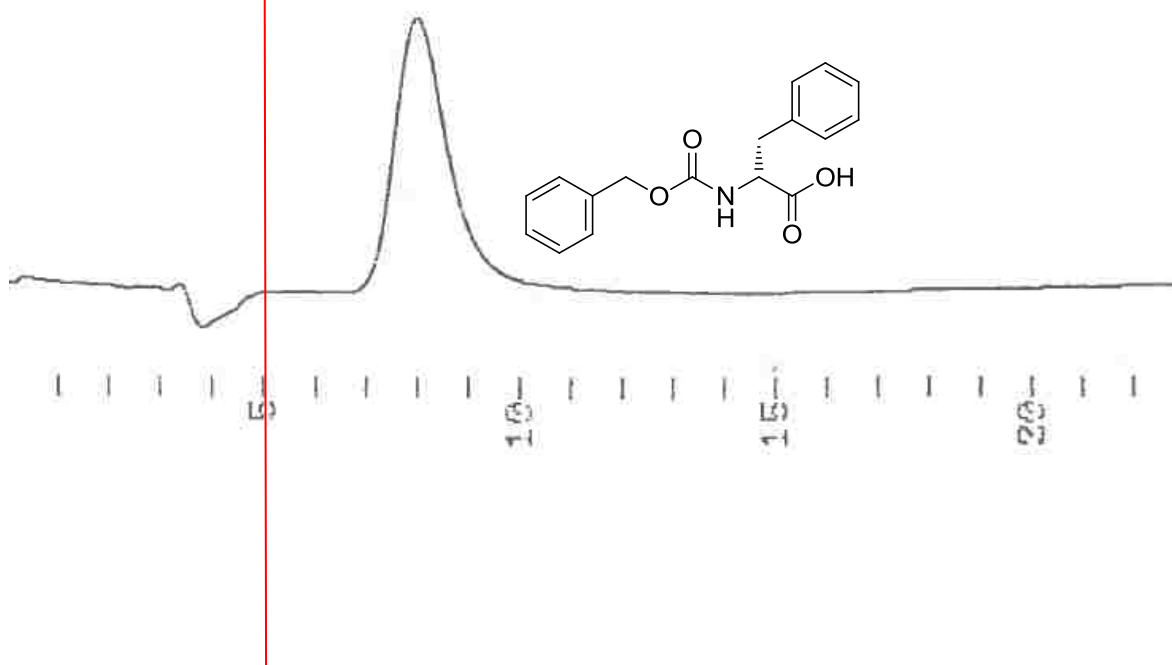
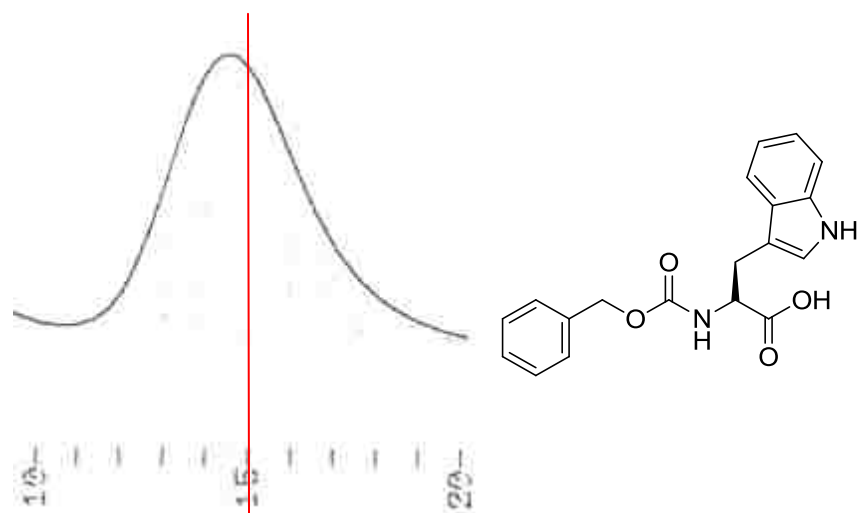


Figure C5: *R*-Z-Phe (75b) on the DuoMIPs.

0.2 mM *S*-Z-Trp (76a) on the 20% *R*-BOC-Tyr imprinted column ($D_v = 3.61$)



0.2 mM *S*-Z-Trp (76a) on the 20% *S*-BOC-Tyr imprinted column ($D_v = 3.23$)

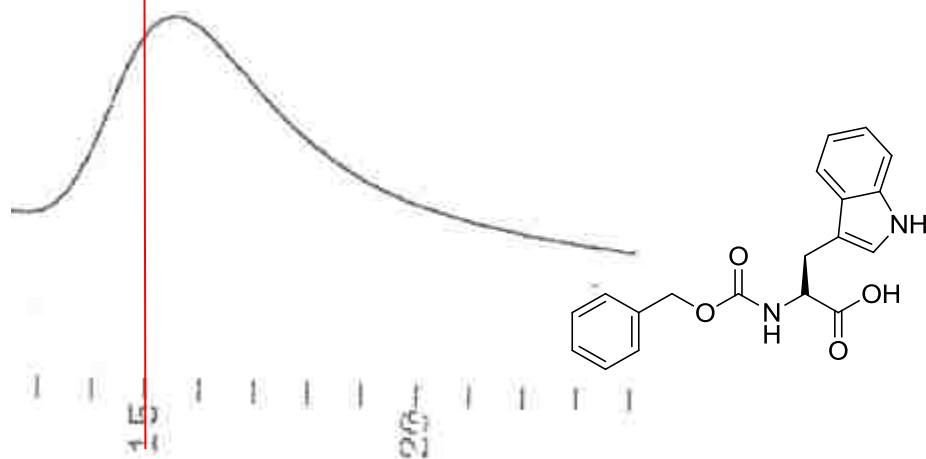
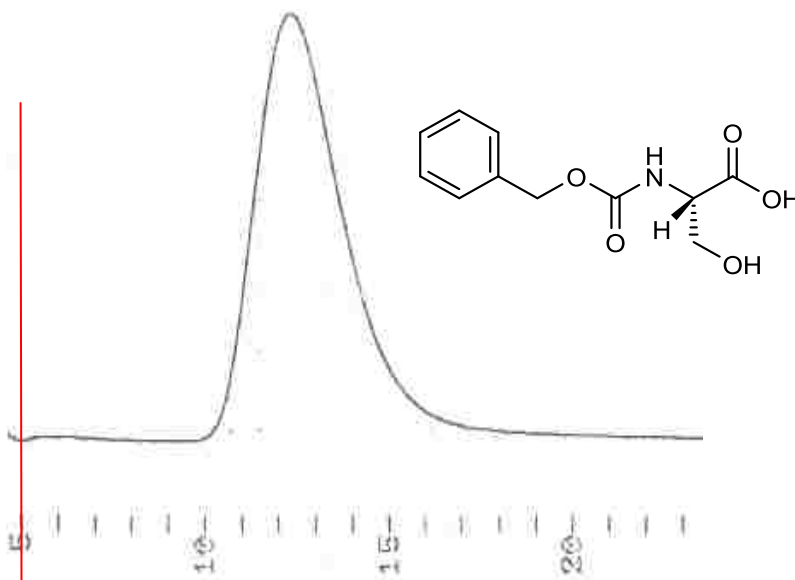


Figure C6: *S*-Z-Trp (76a) on the DuoMIPs.

Important Note: Although the retention time on the *R*-MIP is higher, the k' values of the analyte on both DuoMIPs are the same, as shown in Table 1. This is due to the difference in dead volume values. Thus, AC cannot be determined for this analyte.

1 mM *S*-Z-Ser (77a) on the 20% *R*-BOC-Tyr imprinted column ($D_v = 3.61$)



1 mM *S*-Z-Ser (77a) on the 20% *S*-BOC-Tyr imprinted column ($D_v = 3.23$)

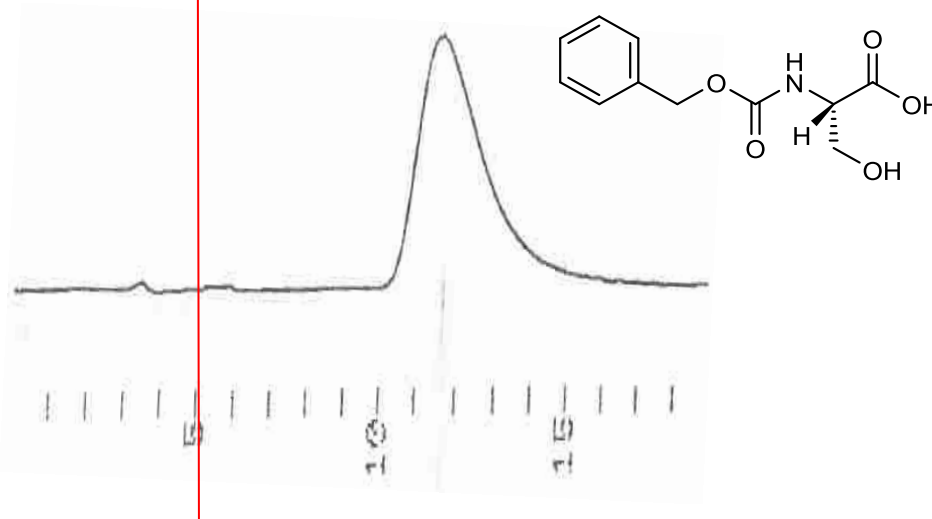
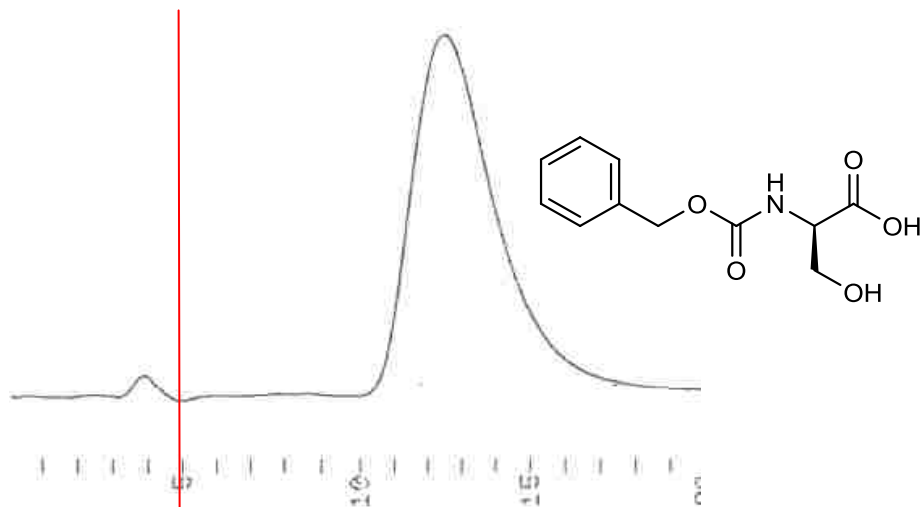


Figure C7: *S*-Z-Ser (77a) on the DuoMIPs.

Important Note: Although the retention time on the *R*-MIP is higher, the k' values of the analyte on both DuoMIPs are the same, as shown in Table 1. This is due to the difference in dead volume values. Thus, AC cannot be determined for this analyte.

1 mM *R*-Z-Ser (77b) on the 20% *R*-BOC-Tyr imprinted column ($D_v = 3.61$)



1 mM *R*-Z-Ser (77b) on the 20% *S*-BOC-Tyr imprinted column ($D_v = 3.23$)

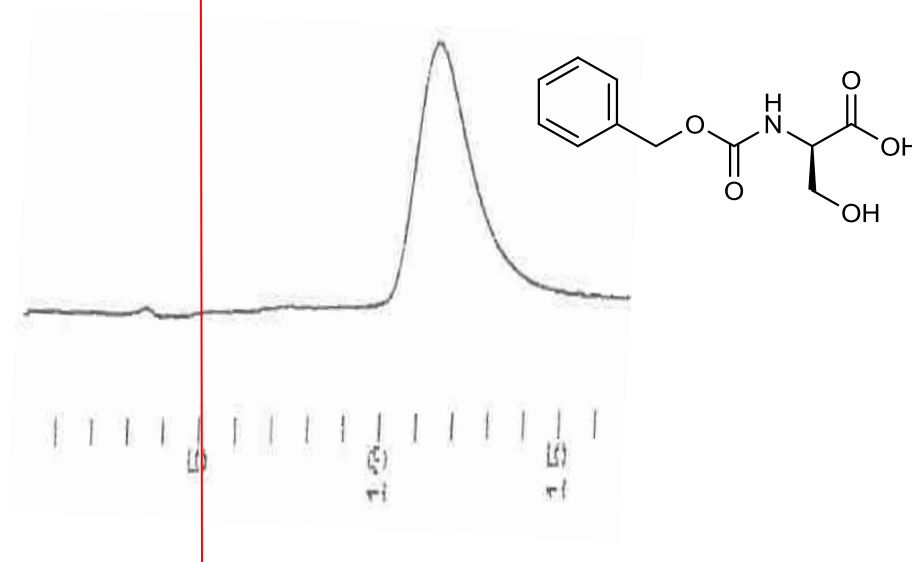
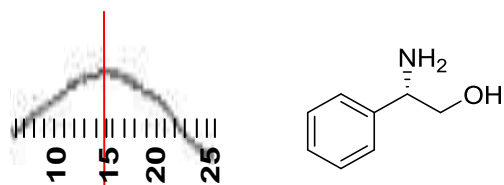


Figure C8: *R*-Z-Ser (77b) on the DuoMIPs.

1.0 mM *S*-phenyl-glycinol (78) on the 20% *R*-BOC-Tyr imprinted column ($D_v = 3.61$)



1.0 mM *S*-phenyl-glycinol (78) on the 20% *S*-BOC-Tyr imprinted column ($D_v = 3.23$)

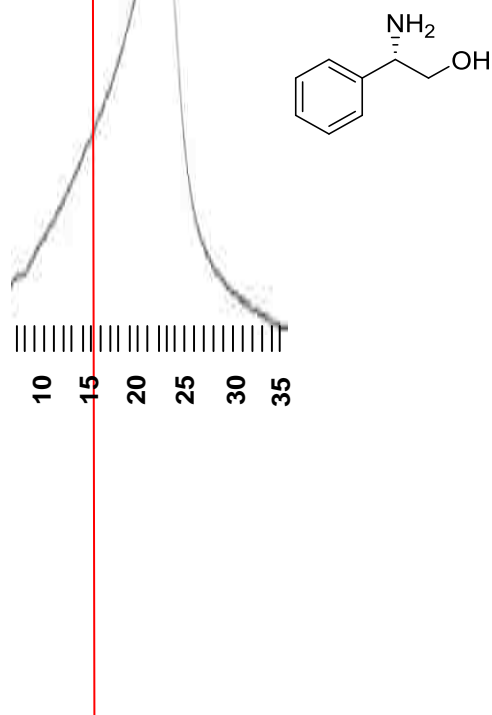
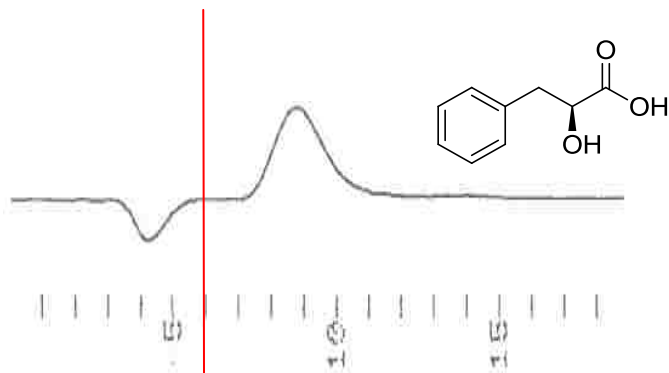


Figure C9: *S*-phenyl glycinol (78) on the DuoMIPs.

Important Note: Although the retention time on the *R*-MIP is higher, the k' of the analyte on the *S*-MIP is higher, as shown in Table 1. This is due to the difference in dead volume values. Thus, AC is still accurately accounted for.

1 mM *S*-phenyl lactic acid (79) on the 20% *R*-BOC-Tyr imprinted column ($D_v = 3.61$)



1 mM *S*-phenyl lactic acid (79) on the 20% *S*-BOC-Tyr imprinted column ($D_v = 3.23$)

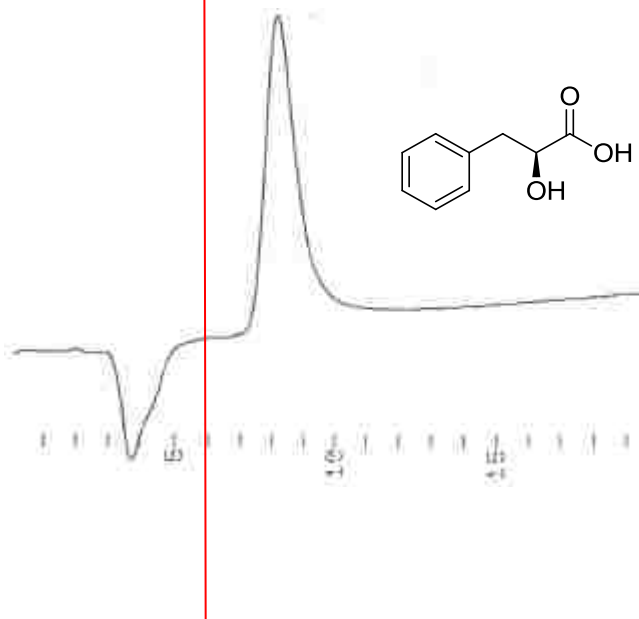
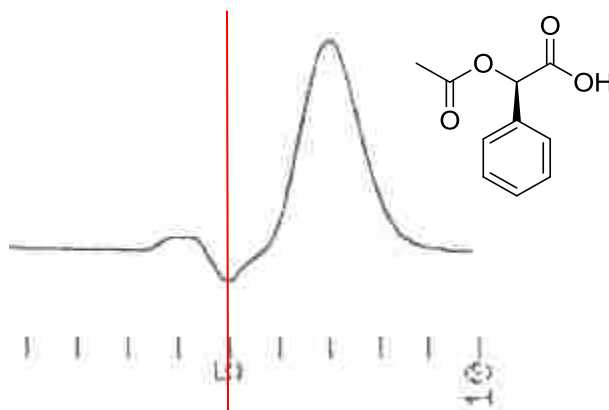


Figure C10: *S*-phenyl lactic acid (79) on the DuoMIPs.

Important Note: Although the retention time on the *R*-MIP is higher, the k' values for *R* mandelic acid on both DuoMIPs are the same, as shown in Table 1. This is due to the difference in dead volume values. Thus, AC cannot be determined for this analyte.

1 mM *R*-acetyl mandelic acid (86) on the 20% *R*-BOC-Tyr imprinted column ($D_v = 3.61$)



1 mM *R*-acetyl mandelic acid (86) on the 20% *S*-BOC-Tyr imprinted column ($D_v = 3.23$)

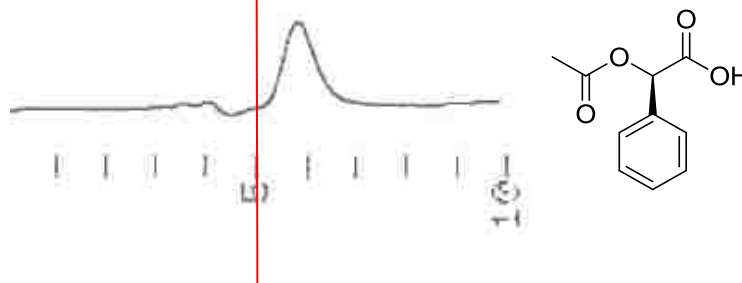
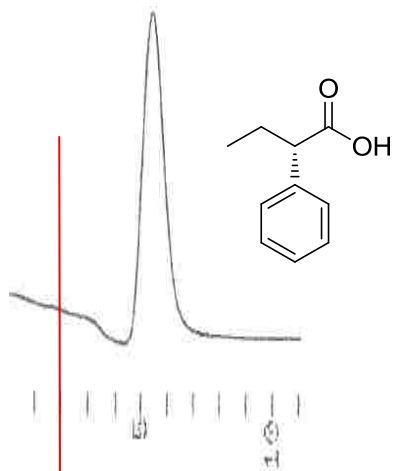


Figure C11: *R*-acetyl mandelic acid (86) on the DuoMIPs.

Important Note: Although the retention time on the *R*-MIP is higher, the k' values of the analyte on both DuoMIPs are the same, as shown in Table 1. This is due to the difference in dead volume values. Thus, AC cannot be determined for this analyte.

2 mM *S*-phenyl butyric acid (81a) on the 20% *R*-BOC-Tyr imprinted column ($D_v = 3.61$)



2 mM *S*-phenyl butyric acid (81a) on the 20% *S*-BOC-Tyr imprinted column ($D_v = 3.23$)

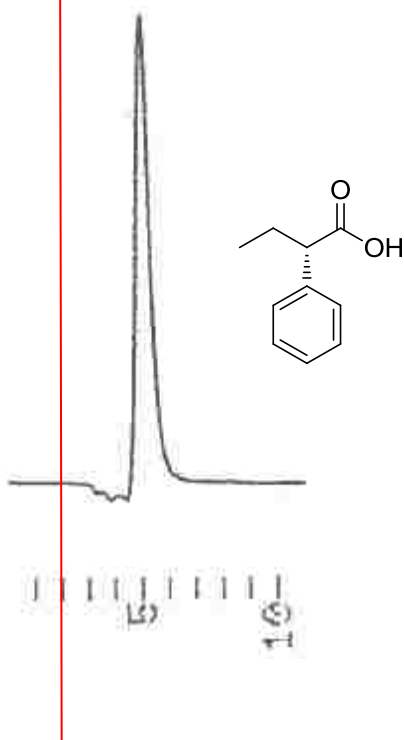
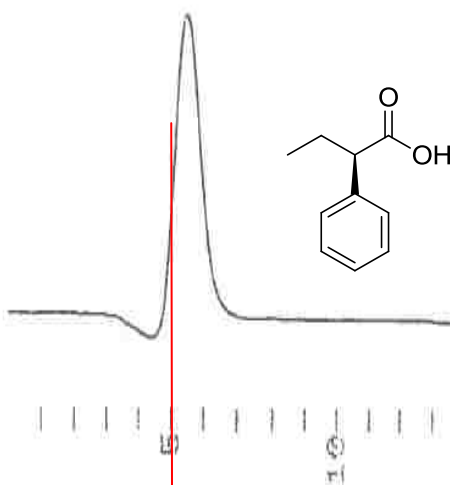


Figure C12: *S*-phenyl butyric acid (81a) on the DuoMIPs.

Important Note: Although the retention time on the *R*-MIP is higher, the k' values of the analyte on both DuoMIPs are the same, as shown in Table 1. This is due to the difference in dead volume values. Thus, AC cannot be determined for this analyte.

2 mM *R*-phenyl butyric acid (81b) on the 20% *R*-BOC-Tyr imprinted column ($D_v = 3.61$)



2 mM *R*-phenyl butyric acid (81b) on the 20% *S*-BOC-Tyr imprinted column ($D_v = 3.23$)

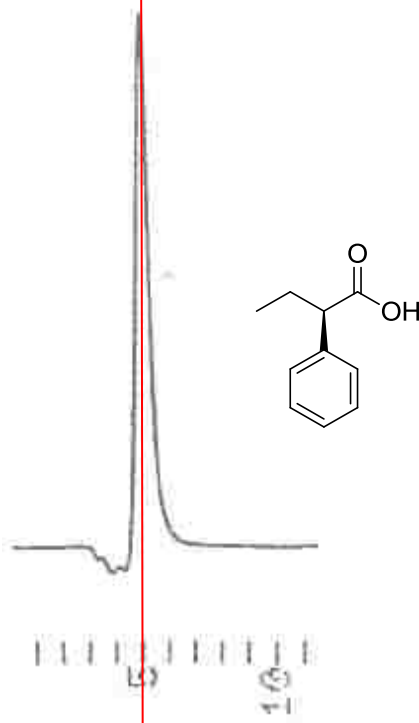


Figure C13: *R*-phenyl butyric acid (81b) on the DuoMIPs.

APPENDIX D: SPECTRA FOR CHAPTER FIVE

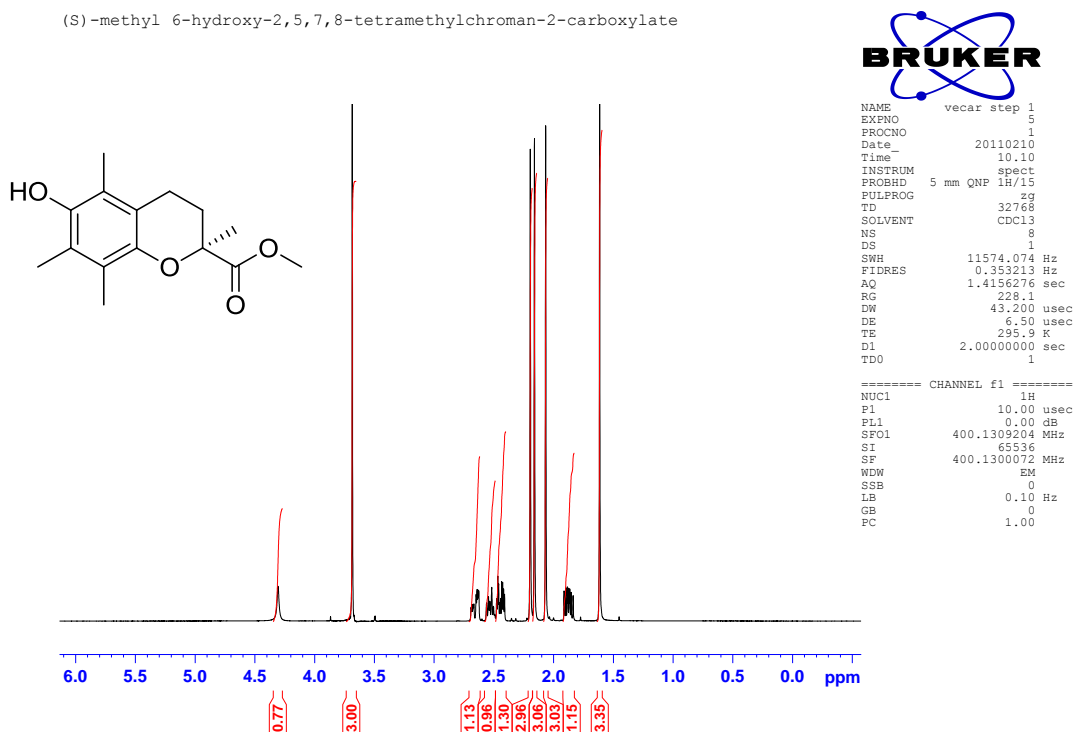


Figure D1: (S)-methyl 6-hydroxy-2,5,7,8-tetramethylchroman-2-carboxylate (109) ^1H NMR.

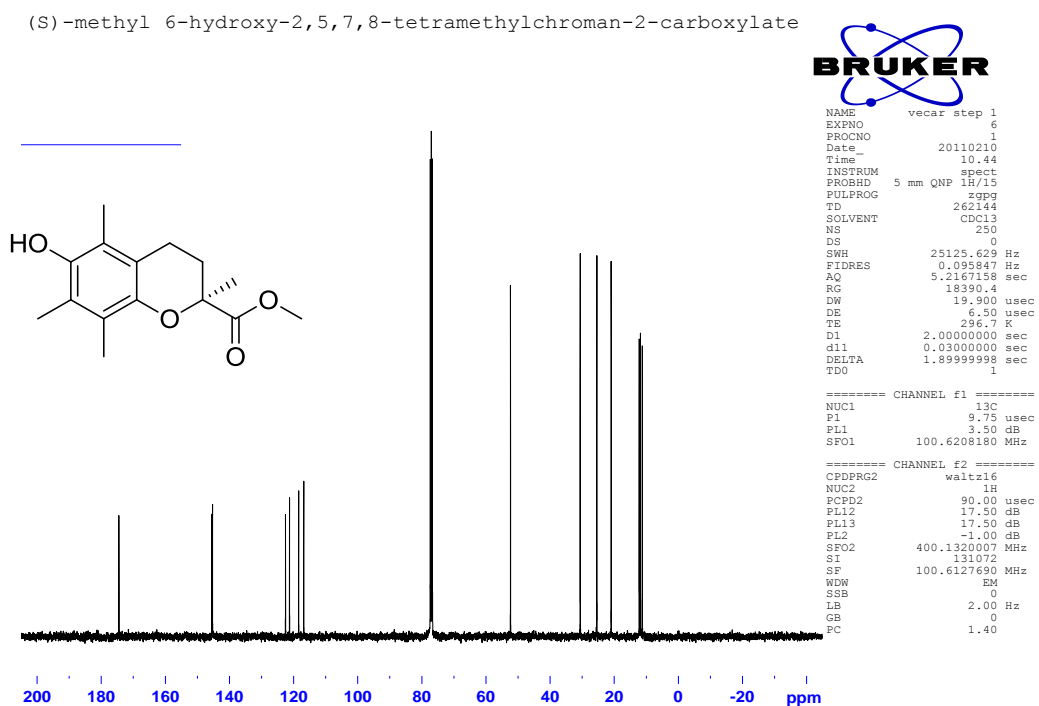


Figure D2: (S)-methyl 6-hydroxy-2,5,7,8-tetramethylchroman-2-carboxylate (109) ^{13}C NMR.

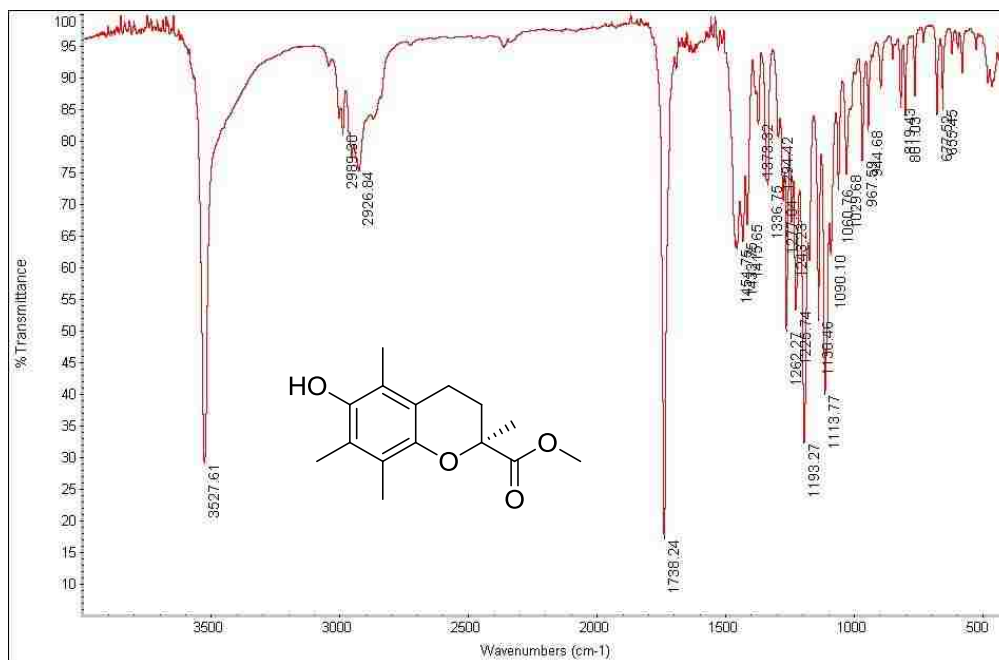


Figure D3: (*S*)-methyl 6-hydroxy-2,5,7,8-tetramethylchroman-2-carboxylate (109) IR.

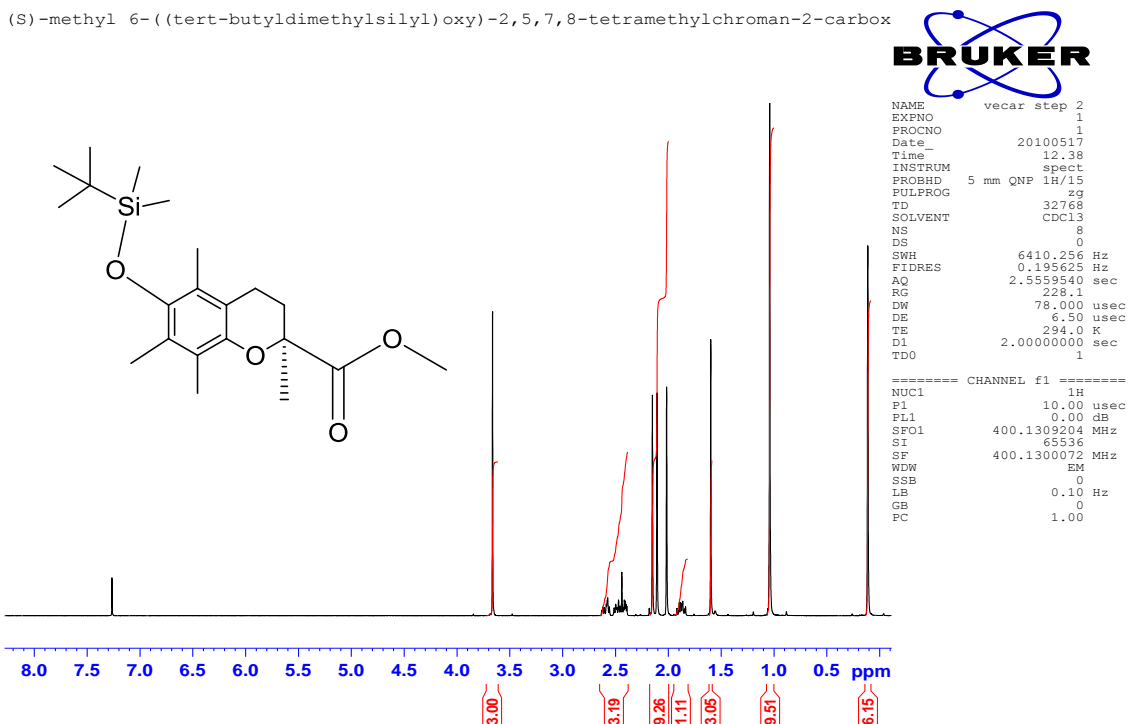


Figure D4: (*S*)-methyl 6-((tert-butyldimethylsilyloxy)-2,5,7,8-tetramethylchroman-2-carboxylate (110) ^1H NMR.

(S)-methyl 6-((tert-butyldimethylsilyloxy)-2,5,7,8-tetramethylchroman-2-carboxylate

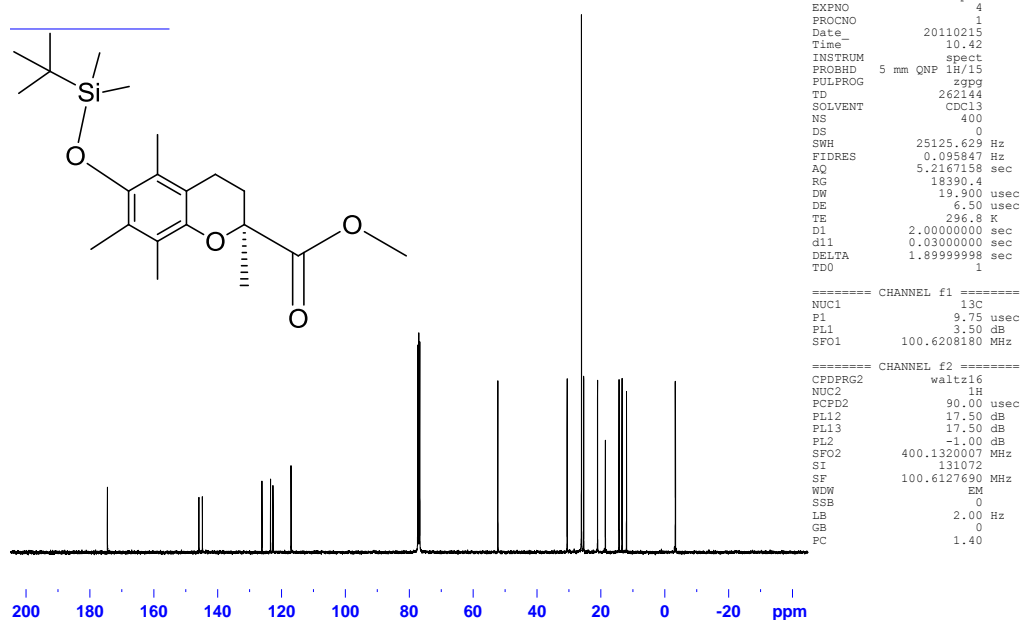


Figure D5: (S)-methyl 6-((tert-butyldimethylsilyloxy)-2,5,7,8-tetramethylchroman-2-carboxylate (110) ^{13}C NMR.

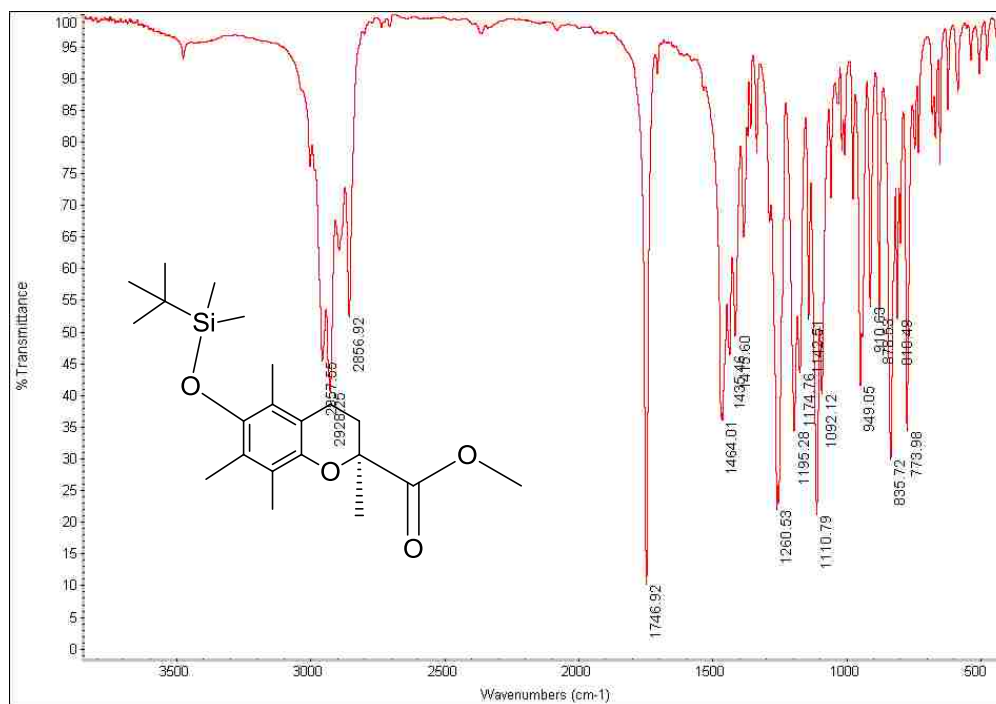


Figure D6: (S)-methyl 6-((tert-butyldimethylsilyloxy)-2,5,7,8-tetramethylchroman-2-carboxylate (110) IR.

(S)-6-((tert-butyldimethylsilyloxy)-2,5,7,8-tetramethylchroman-2-carbaldehyde

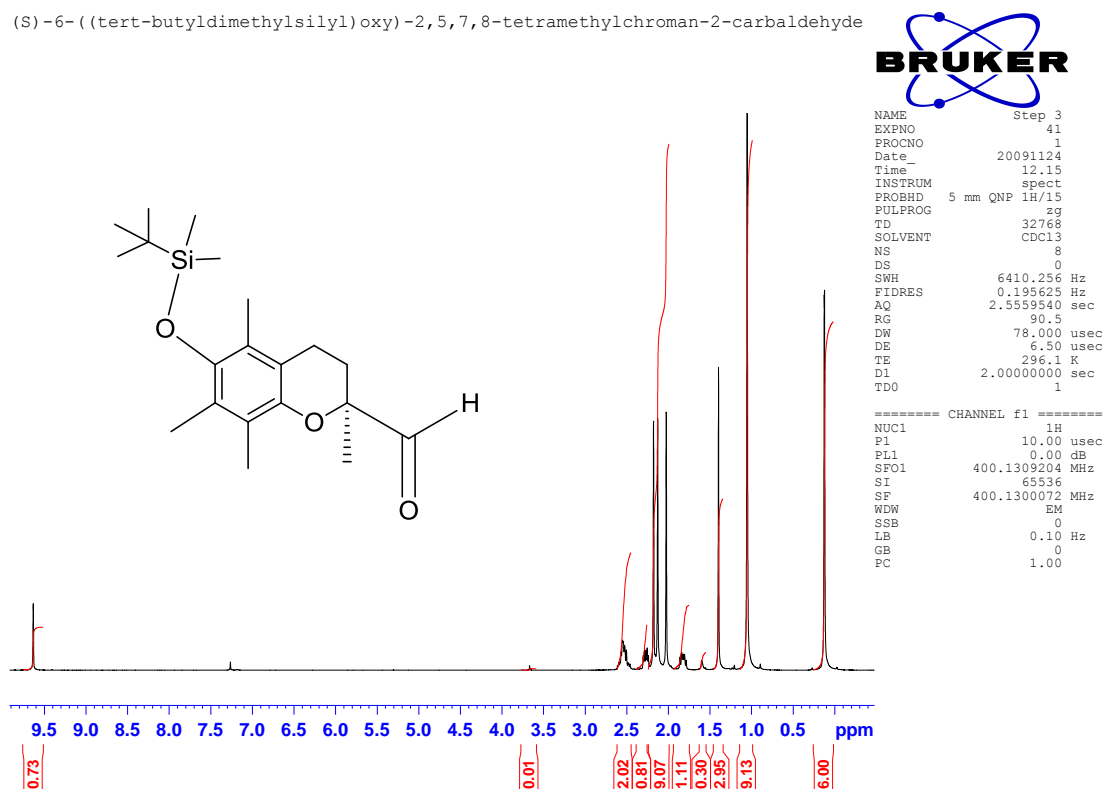


Figure D7: (S)-6-((tert-butyldimethylsilyloxy)-2,5,7,8-tetramethylchroman-2-carbaldehyde (111) ¹H NMR.

(S)-6-((tert-butyldimethylsilyloxy)-2,5,7,8-tetramethylchroman-2-carbaldehyde

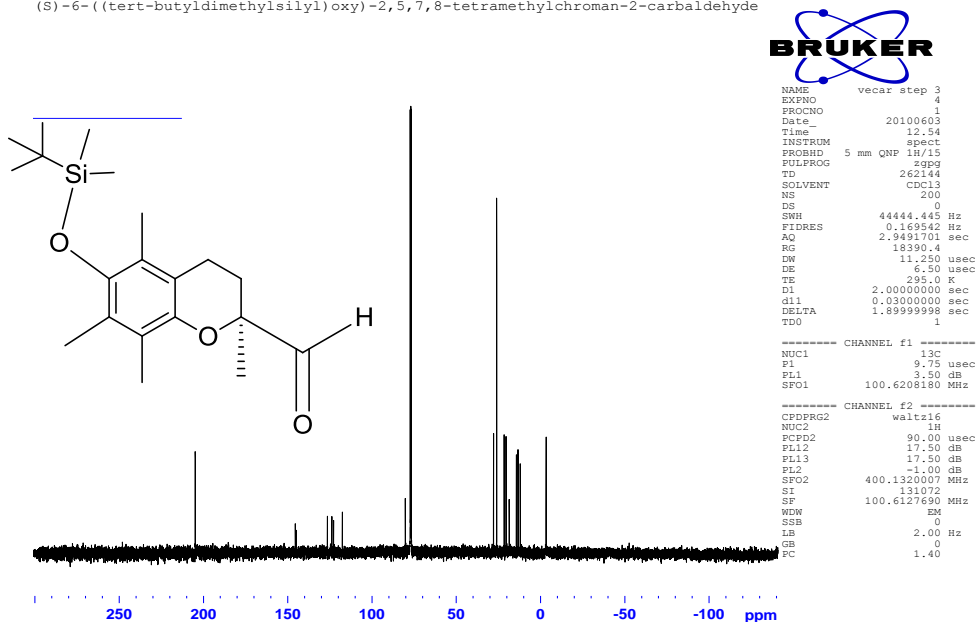


Figure D8: (S)-6-((tert-butyldimethylsilyloxy)-2,5,7,8-tetramethylchroman-2-carbaldehyde (111) ¹³C NMR.

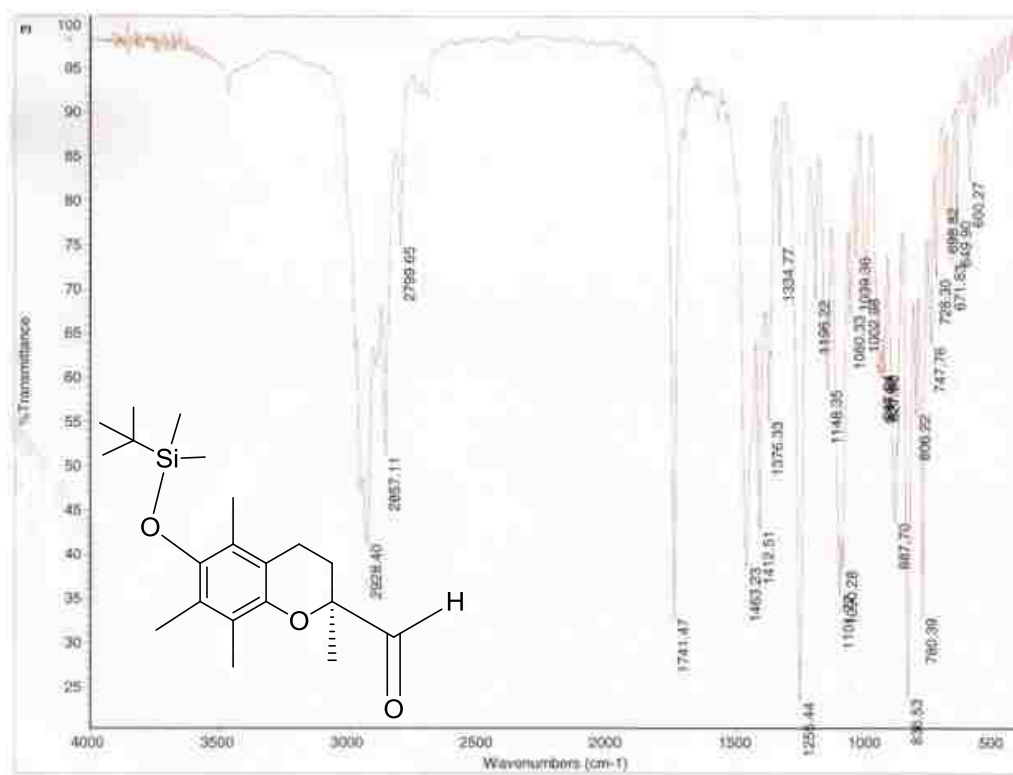


Figure D9: (S)-6-(tert-butyldimethylsilyloxy)-2,5,7,8-tetramethylchroman-2-carbaldehyde (111) IR.

(11-carboxyundecyl)triphenylphosphonium bromide

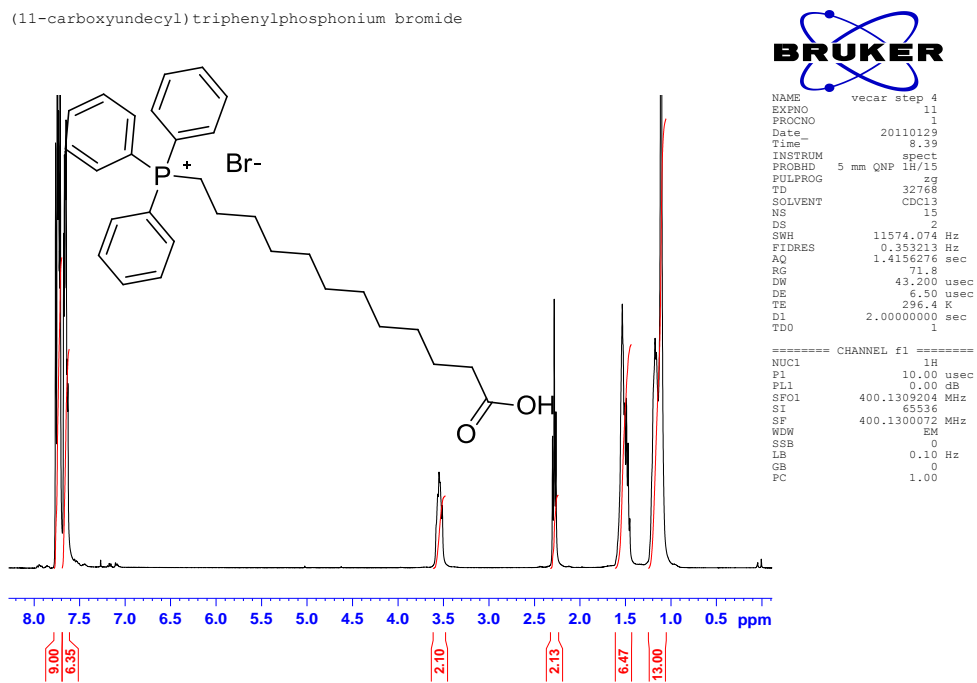


Figure D10: 11-(carboxyundecyl)triphenylphosphonium bromide (114) ^1H NMR.

(11-carboxyundecyl) triphenylphosphonium bromide

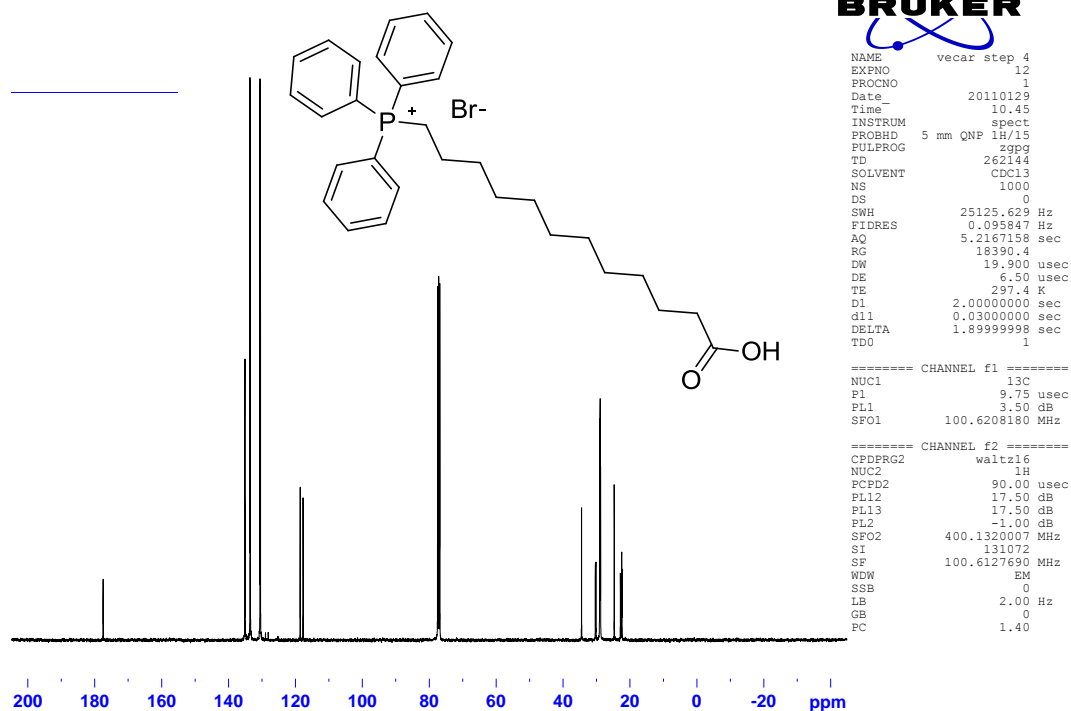


Figure D11: 11-(carboxyundecyl)triposponium bromide (114) ^{13}C NMR.

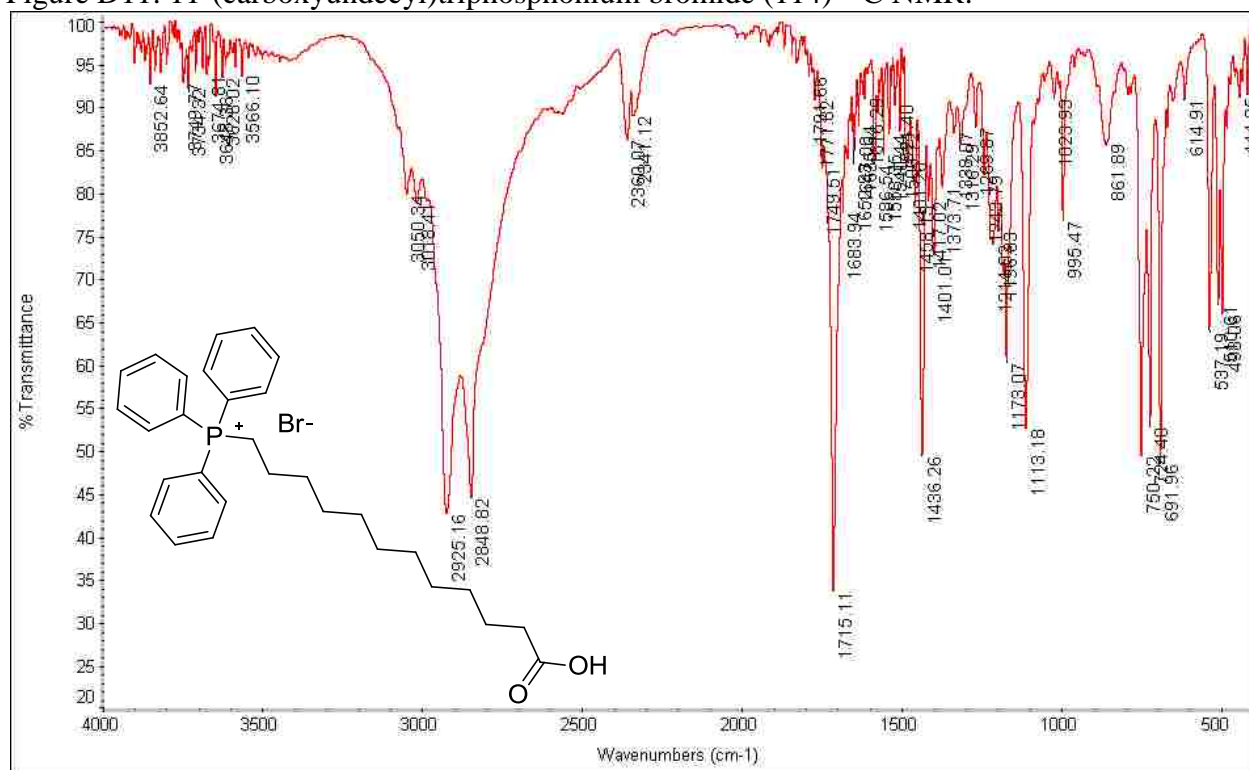


Figure D12: 11-(carboxyundecyl)triposponium bromide (114) IR.

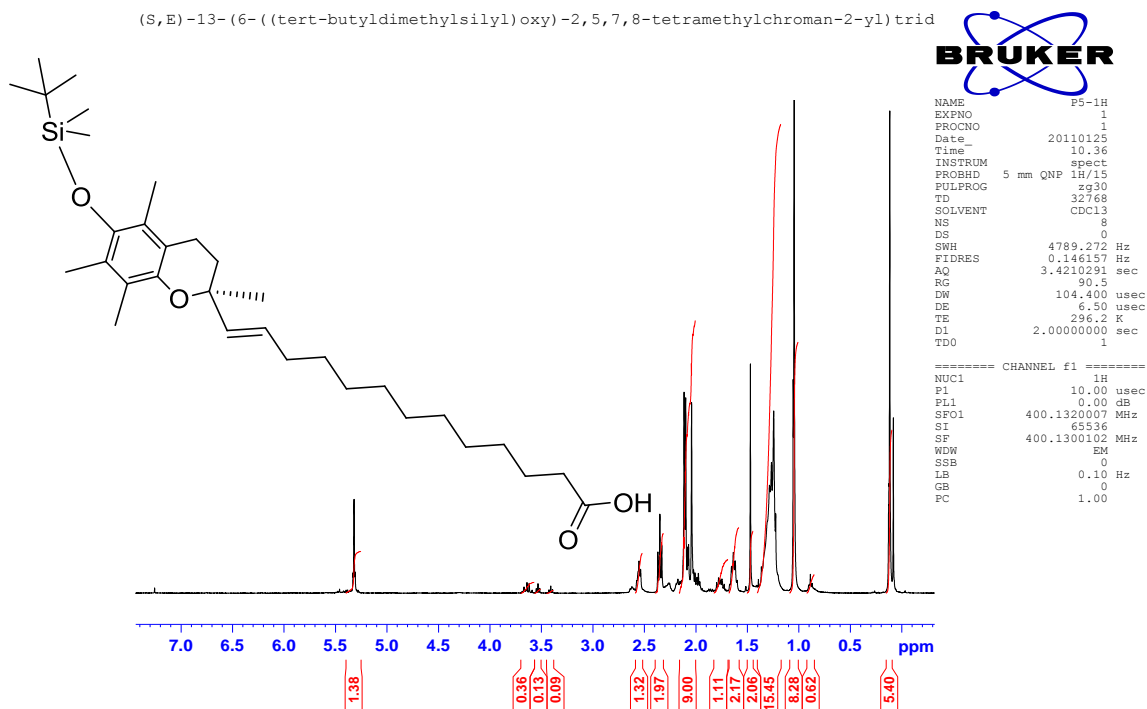


Figure D13: (S,E)-13-(6-((tert-butyldimethylsilyloxy)-2,5,7,8-tetramethylchroman-2-yl)tridec-12-enoic acid (116) ¹H NMR.

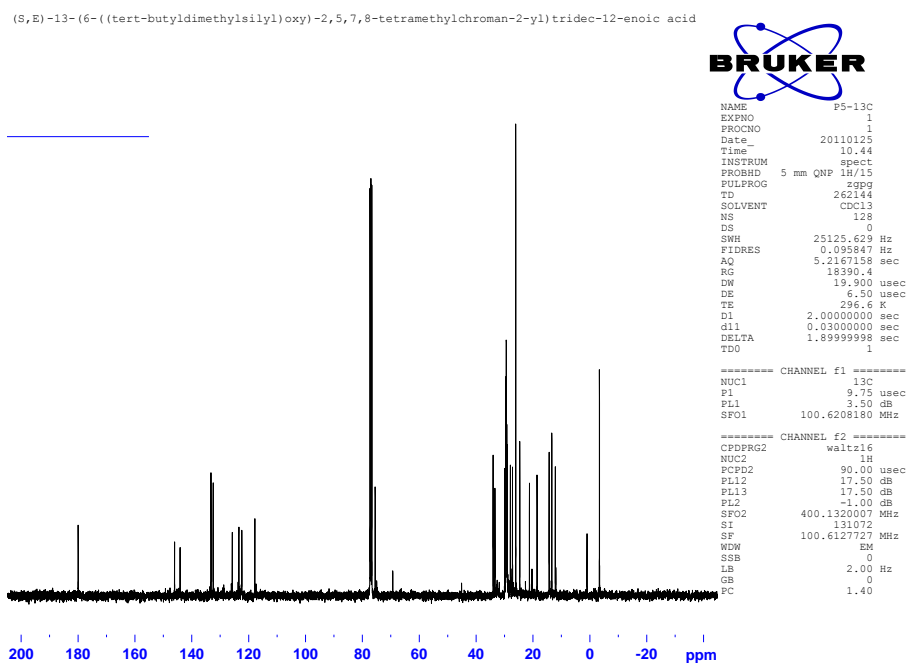


Figure D14: (S,E)-13-(6-((tert-butyldimethylsilyloxy)-2,5,7,8-tetramethylchroman-2-yl)tridec-12-enoic acid (116) ¹³C NMR.

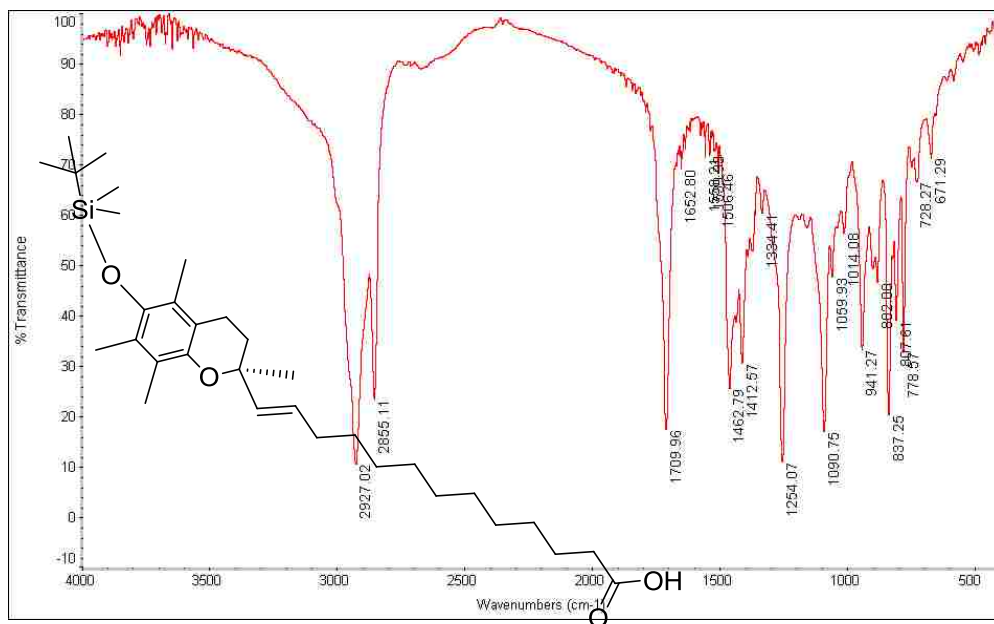


Figure D15: (*S,E*)-13-(6-(*tert*-butyldimethylsilyloxy)-2,5,7,8-tetramethylchroman-2-yl)tridec-12-enoic acid (116) IR.

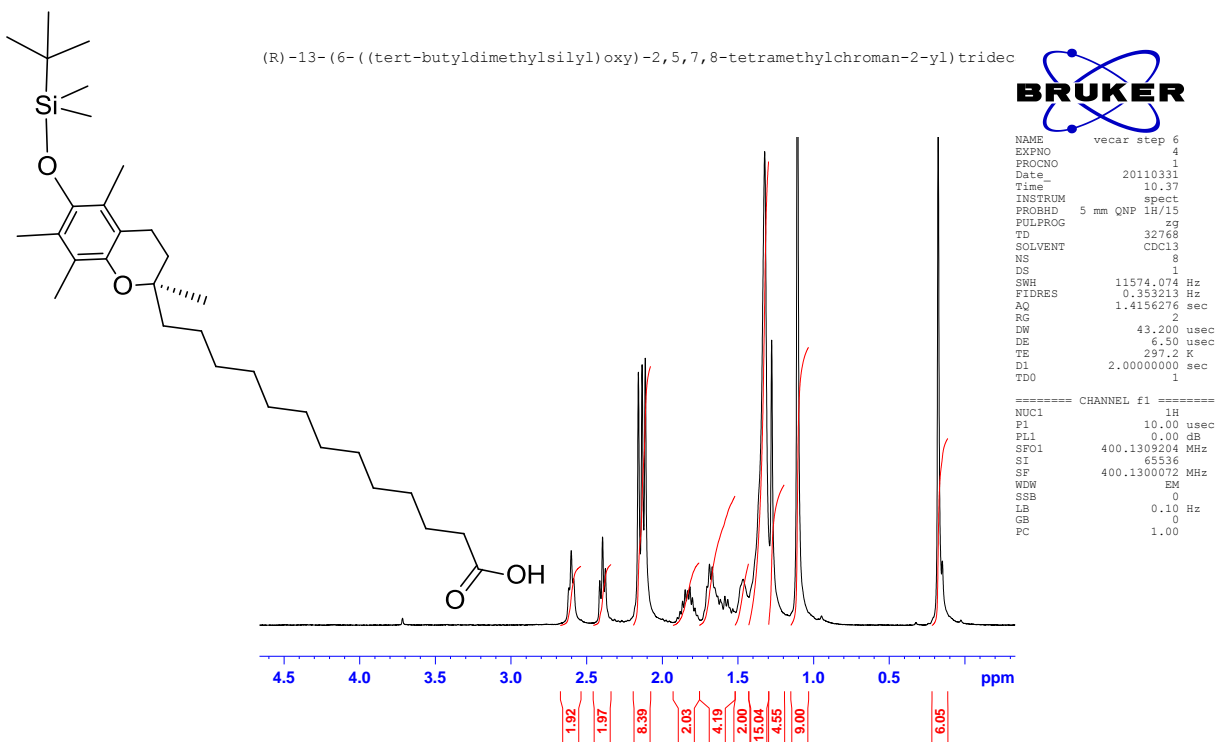


Figure D16: (*R*)-13-(6-(*tert*-butyldimethylsilyloxy)-2,5,7,8-tetramethylchroman-2-yl)tridecanoic acid (119) ^1H NMR.

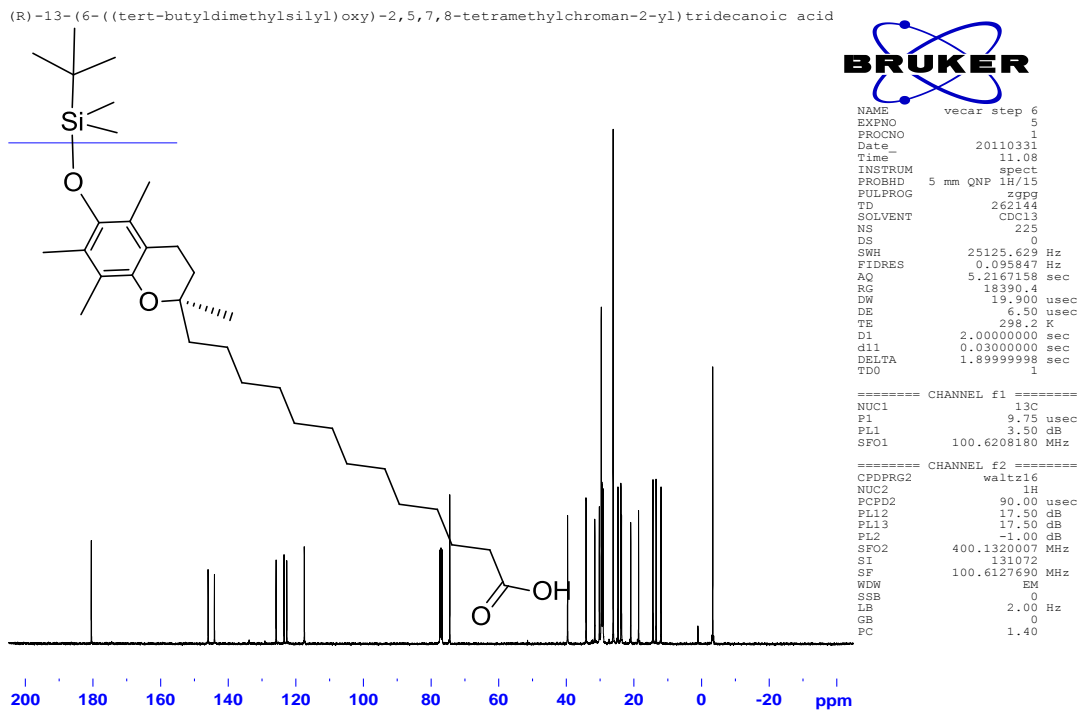


Figure D17: (R)-13-(6-((tert-butyldimethylsilyloxy)-2,5,7,8-tetramethylchroman-2-yl)tridecanoic acid (119) ^{13}C NMR.

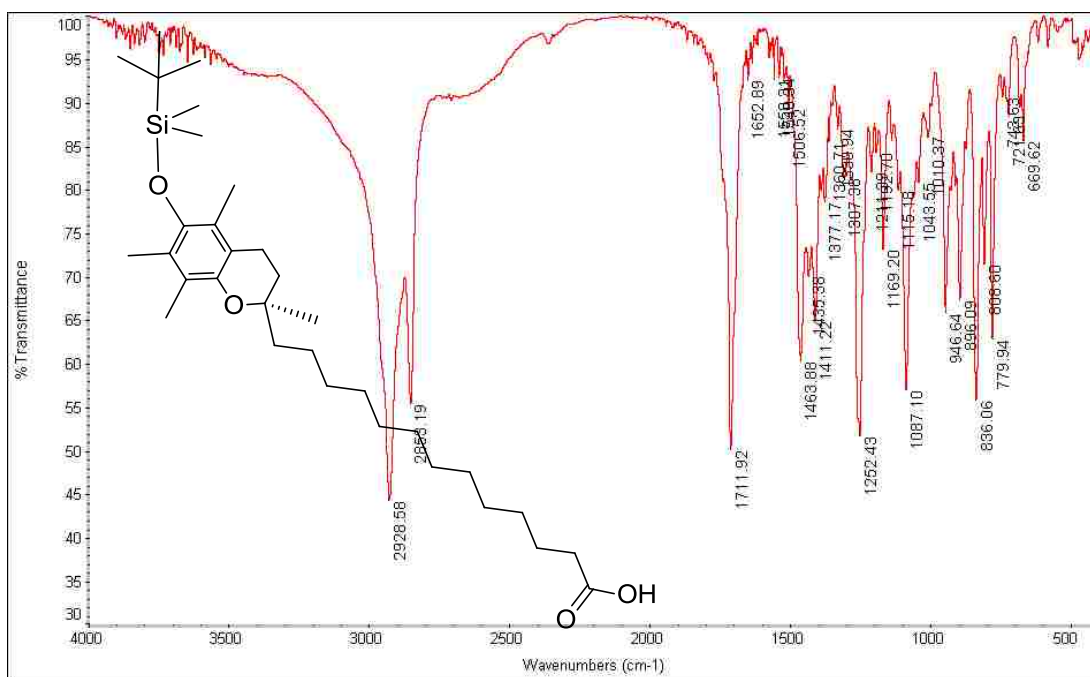


Figure D18: (R)-13-(6-((tert-butyldimethylsilyloxy)-2,5,7,8-tetramethylchroman-2-yl)tridecanoic acid (119) IR.

(R)-methyl 2-(3-aminopropanamido)-3-(1H-imidazol-4-yl)propanoate

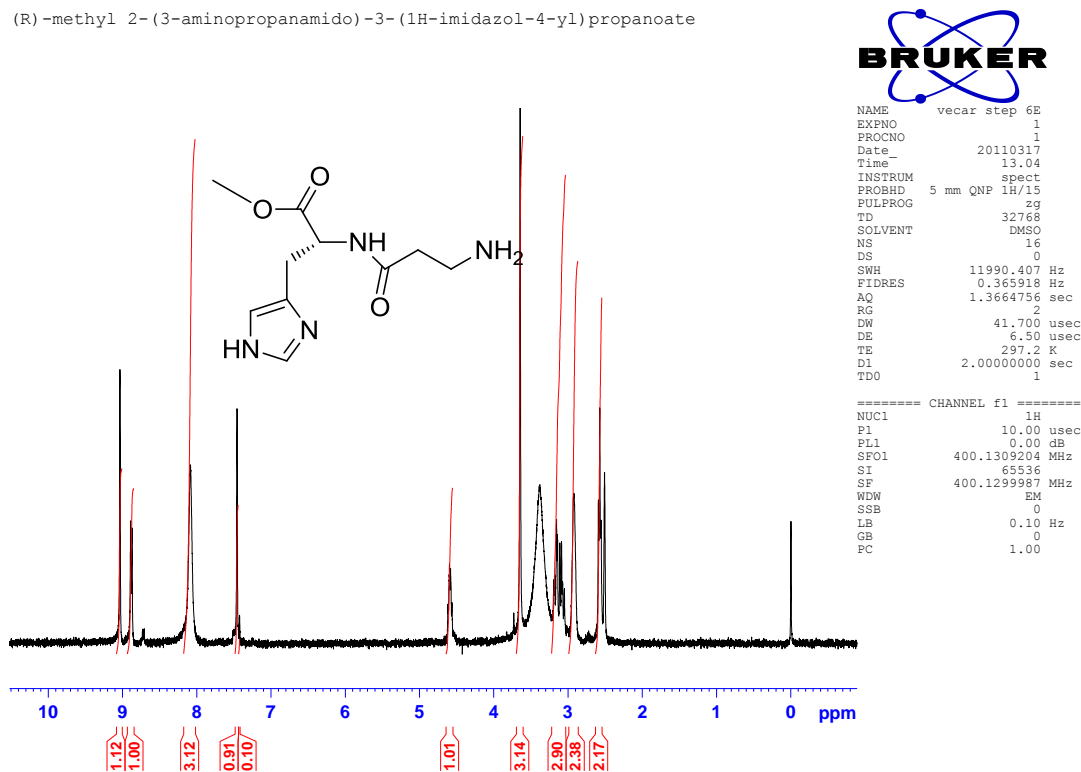


Figure D19: Carnosine Methyl Ester Dihydrochloride (115) ¹H NMR.

(R)-methyl 2-(3-aminopropanamido)-3-(1H-imidazol-4-yl)propanoate

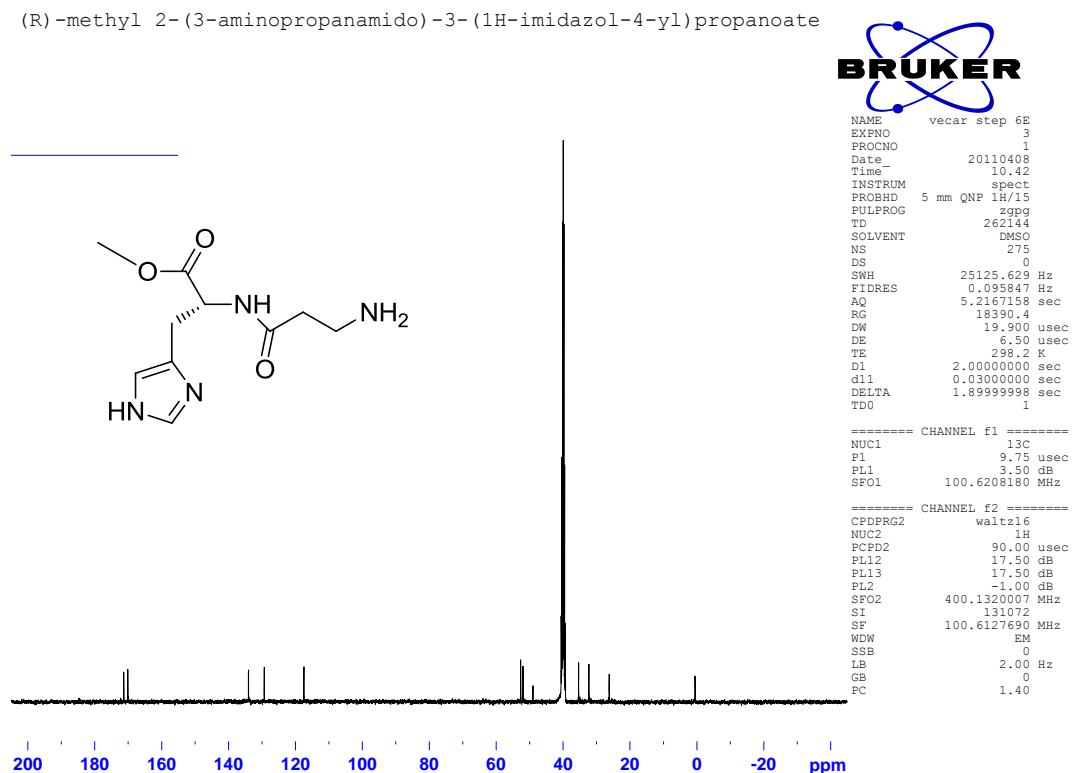


Figure D20: Carnosine Methyl Ester Dihydrochloride (115) ¹³C NMR.

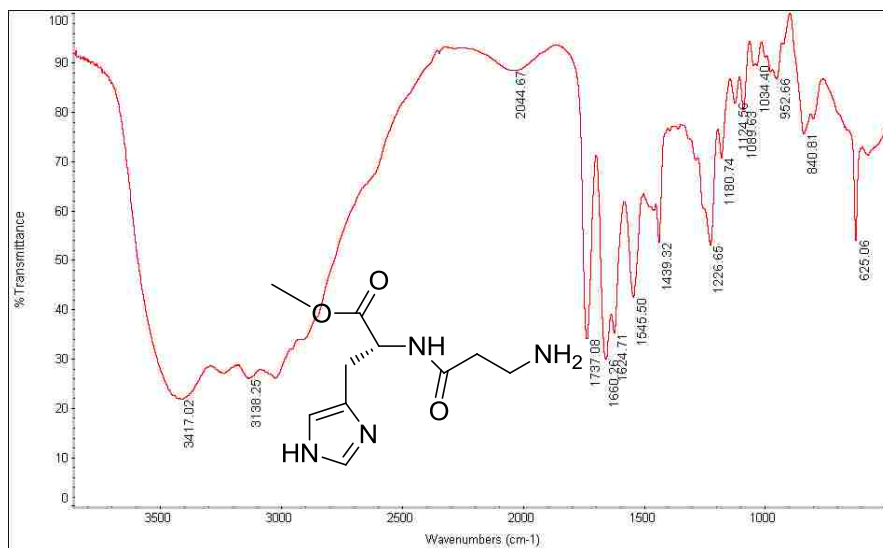


Figure D21: Carnosine Methyl Ester Dihydrochloride (115) IR.

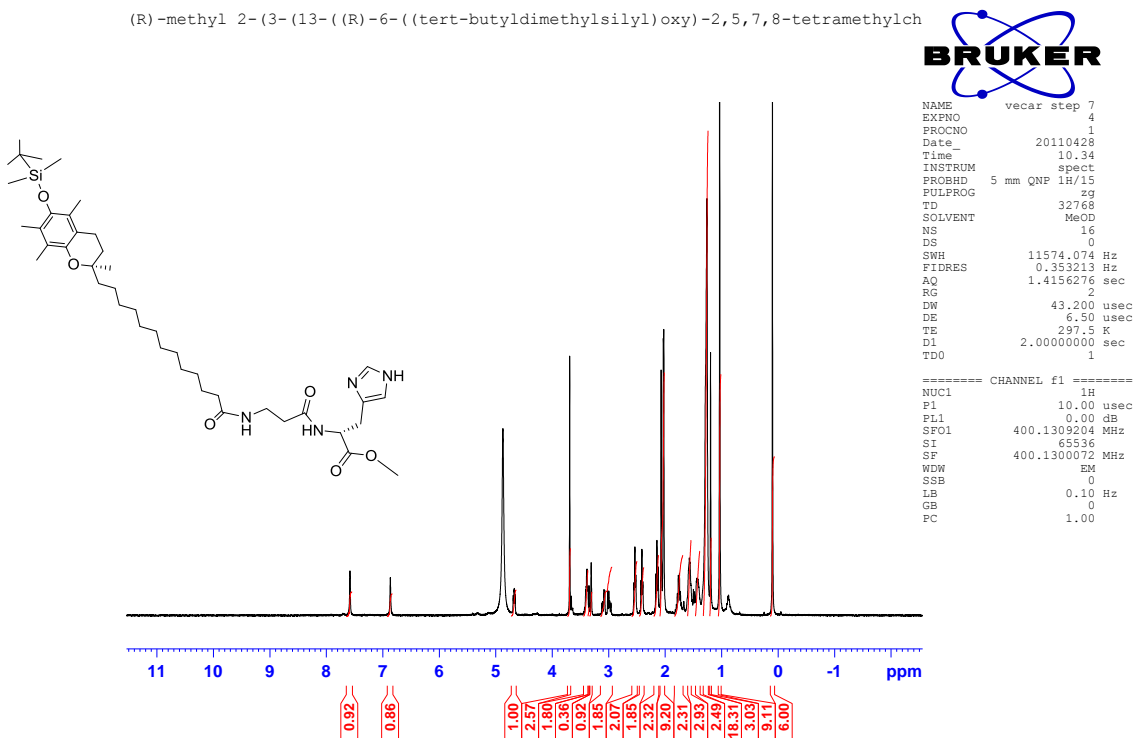


Figure D22: (R)-methyl 2-(3-(13-((R)-6-((tert-butyl dimethylsilyl)oxy)-2,5,7,8-tetramethylchroman-2-yl)tridecanamido)propanamido)-3-(1H-imidazol-4-yl)propanoate (119) ¹H NMR.

(R)-methyl 2-(3-(13-((R)-6-((tert-butylidimethylsilyl)oxy)-2,5,7,8-tetramethylchroman-2-yl)tridecanamido)propanamido)-3-(1H-imidazol-4-yl)propanoate

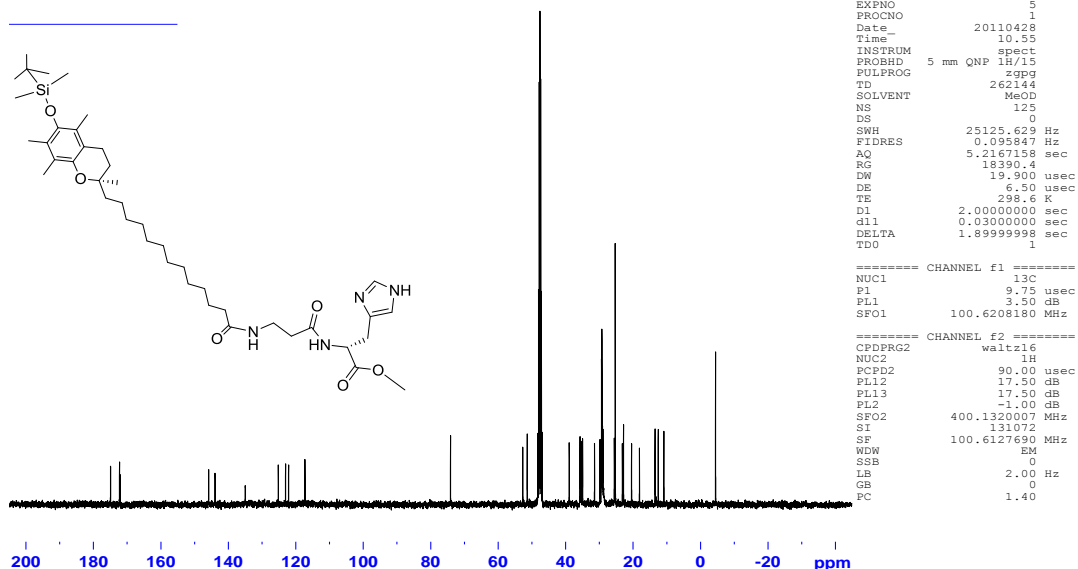


Figure D23: (R)-methyl 2-(3-(13-((R)-6-((tert-butylidimethylsilyl)oxy)-2,5,7,8-tetramethylchroman-2-yl)tridecanamido)propanamido)-3-(1H-imidazol-4-yl)propanoate (119) ¹³C NMR.

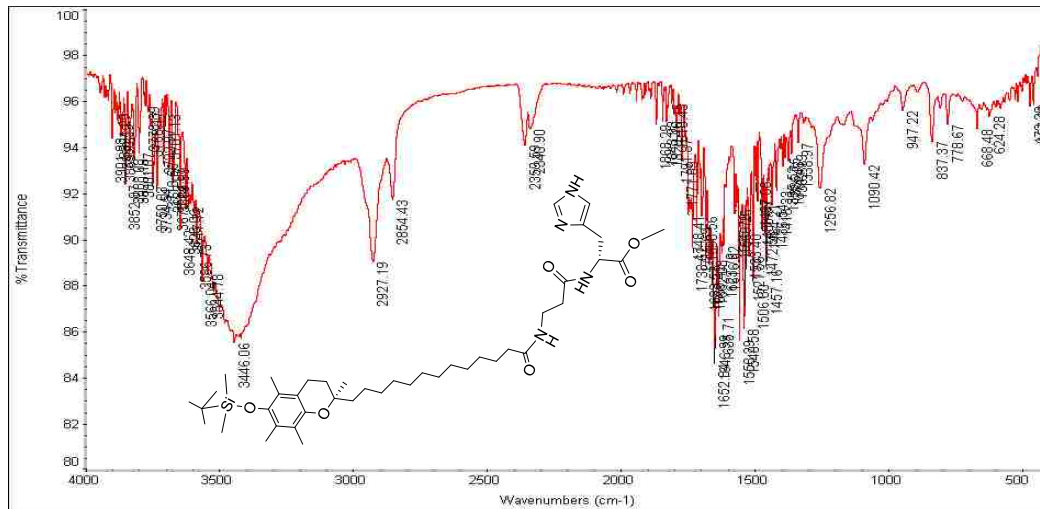
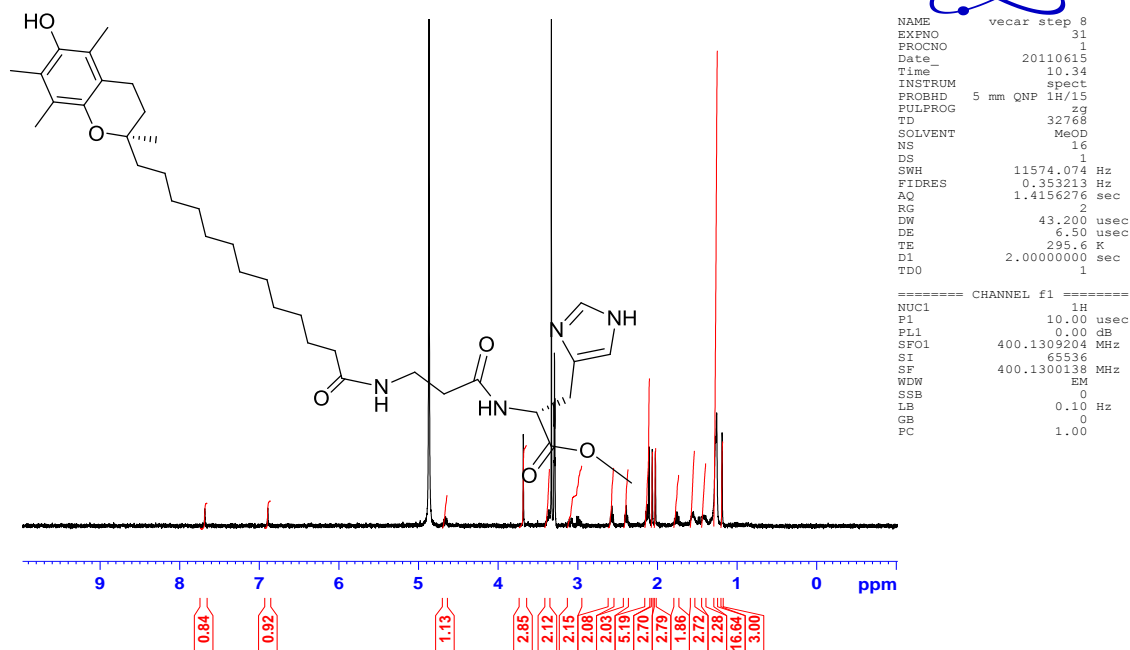


Figure D24: (R)-methyl 2-(3-(13-((R)-6-((tert-butylidimethylsilyl)oxy)-2,5,7,8-tetramethylchroman-2-yl)tridecanamido)propanamido)-3-(1H-imidazol-4-yl)propanoate (119) IR.

(R)-methyl 2-(3-(13-((R)-6-hydroxy-2,5,7,8-tetramethylchroman-2-yl)tridecanamid)propanamido)-3-(1H-imidazol-4-yl)propanoate



```

NAME      vecar step 8
EXPNO    31
PROCNO   1
Date_    20110615
Time     10.34
INSTRUM  spect
PROBHD   5 mm QNP 1H/15
PULPROG  zg
TD        32768
SOLVENT  MeOD
NS        16
DS        1
SWH       11574.074 Hz
FIDRES   0.353213 Hz
AQ        1.4156276 sec
RG        2
DW        43.200 usec
DE        6.50 usec
TE        295.6 K
D1        2.0000000 sec
TD0       1

----- CHANNEL f1 -----
NUC1     1H
P1       10.00 usec
PL1      0.00 dB
SFO1    400.1309204 MHz
SI       65536
SF       400.1300138 MHz
WDW      EM
SSB      0
LB       0.10 Hz
GB       0
PC       1.00
    
```

Figure D25: (R)-methyl 2-(3-(13-((R)-6-hydroxy-2,5,7,8-tetramethylchroman-2-yl)tridecanamido)propanamido)-3-(1H-imidazol-4-yl)propanoate (106) ¹H NMR.

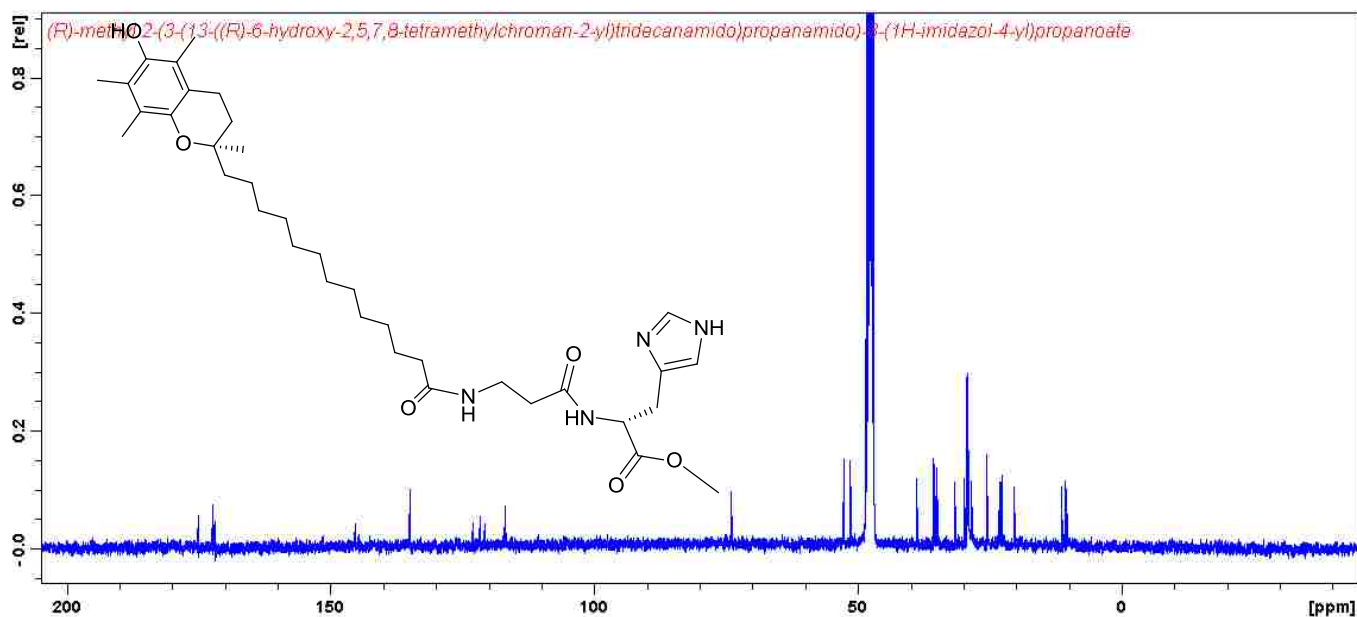


Figure D26: (R)-methyl 2-(3-(13-((R)-6-hydroxy-2,5,7,8-tetramethylchroman-2-yl)tridecanamido)propanamido)-3-(1H-imidazol-4-yl)propanoate (106) ¹³C NMR.

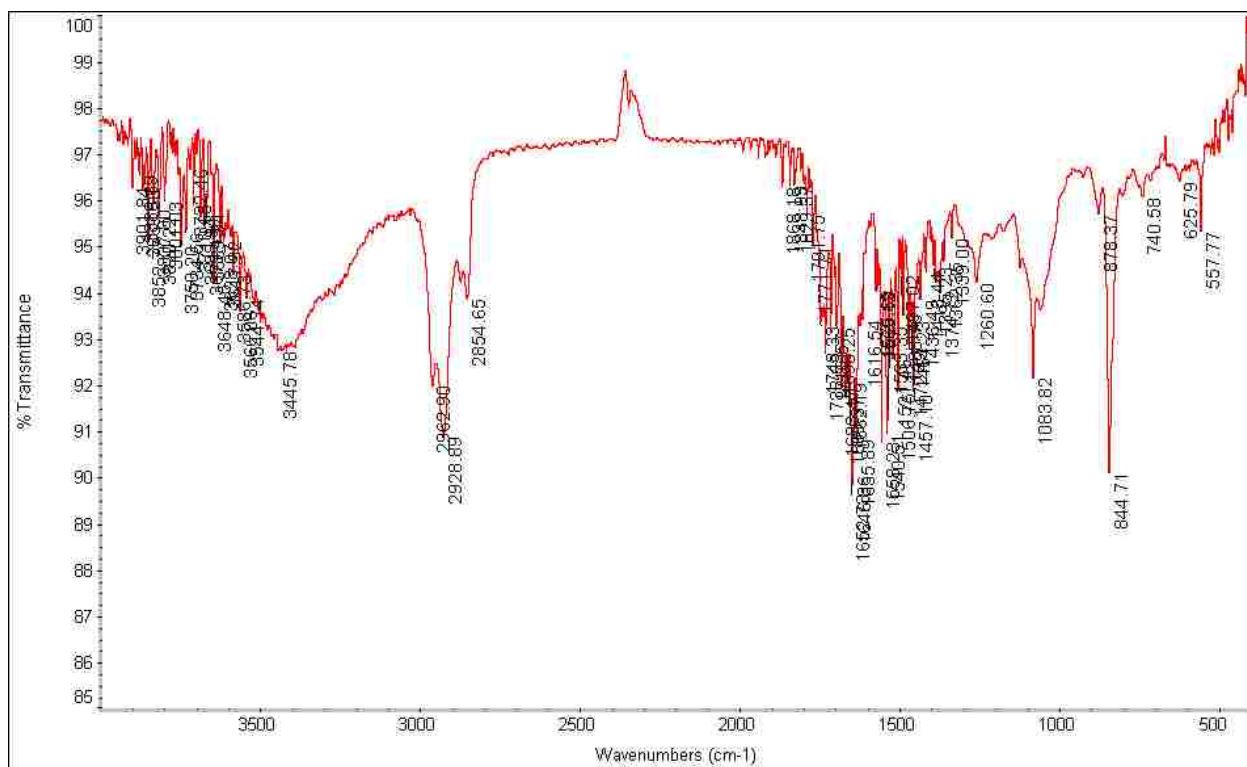


Figure D27: (*R*)-methyl 2-(3-(13-((*R*)-6-hydroxy-2,5,7,8-tetramethylchroman-2-yl)tridecanamido)propanamido)-3-(1H-imidazol-4-yl)propanoate (106) IR.

APPENDIX E: LETTERS OF PERMISSION

Permission Request
12/11/2013



RightsLink®

[Home](#)[Create Account](#)[Help](#)

Title: Synthesis of Vitamin E-Carnosine (VECAR): New Antioxidant Molecule with Potential Application in Atherosclerosis

Author: Carlos E. Astete, Danielle Songe Meador, David Spivak et al.

Publication: Synthetic Communications

Publisher: Taylor & Francis

Date: May 3, 2013

Copyright © 2013 Taylor & Francis

User ID:
Password:
<input type="checkbox"/> Enable Auto Login
<input type="button" value="LOGIN"/>
Forgot Password/User ID?
If you're a copyright.com user, you can login to RightsLink using your copyright.com credentials. Already a RightsLink user or want to learn more?

Thesis/Dissertation Reuse Request

Taylor & Francis is pleased to offer reuses of its content for a thesis or dissertation free of charge contingent on resubmission of permission request if work is published.

[BACK](#)[CLOSE WINDOW](#)

Copyright © 2013 [Copyright Clearance Center, Inc.](#) All Rights Reserved. [Privacy statement](#).
Comments? We would like to hear from you. E-mail us at customercare@copyright.com



RightsLink®

Home

Create Account

Help



ACS Publications
High quality. Right impact.

Title: Absolute Configuration Determination Using Enantiomeric Pairs of Molecularly Imprinted Polymers
Author: Danielle S. Meador and David A. Sliyak
Publication: Organic Letters
Publisher: American Chemical Society
Date: Mar 1, 2014
Copyright © 2014, American Chemical Society

User ID
<input type="text"/>
Password
<input type="text"/>
Enable Auto-Login
<input type="button" value="LOGIN"/>
Forgot Password/User ID?
If you're a copyright.com user, you can login to RightsLink using your copyright.com credentials. Already a RightsLink user or want to learn more?

PERMISSION/LICENSE IS GRANTED FOR YOUR ORDER AT NO CHARGE

This type of permission/license, instead of the standard Terms & Conditions, is sent to you because no fee is being charged for your order. Please note the following:

- Permission is granted for your request in both print and electronic formats, and translations.
- If figures and/or tables were requested, they may be adapted or used in part.
- Please print this page for your records and send a copy of it to your publisher/graduate school.
- Appropriate credit for the requested material should be given as follows: "Reprinted (adapted) with permission from (COMPLETE REFERENCE CITATION). Copyright (YEAR) American Chemical Society." Insert appropriate information in place of the capitalized words.
- One-time permission is granted only for the use specified in your request. No additional uses are granted (such as derivative works or other editions). For any other uses, please submit a new request.

THE VITA

Danielle Songe Meador, a native of Meraux, Louisiana, received her bachelor's degree in chemistry at Louisiana State University in 2009. She decided to deepen her knowledge of chemistry and joined Professor David Spivak's research group in 2010 where she designed, synthesized, and explored a chimeric antioxidant and new crosslinkers for molecular recognition. As a graduate student, Danielle has also earned several awards; including, the Coates Travel Award and Outstanding LSU Teaching Award. Danielle is a GAANN fellow and a candidate for the degree of Doctor of Philosophy in chemistry, which will be awarded at LSU's spring commencement in May 2014.